Dielectrophoretic characterization of living cells in real-time on a point-and-planar microwell (PPM) platform

A Dissertation
Presented in Partial Fulfillment of the Requirements for the
Degree of Doctor of Philosophy
with a
Major in Chemical Engineering
in the
College of Graduate Studies
University of Idaho
by
Ezekiel O. Adekanmbi

Major Professor: Soumya Srivastava, Ph.D.
Committee Members: Wudneh Admassu, Ph.D.; James Moberly, Ph.D.; Nathan Schiele, Ph.D.
Department Administrator: Eric Aston, Ph.D.

August 2019

Authorization to Submit Dissertation

This dissertation of Ezekiel O. Adekanmbi, submitted for the degree of Doctor of Philosophy with a Major in Chemical Engineering and titled "Dielectrophoretic characterization of living cells real-time on a point-and-planar microwell (PPM) platform", has been reviewed in final form. Permission, as indicated by the signatures and dates below, is now granted to submit final copies to the College of Graduate Studies for approval.

Major Professor: _____ Date: _____
Soumya Srivastava, Ph.D.

Committee Members: _____ Date: _____
Wudneh Admassu, Ph.D.

_____ Date: _____
James Moberly, Ph.D.

_____ Date: _____
Nathan Schiele, Ph.D.

Department Administrator: _____ Date: _____
Eric Aston, Ph.D.

Abstract

Electrical, dielectric, or electrophysiological properties of bioparticles, i.e. cells in particular, define their response to the external electric fields. They provide important information that aids in the prediction of bioparticle pathways, discernment of infections, phenotypic and genotypic variations, as well as pneumographic analysis, and biosensing. These dielectric properties are also essential in the development of diagnostic and therapeutic procedures. A review of the current state-of-the-art techniques for obtaining these properties was compiled and significant shortcomings ranging from cost and fabrication challenges for sub-micron bioparticles to the limitation of real-time exploration of electrode spacing were found. To address these shortcomings, a point-and-planar microwell (PPM) platform is developed. This device platform, which was fabricated with poly(dimethylsiloxane) (PDMS) polymer and assembled through a novel and economical in-house microwave plasma generator (compared and validated with commercial Harrick Plasma cleaner), is validated with O-type human erythrocytes or red blood cells (RBCs). Following validation, it was utilized for characterizing bioparticles related to applications in 1) medical diagnostics and 2) environmental biotechnology i.e. synergy of biosorption and dielectrophoresis. In medical diagnostics, the device was used to explore the properties of early stage infiltrating ductal adenocarcinoma cells (ADCs) i.e. breast cancer from peripheral blood and numerically quantifying their isolation in a microdevice using particle tracking module. This revealed the potential solution to the problem of device instability currently been experienced in the bioseparations field. The device also revealed the variations in the electrophysiological properties of human red blood cells as they age and when they are osmotically stressed. Furthermore, with the environmental challenges associated with recovering rare earth elements (REEs) and the subsequent utilization of biosorption to alleviate these challenges, this work introduces, for the first time, the utilization of dielectrophoretic crossover frequency (measured through the point- and-planar device platform) as a potential complementary quantification methodology to spectroscopy and a unique method of identifying organisms (*C. Necator*) that can hyperaccumulate metals (Samarium, Neodymium, and Europium).

Acknowledgements

My special thank you goes to my Major Professor, Dr. Soumya Srivastava, for her guidance through the execution stage of various work reported in this dissertation. Alumni and current members of MESA research group have been very helpful in the lab. Anthony Giduthuri, Archana Dulal, Courtney Molvig, Sahara Waymire, Abigeal Ilesanmi-Odubiyi, Amanda Vu, Sheilla Briggs, Jeremiah Dustin, Milad Nahavandi, your contributions have saved me time, sleep and money. Special appreciation also goes to Drs. Wudneh Admassu, James Moberly and Nathan Schiele for their guidance, teaching and unflinching supports.

How would I have carried out the visualization of these microorganisms without using microscopes? Thanks to Dr. Eric Aston, the Chair of the Department of Chemical and Materials Engineering, who made available both inverted and upright microscopes for my use. Oscilloscopes are important tool that helps one tracks the functionality a waveform generator. This was made available by Dr. David McPherson. Thank you so much DMAC. Charles Cornwall, Gail Bergman and Margaret Baker, knowing you since 2014 has been a great benefit to me and the completion of this dissertation.

University of Idaho's co-graduate students: Bennet Carv, Jonathan Counts, and Washington State University staffers: Powell Alyxandria, Kirubananthah Rubika, Kim Lam Chiok, Drs. Narayan Paul, Massaro Ueti, and Devendra Shah are also important parts of this dissertation story. I say thank you all for your patience even when it appeared I was pushing too hard so as to get things done.

Finally, I want to immensely thank the National Science Foundation (NSF) for providing the fund [NSF/CBET #1500815] to executive the projects reported in this dissertation. I also want to thank the Graduate and Professional Student Association (GPSA), National Institutes of Health (NIH), National Society of Black Engineers (NSBE) and National Organization for the professional advancement of Black Chemists and Chemical Engineers (NOBCChE) for making funds available to attend conferences and programs that helped me throughout this work.

Dedication

I dedicate this work to my mother, Mrs. Abosede Adekanmbi - who motivated me to strive for excellence, my wife Olufunke Adekanmbi - who endured my frequent absence from home for laboratory work or conferences, and my trio - David, Pelumi and Danielle Adekanmbi for their patience and understanding when I constantly denied them appropriate fatherly presence while pursuing this doctoral degree.

Table of Contents

List of Tables

List of Figures

Chapter 1: Introduction

Electrical properties of bioparticles (cells, in particular) define their response to the external electric fields [1]. Characterizing bioparticles and identifying these dielectric properties is very important in the prediction of bioparticle pathways, discerning infections, recognizing phenotypes and genotype, pneumographic analysis and biosensing. On the engineering side of developing and designing point-of-care diagnostic platforms, recognizing these dielectric properties will aid in the simulation of bioparticle-electromagnetic field interaction [1]. These electrophysiological properties are also essential in the development of diagnostic and therapeutic procedures [1]. For instance, when a bioparticle is suspended in an external electric field (AC or DC), the electric current densities [2], electric current pathways [3-5], and energy absorption depend largely on the intrinsic electrical characteristics of the bioparticle. Such intrinsic electrical properties include permittivity, conductivity, impedance, conductance, capacitance, resistance, etc.

To measure these dielectric properties, three central methods are most commonly used: (1) impedance cytometry, (2) electrorotation (ROT), and (3) dielectrophoresis have been utilized for both single and multiple cell analyses [6]. In impedance cytometry, an AC electric potential is applied between a pair of electrodes and the resulting current flowing through the system is measured [7]. The impedance of the system is then found as a function of the applied voltage and the electric current passing through the system. Data from such impedance experiments are then fitted with appropriate shell models i.e. single and multiple shell to extract the dielectric properties of these bioparticles [8-10]. However, impedance cytometry is usually limited to two frequencies per single bioparticle unless it is combined with other methods, such as fluorescence [6] and optics [11]. Apart from this holdup, cytometry is notorious for rolling out an overwhelming amount of information that can be unnecessary. Also, the quantification of these properties itself is too slow when compared with other methods and it is often limited to particles <70 μm in size [12].

Electrorotation (ROT) on the other hand commonly uses a four-phase quadrature applied to quadrupolar electrodes to generate electrical torque from the rotating electric field that induces the rotation of a bioparticle (suspended between the electrodes) [13-22]. The magnitude of the rotating particle velocity is a function of the electrical characteristics i.e. dielectric properties of the bioparticle. From the velocity measurement, the electrical properties of the bioparticle can be obtained [23-27]. A major disadvantage of the electrorotation technique is its lower throughput because of the time required to obtain bioparticle velocity data [6].

The third characterization method, dielectrophoresis (DEP), involves the use of spatially nonuniform electric field as a driving force to induce translational motion of the bioparticle [28-30]. DEP is the focus of this work. In DEP, neutral or charged bioparticles in applied alternating current

(AC) electric fields become polarized and form dipoles, which move according to their electrical properties and other surrounding factors like the field gradient, particle size, and properties of the suspending medium. Information from such translational orientation of bioparticles can reveal their electrical properties [31, 32]. DEP has the advantage of obtaining quick response of bioparticles to electric field effects. This is a huge benefit as the bioparticle viability tends to be preserved when they are not exposed to the electric field for a period longer than 5 min [33]. In terms of throughput, however, DEP tends to be lower than impedance cytometry though higher when compared to electrorotation [6]. Cost advantage, ease of operation, flexibility in fabrication, and a balance between testing time and throughput are the rationales behind the exploration of DEP methodology in this work.

Research goal and objectives

The principal goal of this dissertation is to design, fabricate, validate and utilize a dielectrophoretic characterization device for medical diagnostics and environmental applications. The objectives of this body of work are to;

Objective 1: Design, fabricate, and validate a characterization device that works on the principle of dielectrophoresis.

> **Objective 1a**: Fabricate a point and planar electrode microwell system. Numerically and experimentally explore its operation. (Chapter 3)
>
> **Objective 1b**: Construct a microwave plasma cleaner for the irreversible hydrophobic assembly of the point and planar microwell system. (Chapter 4)

Objective 2: Apply the device for medical diagnostics to;

> **Objective 2a**: Detect subtle differences in early stage (stage 0) breast cancer by understanding the electrical properties of infected peripheral blood samples. (Chapter 5)
>
> **Objective 2b**: Use the information to numerically simulate the separation of infected cells from healthy ones. (Chapter 5)
>
> **Objective 2c**: Explore the effect of cell age on their dielectrophoretic signatures (Chapter 8)

Objective 3: Apply the device for environmental biotechnology to;

> **Objective 3a**: Characterize gram negative bacteria (*Cupriavidus necator*) in its native and allied states with rare earth elements (Chapter 6)
>
> **Objective 3b**: Utilize crossover frequency measurement as a novel quantitative tool for rare earth elements (Chapter 7)

By these objectives, this work is divided into eight (8) chapters. In Chapter 1, an introduction and motivation for the electrical characterization of bioparticle is presented. The three (3) main methods

of obtaining the electrical properties of bioparticles, their pros and cons, as well as the rationale behind choosing DEP in this dissertation are succinctly delivered. Chapter 2 discusses these three methods in detail. It also reports various bioparticles that have been characterized using each of these methods. Particles of interest, choice of suspending medium, electrode configuration, choice of applied voltage, and other pertinent factors related to each of these electrical characterization techniques are discussed in detail. This leads to the introduction of point-and-planar microwell (PPM) in Chapter 3. PPM is a novel characterization device introduced in this dissertation to contain sizable amount of bioparticle suspension for onward particle property determination. This chapter discusses the choice of polymer used in the fabrication of PPM. The device, which works on the dielectrophoretic principle of crossover frequency measurement, is functionalized with alternative current through high-grade platinum electrodes. It also discusses the choice of electrode and the technique for sealing of the device platform. Numerical and experimental exploration of the influence of inter-electrode spacing and shape of the electrode on DEP factor is revealed.

In Chapter 4, effort is geared towards the comparative analysis of the efficiency of commercial plasma cleaner (COM-PC) and our in-house microwave plasma generator (MESA-Mgen). While assembling the parts of the proposed microwell system, a hydrophilic sealing is required. MESA-Mgen was fabricated and evaluated for its influence on bulk electro-osmotic and polystyrene particle velocities. Factors including contact angles, storage-solvent, and half-way hydrophobicity period were explored using polymer materials treated with MESA-Mgen and the outcomes were compared with other sealing technology. Chapter 5 details the application of PPM to the characterization of peripheral mononuclear blood cells (PBMCs) and infiltrating ductal adenocarcinoma cells (ADCs) for the first time. In this chapter, extracted electrical properties are used to model and simulate the separation of PBMCs from ADCs, that would further lead to developing a diagnostic tool for early detection of breast cancer, especially in young women. The dielectric properties of PBMCs available from the literature were utilized to validate the measurement and the PPM platform. The Multiphysics simulation of the particle trajectories revealed a unique mechanism which can solve the age-long instability issues experienced in the microfluidic devices especially DEP driven devices.

Chapters 6 and 7 is about the application of PPM in environmental science. In Chapter 6, PPM was used to find the electrical properties of biosorbent (*Cupriavidus necator*) in its native state and allied states with rare earth elements (REEs): Europium (Eu), Samarium (Sm) and Neodymium (Nd). While characterizing the bio-sorbent, *C. Necator* another important observation was revealed: although the first crossover frequencies were changing, the second crossover frequency remained constant. The observation of this no-change in the second crossover frequency in Chapter 6 led to further correlations as discussed in Chapter 7.

The adsorption of REEs were further correlated with the electrical characterization of the biosorbent to quantify adsorbed metals with the goal of providing an alternative technique to expensive mass spectroscopy (ICP-MS). In this chapter (Chapter 7), *Cupriavidus necator* was cultured and incubated in REE solutions. Supernatant, after centrifugation, was quantified for REEs using UV-Vis spectrophotometry. The resultant biosorbent pellets were quantified for their electrical properties and the correlation between these measurements were utilized to predict the efficiency of *Cupriavidus necator* during the adsorption of REEs.

The dissertation finally concludes with Chapter 8 where the device was validated using O type red blood cells (RBCs) and were compared to the results obtained from ROT research. Additionally, the key achievements and novel conclusions from each chapter are highlighted alongside some stated future directions regarding the application of PPM.

References

[1] D. Miklavcic, Paveselj, N, Hart, F. X, "Electrical properties of Tissues," in *Encyclopedia of Biomedical Engineering*, M. A. (Ed), Ed., ed, 2006.

[2] R. Pethig, "Review article-dielectrophoresis: status of the theory, technology, and applications," *Biomicrofluidics,* vol. 4, p. 022811, 2010.

[3] Y. A. Chizmadzhev, A. V. Indenbom, P. I. Kuzmin, S. V. Galichenko, J. C. Weaver, and R. O. Potts, "Electrical properties of skin at moderate voltages: contribution of appendageal macropores," *Biophysical journal,* vol. 74, pp. 843-856, 1998.

[4] M. D. Vahey, L. Quiros Pesudo, J. P. Svensson, L. D. Samson, and J. Voldman, "Microfluidic genome-wide profiling of intrinsic electrical properties in Saccharomyces cerevisiae," *Lab on a chip,* vol. 13, pp. 2754-2763, 2013.

[5] C. Trainito, "Study of cell membrane permeabilization induced by pulsed electric field – electrical modeling and characterization on biochip," Université Paris-Saclay, 2015.

[6] A. Jaffe and J. Voldman, "Multi-frequency dielectrophoretic characterization of single cells," *Microsystems & Nanoengineering,* vol. 4, p. 23, 2018/09/10 2018.

[7] D. Holmes and B. L. J. Webb, "Electrical Impedance Cytometry," in *Encyclopedia of Nanotechnology*, B. Bhushan, Ed., ed Dordrecht: Springer Netherlands, 2012, pp. 662-671.

[8] T. Sun and H. Morgan, "Single-cell microfluidic impedance cytometry: a review," *Microfluidics and Nanofluidics,* vol. 8, pp. 423-443, 2010/04/01 2010.

[9] Y. Zhang, Y. Zhao, D. Chen, K. Wang, Y. Wei, Y. Xu, C. Huang, J. Wang, and J. Chen, "Crossing constriction channel-based microfluidic cytometry capable of electrically phenotyping large populations of single cells," *Analyst,* vol. 144, pp. 1008-1015, 2019.

[10] D. Holmes and H. Morgan, "Single Cell Impedance Cytometry for Identification and Counting of CD4 T-Cells in Human Blood Using Impedance Labels," *Analytical Chemistry,* vol. 82, pp. 1455-1461, 2010/02/15 2010.

[11] N. Haandbæk, S. C. Bürgel, F. Rudolf, F. Heer, and A. Hierlemann, "Characterization of Single Yeast Cell Phenotypes Using Microfluidic Impedance Cytometry and Optical Imagingtime," *ACS Sensors,* vol. 1, pp. 1020-1027, 2016/08/26 2016.

[12] M. E. Piyasena, P. P. Austin Suthanthiraraj, R. W. Applegate, A. M. Goumas, T. A. Woods, G. P. López, and S. W. Graves, "Multinode Acoustic Focusing for Parallel Flow Cytometry," *Analytical Chemistry,* vol. 84, pp. 1831-1839, 2012/02/21 2012.

[13] Y. K. Ren, D. Morganti, H. Y. Jiang, A. Ramos, and H. Morgan, "Electrorotation of Metallic Microspheres," *Langmuir,* vol. 27, pp. 2128-2131, 2011/03/15 2011.

[14] H. R. Fuhr G., "Cell Electrorotation," in *Electrical Manipulation of Cells*, D. M. R. e. Lynch P.T., Ed., ed Boston, MA: Springer, (1996).

[15] C. Dalton, A. D. Goater, J. Drysdale, and R. Pethig, "Parasite viability by electrorotation," *Colloids and Surfaces A: Physicochemical and Engineering Aspects,* vol. 195, pp. 263-268, 2001/12/30/ 2001.

[16] A. a. R. Bonincontro, G., "Electrorotation: A Spectroscopic Imstorage time Approach to Study the Alterations of the Cytoplasmic Membrane. ," *Advances in Molecular Imaginge time,* vol. 5, pp. 1-15, 2015.

[17] G. D. Gasperis, X. Wang, J. Yang, F. F. Becker, and P. R. C. Gascoyne, "Automated electrorotation: dielectric characterization of living cells by real-time motion estimation," *Measurement Science and Technology,* vol. 9, pp. 518-529, 1998/03/01 1998.

[18] M. Esch, V. L. Sukhorukov, M. Kürschner, and U. Zimmermann, "Dielectric properties of alginate beads and bound water relaxation studied by electrorotation," *Biopolymers,* vol. 50, pp. 227-237, 1999/09/01 1999.

[19] L. Huang, W. He, and W. Wang, "A cell electro-rotation micro-device using polarized cells as electrodes," *ELECTROPHORESIS,* vol. 40, pp. 784-791, 2019/03/01 2019.

[20] Y.-S. Lin, S. Tsang, R. Ghasemi, S. Bensalem, O. Français, F. Lopes, H.-Y. Wang, C.-L. Sun, and B. L. Pioufle, "Dielectric Characterisation of Single Microalgae Cell Using Electrorotation Measurements," *Proceedings,* vol. 1, 2017.

[21] Y. Huang, R. Holzel, R. Pethig, and X.-B. Wang, "Differences in the AC electrodynamics of viable and non-viable yeast cells determined through combined dielectrophoresis and electrorotation studies," *Physics in Medicine and Biology,* vol. 37, pp. 1499-1517, 1992/07/01 1992.

[22] D. Voyer, M. Frénéa-Robin, F. Buret, and L. Nicolas, "Improvements in the extraction of cell electric properties from their electrorotation spectrum," *Bioelectrochemistry,* vol. 79, pp. 25-30, 2010/08/01/ 2010.

[23] A. B. Tomáš Michálek, Zdeněk Hurák, Michaël Gauthier, "Control-oriented model of dielectrophoresis and electrorotation for arbitrarily shaped objects," *PHYSICAL REVIEW E,* vol. Accepted Paper, 2019.

[24] A. D. Goater and R. Pethig, "Electrorotation and dielectrophoresis," *Parasitology,* vol. 117 Suppl, pp. S177-89, 1998.

[25] P. Benhal, G. Chase, P. Gaynor, B. Oback, and W. Wang, "Multiple-Cylindrical Electrode System for Rotational Electric Field Generation in Particle Rotation Applications," *International Journal of Advanced Robotic Systems,* vol. 12, p. 84, 2015/07/01 2015.

[26] C. Dalton, A. D. Goater, J. P. H. Burt, and H. V. Smith, "Analysis of parasites by electrorotation," *Journal of Applied Microbiology,* vol. 96, pp. 24-32, 2004/01/01 2004.

[27] M. Cristofanilli, G. De Gasperis, L. Zhang, M.-C. Hung, P. R. C. Gascoyne, and G. N. Hortobagyi, "Automated Electrorotation to Reveal Dielectric Variations Related to HER-2/< strong> neu Overexpression in MCF-7 Sublines," *Clinical Cancer Research,* vol. 8, p. 615, 2002.

[28] T. B. Jones, "Basic theory of dielectrophoresis and electrorotation," *IEEE Engineering in Medicine and Biology Magazine,* vol. 22, pp. 33-42, 2003.

[29] W. Xiao-Bo, H. Ying, P. R. C. Gascoyne, and F. F. Becker, "Dielectrophoretic manipulation of particles," *IEEE Transactions on Industry Applications,* vol. 33, pp. 660-669, 1997.

[30] Q. Chen and Y. J. Yuan, "A review of polystyrene bead manipulation by dielectrophoresis," *RSC Advances,* vol. 9, pp. 4963-4981, 2019.

[31] P. R. C. Gascoyne, J. Noshari, F. F. Becker, and R. Pethig, "Use of dielectrophoretic collection spectra for characterizing differences between normal and cancerous cells," *IEEE Transactions on Industry Applications,* vol. 30, pp. 829-834, 1994.

[32] P. Gascoyne, R. Pethig, J. Satayavivad, F. F. Becker, and M. Ruchirawat, "Dielectrophoretic detection of changes in erythrocyte membranes following malarial infection," *Biochimica et Biophysica Acta (BBA) - Biomembranes,* vol. 1323, pp. 240-252, 1997/01/31/ 1997.

[33] J. Lu, C. A. Barrios, A. R. Dickson, J. L. Nourse, A. P. Lee, and L. A. Flanagan, "Advancing practical usage of microtechnology: a study of the functional consequences of dielectrophoresis on neural stem cells," *Integrative Biology,* vol. 4, pp. 1223-1236, 2012.

Chapter 2: Dielectric spectroscopy of biological cells via electrokinetics: the past, present, and the future

Ezekiel O. Adekanmbi[1], Soumya K. Srivastava[1*]
[1]Department of Chemical & Materials Engineering, University of Idaho, Moscow, ID 83844

Abstract

Electrical properties of biological cells are useful to distinguish cells either in their homogenous or heterogenous populations. They provide insight into the health, geometry, growth, differentiation, function, physiological state including death of any biological cell i.e. phenotype and genotype of a cell. These properties play an important role in designing of various microfluidic chip-based diagnostic tools that utilize electric field gradients for cell movement. Reported studies over several decades have revealed that electrorotation, dielectric spectroscopy, and dielectrophoresis are the most common cell characterization techniques to obtain electrical parameters. However, in each of these characterization techniques, several advancements have been reported especially within the last decade. Details of these advances vary from sophisticated methods like grinding electrode materials and mixing them with polymer composite for use as electrorotation electrodes to simple targeted means like using biological cells itself as electrodes. These advances in technologies are very well discussed in this review. Sequentially, a complete description of the characterized electrical properties targeted to specific bioparticles of interest are presented. The main concepts of dielectrophoresis, electrorotation, and impedance cytometry are given alongside the generated spectra including their analyses for both single and multiple cells. Also, various methods of electrode design, spacing, and fabrication are adequately discussed. The materials used for fabricating the electrodes and its advancement over time with respect to the choice of the materials are also substantially addressed. Finally, with the growing trend observed within this time frame, the future direction of bioparticle characterization could be predicted.

2.1 Introduction

The 2017 World Health Statistics on monitoring global heath for sustainable development goals (SGDs) has revealed how global health is centrally positioned within the 2030 agenda, with one comprehensive goal (SDG 3) and its 13 targets covering all major health priorities [34]. Departments of Health and Family Welfare in U.K., U.S., Australia, India, China as well as the World Health Organization (WHO) are all prepared through the provision of funding and technical assistance towards protecting public health [35-37]. With more than 36 million annual global death resulting from non-communicable diseases alone, one cannot oppose the essence of detecting these diseases at teething stages. One of the several ways by which these diseases can be detected early enough is through microfluidic technology [38-50]. Over the last decade, several patents have been granted in this regard

resulting in the surge of point-of-care diagnostic device start-up companies scattered all around U.S. and Europe [51].

In cases where disease conditions have already developed or approached its terminal stage, such as stage-4 breast cancer, these microfluidic devices are still important in monitoring disease progression and treatment effectiveness [52-56]. For instance, quantifying circulating tumor cells (CTCs) in the blood through microfluidics could help the medics to reach to a judgement that could avert extreme measures like surgery. Common microfluidic devices for detecting/monitoring these diseases are designed using the known electrical properties of the bioparticles. These properties measure the extent of interaction a bioparticle would have with any externally generated electromagnetic fields [57]. Measuring electrical properties of cells has been the choicest cell characterization technique (as against other methods such as mechanical [58, 59], magnetic [60, 61], optical [62, 63] and acoustic means [64, 65]) because of its ease of control, higher efficiency, lower cost, and versatility that can be used for both single and multiple cells [66].

Currently, there is a dire need of a compendium of methodologies required to obtain these electrical properties and that is the purpose this collation of research works is meant to serve. Not only will this collation serve as a one-stop shop for all researchers who desire to know the intrinsic characteristics of their bioparticles of interest, it will also enable researchers to compare various methodologies and choose therefrom depending on multiple determining factors including but not limited to economics and ease of fabrication. This chapter starts with the description of biological cells and their electrical properties. It then gives a succinct overview of the importance of electrical properties of biological cells and the methods through which these properties can be obtained. Thereafter, the chronological procedure on how to obtain and analyze these properties using Excel software are provided with sample steps. Following this is a compendium of the research studies involving the quantification of the electrical properties of interest as reported by various research groups. This chapter finally ends with a glimpse into the future of cell characterization techniques.

2.2 Biological cells and their membranes

Biological cells are known to have two main structural components: the membranes/walls and the internal constituents. Membranes are a critical part of all forms of biological material because they separate the cellular contents from the external world [67]. They are very important in the microfluidic arena and can, therefore, be represented as single, double, or multiple shell entities depending of the nature of the cell. Matured human red blood cell, for example, does not have any nucleus and can therefore be represented with only one membrane (single shell). When bioparticles are represented as a single shell, it means they occur as a bag of cytoplasm covered with a shell/membrane. Membranes allow biological cells to maintain differences in the chemical composition between their internal and

external environment [67]. Despite their fencing roles, they are also the gate keepers that allow or debar critical materials like nutrients, waste products, etc. into or out of the cell. The interaction of a cell with its external environment and other cells (identifying themselves and sharing information) is also selectively controlled via the membrane. Evolutionary history reveals that beyond the roles of being a barrier, cell membranes are also structural elements contributing to many aspects of cell function and behavior [67]. Composition wise, the cell membrane has lipid (phospholipids) molecules as its most common constituent [67-69] with their hydrophobic (fatty acid) heads sandwiched between the hydrophilic (phosphate) heads as shown in Figure 2.1.

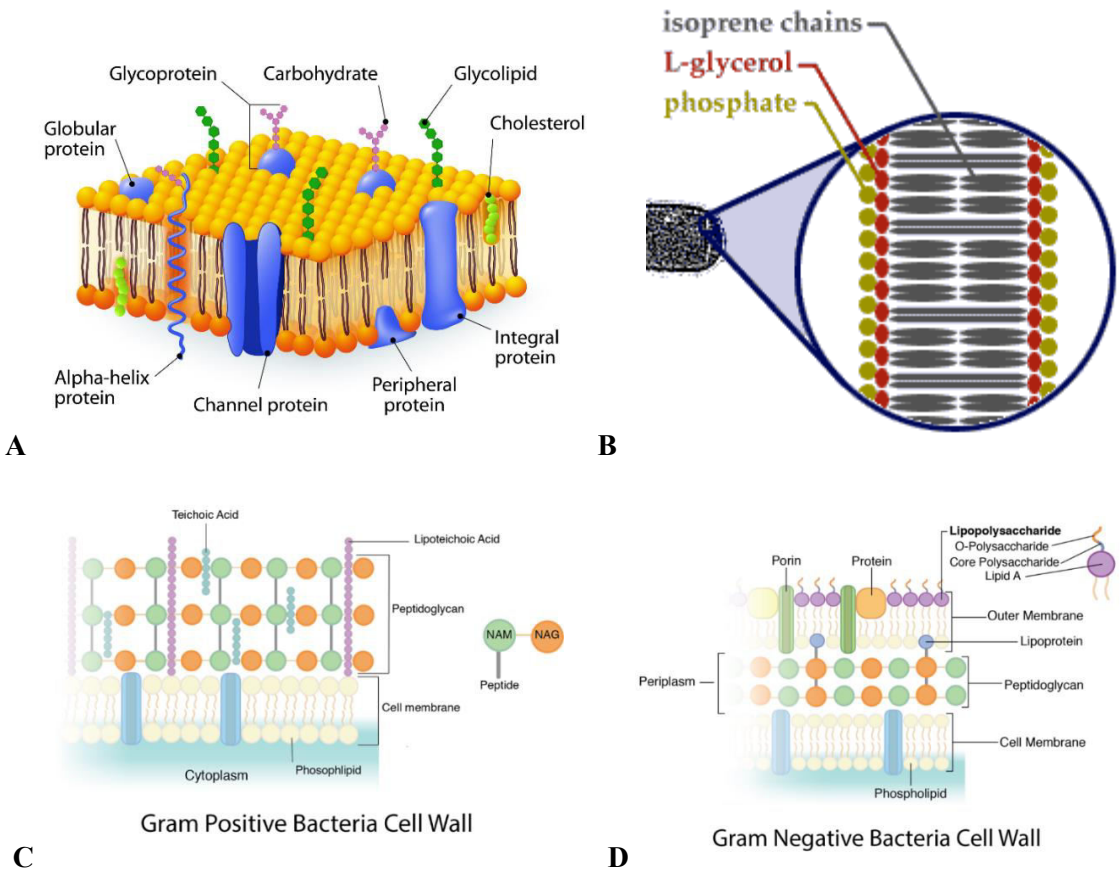

Figure 2.1 *(A) The schematic representation of a cell membrane of a eukaryotic cell; (B) Cell membrane of an archaea. It is different form all other forms of living cells; and C, D are the cell wall of gram positive and gram-negative bacteria respectfully. Unlike Archaea and eukaryotes, bacteria have a cell wall made of peptidoglycan, comprised of sugars and amino acids, and many have a polysaccharide capsule. The cell-wall acts as an extra layer of protection helping the cell maintain its shape and preventing dehydration.*

This hydrophobic region ~5-10 nm thick, is responsible for the formation of a strong deterrence against the diffusion of any hydrophilic molecule across the selected portion of the membrane. Apart from lipid molecules, the cell membrane also contains hundreds of proteins (for cross-membrane transport and cell communication), carbohydrates (for assistance in cell-cell recognition), and

cholesterol thereby rendering the membrane to be very complex in nature [67]. These proteins and lipids specifically determine many of the membrane properties. The characteristics of the membrane, therefore, make them possess electrical properties that distinguish them from the properties of both the cell interior and cell external environment [41, 68-73]. Electrical properties that are usually of interest in microfluidic arena include but not limited to capacitance and conductance of the membrane, permittivity and conductivity of the cytoplasm, and other related factors (depending on the shell model in focus) are discussed in the next section (cf. Sec. 3.0).

2.3 Electrical properties of the cell membrane

Since the membrane acts as an interface between the cell and its environment, knowing its electrical properties is very important to evaluate cell's response to any external electric field effect. First, it is crucial to know that the cell's membrane behaves like a dielectric material sandwiched between the conducting inner (cytoplasmic) and outer surfaces. This representation is similar to a dielectric material placed between two parallel conducting plates forming an electric capacitor. The behavior of the membrane as an insulator (a dielectric) is caused by the pure phospholipid bilayers that have no free ions, hence, no carriers to transport charges. For a bioparticle i.e. a cell suspended in a homogenous dielectric medium, two forms of particle-field interactions can occur under the influence of electric field. This interaction could be in the form of conduction (when the charges can move about) or as polarization (when the charges are restricted from moving) [74]. The combination of these two forms i.e. conduction and polarization is usually represented by the Kramer-Kronig relation- a bidirectional mathematical relation that lumps the real and imaginary parts together as a single 'complex entity'.

$$\varepsilon^* = \varepsilon' - i\varepsilon'' \tag{2.1}$$

where, ε' is the part due to polarization and $i\varepsilon''$ is due to conduction. When the conduction part ε'' is replaced by the conductivity relation $\sigma' = \omega\varepsilon''$, the permittivity relation above can be rewritten as:

$$\varepsilon^* = \varepsilon' - i\frac{\sigma'}{\omega} \equiv \varepsilon - i\frac{\sigma}{\omega} \tag{2.2}$$

with passive electrical permittivity given as:

$$\varepsilon^* = \varepsilon^*(\omega) = \varepsilon_\infty + \frac{\varepsilon_s - \varepsilon_\infty}{1 + i\omega\tau} \tag{2.3}$$

$\varepsilon^*$is the complex dielectric constant, ε_s is the permittivity at the low frequency limit, and ε_∞ is the permittivity at the high frequency limit, ω is the angular frequency and τ is the charge relaxation time constant (the time taken by the dielectric to return to its equilibrium state after being disturbed by an external electric field)

This new relation, the Cole-Cole (Debye model) relation given by eqn. 2.3, emphasizes the importance of frequency on complex (including polarization effects) permittivity and that is one of the reasons of using frequency dependency (as detailed in section 6.0) to determine the permittivity of

bioparticles. It is sufficing to say that the real and the imaginary parts, both represent two states where the field is in-phase and out-of-phase with the dipole respectively. In general, polarization of any material in an electric field can occur in five modes: electronic, atomic, dipolar, nomadic, and interfacial [74]. Out of these 5 modes, interfacial polarization, is the most commonly observed phenomenon in bioparticles [75]. This interfacial polarization occurs when the charges within the bioparticle get positioned in such a way as to generate non-uniform charge accumulations at the particle-field interfaces. This implies that when a bioparticle is placed within an electric field, the charges within them initially shift to align with the electric field.

However, their motion may be restricted either through trapping at the interface or at the impurities centers and this leads to space-charge formation that is seen as polarization - the formation of dipoles [74]. It is important that the field strength be sufficiently high, otherwise, interfacial polarization will be negligible [75]. As the frequency of the electric field increases, the relative permittivity of the bioparticle decreases resulting in dielectric dispersion (i.e. change in property of interest with frequency). As reported by Schwan in 1957, there are three forms of dispersion depending on the frequency range of the field; Alpha (10 Hz - few kHz), Beta (kHz to several MHz) and Gamma dispersion (> 10 GHz) [76]. While alpha and beta dispersions could be related to cellular interfaces such as the membrane [77], gamma dispersion is associated with the polarization of water molecules [77]. Beta dispersion technically represents the ability of a bioparticle's cell membrane to filter out low frequency currents and allow high-frequency current to pass through [78] the membrane. This is also known as "Maxwell-Wagner" dispersion since this was first explored for DC electric fields by Maxwell, and was later extended by Wagner to accommodate AC fields [79]. If a bioparticle is subjected to an AC electric field in the radio frequency range (100 kHz – 10 MHz), its polarization will be due to Maxwell-Wagner interfacial polarization [75].

In a non-uniform field of moderate strength, the suspended bioparticle forms an induced dipole whose moment, $\mu^{(i)}$, is given as;

$$\mu^{(i)} = \propto E \tag{2.4}$$

where $\propto$ is the polarizability of the particle (i.e the measure of the displacement of the particle's electron by the electric field) and E is the electric field strength [80]. The polarizability, $\propto$, is inevitably known if the dielectric property of the bioparticle is known. For a suspension of particles, polarizability can also be calculated from index-of-refraction data [80]. When the dipole is formed, the net charge on the particle is still zero; however, there is an electric field that is set up within the particle and this field can interact with the internal dipole field. This dipole resists the flow of the external electric field thereby storing charges. This charge storing capability of the particle is called its *capacitance* [81]. At low frequencies, the plasma membrane is highly resistive to current flow (capacitance is at the highest

value) across it (see Figure 2.2).

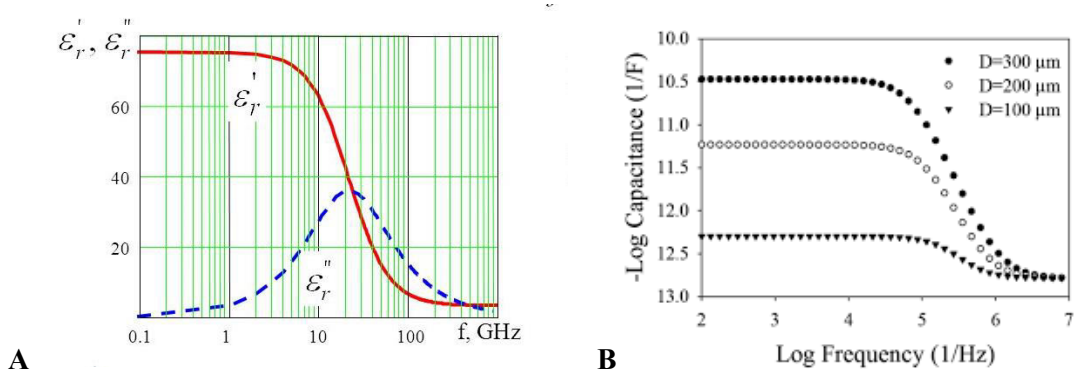

Figure 2.2 *(A) The variation of dielectric constant with frequency of the applied field. At low frequencies, the membrane permittivity is at the highest value (red curve). At high frequencies, the membrane is capacitively short circuited [82]. The blue dotted line represents heat generation as stated by Cole-Cole (B) The variation of capacitance (a function of the permittivity) with frequency at various particle size: the larger the size of the particle, the greater is its capacitance at lower frequencies. At high frequencies, the influence of size on permittivity is rendered null.*

As the frequency increases, the membrane is capacitively short circuited so that the ions in the cell interior as well as the cell membrane / wall begin to conduct electric current [83]. At this state the membrane is electrically transparent, hence, the internal components of the cell can be probed [84]. The cell membrane capacitance also helps in the design of device platforms that could use non-uniform electric fields to separate heterogeneous cell populations into unique homogeneous components. Besides, the charges on the surface of the membrane play an importance role in defining the capacitance of the membrane [85] as they can affect the voltage across the membrane; since the capacitance (C) and charges (Q) are related to the voltage (V) by $Q = CV$. For multilayer cytoplasmic strata, such as in bacteria, each layer is treated as a capacitor in series with the other layer and thus effective capacitance can be obtained. This charge storing capacity of the membrane is related to another important electrical property called permittivity. Permittivity of a dielectric material such as the cell membrane is a measure of how far the dipole charges are separated (electrical polarization) under the influence of an external electric field. In other words, it is the bioparticle's ability to resist an electric field. Permittivity of a spherical cell membrane is related to its capacitance through eqn. 2.5 below:

$$\varepsilon_{mem} = \frac{C_{mem} d}{4\pi r^2 \varepsilon_o} \tag{2.5}$$

where ε_{mem} is the permittivity of the membrane, C_{mem} the capacitance of the membrane, d the membrane thickness, r the particle radius, and ε_o the permittivity of vacuum. Several researchers have taken advantage of the permittivity and capacitance to characterize bioparticles such as neural stem cells [75], neurons [86], protoplasts [87], pancreatic β-cells [88], breast cancer cells [89], myelogenous leukemia (K562) cells [90], erythrocytes [50], and many other cells [53, 91-108].

Another important electrical property is the conductance of the cell membrane. Conductance of a cell membrane signifies the ease with which electric current flows through the membrane. Both conductance and capacitance are the two main electrical properties that can reveal the morphological peculiarities or the phenotypical behavior of the cell membrane with respect to the cell's response to external electric field. They serve as crucial electrophysiological biomarkers for cellular identities including, health, growth, division, function, physiological state including death [82, 109-116]. The presence of many ion channels and other *pores* in the membrane enhances current flow leading to the explanation behind high conductance usually observed in a cell membrane [117].

2.4 Quantification of electrical properties in bioparticles

From Sec. 2.3, membrane capacitance and conductance are crucial in providing information about the cell membrane. In this section, the focus is on how to obtain these electric properties.

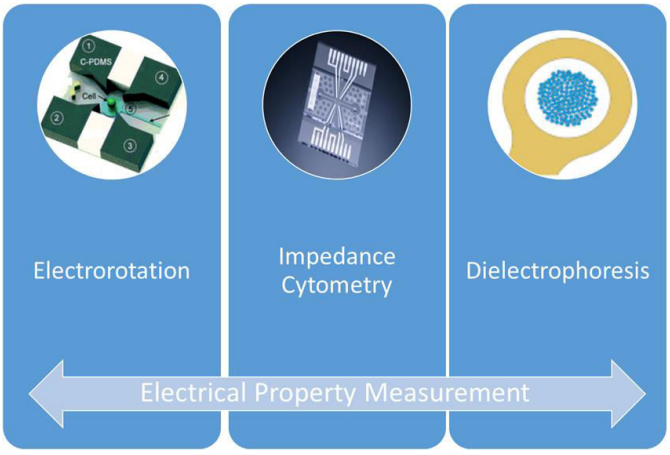

Figure 2.3 *The representation of the main electrical characterization techniques for biological materials. impedance cytometry and dielectrophoresis were respectively adapted with permission from [66, 118].*

In the domain of cellular characterization, there are three broad methods commonly used to obtain cell dielectric properties (**Figure 2.3**). These are impedance (cytometry) spectroscopy [93, 119-122], dielectrophoresis [72-75, 123-125], and electrorotation [13, 66, 126-131]. The last two methods are collectively referred to as AC electrokinetics [8].

2.4.1 Electrical impedance spectroscopy

Electrical impedance spectroscopy, also called dielectric spectroscopy or impedance cytometry, is one of the noninvasive bioparticle characterization techniques. It measures in real-time the impedance of biological cells [132]. From the impedance data, a spectrum can be generated i.e. impedance vs. frequency plot to obtain the dielectric properties such as membrane capacitance of the cell. In relation to a cell, impedance is a form of total restriction by the cell to current flow due to the capacitance of its membrane as well as the innate resistance of the cell. Pure (ohmic) resistance does not vary with frequency of the AC field, however, the resistance is frequency dependent due to the

capacitance of the cell membrane (capacitive reactance). Impedance is a combination of both these resistances: Ohmic resistance and capacitive reactance. The origin of the physics governing the impedance measurement of bioparticle can be traced back to the 18th century by Maxwell [133]. However, the first report on impedance measurement of bioparticle was published around the first world war period [134]. About 10 years after the end of the world war I, series of works were reported on the estimation of cytoplasmic electrical properties using suspended cells [135]. Since then, scientists have advanced the characterization technique for cell dielectric property measurement using impedance [76, 136-138]. The set up for impedance spectroscopy simply involves the application of a very low AC voltage (commonly sinusoidal potential excitation) through two electrodes between which the cell suspension can flow through (**Figure 2.4**).

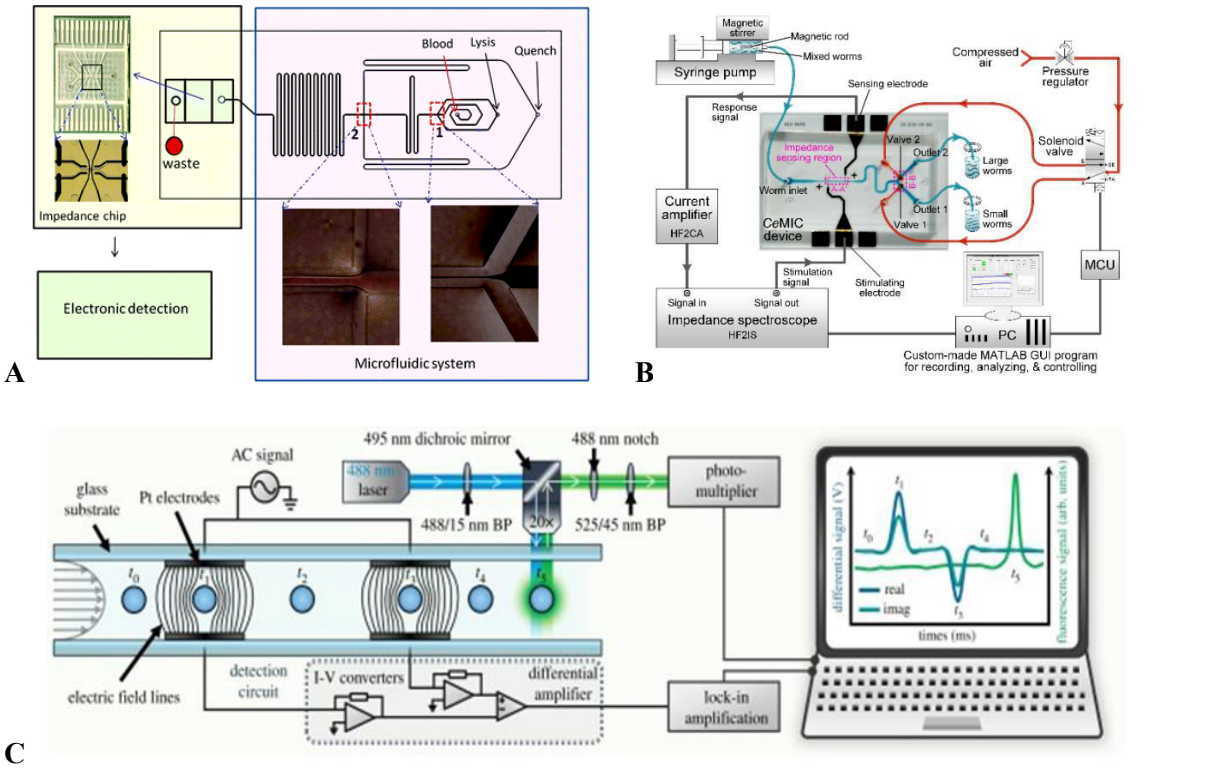

Figure 2.4 *The representation of electrical impedance measurement. A-C shows how single cells can be conditioned to move through an electric field for the detection of impedance when related to baseline measurements. Images A (Characterization of Plasmodium falciparum-infected red blood cells, B (Lysis of Human Blood for Leukocyte Analysis), and C (tracking of C. elegans worms) are reproduced with permission from the following sources [93, 139, 140].*

As the suspended bioparticles experience the influence of electric field that is set up between the two electrodes, the resistive effect of the cell on the field is measured in the form of a response current. This response current can be analyzed using Fourier series, for e.g., if the voltage applied is classified as sinusoidal potential excitation. The applied voltage is usually low so that a pseudo-linear response current can be obtained at the same frequency but at a phase different from the excitation

potential. By dividing the applied voltage by the response current, the electrical impedance is calculated. Thereafter, the frequency of the field is changed and the whole experiment is repeated to obtain another impedance value thus generating an impedance spectrum at varying frequencies. On the other hand, the cells can be immobilized, and the measurement could be made relative to the electrodes at several signal frequencies [66, 141]. This method of impedance measurement is called electrical cell-substrate impedance sensing (ECIS).

2.4.2 Electrorotation

Electrorotation (ROT), an important cell characterization technique utilizes the imaginary part of the Clausius-Mossotti (CM) factor, where the dipole and the field are out of phase [127]. CM factor relates the permittivity and conductivity of the medium to that of the bioparticle. It is given by:

$$CM = \frac{\varepsilon_p^* - \varepsilon_m^*}{\varepsilon_p^* + 2\varepsilon_m^*} \quad \text{where} \quad \varepsilon_k^* = \varepsilon_k - \frac{i\sigma_k}{\omega}; k = p, m \tag{2.6}$$

where the symbol * represents complex entity with σ as the conductivity, ε; the permittivity, ω; the field frequency, and *p, m* as the bioparticle and the suspending medium respectively.

In classical electrorotation, three (3) or more electrodes are each charged with AC voltage and frequency at different phases to generate a rotating electric field, thus setting up an electrical torque (Figure 2.5) [142].

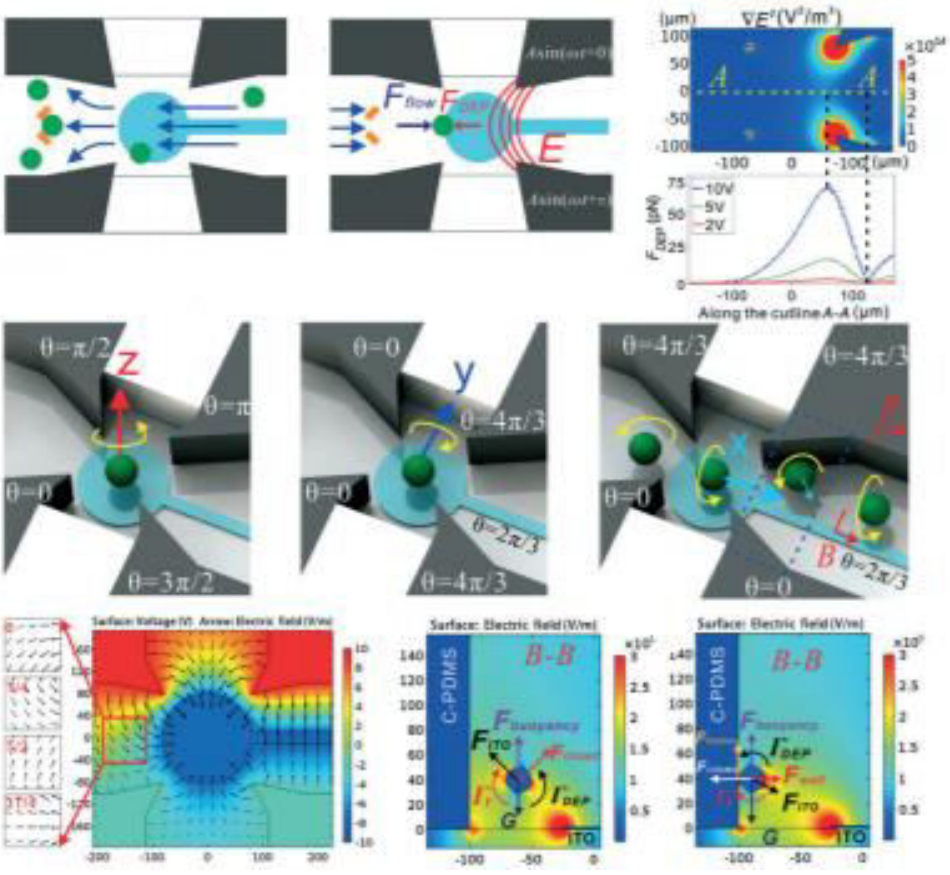

A

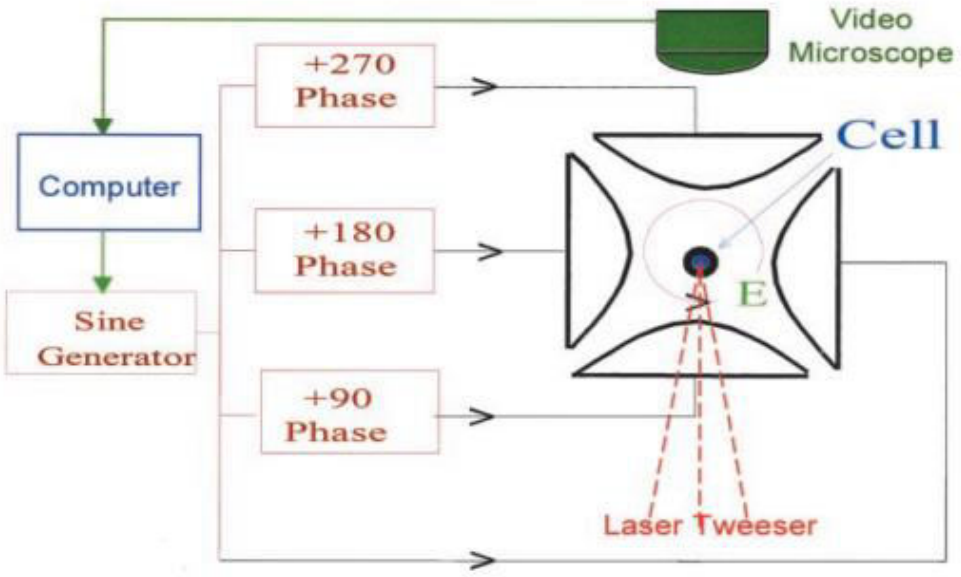

B

Figure 2.5 *The working principle of electrorotation. A bioparticle can rotate with the rotating field and their angular velocity can be related to the frequency of the electric field signals. Images reproduced with permission from [66, 143]. (A) In the first row, one single cell flowing with the solution streamline was trapped hydrodynamically, released by back flow as predicted by simulation. In the second row, cell displaying different rotation patterns in different locations along the channel. Third row shows the simulation results of the rotating electric field and its distribution. (B) The demonstration of the physics of electrorotation in a 4- electrode arrangement with 90^{o} phase difference.*

However, it is now possible to achieve electrorotation by using only two (2) electrodes [19]. When a (spherical) bioparticle is suspended within this rotating field, it becomes polarized inducing a dipole. This induced dipole within the bioparticle rotates with (or against) the electric field at certain velocity. The rotation of the bioparticle with (or against) the electrical field depends on the sign (positive or negative) of the imaginary part of the Clausius-Mossotti factor in equation 2.6 [144]. Further, the rotation of the particle depends on whether the charge relaxation time constant, τ (eqn. 2.3) for the bioparticle is greater than that of the suspending medium or vice versa [144]. Usually, the particle will rotate against (or with) the direction of field if the charge relaxation time constant for the particle is more (or less) than that of the medium and the angular velocity of rotation, ω will be constant if the particle is suspended in a liquid of known viscosity [144]. However, the multiphase nature of the driving force on the four electrodes causes the particle to lag the field by a factor that depends on the frequency of the rotating field. Since the particle velocity is determined by the torque in the rotating electric field, electrical properties of the particle can be extracted by measuring the dependence of the torque on the field frequency.

If the dipole caused by the rotating electric field is perfectly in phase with the field, no torque

is generated since the Clausius-Mossotti factor is valid only for the out of phase (imaginary part) mode [42]. When a torque is generated, it is usually dependent on the bioparticle size as well as the dielectric properties of both the particle and the suspending medium [66]. It is important to note that at higher frequencies, the obtained electrical properties from electrorotation and impedance cytometry are the alike as evident from many reports [145-153]. One of the main advantages of electrorotation is its versatility in obtaining the dielectric (interior and membrane) properties of a single. However, the possibility of cell lysis at high frequency and the fabrication of the device for submicron particles can be a challenge. [145, 146, 149, 152, 154-156].

2.4.3 Dielectrophoresis

Dielectrophoresis (DEP) experimentation for bioparticles started in 1939 [157] even though its theory has been in existence about the first world war period. DEP, an electrokinetic phenomenon involves the application of a force on neutral or charged particle by employing nonuniform electric field [53, 158-162]. The electric field signal can be direct current (DC) or alternating (AC) in nature [157]. For bioparticle characterization, DEP has been used always with AC signals so that the source frequency can be easily varied (if necessary) for dielectric dispersion measurements. The principle of dielectrophoresis as a characterization tool involves the fabrication of electrodes capable of generating non-uniform electric field due to their existence in space. Pure DEP operations for bioparticle characterization could be accomplished by different modes: crossover frequency measurement, collection spectrum, and capture voltage spectrum.

2.4.3.1 Crossover frequency measurement

When a charged or an uncharged spherical bioparticle is subjected to an AC field utilizing unequally dimensioned electrode-pair that is creating non-uniform electric field, (Figure 2.6A) the bioparticle becomes polarized just as the medium in which the bioparticle is suspended. The bioparticle could then move towards the region of high field (short electrode), low field (long electrode) or remain unperturbed by the electric field depending on the frequency of the applied AC voltage, properties of the suspending medium, and the bioparticle. The low and high field existing at the electrodes is because of the electrode arrangement. When the bioparticle moves toward the high field region, the phenomenon is termed positive dielectrophoresis (pDEP) while it is called negative dielectrophoresis (nDEP) if the particle's translational motion is toward the low field region. Usually, when a bioparticle is experiencing nDEP, for instance, it does so over a range of frequency. As the frequency changes further, the particle can translate to the pDEP regime. Before this happens, there occurs a specific inflection point wherein the bioparticle comes to a freeze before changing the regime i.e. nDEP to pDEP. The frequency at that point of inflection is termed as first crossover frequency. The continuous increase in the second cross over frequency.

During laboratory experiments, the crossover frequency is usually detected when, after the application of the AC voltage and frequency, the bioparticle is seen vibrating at a spot without any appreciable translational motion. At this point, the particle experiences no DEP force (F_{DEP}=0).

$$F_{DEP} = 2\pi r^3 \varepsilon_0 \varepsilon_m Re[CM] \nabla E^2 = 0 \quad (2.7)$$

where F_{DEP} is the dielectrophoretic force; r the particle radius; ε_0 the permittivity of the vacuum; ε_m the permittivity of the suspending medium; E the electric field; ε_p^* and ε_m^* are the complex permittivity of the bioparticle and the suspending medium respectively; and CM is the Clausius-Mossotti factor as defined in Equation 2.6. Benguigui *et al.* in 1982 [163] leveraged the work of Molibari and Viviani [164] to show that the first crossover frequency, f_{co1} can be obtained mathematically. Their work was further explored in 1996 by Huang *et al.* [165] leading to an approximation shown below:

$$f_{co1} = \frac{1}{2\pi}\sqrt{\frac{2\sigma_m^2 - A\sigma_{mem}\sigma_m - A^2\sigma_{mem}^2}{A^2\varepsilon_{mem}^2 - A\varepsilon_{mem}\varepsilon_m - 2\varepsilon_m^2}} \quad (2.8)$$

where $A = \frac{cell\ radius}{membrane\ thickness} = \frac{\varepsilon_p}{\varepsilon_{mem}}$ with σ_{mem}, σ_m, ε_{mem}, ε_m, and ε_p representing the conductivity and permittivity respectively with subscript *mem*, *m*, and *p* depicting membrane, suspending medium, and particle. Using a Maple-assisted computational method, Broche *et al.* [166] obtained the second crossover frequency, f_{co2} (using up to 20:1, size-thickness ratio approximation) at higher frequencies given as:

$$f_{co2} = \frac{1}{2\pi}\sqrt{\frac{\sigma_{cyto}^2 - \sigma_{cyto}\sigma_m - 2\sigma_m^2}{2\varepsilon_m^2 - \varepsilon_{cyto}\varepsilon_m - \varepsilon_{cyto}^2}} \quad (2.9)$$

where the subscript *cyto*, refers to the cytoplasm along with other subscripts and symbols remaining the same. The equations (eqns. 2.8 and 2.9) above represent a simplified presentation of the first and second crossover frequencies of a particle in relation to the permittivity and conductivity (electrical properties) of both the particle (membrane and cytoplasm) and its suspending medium. To extract the electrical properties of the particle, it is common to obtain a data set comprising of varied medium conductivity and hence, varied first crossover frequency.

The conductivity-frequency data is then fitted with the appropriate shell model i.e. single or multiple [157, 168] representing the bioparticle of interest. Crossover frequency has the advantage over other techniques since only one frequency point is desired for each bioparticle unlike electrorotation (ROT) that requires several frequency points [50]. As a result, crossover frequency measurement is faster than electrorotation measurements. Additionally, this technique causes the cytoplasmic ion loss less of a problem unlike ROT measurement. However, crossover frequency method is only good for

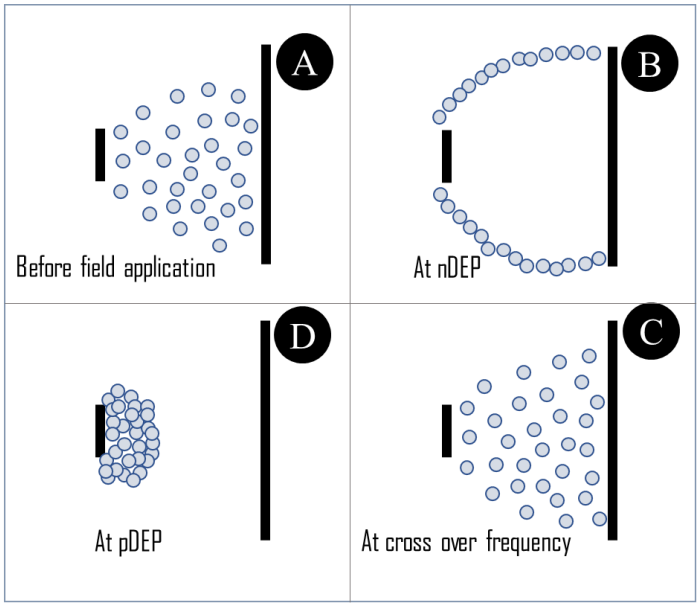

Figure 2.6 *Images of the particle behavior under different field frequencies. (A) particles well dispersed before field application (B) particles undergoing nDEP forming chains with increased particle-particle interaction. (C) particles at cross-over frequency; no response to the dielectrophoretic force. (D) particles clinging to the high field region depicting pDEP. Reproduced with permission from [167].*

average cell population. It does not have the capacity to cater towards single cell dielectric properties [50]. In this dissertation, the focus is on characterizing bioparticle population rather than single bioparticle, hence the choice of crossover frequency measurement.

2.4.3.2 Dielectrophoretic Capture-Voltage Spectrum

In 2011, Wu *et al.* [169] introduced a new method to obtain electrical properties called the capture-voltage spectrum. DEP capture-voltage technique is a direct opposite of the cross-over frequency method. Here, a low conducting medium is used to suspend the bioparticle for enhancing pDEP force experienced by them. When a suspension of bioparticles is transferred into the microfluidic channel, the frequency of the AC signal is fixed while the voltage is slowly adjusted until a point is reached where the cells are seen trapped at the electrode (pDEP); unlike crossover frequency method that usually involves fixing the AC voltage while changing the frequency. This specific AC voltage at which pDEP is observed is referred to as the capture-voltage and it is at this point that the DEP force is said to be balanced out by the Stokes drag force. At varying medium conductivities and AC frequencies, a spectrum of capture-voltage is generated. Using the capture-voltage relation (equation 2.10 below), the capture-voltage spectrum data can be fitted to obtain the dielectric properties of interest.

$$Re[K^*(\omega)] = \frac{6c\mu\pi u_f}{\left(\frac{\varepsilon_o \varepsilon_m r^2 \partial |E|^2_{V_o=1}}{\partial x} V^2\right)} \tag{2.10}$$

where V is the amplitude of the AC signal, u_f; the local flow velocity in the microchannel, c; the correction factor to account for near-wall effects, and all parameters have been previously defined in

section 4.3.1. The main advantage of this method is that both interior and membrane bioparticle properties can be found simultaneously unlike crossover frequency method that requires generating second crossover spectra to obtain cells' interior properties.

2.4.3.3 Dielectrophoretic collection spectra

Another DEP-based technique that is used to obtain the dielectric properties is the collection spectra [170, 171]. This method tracks and records the rate at which cells accumulate while experiencing positive and negative dielectrophoresis. Here, interdigitated electrode configuration is used to aid the simultaneous discrimination of pDEP and nDEP during cell collection. The collection rate and frequency data is then plotted and fitted with shell model to extract the dielectric properties.

2.5 Obtaining electrical properties of bioparticles experimentally

Dielectrophoretic force is known to depend on the particle size, particle's electrical properties (permittivity or conductivity), suspending medium properties as well as the gradient of the applied electric field as shown in eqns. 2.6 and 2.7. This subsection explores the experimental technique followed to obtain the electric properties of bioparticles. It details how independent factors are carefully chosen to ensure reliable bioparticle electrical property estimation.

2.5.1 Suspending medium selection (and how to vary its conductivity)

When bioparticles are suspended within a nonuniform electric field, one of the independent factors that determine their translational motion is the Clausius-Mossotti factor (CM). This factor, as shown in eqn. 2.7, depends on both the bioparticles and suspending medium properties. It is therefore important to cautiously select and characterize this medium for the desired dielectrophoretic experimentation. Depending on the concentration of the solute, a medium can be classified as hypotonic, isotonic, or hypertonic. Hypotonic medium has lesser solute (more water) concentration than the solute concentration inside the bioparticle. Therefore, water, which is highly permeable through the bioparticle membrane moves into it and causes the bioparticle (e.g. any cell) to swell and thus increase in size. In an isotonic solution, the solute (water) concentration is the same as that of the cell interior. Hence, there is no net movement of water. Therefore, cell size remains the same. Hypertonic solution, on the other hand, causes cells to reduce in size owing to net water movement out of the cell. In the dielectrophoretic characterization experiments, isotonic solutions are usually employed.

Most commonly used suspending medium are normal saline (0.9% NaCl) and 5% dextrose. Many researchers have reported using various other isotonic medium: 280 mM mannitol [172], sucrose (8.5% sucrose + 0.3% glucose) [48], sterile deionized water [171], etc. to achieve DEP experiments. It is not uncommon to use dextrose since it is a covalent compound and cannot conduct electric current. However, when it is dissolved in deionized water, the -OH groups in dextrose are attracted to the water

molecules via dipole-dipole force. The hydrogen bonding between the water molecules and glucose also makes the glucose more soluble in water. Since suspending medium solutions in particle characterization is not highly concentrated (to prevent electrolysis), it is normal to use molality (moles of solute per kg of solvent) as the unit for solute concentration [80]. Furthermore, it is necessary, in some experiments, to modify the conductivity of the medium to obtain a relation with field frequency. So, the chemicals utilized for modifying medium conductivity should be bioparticle friendly and not generate any osmotic gradient. EDTA, KCl, PBS (Phosphate buffer saline), Dextrose, NaCl, Inositol, HEPES and dextrose have been reported as good modifiers. For instance, Gascoyne *et al.* [89] reported that when Hemisodium EDTA was used to adjust the conductivity of the cell suspension, it helped to maximize the derived dielectric properties and prevent cell adhesion to the surface of the characterization chamber. In addition, Inositol was reported as being very useful to reduce the conductivity of the suspension and still maintain osmolarity [126].

2.5.2 Electrode configuration for bioparticle characterization

Electrodes are an important part of the cell characterization process because they establish the electric field when functionalized with electric signals. Their spacing, shapes, and electric potential affect the distribution of the electric field within the cell characterization device platform. Over the years, several electrode configurations have been reported [77, 113, 144]: polynomial, interdigitated, strip, U and T, needle, and many more. Electrode design is basically dictated by the desired output of any research.

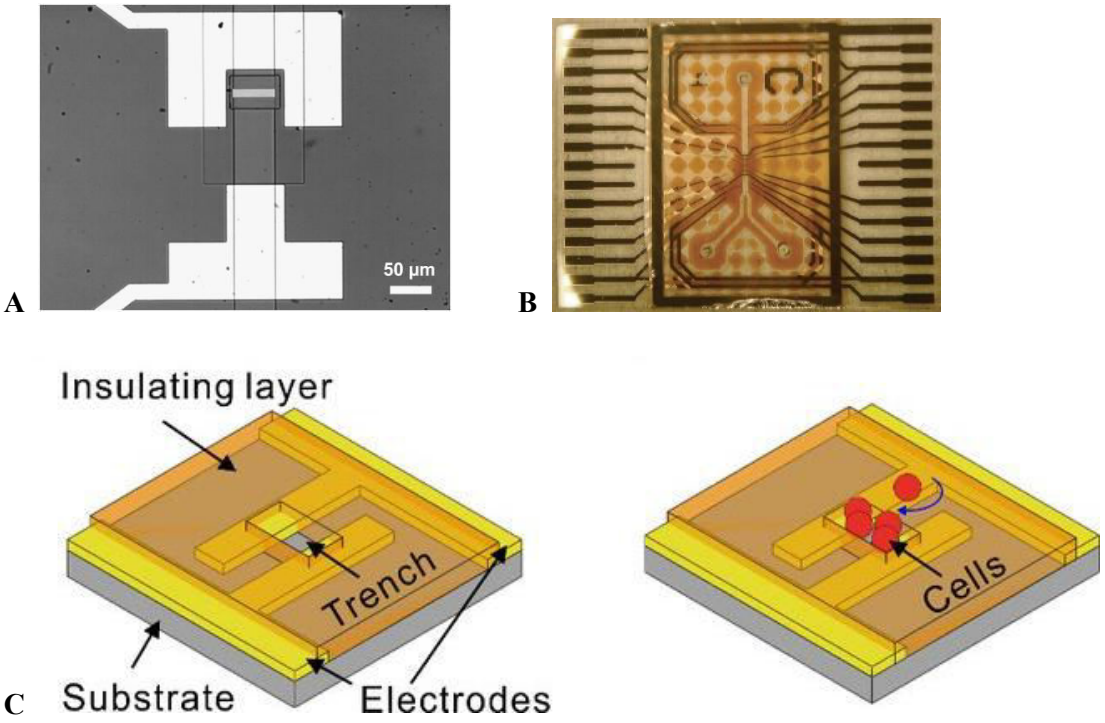

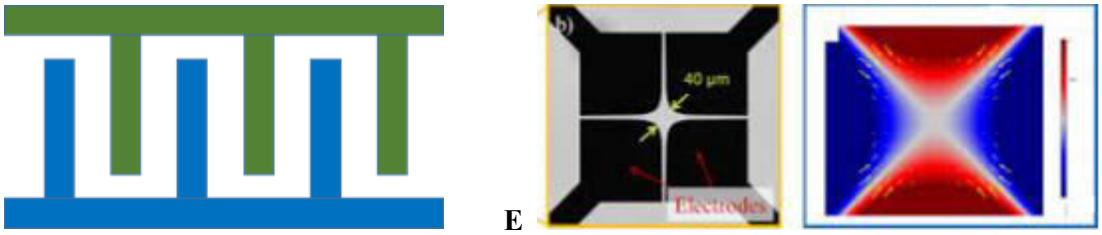

Figure 2.7 *Electrode configuration are characteristically important in the generation of field non-uniformities for dielectrophoretic applications. (A) A U-and-T configuration of electrode used for characterizing Escherichia coli [173]. (B) An on-chip label-free characterization electrode arrangement for cell differentiation [110]. (C) An electrode arrangement that utilized cells as electrode [19]. (D) A simplified representation of interdigitated electrodes. The electrode pair is charged with signals using each of the two structures in the figure. A typical polynomial electrode arrangement for electrorotation [174]. All figures are reproduced with permission.*

For example, Gascoyne *et al.* [170] utilized interdigitated electrode (Figure 2.7) because of the ease of observing both nDEP and pDEP simultaneously while Sanchis *et al.* [171] constructed a microelectrode chamber for the ease of enhancing cell collection. Figure 2.7 shows various electrode formats that have been reported for electrorotation, impedance cytometry, and dielectrophoresis. Apart from using solid materials as an electrode, bioparticles themselves can also be used as an electrode. This concept is called cell-electrode. In 2019, Huang *et al.* utilized this concept to aid the electrorotation of HeLa and HepaRG (hepatic stem cell line) cells; however the electric properties of the cells were not extractable [19].

2.5.3 Data collection methods

The types of data collected from cell characterization experiments depend on the nature and form of the experiments. In dielectrophoretic experiments, it is not uncommon to subject bioparticles to discriminatory field effects that would reveal their first and second crossover frequencies. For these data to be useful in curve fitting procedure, they must be collected at different medium conductivities. These medium conductivities are varied utilizing bioparticle-friendly medium solutions. Other dielectrophoretic characterization techniques focus on the number of cells trapped at high field regions at different AC frequency conditions. Additionally, the velocity at which these bioparticles are collected can also be the desired data for cellular characterization. In general, for DEP dielectric characterization experiments, the following methods could be considered for data collection purposes: number of trapped cells at the high field (HF) region, number of streamed cells from the high field region i.e. towards the low field (LF) region, rate of cell trapping, voltage of cell trapping, cross-over frequency, and levitation [175]. It should be noted that if the desired goal is to trap cells to obtain dielectric properties, then, the conductivity of the suspending medium should be as low as possible. In electrorotation experiments, the focus is on measuring the angular velocity at which the bioparticle rotates at varying AC frequencies. For impedance characterizations, the only data required is the signal (measured current) imparted by the cell when it passes through the region of interest. As discussed in

sec. 4.1, it is important that the applied voltage for impedance characterization be very small to obtain meaningful cell response.

2.5.4 Models for biological cells

When bioparticles are under the influence of an external electric field, their movement can be interpreted by applying diverse analytical models [176-187]. Depending on the morphology of the bioparticles i.e. sphere, ellipse, cylinder, or rod with single or multiple shells, the models could be fine-tuned to extract the electrical properties [184, 185]. To overcome, computational limitations several researchers have resorted towards simplifying these models to obtain fairly accurate characterization properties. For example, *Escherichia coli* is a rod-shaped gram-negative bacterium that is usually modeled as a spherical or ellipsoidal bioparticle [184, 185]. Besides, numerical computation tools such as COMSOL Multiphysics software are not currently equipped with functionalities for handling biological models of diverse shapes. Besides, deriving an analytical model representation for different shapes of bioparticles is currently a herculean task. Until a foreseeable future, spherical shell models will dominate the domain of bioparticle characterization. Details of each shell model has been reported elsewhere [157, 168].

2.5.5 Data analysis and dielectric property extraction

With adequate understanding of different data collection techniques and shell modeling, it is literally less cumbersome to obtain the much-needed electrical properties of bioparticles. In this section, a step-by-step procedure to obtain the electrical properties are presented. Once, the required data is obtained from DEP experiments, there are several ways by which they could be analyzed. While there are many commercial software packages that could be utilized to obtain these properties, the example here will involve the use of a readily available versatile software package, Microsoft Excel. Suppose a set of crossover frequency *vs.* suspending medium conductivity data is collected from the DEP experiments and the specific membrane capacitance (C_{mem}) and conductance (G_{mem}) are required to be estimated from an ellipsoidal single shell model using Excel, the following procedure could, amongst other procedures, be used;

1. Transfer or export data to Excel. Repetitions of the crossover frequency measurement for each suspending medium conductivity is averaged such that only two columns are obtained for curve fitting. The crossover frequency column can be renamed as “measured” while the other column serves as the conductivity of the medium
2. Guess the initial values of C_{mem} and G_{mem} and on a third column (named as predicted), type-in the single-shell model on the same first row as the experimental data. Copy the model to the other rows using any convenient method. By this time, there should be three columns: medium conductivity, measured, and predicted. Two errors may show-up: (1) *#Name?* if you fail to

define the initial guesses for C_{mem} and G_{mem}; (2) *#Num!* if the number is too large. Therefore, a simple number such as (1, 1) may be a good place to start.

3. Plot these values to visualize the comparison of the data with the model. Further, construct a fourth column to compute the square error i.e. $(\text{measured} - \text{predicted})^2$ and finally sum them up to obtain the sum of squares error (SSE).
4. Using the Excel solver (go to *add ins* to add the solver box if solver not found) and selected SSE as the function, select the C_{mem} and G_{mem} units as the changing variable. A constraint can be set for this optimization problem if required. Run the set up to obtain the values of G_{mem} and C_{mem} that gave the minimum SSE. Once the minimum SSE is reached, the plots of the measured and predicted should be substantially aligned provided the model is good. Other plots such as residual by predicted, R^2, Q-Q plot, etc. can also be made to verify the reliability of curve fitting process and the dielectric parameters obtained. Sensitivity analysis can also be conducted prior to optimization to determine the parameters affecting the model significantly.

It is also more common to use Levenberg-Marquardt [82] or least-square optimization algorithm [188] in MATLAB to achieve similar results as described for Microsoft Excel above. Once the electrical properties are obtained through any computational tool i.e. Microsoft Excel, MATLAB, etc., they are fed back into the theoretical equations to obtain plots that are easily interpretable with respect to the behavior of the bioparticles at diverse electrical signal conditions.

2.6 Electrical characterization of bioparticles / cells

This section captures relevant publications on diverse methods of characterizing bioparticles, in particular, cells. Details involving electrode configuration, charging at diverse voltages and frequencies to achieve target goals has been presented. In some cases, there was a need to modify the nature of the electrode or the properties of the suspending medium.

2.6.1 Impedance spectroscopy method

In 1873, Maxwell published a book titled "A treatise on electricity and magnetism" (Vol 1) [189] to lay the foundation of the mixture theory (eqn. 2.11), which later became very useful in describing the dielectric behavior of bioparticles suspended in a medium without any consideration for the interaction between the induced dipoles (because the suspension of particles is very dilute) [190].

$$\tilde{\varepsilon}_{mix} = \tilde{\varepsilon}_m \frac{1+2f\widetilde{K}(\omega)}{1-2f\widetilde{K}(\omega)} \tag{2.11}$$

where, $\tilde{\boldsymbol{\varepsilon}}$ is the complex permittivity, $\boldsymbol{f}$ the volume fraction, $\widetilde{\boldsymbol{K}}(\boldsymbol{\omega})$ the complex Clausius-Mossotti factor given by:

$$\widetilde{K}(\omega) = \frac{\tilde{\varepsilon}_p - \tilde{\varepsilon}_m}{\tilde{\varepsilon}_p - 2\tilde{\varepsilon}_m} \tag{2.12}$$

$$\tilde{\varepsilon} = \varepsilon - i\frac{\sigma}{\omega} \tag{2.13}$$

$$i^2 = -1;$$

$$\tilde{\varepsilon}_p = \tilde{\varepsilon}_{mem} \frac{\gamma^3 + 2\left(\frac{\tilde{\varepsilon}_{cyto} - \tilde{\varepsilon}_{mem}}{\tilde{\varepsilon}_{cyto} + 2\tilde{\varepsilon}_{mem}}\right)}{\gamma^3 - 2\left(\frac{\tilde{\varepsilon}_{cyto} - \tilde{\varepsilon}_{mem}}{\tilde{\varepsilon}_{cyto} + 2\tilde{\varepsilon}_{mem}}\right)} \tag{2.14}$$

$$\gamma = \frac{R+d}{R} \tag{2.15}$$

where d is the membrane thickness, R the cell radius, and subscripts p, m, mem, and cyto are particle, medium, membrane, and cytoplasm respectively. The impedance of a mixture of cells, eqn. 2.16, can be obtained if $\tilde{\varepsilon}_{mix}$ in eqn. 2.11 is known. However, this can be simplified using the equivalent circuit model developed by Foster and Schwan [190] (interested readers can consult this reference for further studies).

$$\tilde{Z}_{mix} = \frac{1}{i\omega\tilde{\varepsilon}_{mix}G_f} \tag{2.16}$$

where $\tilde{\boldsymbol{Z}}$ is the complex impedance, and G_f the electrode characteristic. Eqn. 2.16 and its modified versions have been used to reveal the characteristics of several bioparticles [93, 119-122, 191, 192]. Some of the relevant publications on cell characterization using impedance method has been discussed below.

Early 2019, Zhang *et al.* [9] adopted a crossing constriction channel to characterize paired salivary adenoid cystic carcinoma cells (SACC-83) and lung metastasis cells (SACC-LM). Here the cells were forced through a major constriction channel (Figure 2.8A) to seal the side constriction, blocking the electric field lines within the region, hence varying the impedance digital signal on the impedance analyzer [9].

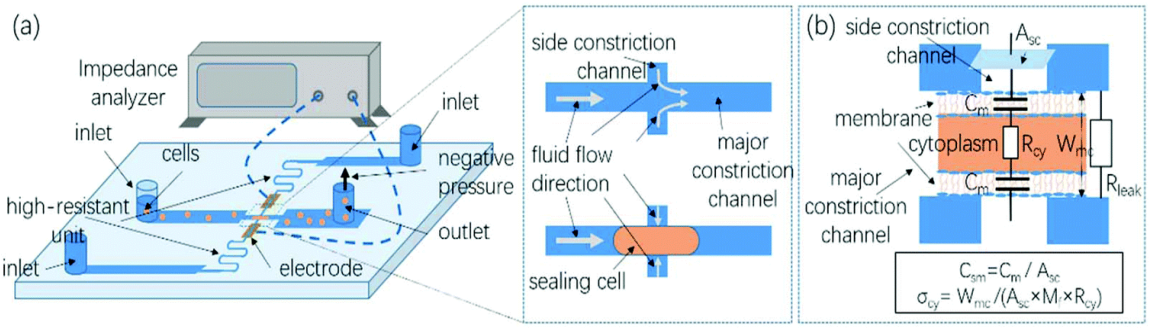

Figure 2.8 *Device designed and fabricated by Yi Zhang et al. for the characterization of paired salivary adenoid cystic carcinoma cell (SACC-83) and lung metastasis cells (SACC-LM). Reproducibility permission granted by [9].*

These digital signals from the impedance analyzer were translated into electrical properties of the cells through equivalent circuit model. This marker-free technique was able to differentiate the two carcinomas SACC-83 and SACC-LM in terms of their specific membrane capacitance (3.16 ± 0.90 *vs.* 2.79 ± 0.67 μF/cm^2) and cytoplasmic conductivity (0.36 ± 0.06 *vs.* 0.41 ± 0.08 S/m) [9]. Zhao *et al.* [193] utilized the crossing constriction channel to study the lung cancer cell line (H1299), human

cervical cancer cell line (Hela), and adenocarninomic human alveolar basal epithelial cells (A549). A droplet of cell suspension (3–5×10^6 cells/ml) was fed into the characterization channel and impedance profile of the traveling cells was captured when the channel was functionalized with frequencies 100 kHz and 250 kHz. Further, neural network-based pattern recognition was utilized to classify H1299 and A549 cells based on the scatter plots generated by MATLAB. The specific capacitance for H1299 and HeLa cells were 1.32 ± 0.58 μF/cm^2 and 2.33 ± 0.60 μF/cm^2 respectively while their cytoplasmic conductivities were 0.27 ± 0.08 S/m and 0.19 ± 0.05 S/m respectively. Native A459 cells had specific capacitance and cytoplasmic conductivity values of 1.86 ± 0.45 μF/cm^2 and 0.22 ± 0.06 S/m respectively. In 2014, Spencer *et al.* [84] utilized microfluidic impedance cytometry to characterize breast cancer tumor MCF7 cells both individually and mixed with leukocytes. The results revealed that MCF7 cells have a large membrane capacitance and size than the leukocytes [84].

Acquired Immune Deficiency Syndrome (AIDS) is a deadly disease that has killed millions of people since it was first reported in 1981. The disease is caused by the Human Immunodeficiency Virus (HIV), which weakens the CD4+ T-Lymphocyte cells. For monitoring the progression of this disease, an absolute CD4+ T-lymphocyte count is the most widely used method [194]. Holmes *et al.* used two sinusoidal voltages, 503 kHz and 10 MHz, and a low frequency in-phase impedance signal to trigger data acquisition when the cells passed between the electrodes. With sample flow rate held constant at 5 μL/min, CD4+ T-Lymphocytes were distinguished from their mixture of other blood components, even though the signal range for operating the device was limited. Holmes *et al.* used this technique to prove that CD4+ T- Lymphocytes can be identified in a low-resource setting. Although the spectrum revealed the characteristics of the cells, it also aided in quantification of the cells.

By measuring the resistive and reactive impedance of human peripheral blood granulocytes, Fuller *et al.* [195] developed a multi-frequency characterization platform to quantify membrane capacitance and cytoplasmic conductivity. This device platform yielded 0.9 μF/cm^2 membrane capacitance and 0.66 S/m cytoplasmic conductivity that accommodated a range of medium conductivities 50 - 250 mS/m to maximize the operational bandwidth [195].

Another application of impedance cytometry is in the characterization of bioparticle reported by Cheung *et al.* [110]. In the research, three (3) bioparticle models were used: native red blood cells (RBCs), hypotonically ruptured RBCs, and glutaraldehyde-based RBC. A micro-chip fabricated through lift-off, sputtering, and electrochemical etching was operated at two AC frequency ranges: a reference frequency (which was kept low and constant at 602 kHz) and a variable frequency, which was varied between 350 kHz and 20 MHz. These low and high frequencies were compared as a ratio to produce the opacity value that helped differentiate the cells moving at 10 mm/s and at a rate of 1,000/min during which the impedance spectrum for the entire population were obtained.

Dielectric characterization of *Plasmodium falciparum*-infected red blood cells has also been reported [93]. This work by Honrado *et al.* monitored changes in the dielectric properties of the RBCs as they were being infected by *P. falciparum* for up to 42 h. The results showed increased membrane and cytoplasmic conductivity/permittivity as infection progressed [93].

Discriminating wild-type yeast cells from that of a mutant, which differs in size and distribution of vacuoles is another application of impedance cytometry. Haandbaek *et al.* [196] fabricated a novel microfluidic impedance cytometer that differentiated the two cell populations based on their intrinsic dielectric properties at frequencies up to 200 MHz. The differences were measured in terms of the opacity indicated by the impedance differences. Haandbaek *et al.* further explored the dielectric properties of these cell populations at higher frequencies, up to 500 MHz and Table 2.1 demonstrates the properties obtained for the yeast cells (wild-type and mutant) with a medium conductivity of 1.34 S/m [196].

Table 2.1 *Dielectric properties of the wild type and mutant yeast strains suspended in PBS of conductivity 1.34 S/m and extracted through nonlinear least squares curve-fitting algorithm. Data reproduced with permission from [196].*

Strain	Cell wall		Cell membrane	Cytosol		Vacuole membrane	Vacuole
	σ (S/m)	ε_r	ε_r	σ (S/m)	ε_r	ε_r	σ (S/m)
Wild-type	0.20	64–72	8.6–9.5	1.1–1.2	53–74	4.4–6.2	0.87–1.3
vac8Δ::KanMX	0.11	62–63	8.0	0.84	57–58	N/A	N/A

Using lithography-fabricated integrated microneedles, Mansor *et al.* [197] experimented on 4-7 μm sized, $10^2 – 10^9$ cfu/ml *Saccaromyces cerevisiae* suspended at 1:10 dilution ratio in DI water of conductivity 6 mS/m flowing at a fixed rate of 6 μL/min. Impedance was found to decrease with increase in cell concentration. Mansor *et al.* claimed that the device could help detect water contamination based on the results obtained. It is cost effective and the microneedles were reusable.

2.6.2 Electrorotation (rot)

Rotation effects set up by an electric field can be traced to a physics report in 1877 when mechanically generated rotating electric field was explored in solar radiometer [198]. Since then, several developmental steps have been taken to maximize the utilization of rotating effects of electric fields: from the physical application of Steinmetz's quasi-rotating fields in 1892, theory of rotation of permanent dipole by Born in 1920 to biological utilization of rotating fields as reported by Sauer (1983), Pohl (1983), and Zimmermann (1987). In the past decade, several research reports have been published on electrorotation. Few of those research results are discussed here.

More recently, electrorotation was utilized by Huang *et al.* [156] to characterize Friend murine erythroleukemia (MEL) DS19 cells in its natural and differentiated (with hexamethylene bis(acetamide), HMBA) forms. In both cases, electrorotation spectra was obtained using a well characterized dextrose/sucrose medium. Cell suspension at a dilution ratio of 1:22 was fed into the electrorotation chamber, at a fixed RMS (root mean square) AC voltage of 0.9 V_{rms} with varying frequencies ranging from 10 kHz to 100 MHz. The electrorotation spectra obtained was utilized to derive the dielectric properties of the cells through an optimization procedure in conjunction with the single-shell model. Membrane capacitance was sacrificed and a scaling factor was calculated that accounted for the viscous drag of the suspending medium as well as the applied field strength [156]. Results showed that with increasing suspension osmolality, the average interior conductivity increased while permittivity decreased. Having realized that the average permittivity of cell interior was larger than that of the medium (pure water at 20^{o}C) at all conditions, it was suggested that other cytoplasmic polarization mechanisms might be present.

Another research involved cell characterization by electrorotation utilizing healthy and infected RBCs by Gascoyne *et al.* [50]. The cells characterized were twenty (20) healthy blood group 'O' human RBCs and 20 *P. falciparum*-parasitized RBCs that were timed at five (5) points ranging from 1 kHz-100 MHz i.e. 1 kHz-10 kHz, 10 kHz-100 kHz, 100 kHz-1 MHz, 1 MHz-10 MHz, and 10 MHz-100 MHz. The characterization of the RBCs was conducted using base supports comprising of four polynomial electrodes charged with sinusoidal signals in a four-phase quadrature (0^{o}, 90^{o}, 180^{o}, 270^{o}) that generated the rotating electric field. The analysis of the ROT data for normal RBCs provided the membrane specific capacitance value of 12±1.2 mF/m^2, 0.52±0.05 S/m^2 for the cytoplasmic conductivity, and 57±5.4 for the internal relative permittivity. Gascoyne *et al.* observed some instabilities in the ROT measurements for infected RBCs that prevented their characterization [50].

Huang *et al.* also worked on electrorotation by using 3D cell electrorotation to find cellular biophysical properties, specifically C_{mem} and σ_{cyto}. 3D electrodes were fabricated using carbon-PDMS obtained by adding blended carbon black particle at 1:3 to the regular silicon-curing agent mixture. This approach was utilized because it was time-consuming and relatively costly to employ the common 3D electrode-building methods such as micromachining, ion implantation, electroplating, or pyrolysis. Operating this carbon-PDMS electrode, trapping of a single cell was achieved from where an in-plane electrorotation spectrum was obtained. C_{mem} and σ_{cyto} was obtained when the experimental data was fitted with a single-shell model for spherical particle. Even though this novel device yielded the electric properties of Hela, C3H10, B Lymphocytes and HepaRG cells, it required that these cells be spherical. This implies that this novel technique cannot be utilized to characterize non-spherical prokaryotes. Besides, the technique employed several AC frequencies to the cells to generate its in-plane rotation.

This prolonged exposure of cells to the electric field questions the viability of cells, to which the authors mentioned time of 5-10 min [66].

Apart from using the 3D construct, Huang *et al.* delved into turning a cell into an electrode: a concept that is popularly known as cell-electrode [19]. In this work, an electrorotation device was fabricated using only two (2) planar electrodes unlike the common quadrupoles (Figure 2.7 C). The device was made from ITO (Indium tin oxide), because of its optical transparency, and gold, due to its higher conductivity. When a high-density cell suspension was equilibrated in the device and the signal was switched on, a portion of the cell mixture was trapped by pDEP while the other cells were swept away by the flowing fluid medium. Thereafter, a lower-density cell suspension was fed into the chamber where the trapped polarized cells acted as an electrode, since its capacitance causes a phase delay in the transmitted signal. On changing the amplitude of the AC signal, the cells trapped onto the insulating layer (near the cell-electrode) were seen rotating (Figure 2.7C). This group of researchers neither generated nor analyzed any ROT spectrum, however they did emphasize that the utilization of polarized cells as electrode source could reduce design and handling difficulty associated with electrorotation devices [19].

Human leukocyte subpopulations (T and B lymphocytes, granulocytes, and monocytes), metastatic human breast cancer cell line (SkBr3), and lung cancer (A549) cell line, suspended in 32.6 mS/m medium, characterized using ROT-microchip, operating with 90^{o} phase difference and superimposed on negative dielectrophoretic (nDEP) signals was another application of electrorotation to bioparticles [126]. Using varying peak voltages (0-5 V_{pp}) at 20 kHz nDEP signal that is superimposed on 100 kHz, 0.4 V_{pp} ROT signal, the influence of nDEP on ROT was measured. The leukocytes were trapped at 2 V_{pp} while the metastatic human cancer cell lines were trapped at 1.5 V_{pp}. This ensured that the integrity of the cells was retained. Through a ROT frequency range of 10 kHz to 10 MHz, the trapping region for each of the subpopulations was found. By using a single-shell dielectric model, the properties (C_{mem} and σ_{cyto}) for the six (6) types of cells were obtained.

2.6.3 Dielectrophoresis

Dielectrophoresis is the most common method for bioparticle characterization. This is not only because of the quick response of cells to the field effects, other factors such as its versatility play a major role. Bioparticles that were characterized using DEP was healthy and *P. falciparum*-parasitized RBCs [50]. Here, Gascoyne *et al.* obtained human blood cells (group 'O') as well as type A, B, O, and AB serum from healthy donors and cultured chloroquine-resistant strain T9/94 of *Plasmodium falciparum* to obtain parasitized erythrocytes synchronized at the ring stage. With suspending medium conductivity varying between 1-75 mS/m (conductivity adjusted with KCl), DEP crossover frequency responses were obtained by charging the polynomial electrodes (at inter-electrode (pole tip to pole tip)

spaced 400 μm apart) at peak-to-peak voltage range of 3-8 V_{pp}. While assuming that the cell interior is much more conductive than the membrane and conducting the DEP crossover experiments with frequencies confined below the Maxwell-Wagner dispersion frequency, single-shell oblate spheroid dielectric model was used to fit the crossover frequency data through an optimization algorithm. Through this numerical computation, the specific conductance and capacitance of the healthy RBCs were obtained as 271 S/m^2 and 11.8 mF/m^2 respectively. Single-shell oblate spheroid dielectric model could not be used to fit the crossover frequency data for the parasitized RBCs because of the possible variation of the membrane specific capacitance, conductance, and cell shape with the conductivity of the suspending medium [50]. Modified model was then used to obtain specific membrane capacitance and specific membrane conductance i.e. 9±2 mF/m^2 and 1130 S/m^2 respectively for the parasitized RBCs.

DEP was also used to explore a shift in the second crossover frequency of an algae, *Chlamydomonas reinhardtii*, a single-cell green alga of 10 μm in diameter, when it was cultured in nitrogen-based and nitrogen-free media [199]. The authors, Michael *et al.* hypothesized that by the removal of ammonium nitrate from the agar slant used in the growth medium, the algae will be stressed and thereby have a retarded growth. The algae due to osmotic stress will further accumulate lipids (within the cytoplasm) causing a reduction in the cytoplasmic conductivity, thus causing a shift in the 2nd crossover frequencies to lower values. By suspending the cells in deionized water, adjusting the medium conductivity to 0.064 S/cm with potassium chloride and by maintaining the osmotic pressure of the suspension with 85 g/L glucose solution, the movement of the cells (within the needle-shaped gold-patterned glass slide) under pDEP and nDEP was observed under an AC amplitude of 30±3 V_{pp} with a frequency sweep of 20-110 MHz (Figure 2.9). Second crossover frequency for *C. reinhardtii* cells cultured in regular media was found to be 75±5 MHz while that of the cells cultured in nitrogen-free media was 40±5 MHz. The reduction in the second crossover frequency was attributed to the accumulated lipids which, due to their oily nature, reduced the effective permittivity of the cytoplasm [199]. Gascoyne *et al.* also used dielectrophoretic collection spectra to characterize the differences between normal and cancerous cells in a glass-supported periodic interdigitated gold electrode array [170].

By arranging the electrodes with a spacing of 80 μm, the highest field strengths of up to $6.8*10^4$ V_{rms}/m was obtained when a sinusoidal amplitude ($V_{rms)}$ of 3 with frequency ranging between 500 to 10^5 Hz was applied using a waveform generator. This high-field region serves as the dielectrophoretic collection zone for the cells. The whole setup was automated through which the spectra, AC voltage and frequency adjustment, sample changing, and image analyses were performed. Suspension of friend murine erythroleukemia (MEL) cells were fed into the automated platform. Therein, the collection rate

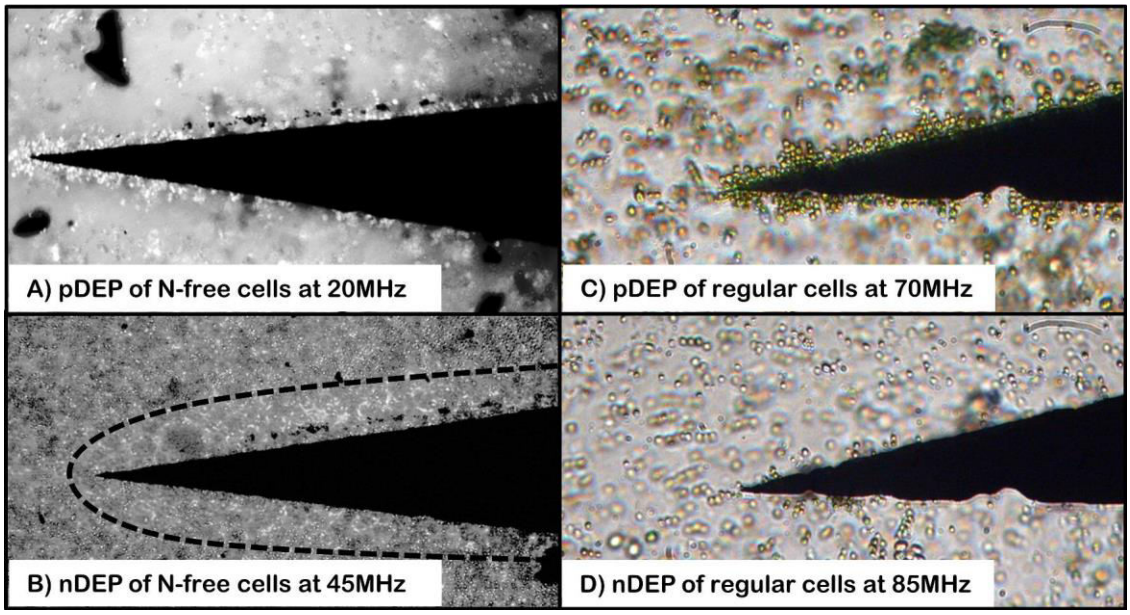

Figure 2.9 *Micrographs of pDEP and nDep. A) Microalgae cells grown in N-free media fluoresce when stained and undergo pDEP at 30 MHz. B) At 55 MHz, these cells have been pushed away from the electrodes indicating nDEP. The N-free cells are approximately the same size as the regular cells but appear smaller due to the bright fluorescence of the lipid rich regions of the cell. C) Microalgae cells grown in regular culture experience pDEP at 70 MHz. D) At 85 MHz these cells have been pushed away from the electrodes due to nDEP except for cells that have adhered to the electrode. The regular cells do not fluoresce when stained due to a lack of lipids. The micrographs have been converted to greyscale and uniformly adjusted for proper contrast. Reproduced with permission from Micheal et al[199]*

of the cells both at the low-field and high-field regions were obtained at suspending medium conductivities ranging from 1-4 mS/m. At the same medium conductivities (1-4 mS/m), the crossover frequencies of the cells were also noted. Friend MEL cells (DS19), herein referred to as HMBA-DS19 after being treated with hexamethylene bis(acetamide) (HMBA), was then suspended and used as described for pure DS19 above [170]. By assuming that both DS19 and HMBA-DS19 were single dielectric particles of inner sphere surrounded by thin, homogenous, spherical membrane, Gascoyne *et al.* used computer simulation to perform regression analysis on the experimental data while assuming cytoplasmic conductivity of 0.5 S/m and interior permittivity of $59\varepsilon_0$. This regression analysis yielded $5.4*10^{-7}$ S/m, 6.3 ε_0 F/m, 12.6 mF/m^2 for DS19 and < 10^{-7} S/m, $4.49\varepsilon_0$ F/m, 8.8 mF/m^2 for HMBA-DS19 cells σ_{mem} , ε_{mem}, and C_{mem} respectively [170].

Apart from the dielectrophoretic collection spectra, researchers have also leveraged the power of positive dielectrophoresis (pDEP) to obtain the capture-voltage spectrum [169]. Dielectrophoretic capture-voltage spectrum (DCS) is a method of obtaining the dielectric properties of bioparticles through the balancing of dielectrophoretic force and Stokes drag force acting on a cell in a microfluidic device equipped with fluid flow and field gradient functionalities. DCS has been applied for the characterization of human colon cancer cell lines (HT-29) by Wu *et al*. utilizing a microfluidic channel with embedded interdigitated ITO electrodes and high channel aspect ratio to render it safe for assuming

parabolic velocity profile. When the fluid flow rate and the frequency of the applied electric field are fixed, a critical voltage at which DEP force and Stokes drag force are balanced can be obtained. This critical voltage at different frequencies gives the information about the dielectric properties of the cells, which can be determined from the Clausius-Mossotti (CM) factor. Wu *et al*. cultured HT-29 cells and suspended them in 8.5% sucrose and 0.3% glucose medium with conductivities of 0.01 S/m, 0.05 S/m, and 0.1 S/m. The cell suspension was made such that the final concentration was ~10^6 cells/ml. With up to 20 Vpp amplitude applied through a sinusoidal function generator, HT-29 cells were trapped at the electrodes [169]. By changing the operating frequency from 5 kHz to 20 MHz, several capture-voltages were obtained at each medium conductivity. Curve-fitting the real part of the Clausius-Mossotti factor using nonlinear least square method gave the dielectric parameters of HT-29 cells [169].

Using a U- and T- electrode configuration (Figure 2.7A), Castellarnau *et al*. utilized dielectrophoresis as a characterization tool to identify changes that occur in four *Escherichia coli* (*E. coli*) isogenic strains with different mutant alleles [188]. It is noteworthy to mention that the results recognized mutant genotypes of the bacteria. The integrated U-and-T DEP electrode device (Figure 2.7A) was fabricated and operated such that the bacteria suspension in contact with the electrode did not experience any form of electrolysis (due to the use of alternating electric field and relatively high frequency). Using water, whose conductivity was progressively increased through NaCl, each of the mutants was suspended and subjected to non-uniform electric field when the U-and-T electrode was charged with AC signals (6-10 V_{pp}, 10 kHz-200 MHz). Within the range of suspension conductivity used (1-130 mS/m) at the stated frequency range, the first and second crossover frequencies were obtained. These two frequencies enabled the estimation of the dielectric properties of the parent *E. coli* strain (5K) when fitted with a double-shell model using values available in the literature as initial guesses. As expected, the first crossover frequency for 5K strain differ substantially from that of the mutants but Castellarnau *et al*. could not account for the rationale behind the disparity. The only suggestion was that the change might be due to the protein composition of the cytoplasmic membrane or the lipopolysaccharide composition in the outer membrane [188].

However, Chiok *et al*. while working on a similar project involving not *E. coli*, but *Salmonella enteritidis* found a change in the crossover frequencies of wild-type *S. enteritidis* and its KsgA-based mutants (dimethyl adenosine transferase) [123]. They attributed the change partly to the disruption of the cell envelope as evident in the series of electron micrographs of the bacteria and their mutants (Figure 2.10).

Dielectrophoretic crossover frequency method has also been applied to study the behavior of Herpes simplex virus type 1 (HSV-1) by Hughes *et al.* [200]. HSV-1 is the etiologic agent for cold sores [172]. HSV-1 virions were cultured, suspended in a mannitol/KCl solution and characterized by

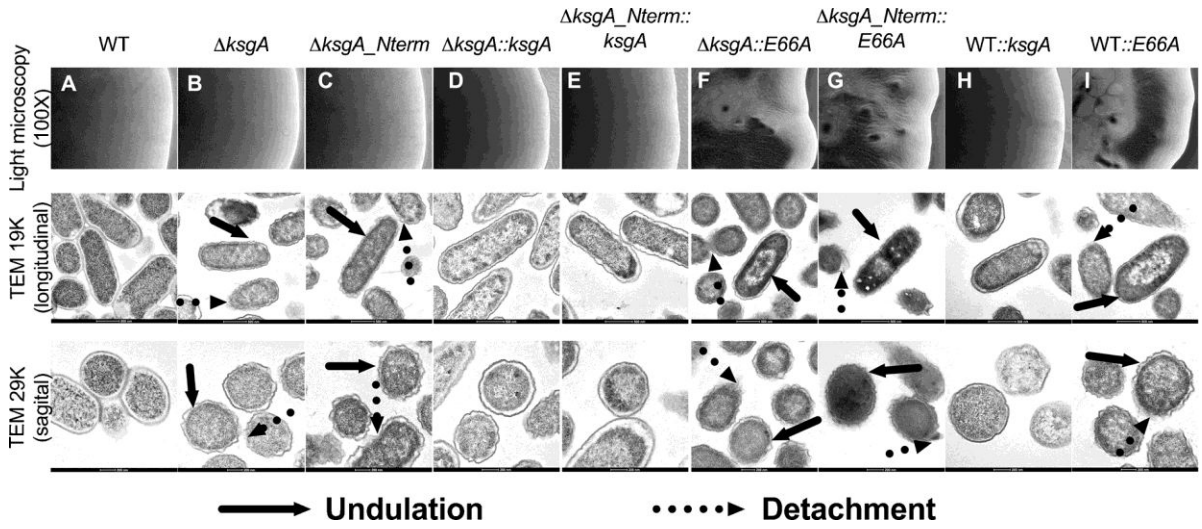

Figure 2.10 *Colony morphology (Top panel) and Transmission electron microscopy (TEM, middle and bottom panels) of S. Enteritidis strains. Bacterial colonies were collected from LB plates containing L-arabinose 0.04% incubated at 42 °C for 24 h. Colony morphology was examined with light microscopy at 100X magnification. Bacterial thin sections infiltrated with osmium tetroxide and stained with 4% uranyl acetate were examined by TEM. Images correspond to longitudinal (19 K) and sagittal (29 K) views captured at 200 kV in a FEI Technai G2 20 Twin Transmission Electron Microscope (FEI, Oregon-USA). Solid black arrows = Undulation of the cell envelope. Dashed black arrows = Loss of envelope continuity and detachment from the cell. Reproduced with permission from [90]*

applying 5 V_{pp} and 1 kHz-20 MHz to a set of polynomial electrodes. The approximate crossover frequencies for pure virions and virions treated with saponin, valinomycin, and trypsin were obtained at certain conductivity of the suspending medium. Effects of chemical agents (saponin, valinomycin and trypsin) on the biochemistry of the HSV-1 virion were explored through crossover frequency measurements at varied medium conductivity. The frequency-conductivity data points were fitted with single-shell model to obtain the dielectric properties that vividly revealed almost the same interior permittivity but considerably different membrane permittivity. Hughes *et al.* also confirmed that the surface charge density of HSV-1 reduced considerably when treated with trypsin, an observation that corroborates trypsin's capability in stripping glycoproteins from viral membranes. While valinomycin-treated HSV-1 had a modified membrane capability that facilitates the free flow of potassium ions (K+) across the membrane, Saponin-treated HSV-1 were observed to have a leaky membrane structure that enhanced the leakage of ions from the virus interior. These observations were adjudged as the rationale behind the variation in the surface conductance (0.3±0.1 nS, <0.05 nS, 0.3±0.05 nS, <1 (insensitive) nS) and interior conductivity (100±5 mS/m, 85±1 mS/m, 83±3 mS/m,40-60 mS/m, 30 mS/m) for HSV-1, HSV-Trypsin, HSV-Saponin, and HSV-valinomycin respectively [200].

Attempt by Ermolina *et al.* to find the dielectric properties of another virus (Tobacco Mosaic Virus (TMV)) using time-domain dielectric spectroscopy faced challenges as their experimental data could not be fitted through the currently available shell models [201]. Hughes *et al*. again worked on

HSV-1 but used the dielectrophoretic collection spectra in lieu of the previously reported crossover method [172]. This time, the viruses were labelled with NBD (dihexadecylamine) with the assumption that the dye would not affect the infectious nature of the virions. Hughes *et al*. also replaced the medium conductivity-modifier (KCl) with ethylenediaminetetraacetic acid (EDTA) possibly for enhancing dispersion (reducing coagulation) and preventing the adhesion of the virions to the measuring chamber. A limiting value of the suspending medium conductivity (5 mS/m) and the AC signal frequency (4.5 MHz) was obtained below which the virion displayed pDEP [172]. Below this limiting condition, the rate of virion collection at various operating frequencies was found based on the intensity of the light (increase in fluorescence) and total illuminated frame area. Fitting the collection data with a single shell model was highly insensitive to membrane permittivity [172].

DEP crossover measurement was again applied to characterize murine myeloma cell line (Tib9) and *Neurospora crassa* flowing in a 1-30 mS/m suspension under the influence of gravity in an applied, horizontal, and non-uniform AC field of strength 200 V/cm and frequency 8 kHz to 12 kHz [202]. In the project, each single cell was tracked and its deflection to the field for pDEP and nDEP at 12 kHz (pDEP condition) and 8 kHz (nDEP) were recorded. The frequency at which the cells began to sediment with gravitation, at constant speed, is termed the crossover frequency or the critical frequency. A very important finding by Marszalek *et al.* is that the strength of the electric field may affect both nDEP and pDEP but is not critical for the determination of the crossover point. More so, the crossover frequency for *N. crassa* was found to decrease with increasing cell size at the same medium conductivity. Since only one critical frequency was possible (second crossover could not be measured in this case), only the properties of the cell membrane was quantified [202].

Dielectrophoretic exploration of the differences in dielectric properties of drug sensitive and multidrug resistant (MDR) cancer cells has also been reported [203] by Labeed *et al*. Cultured human chronic myelogenous leukemia (K562) and doxorubicin human leukemic resistant cell line (K562AR) was validated using chemosensitivity and western immune-blotting testing to confirm the MDR phenotype in K562AR. Using 8.5% w/v sucrose plus 0.3% w/v dextrose medium, whose conductivity was progressively adjusted to 2.5 mS/m with PBS, a $3*10^5$ cells/ml suspension was formulated. Labeed *et al.* utilized two specially-cut shallow-angled needle-shaped electrodes with interelectrode distance of 100 μm to collect cells after being charged with 20 Vpp, 10 kHz - 20 MHz using a waveform signal generator. Collection spectra of both K562 and K562AR began at 10 kHz but while K562 showed a decline in the collection rate between 2-3 MHz, K562AR did not show any decline until 8-10 MHz. This observation resulted in lower cytoplasmic conductivity (0.23 S/m) for K562 than 0.5 S/m for K562AR representing different ionic strengths in the cytoplasm of both cells [203].

Sanchis *et al.* reported dielectrophoretic collection spectra that intrinsically differentiated gram-negative bacteria (*Escherichia coli*) from gram-positive bacteria (*Staphylococcus aureus*) [171]. Prior knowledge about the gram-stain can help in the choice of antibiotic therapy. However, it is procedurally time consuming and that some bacteria of medical importance do not stain effectively which leads to the possibility of utilizing DEP in place of gram staining procedure. By constructing a microelectrode chamber sputter with chromium, this group of researchers were able to aggregate cells at the electrodes, relate the cell collection to the dielectric polarizability of the cells, and utilize boundary element methodology to obtain the polarizabilities of both *E. coli* (which is treated as a rod-like shape) and *S. aureus* (treated as a spherical entity). On fitting the collection spectra with their developed model, they were able to obtain the plasma membrane dielectric constant for *S. aureus*, which was 1.6 times greater than that of *E. coli*. They also found out that the internal conductivity of the gram-positive bacteria (*S. aureus*), 0.8 ± 0.05 S/m is about ten(10) times greater than that of *E. coli*, which is in tune with the fact that gram-positive bacteria have higher concentration of potassium ions than their gram-negative counterparts [171].

Conclusions

This review has been able to provide the necessary background for the three main bioparticle characterization techniques for obtaining the electrical properties. A detailed overview of how biological cells are represented in terms of cytoplasmic and membrane characteristics has been discussed. The concept of conduction and polarization of bioparticle under electric field effects leading to a consideration of real and imaginary parts of the Kramer-Kronig relation was introduced. This also led to the discussion on Cole-Cole dispersion model as a function of AC frequency: a concept that underscores the DC/AC Maxwell-Wagner interfacial dispersion at the radio frequency range. Here the capacitance and conductance, which are related to permittivity and conductivity was given a pride of place. This is due to their relation to dielectrophoretic force which directs bioparticles under non-uniform electric field. When a bioparticle is suspended between two electrodes charged with low-voltage, a dynamically linear response current can be obtained. This is the concept of dielectric spectroscopy and has been well detailed in this review. If, however, the cells are contained in a quadrupole, a torque is created, and the cells can rotate with the rotating electric field depending on the frequency in use. This principle called, electrorotation (ROT), has been well utilized in characterizing many bioparticles. Details of these applications have been reported in this summary. Two charged electrodes can be arranged such that the strength of the field between them are unequally distributed. This non-uniformity in electric field strength can be advantageous in moving cells to various locations within the field space. Dielectrophoresis is a phenomenon that describes how this non-uniform field can generate a gradient electric field force that would cause cells to move away or toward high-fielf

Table 2.2 *Some of the biological materials that have been electrically characterized and the method used to obtain their intrinsic electrical properties. Single shell model of cells is the most common characterization model possibly because of its simplicity*

Type Method	**Electrode configuration**	**Target cells**	**Medium Type Medium pH Medium conductivity (mS/m)**	**Cell viability**	**Cell density (cells/ml)**	**Applied Voltage**	**Frequency range**	**Fitting Model**	**Extracted parameters**
Electroro-tation	Four-point	(1) Friend murine Erythroleukemia (MEL) DS 19 (2) HMBA-treated FME	Sucrose/dextrose 7.6 6.1-56	≥ 98%	$5\,X\,10^4$	0.9 V_{rms}	10kHz – 100 MHz	Single-shell spherical	C_{mem}, σ_{int}, ε_{int} G_{mem} (not calculated)
Dielectro-phoresis (crossover frequency)	Polynomial	Healthy and plasmodium-infected erythrocytes	Sucrose/dextrose N/A 1-75	N/A	≥ 10	3-8 Vpp	1 kHz- 100 MHz	Single-shell oblate spherical	C_{mem} G_{mem}
Electroro-tation	Polynomial	Healthy erythrocytes	Sucrose/dextrose N/A 56	N/A	$5\,X\,10^5$	four phase quadrature	1 kHz- 100 MHz	Single-shell spherical	C_{mem} ε_{int} σ_{int}
Dielectro-phoresis (collection spectra)	Interdigitated	1) Friend murine Erythroleukemia (MEL) DS 19 (2) HMBA-treated FME	Sucrose/dextrose N/A 1-4	N/A	$1\,X\,10^7$	3.0 Vrms	500 Hz-10 kHz	Single shell	C_{mem} σ_{mem} ε_{mem}
Dielectro-phoresis (capture voltage spectrum)	Strip	Human colon cancer cells (HT-29 cells)	Sucrose pH 10-100	N/A	~ 10^6	Up to 20 Vpp	5kHz-20MHz	Single shell	σ_{mem} ε_{mem} σ_{int} ε_{int}
Dielectro-phoresis (crossover frequency)	U- and-T	*Escherichia coli* (5K) and its Mutants (Hha-3, 5K hns and Hha-3 hns)	Distilled water N/A 1-130	N/A	N/A	6- 10 Vpp	10kHz- 200MHz	Double shell	σ_{mem} ε_{mem} ε_{wall} σ_{int} ε_{int} σ_{wall}

Table 2.2 (contd)	*Some of the biological materials that have been electrically characterized and the method used to obtain their intrinsic electrical properties. Single shell model of cells is the most common characterization model possibly because of its simplicity*								
Dielectro-phoresis (crossover frequency)	Polynomial	Herpes simplex virus type 1 (HSV-1)	Mannitol/KCl 6.4 ± 0.2 1-100	N/A	Low enough to assume negligible particle-particle interaction	5Vpp	1kHz-20MHz	Single shell	σ_{mem} ε_{mem} σ_{int} ε_{int}
Dielectric Spectro-scopy (time domain)	(N/A) Dielectric spectrometer	Tobacco mosaic virus	KCl/HEPES 7.0 3.5-5	N/A	$4.0\ X\ 10^7$	N/A	N/A	N/A	N/A
Dielectroph oresis (Collection Spectra)	Polynomial	Herpes simplex virus type 1 (HSV-1)	Mannitol/EDTA N/A 5	N/A	N/A	10 Vpp, 180^0 phase difference	1kHz-20MHz	Single shell	N/A
Dielectroph oresis (cross over frequency)	Parallel wire-sheet (polynomial)	Murine myeloma cell line and Neurospora crassa	Sorbitol/NaCl N/A 1-30	N/A	N/A	Field strength (200V/cm)	8 kHz-12 kHz	Single shell	σ_{mem} ε_{mem}
Dielectroph oresis (Collection spectra)	Needle-shaped	Human chronic myelogenous leukemia (K562) and doxorubicin human leukemic resistant cell line (K562AR)	Sucrose/Dextrose/PBS N/A 2.5	N/A	$\sim 3.0\ X\ 10^5$	20 Vpp	10-20 MHz	Single shell	σ_{mem} ε_{mem}
Electrorotation	3D Carbon-PDMS	Hela C3H10 B Lymphocytes HepaRG	Sucrose/PBS N/A 36.5	unknown	$1.5\ X10^5$	$\leq 14.5\ Vpp$	100kHz-10MHz	Single shell	C_{mem} σ_{int}
Electrorotation	Planar	HeLa and HepaRG cells	Sucrose/PBS N/A 36.5	N/A	$1\ X\ 10^8$ (High-density) $1\ X\ 10^7$ (Low-density)	up to $12\ V_{pp}$	Up to 1 MHz	N/A	N/A

region. This technique, together with its hybrids, have revealed the electrical properties of many bioparticles ranging from algae to cancerous cells are well discussed here.

The advancement in cellular characterization over the years would have been impossible but for the improvement in microfabrication techniques. The minimum microfluidic channel size (critical dimension) that can be made for cellular characterization is governed by its relation to the wavelength of illumination and the numerical aperture of the scanning lens. This has been facilitated by Moore's, which proposed that the size of a transistor, for instance, will keep reducing by half every 2 years. Current moves by major players in the semiconductor industry from immersion (DUV) lithography to EUV will further advance the miniaturization of cellular characterization devices, though it may be very costly to fabricate at the initial stage.

Many of the techniques reported here require cells to be cultured, washed, and reconstituted to certain concentration/density before their characterization. This is a tedious and time-consuming process that researchers are still hanging with. In the future, scientists will likely delve into a single device application that will culture, wash, reconstitute and electro-physically characterize cells. For examples, Vasdekis and many other researchers have over the years worked on trapping techniques for single cells [204-208]. Their initiatives can further be advanced such that micro- nano- valves, pumps, sieves, and other useful unit operations can be integrated into a single device for cellular characterization and atomization.

With the advancement in machine/artificial intelligence, the future of cellular dielectric property quantification is very bright. However, researchers must start compiling computerized databases and digitalized informatics for biological cells with respect to their capacitance and conductance obtained through diverse characterization techniques. Through this, the computer can learn and utilize online image recognition (computer vision) for cellular properties that are closely estimated as possible to their true values.

References

[1] "Six lines of action to promote health in the 2030 agenda for sustainable development," in "World Health Statistics 2017," 2017.

[2] (2018, May 21). *Spending on Health: Latest Trends*. Available: http://www.oecd.org/health/health-data.htm

[3] W. H. Organization. (2018, May 21). *Global Health Expenditure Database*. Available: http://apps.who.int/nha/database

[4] J. Cooper, "Healthcare expenditure, UK Health Accounts: 2017," Office for National Statistics, UK2017, Available: https://www.ons.gov.uk/peoplepopulationandcommunity/-healthandsocialcare/healthcaresystem/bulletins/ukhealthaccounts/2017.

[5] K. L. Chan, H. Morgan, E. Morgan, I. T. Cameron, and M. R. Thomas, "Measurements of the dielectric properties of peripheral blood mononuclear cells and trophoblast cells using AC electrokinetic techniques," *Biochimica et Biophysica Acta (BBA) - Molecular Basis of Disease,* vol. 1500, no. 3, pp. 313-322, 2000/03/17/ 2000.

[6] A. Koji, H. Tetsuya, and K. Naokazu, "Dielectric Approach to Suspensions of Ellipsoidal Particles Covered with a Shell in Particular Reference to Biological Cells," *Japanese Journal of Applied Physics,* vol. 19, no. 2, p. 359, 1980.

[7] M. A. Mansor and M. R. Ahmad, "Single Cell Electrical Characterization Techniques," *Int J Mol Sci,* vol. 16, no. 6, pp. 12686-712, Jun 4 2015.

[8] R. R. Pethig, *Dielectrophoresis: Theory, Methodology and Biological Applications*. Wiley, 2017.

[9] B. J. Kirby, *Micro- and Nanoscale Fluid Mechanics: Transport in Microfluidic Devices*. Cambridge: Cambridge University Press, 2010.

[10] H. A. Pohl, *Dielectrophoresis: The Behavior of Neutral Matter in Nonuniform Electric Fields*. Cambridge: Cambridge University Press, 1978.

[11] P. R. Gascoyne and J. Vykoukal, "Particle separation by dielectrophoresis," *Electrophoresis,* Review vol. 23, no. 13, pp. 1973-83, Jul 2002.

[12] B. H. Lapizco-Encinas, B. A. Simmons, E. B. Cummings, and Y. Fintschenko, "Dielectrophoretic concentration and separation of live and dead bacteria in an array of insulators," *Anal Chem,* Research vol. 76, no. 6, pp. 1571-9, Mar 15 2004.

[13] B. H. Lapizco-Encinas and M. Rito-Palomares, "Dielectrophoresis for the manipulation of nanobioparticles," *Electrophoresis,* Review vol. 28, no. 24, pp. 4521-38, Dec 2007.

[14] C. Zhang, K. Khoshmanesh, A. Mitchell, and K. Kalantar-Zadeh, "Dielectrophoresis for manipulation of micro/nano particles in microfluidic systems," *Anal Bioanal Chem,* Review vol. 396, no. 1, pp. 401-20, Jan 2010.

[15] P. Gascoyne, C. Mahidol, M. Ruchirawat, J. Satayavivad, P. Watcharasit, and F. Becker, "Microsample preparation by dielectrophoresis: isolation of malaria," *Lab Chip,* vol. 2, no. 2, pp. 70-5, May 2002.

[16] E. O. Adekanmbi, M. W. Ueti, B. Rinaldi, C. E. Suarez, and S. K. Srivastava, "Insulator-based dielectrophoretic diagnostic tool for babesiosis," *Biomicrofluidics,* vol. 10, no. 3, p. 033108, May 2016.

[17] P. Gascoyne, R. Pethig, J. Satayavivad, F. F. Becker, and M. Ruchirawat, "Dielectrophoretic detection of changes in erythrocyte membranes following malarial infection," *Biochim Biophys Acta,* vol. 1323, no. 2, pp. 240-52, Jan 31 1997.

[18] (May 15). *United States patent and trademark office*. Available: https://www.uspto.gov

[19] M. Li and R. K. Anand, "High-Throughput Selective Capture of Single Circulating Tumor Cells by Dielectrophoresis at a Wireless Electrode Array," *Journal of the American Chemical Society,* vol. 139, no. 26, pp. 8950-8959, 2017/07/05 2017.

[20] P. R. Gascoyne and S. Shim, "Isolation of circulating tumor cells by dielectrophoresis," (in eng), *Cancers (Basel),* vol. 6, no. 1, pp. 545-79, Mar 12 2014.

[21] J. Zhang, K. Chen, and Z. H. Fan, "Chapter One - Circulating Tumor Cell Isolation and Analysis," in *Advances in Clinical Chemistry*, vol. 75, G. S. Makowski, Ed.: Elsevier, 2016, pp. 1-31.

[22] M. Aghaamoo, A. Aghilinejad, X. Chen, and J. Xu, "On the design of deterministic dielectrophoresis for continuous separation of circulating tumor cells from peripheral blood cells," *ELECTROPHORESIS,* vol. 40, no. 10, pp. 1486-1493, 2019.

[23] I. Cheng, T. Chen, Y. Lin, W. Huang, C. Liu, and W. Su, "A novel dielectrophoresis-based microfluidic chip for antibody-free isolation of circulating tumor cells from blood," in *2015 IEEE 15th International Conference on Nanotechnology (IEEE-NANO)*, 2015, pp. 1525-1527.

[24] C. Gabriel, "The Dielectric Properties of Biological Materials," in *Radiofrequency Radiation Standards: Biological Effects, Dosimetry, Epidemiology, and Public Health Policy*, B. J. Klauenberg, M. Grandolfo, and D. N. Erwin, Eds. Boston, MA: Springer US, 1995, pp. 187-196.

[25] S. M. Hosseini, M. Hajian, F. Moulavi, V. Asgari, M. Forouzanfar, and M. H. Nasr-Esfahani, "Cloned Sheep Blastocysts Derived from Oocytes Enucleated Manually Using a Pulled Pasteur Pipette," *Cellular Reprogramming,* vol. 15, no. 1, pp. 15-23, 2013.

[26] S. M. Hosseini *et al.*, "Simple, fast, and efficient method of manual oocyte enucleation using a pulled Pasteur pipette," *In Vitro Cellular & Developmental Biology - Animal,* journal article vol. 49, no. 8, pp. 569-575, September 01 2013.

[27] H. Ebrahimian, M. Giesguth, K.-J. Dietz, G. Reiss, and S. Herth, "Magnetic tweezers for manipulation of magnetic particles in single cells," *Applied Physics Letters,* vol. 104, no. 6, p. 063701, 2014.

[28] L. Chen, A. Offenhäusser, and H.-J. Krause, "Magnetic tweezers with high permeability electromagnets for fast actuation of magnetic beads," *Review of Scientific Instruments,* vol. 86, no. 4, p. 044701, 2015.

[29] Y.-L. Liang, Y.-P. Huang, Y.-S. Lu, M. T. Hou, and J. A. Yeh, "Cell rotation using optoelectronic tweezers," (in eng), *Biomicrofluidics,* vol. 4, no. 4, pp. 43003-43003, 2010.

[30] G. Carmon and M. Feingold, "Rotation of single bacterial cells relative to the optical axis using optical tweezers," *Optics Letters,* vol. 36, no. 1, pp. 40-42, 2011/01/01 2011.

[31] D. Ahmed *et al.*, "Rotational manipulation of single cells and organisms using acoustic waves," *Nature Communications,* Article vol. 7, p. 11085, 03/23/online 2016.

[32] F. Guo *et al.*, "Three-dimensional manipulation of single cells using surface acoustic waves," *Proceedings of the National Academy of Sciences,* vol. 113, no. 6, p. 1522, 2016.

[33] L. Huang, P. Zhao, and W. Wang, "3D cell electrorotation and imaging time for measuring multiple cellular biophysical properties," *Lab on a Chip,* 10.1039/C8LC00407B vol. 18, no. 16, pp. 2359-2368, 2018.

[34] R. Phillips, J. Kondev, J. Theriot, and H. Garcia, *Physical Biology of the Cell*, 2 ed. CRC Press, 2012.

[35] R. Pethig and D. B. Kell, "The passive electrical properties of biological systems: their significance in physiology, biophysics and biotechnology," *Physics in Medicine and Biology,* vol. 32, no. 8, pp. 933-970, 1987/08/01 1987.

[36] M. P. Hughes, *Nanoelectromechanics in Engineering and Biology*, 1 ed. CRC Press, 2002.

[37] G. H. Markx and C. L. Davey, "The dielectric properties of biological cells at radiofrequencies: applications in biotechnology," *Enzyme and Microbial Technology,* doi: DOI: 10.1016/S0141-0229(99)00008-3 vol. 25, no. 3-5, pp. 161-171, 1999.

[38] T. B. Jones, *Electromechanics of Particles*. Cambridge: Cambridge University Press, 1995.

[39] H. Morgan and N. G. Green, *AC electrokinetics colloids and nanoparticles*. Baldock, Hertfordshire, England; Philadelphia, Pa.; Williston, VT: Research Studies Press ; Institute of Physics Pub. ; Distribution, North America, AIDC, 2003.

[40] R. Pethig, *Dielectric and Electronic Properties of Biological Materials* New York: Wiley & Sons, 1979.

[41] H. A. Pohl, *Dielectrophoresis the behavior of neutral matter in nonuniform electric fields*. Cambridge: Cambridge University Press, 1978.

[42] T. N. G. Adams, A. Y. L. Jiang, P. D. Vyas, and L. A. Flanagan, "Separation of neural stem cells by whole cell membrane capacitance using dielectrophoresis," *Methods,* vol. 133, pp. 91-103, 2018/01/15/ 2018.

[43] H. P. Schwan, *Electrical Properties of Tissue and Cell Suspensions**This work was supported in part by grants from the United States Public Health Service, H-1253(c2-4) and in part by the Office of Naval Research, 119–289* (Advances in Biological and Medical Physics). Elsevier, 1957, pp. 147-209.

[44] D. A. Dean, T. Ramanathan, D. Machado, and R. Sundararajan, "Electrical Impedance Spectroscopy Study of Biological Tissues," (in eng), *Journal of electrostatics,* vol. 66, no. 3-4, pp. 165-177, 2008.

[45] H. P. Schwan, "The Practical Success of Impedance Techniques from an Historical Perspective," *Annals of the New York Academy of Sciences,* vol. 873, no. 1, pp. 1-12, 1999.

[46] H. P. Schwan, "Electrical properties of blood and its constituents: alternating current spectroscopy," (in eng), *Blut,* vol. 46, no. 4, pp. 185-97, Apr 1983.

[47] J. M. Prausnitz, R. N. Lichtenthaler, and E. G. d. Azevedo, *Molecular Thermodynamics of Fluid-Phase Equilibria*, 3 ed. Prentice Hall, 1999.

[48] H. J. Mulhall, F. H. Labeed, B. Kazmi, D. E. Costea, M. P. Hughes, and M. P. Lewis, "Cancer, pre-cancer and normal oral cells distinguished by dielectrophoresis," *Anal Bioanal Chem,* vol. 401, no. 8, pp. 2455-63, Nov 2011.

[49] K. L. Heileman and M. Tabrizian, "Dielectric spectroscopy platform to measure MCF10A epithelial cell aggregation as a model for spheroidal cell cluster analysis," *Analyst,* 10.1039/C6AN02156E vol. 142, no. 9, pp. 1601-1607, 2017.

[50] E. L. Carstensen, R. E. Marquis, S. Z. Child, and G. R. Bender, "Dielectric properties of native and decoated spores of Bacillus megaterium," (in eng), *Journal of bacteriology,* vol. 140, no. 3, pp. 917-928, 1979.

[51] D. Spencer, V. Hollis, and H. Morgan, "Microfluidic impedance cytometry of tumour cells in blood," vol. 8, p. 064124, 2014.

[52] J. L. Nourse *et al.*, "Membrane Biophysics Define Neuron and Astrocyte Progenitors in the Neural Lineage," *Stem Cells,* vol. 32, no. 3, pp. 706-716, 2014.

[53] T. Zhou, Y. Ming, S. F. Perry, and S. Tatic-Lucic, "Estimation of the physical properties of neurons and glial cells using dielectrophoresis crossover frequency," *Journal of Biological Physics,* journal article vol. 42, no. 4, pp. 571-586, October 01 2016.

[54] K. V. Kaler and T. B. Jones, "Dielectrophoretic spectra of single cells determined by feedback-controlled levitation," (in eng), *Biophysical journal,* vol. 57, no. 2, pp. 173-182, 1990.

[55] R. Pethig, L. M. Jakubek, R. H. Sanger, E. Heart, E. D. Corson, and P. J. S. Smith, "Electrokinetic measurements of membrane capacitance and conductance for pancreatic /spl beta/-cells," *IEE Proceedings - Nanobiotechnology,* vol. 152, no. 6, pp. 189-193, 2005.

[56] P. R. Gascoyne, X. B. Wang, Y. Huang, and F. F. Becker, "Dielectrophoretic Separation of Cancer Cells from Blood," *IEEE Trans Ind Appl,* vol. 33, no. 3, pp. 670-678, 1997.

[57] M. M. M. Elnasharty *et al.*, "Cell membrane analysis using modulated dielectrophoresis " *Romanian Journal of Biophysics,* vol. 22, no. 3-4, pp. 235-246, 2012.

[58] X. B. Wang, J. Yang, Y. Huang, J. Vykoukal, F. F. Becker, and P. R. Gascoyne, "Cell separation by dielectrophoretic field-flow-fractionation," *Anal Chem,* vol. 72, no. 4, pp. 832-9, Feb 15 2000.

[59] R. Pethig and M. S. Talary, "Dielectrophoretic detection of membrane morphology changes in Jurkat T-cells undergoing etoposide-induced apoptosis," *IET Nanobiotechnology*, vol. 1, no. 1, pp. 2-9Available: https://digital-library.theiet.org/content/journals/10.1049/iet-nbt_20060018

[60] C. Honrado, L. Ciuffreda, D. Spencer, L. Ranford-Cartwright, and H. Morgan, "Dielectric characterization of Plasmodium falciparum-infected red blood cells using microfluidic impedance cytometry," *J R Soc Interface,* vol. 15, no. 147, Oct 17 2018.

[61] F. H. Labeed *et al.*, "Biophysical Characteristics Reveal Neural Stem Cell Differentiation Potential," *PLOS ONE,* vol. 6, no. 9, p. e25458, 2011.

[62] L. A. Flanagan *et al.*, "Unique Dielectric Properties Distinguish Stem Cells and Their Differentiated Progeny," *STEM CELLS,* vol. 26, no. 3, pp. 656-665, 2008.

[63] J. L. Prieto, J. Lu, J. L. Nourse, L. A. Flanagan, and A. P. Lee, "Frequency discretization in dielectrophoretic assisted cell sorting arrays to isolate neural cells," *Lab on a Chip,* 10.1039/C2LC21184J vol. 12, no. 12, pp. 2182-2189, 2012.

[64] M. G. Simon *et al.*, "Increasing label-free stem cell sorting capacity to reach transplantation-scale throughput," (in eng), *Biomicrofluidics,* vol. 8, no. 6, pp. 064106-064106, 2014.

[65] M. S. Talary, K. I. Mills, T. Hoy, A. K. Burnett, and R. Pethig, "Dielectrophoretic separation and enrichment of CD34+ cell subpopulation from bone marrow and peripheral blood stem cells," *Med Biol Eng Comput,* vol. 33, no. 2, pp. 235-7, Mar 1995.

[66] M. Stephens, M. S. Talary, R. Pethig, A. K. Burnett, and K. I. Mills, "The dielectrophoresis enrichment of CD34+ cells from peripheral blood stem cell harvests," (in eng), *Bone marrow transplantation,* vol. 18, no. 4, pp. 777-782, 1996/10// 1996.

[67] J. Vykoukal, D. M. Vykoukal, S. Freyberg, E. U. Alt, and P. R. C. Gascoyne, "Enrichment of putative stem cells from adipose tissue using dielectrophoretic field-flow fractionation," *Lab on a Chip,* 10.1039/B717043B vol. 8, no. 8, pp. 1386-1393, 2008.

[68] P. O. Bagnaninchi and N. Drummond, "Real-time label-free monitoring of adipose-derived stem cell differentiation with electric cell-substrate impedance sensing," *Proceedings of the National Academy of Sciences,* vol. 108, no. 16, p. 6462, 2011.

[69] C. Hildebrandt, H. Büth, S. Cho, Impidjati, and H. Thielecke, "Detection of the osteogenic differentiation of mesenchymal stem cells in 2D and 3D cultures by electrochemical impedance spectroscopy," *Journal of Biotechnology,* vol. 148, no. 1, pp. 83-90, 2010/07/01/ 2010.

[70] H. Song *et al.*, "Continuous-flow sorting of stem cells and differentiation products based on dielectrophoresis," *Lab on a Chip,* 10.1039/C4LC01253D vol. 15, no. 5, pp. 1320-1328, 2015.

[71] S. Cho, E. Gorjup, and H. Thielecke, "Chip-based time-continuous monitoring of toxic effects on stem cell differentiation," *Annals of Anatomy - Anatomischer Anzeiger,* vol. 191, no. 1, pp. 145-152, 2009/01/01/ 2009.

[72] Y. Hirota and M. Hakoda, "Relationship between Dielectric Characteristic by DEP Levitation and Differentiation Activity for Stem Cells," *Key Engineering Materials,* vol. 459, pp. 84-91, 2011.

[73] M. Muratore, V. Srsen, M. Waterfall, A. Downes, and R. Pethig, "Biomarker-free dielectrophoretic sorting of differentiating myoblast multipotent progenitor cells and their membrane analysis by Raman spectroscopy," (in eng), *Biomicrofluidics,* vol. 6, no. 3, pp. 34113-34113, 2012.

[74] S. Velugotla *et al.*, "Dielectrophoresis based discrimination of human embryonic stem cells from differentiating derivatives," (in eng), *Biomicrofluidics,* vol. 6, no. 4, pp. 44113-44113, 2012.

[75] D. Tsikritsis *et al.*, "Label-free biomarkers of human embryonic stem cell differentiation to hepatocytes," *Cytometry Part A,* vol. 89, no. 6, pp. 575-584, 2016.

[76] W. Liang, Y. Zhao, L. Liu, Y. Wang, W. J. Li, and G.-B. Lee, "Determination of Cell Membrane Capacitance and Conductance via Optically Induced Electrokinetics," (in eng), *Biophysical journal,* vol. 113, no. 7, pp. 1531-1539, 2017.

[77] K. Cheung, S. Gawad, and P. Renaud, "Impedance spectroscopy flow cytometry: On-chip label-free cell differentiation," *Cytometry Part A,* vol. 65A, no. 2, pp. 124-132, 2005.

[78] A. Han, L. Yang, and A. B. Frazier, "Quantification of the Heterogeneity in Breast Cancer Cell Lines Using Whole-Cell Impedance Spectroscopy," *Clinical Cancer Research,* vol. 13, no. 1, pp. 139-143, 2007.

[79] C. Justice *et al.*, "Process control in cell culture technology using dielectric spectroscopy," *Biotechnology Advances,* vol. 29, no. 4, pp. 391-401, 2011/07/01/ 2011.

[80] A. Salmanzadeh, M. B. Sano, R. C. Gallo-Villanueva, P. C. Roberts, E. M. Schmelz, and R. V. Davalos, "Investigating dielectric properties of different stages of syngeneic murine ovarian cancer cells," (in eng), *Biomicrofluidics,* vol. 7, no. 1, pp. 11809-11809, 2013.

[81] J. Leroy *et al.*, "Microfluidic biosensors for microwave dielectric spectroscopy," *Sensors and Actuators A: Physical,* vol. 229, pp. 172-181, 2015/06/15/ 2015.

[82] J. L. Prieto *et al.*, "Monitoring sepsis using electrical cell profiling," (in eng), *Lab on a chip,* vol. 16, no. 22, pp. 4333-4340, 2016.

[83] A. H. Kyle, C. T. Chan, and A. I. Minchinton, "Characterization of three-dimensional tissue cultures using electrical impedance spectroscopy," (in eng), *Biophysical journal,* vol. 76, no. 5, pp. 2640-2648, 1999.

[84] E. Niebur, "Electrical properties of cell membranes," *Scholarpedia,* vol. 3, no. 6, 2008.

[85] B. Yafouz, N. A. Kadri, and F. Ibrahim, "Dielectrophoretic manipulation and separation of microparticles using microarray dot electrodes," (in eng), *Sensors (Basel, Switzerland),* vol. 14, no. 4, pp. 6356-6369, 2014.

[86] M. Tanhaemami, E. Alizadeh, C. Sanders, B. Marrone, and B. Munsky, "Using Flow Cytometry and Multistage Machine Learning to Discover Label-Free Signatures of Algal Lipid Accumulation," *bioRxiv,* p. 497834, 2018.

[87] J.-C. Chien, A. Ameri, E.-C. Yeh, A. N. Killilea, M. Anwar, and A. M. Niknejad, "A high-throughput flow cytometry-on-a-CMOS platform for single-cell dielectric spectroscopy at microwave frequencies," *Lab on a Chip,* 10.1039/C8LC00299A vol. 18, no. 14, pp. 2065-2076, 2018.

[88] C. Simonnet and A. Groisman, "High-Throughput and High-Resolution Flow Cytometry in Molded Microfluidic Devices," *Analytical Chemistry,* vol. 78, no. 16, pp. 5653-5663, 2006/08/01 2006.

[89] C. H. Clausen *et al.*, "Bacteria Detection and Differentiation Using Impedance Flow Cytometry," *Sensors (Basel),* vol. 18, no. 10, p. 3496, Oct 17 2018.

[90] K. L. Chiok, N. C. Paul, E. O. Adekanmbi, S. K. Srivastava, and D. H. Shah, "Dimethyl adenosine transferase (KsgA) contributes to cell-envelope fitness in Salmonella Enteritidis," *Microbiol Res,* vol. 216, pp. 108-119, Nov 2018.

[91] J. Voldman, "Electrical forces for microscale cell manipulation," *Annual Review of Biomedical Engineering,* vol. 8, no. 1, pp. 425-454, 2006.

[92] T. Sun, H. Morgan, and N. G. Green, "Analytical solutions of the dielectrophoretic and travelling wave forces generated by interdigitated electrode arrays," in *Journal of Physics*, 2008, vol. 142, pp. 1-4: IOP publishing.

[93] S.-I. Han, Y.-D. Joo, and K.-H. Han, "An electrorotation technique for measuring the dielectric properties of cells with simultaneous use of negative quadrupolar dielectrophoresis and electrorotation," *Analyst,* 10.1039/C3AN36261B vol. 138, no. 5, pp. 1529-1537, 2013.

[94] W. M. Arnold and U. Zimmermann, "Electro-rotation: development of a technique for dielectric measurements on individual cells and particles," *Journal of Electrostatics,* vol. 21, no. 2, pp. 151-191, 1988/09/01/ 1988.

[95] Y.-L. Chen and H.-R. Jiang, "Electrorotation of a metallic coated Janus particle under AC electric fields," *Applied Physics Letters,* vol. 109, no. 19, p. 191605, 2016.

[96] J. P. Huang, K. W. Yu, G. Q. Gu, and M. Karttunen, "Electrorotation in graded colloidal suspensions," *Physical Review E,* vol. 67, no. 5, p. 051405, 05/19/ 2003.

[97] K. R. Foster, F. A. Sauer, and H. P. Schwan, "Electrorotation and levitation of cells and colloidal particles," (in eng), *Biophysical journal,* vol. 63, no. 1, pp. 180-190, 1992.

[98] E. Alizadeh-Haghighi, S. Jafarmadar, and S. Khalilarya, "Application of genetic algorithm in extracting cell dielectric characteristics with electrorotation," *Journal of Electrical Bioimpedance; Vol 8 (2017),* 2017.

[99] Y. K. Ren, D. Morganti, H. Y. Jiang, A. Ramos, and H. Morgan, "Electrorotation of Metallic Microspheres," *Langmuir,* vol. 27, no. 6, pp. 2128-2131, 2011/03/15 2011.

[100] T. Sun and H. Morgan, "Single-cell microfluidic impedance cytometry: a review," *Microfluidics and Nanofluidics,* vol. 8, no. 4, pp. 423-443, 2010/04/01 2010.

[101] A. Mansoorifar, A. Koklu, S. Ma, G. V. Raj, and A. Beskok, "Electrical Impedance Measurements of Biological Cells in Response to External Stimuli," *Analytical Chemistry,* vol. 90, no. 7, pp. 4320-4327, 2018/04/03 2018.

[102] M. Stubbe and J. Gimsa, "Maxwell's mixing equation revisited: characteristic impedance equations for ellipsoidal cells," (in eng), *Biophysical journal,* vol. 109, no. 2, pp. 194-208, 2015.

[103] R. Schmukler, "Measurements of the Electrical Impedance of Living Cells in the Frequency Domain," in *Charge and Field Effects in Biosystems—2*, M. J. Allen, S. F. Cleary, and F. M. Hawkridge, Eds. Boston, MA: Springer US, 1989, pp. 357-372.

[104] H. Fricke, "A Mathematical Treatment of the Electric Conductivity and Capacity of Disperse Systems I. The Electric Conductivity of a Suspension of Homogeneous Spheroids," *Physical Review,* vol. 24, no. 5, pp. 575-587, 11/01/ 1924.

[105] K. S. Cole, "ELECTRIC IMPEDANCE OF SUSPENSIONS OF ARBACIA EGGS," *The Journal of General Physiology,* vol. 12, no. 1, pp. 37-54, 1928.

[106] K. S. Cole and H. J. Curtis, "ELECTRIC IMPEDANCE OF THE SQUID GIANT AXON DURING ACTIVITY," *The Journal of General Physiology,* vol. 22, no. 5, pp. 649-670, 1939.

[107] K. S. Cole and H. J. Curtis, "Electrical Impedance of Nerve During Activity," *Nature,* vol. 142, no. 3587, pp. 209-210, 1938/07/01 1938.

[108] X. Han, C. van Berkel, J. Gwyer, L. Capretto, and H. Morgan, "Microfluidic Lysis of Human Blood for Leukocyte Analysis Using Single Cell Impedance Cytometry," *Analytical Chemistry,* vol. 84, no. 2, pp. 1070-1075, 2012/01/17 2012.

[109] Z. Zhu *et al.*, "Using microfluidic impedance cytometry to measure C. elegans worms and identify their developmental stages," *Sensors and Actuators B: Chemical,* vol. 275, pp. 470-482, 2018/12/01/ 2018.

[110] C. Rümenapp, M. Remm, B. Wolf, and B. Gleich, "Improved method for impedance measurements of mammalian cells," *Biosensors and Bioelectronics,* vol. 24, no. 9, pp. 2915-2919, 2009/05/15/ 2009.

[111] W. Liu, Y. Ren, Y. Tao, Y. Li, and X. Chen, "Controllable rotating behavior of individual dielectric microrod in a rotating electric field," *ELECTROPHORESIS,* vol. 38, no. 11, pp. 1427-1433, 2017.

[112] M. Cristofanilli, G. De Gasperis, L. Zhang, M.-C. Hung, P. R. C. Gascoyne, and G. N. Hortobagyi, "Automated Electrorotation to Reveal Dielectric Variations Related to HER-2/neu Overexpression in MCF-7 Sublines," *Clinical Cancer Research,* vol. 8, no. 2, pp. 615-619, 2002.

[113] L. Huang, W. He, and W. Wang, "A cell electro-rotation micro-device using polarized cells as electrodes," *ELECTROPHORESIS,* vol. 40, no. 5, pp. 784-791, 2019.

[114] A. Ramos, *Electrokinetics and Electrohydrodynamics in Microsystems*. Springer, 2011, p. 308.

[115] W. M. Arnold and U. Zimmerman, "Rotating-field-induced rotation and measurement of the membrane capacitance of single mesophyll cells of Avena sativa," *Zeitschrift fuer Naturforschung,* vol. 37c, pp. 908-915, 1982.

[116] J. Gimsa, T. Muller, T. Schnelle, and G. Fuhr, "Dielectric spectroscopy of single human erythrocytes at physiological ionic strength: dispersion of the cytoplasm," (in eng), *Biophys J,* vol. 71, no. 1, pp. 495-506, Jul 1996.

[117] W. M. Arnold, H. P. Schwan, and U. Zimmermann, "Surface conductance and other properties of latex particles measured by electrorotation," *Journal of Physical Chemistry,* vol. 91, no. 19, pp. 5093-5098, 1987.

[118] V. P. Pastushenko, P. I. Kuzmin, and Y. A. Chizmadshev, "Dielectrophoresis and electrorotation: A unified theory of spherically symmetrical cells," *Stud. Biophys.,* vol. 110, pp. 51-57, 1985.

[119] E. Donath, M. Egger, and V. P. Pastushenko, "Dielectric behavior of the anion-exchange protein of human red blood cells: Theoretical analysis and comparison to electrorotation data," *Journal of Electroanalytical Chemistry and Interfacial Electrochemistry,* vol. 298, no. 3, pp. 337-360, 1990/06/01/ 1990.

[120] X. B. Wang, Y. Huang, R. Holzel, J. P. H. Burt, and R. Pethig, "Theoretical and experimental investigations of the interdependence of the dielectric, dielectrophoretic and electrorotational

behaviour of colloidal particles," *Journal of Physics D: Applied Physics,* vol. 26, no. 2, pp. 312-322, 1993.

[121] X.-F. Zhou, G. H. Markx, R. Pethig, and I. M. Eastwood, "Differentiation of viable and non-viable bacterial biofilms using electrorotation," *Biochimica et Biophysica Acta (BBA) - General Subjects,* vol. 1245, no. 1, pp. 85-93, 1995/08/17/ 1995.

[122] V. L. Sukhorukov and U. Zimmermann, "Electrorotation of Erythrocytes Treated with Dipicrylamine: Mobile Charges within the Membrane Show their ``Signature" in Rotational Spectra," *The Journal of Membrane Biology,* journal article vol. 153, no. 2, pp. 161-169, September 01 1996.

[123] J. P. Burt, K. L. Chan, D. Dawson, A. Parton, and R. Pethig, "Assays for microbial contamination and DNA analysis based on electrorotation," *Ann Biol Clin (Paris),* vol. 54, no. 6, pp. 253-7, 1996.

[124] M. Egger and E. Donath, "Electrorotation measurements of diamide-induced platelet activation changes," (in eng), *Biophysical journal,* vol. 68, no. 1, pp. 364-372, 1995.

[125] X.-B. Wang, Y. Huang, P. R. C. Gascoyne, F. F. Becker, R. Hölzel, and R. Pethig, "Changes in Friend murine erythroleukaemia cell membranes during induced differentiation determined by electrorotation," *Biochimica et Biophysica Acta (BBA) - Biomembranes,* vol. 1193, no. 2, pp. 330-344, 1994/08/03/ 1994.

[126] Y. Huang, X.-B. Wang, R. Holzel, F. F. Becker, and P. R. C. Gascoyne, "Electrorotational studies of the cytoplasmic dielectric properties of Friend murine erythroleukaemia cells," *Physics in Medicine and Biology,* vol. 40, no. 11, pp. 1789-1806, 1995/11/01 1995.

[127] E. O. Adekanmbi and S. K. Srivastava, "Dielectrophoretic applications for disease diagnostics using lab-on-a-chip platforms," *Lab Chip,* 10.1039/C6LC00355A vol. 16, no. 12, pp. 2148-67, Jun 21 2016.

[128] V. Gupta *et al.*, "ApoStream(™), a new dielectrophoretic device for antibody independent isolation and recovery of viable cancer cells from blood," *Biomicrofluidics,* vol. 6, no. 2, pp. 024133(1-14), 2012.

[129] A. Salmanzadeh *et al.*, "Isolation of prostate tumor initiating cells (TICs) through their dielectrophoretic signature," *Lab on a Chip,* 10.1039/C1LC20701F vol. 12, no. 1, pp. 182-189, 2012.

[130] A. Sonnenberg *et al.*, "Dielectrophoretic isolation and detection of cancer-related circulating cell-free DNA biomarkers from blood and plasma," (in eng), *Electrophoresis,* vol. 35, no. 12-13, pp. 1828-36, Jul 2014.

[131] R. Y. C. P. Xiaoxing Xing, Cesar S.C.Wong, Levent Yobas, "Label-free enumeration of colorectal cancer cells from lymphocytes performed at a high cell-loading density by using interdigitated ring-array microelectrodes," *Biosensors and Bioelectronics,* vol. 61, pp. 434-442, 2014.

[132] C. V. Crowther and M. A. Hayes, "Refinement of insulator-based dielectrophoresis," *Analyst,* 10.1039/C6AN02509A vol. 142, no. 9, pp. 1608-1618, 2017.

[133] L. Benguigui and I. J. Lin, "More about the dielectrophoretic force," *Journal of Applied Physics,* vol. 53, no. 2, pp. 1141-1143, 1982.

[134] G. Molinari and A. Viviani, "Analytical evaluation of the electro-dielectrophoretic forces acting on spherical impurity particles in dielectric fluids," *Journal of Electrostatics,* vol. 5, pp. 343-354, 1978/09/01/ 1978.

[135] Y. Huang, X.-B. Wang, F. F. Becker, and P. R. C. Gascoyne, "Membrane changes associated with the temperature-sensitive P85gag-mos-dependent transformation of rat kidney cells as determined by dielectrophoresis and electrorotation," *Biochimica et Biophysica Acta (BBA) - Biomembranes,* vol. 1282, no. 1, pp. 76-84, 1996/06/13/ 1996.

[136] L. M. Broche, F. H. Labeed, and M. P. Hughes, "Extraction of dielectric properties of multiple populations from dielectrophoretic collection spectrum data," (in eng), *Phys Med Biol,* vol. 50, no. 10, pp. 2267-74, May 21 2005.

[137] E. O. Adekanmbi and S. K. Srivastava, "Applications of Electrokinetics and Dielectrophoresis on Designing Chip-Based Disease Diagnostic Platforms " in *Bio-Inspired Technology*, R. Srivastava, Ed. London, UK: IntechOpen, 2019.

[138] T. Jubery, S. K. Srivastava, and P. Dutta, "Dielectrophoresis separation of bioparticles in microdevices: A review," *Electrophoresis,* vol. 35, no. 5, pp. 691-713, 2014.

[139] L. Wu, L. Y. Lanry Yung, and K. M. Lim, "Dielectrophoretic capture voltage spectrum for measurement of dielectric properties and separation of cancer cells," *Biomicrofluidics,* vol. 6, no. 1, pp. 14113-1411310, Mar 2012.

[140] P. R. C. Gascoyne, J. Noshari, F. F. Becker, and R. Pethig, "Use of dielectrophoretic collection spectra for characterizing differences between normal and cancerous cells," in *Conference Record of the 1992 IEEE Industry Applications Society Annual Meeting*, 1992, pp. 1453-1457 vol.2.

[141] A. Sanchis *et al.*, "Dielectric characterization of bacterial cells using dielectrophoresis," *Bioelectromagnetics,* vol. 28, no. 5, pp. 393-401, 2007/07/01 2007.

[142] M. P. Hughes, H. Morgan, F. J. Rixon, J. P. Burt, and R. Pethig, "Manipulation of herpes simplex virus type 1 by dielectrophoresis," *Biochim Biophys Acta,* doi: DOI: 10.1016/S0304-4165(98)00058-0 vol. 1425, no. 1, pp. 119-26, Sep 16 1998.

[143] M. Castellarnau, A. Errachid, C. Madrid, A. Juárez, and J. Samitier, "Dielectrophoresis as a tool to characterize and differentiate isogenic mutants of Escherichia coli," (in eng), *Biophysical journal,* vol. 91, no. 10, pp. 3937-3945, 2006.

[144] U.-C. Schröder *et al.*, "Combined Dielectrophoresis–Raman Setup for the Classification of Pathogens Recovered from the Urinary Tract," *Analytical Chemistry,* vol. 85, no. 22, pp. 10717-10724, 2013/11/19 2013.

[145] G. H. Markx, R. Pethig, and J. Rousselet, "The dielectrophoretic levitation of latex beads, with reference to field-flow fractionation," *Journal of Physics D: Applied Physics,* vol. 30, no. 17, pp. 2470-2477, 1997/09/07 1997.

[146] I. Turcu and C. M. Lucaciu, "Dielectrophoresis: a spherical shell model," *Journal of Physics A: Mathematical and General,* vol. 22, no. 8, pp. 985-993, 1989/04/21 1989.

[147] Y. Feldman, I. Ermolina, and Y. Hayashi, "Time Domain Dielectric Spectroscopy Study of Biological Systems," *IEEE Transactions on Dielectrics and Electrical Insulation,* vol. 10, no. 5, pp. 728-753, 2003.

[148] D. Vrinceanu and E. Gheorghiu, "Shape effects on the dielectric behaviour of arbitrarily shaped particles with particular reference to biological cells," *Bioelectrochemistry and Bioenergetics,* vol. 40, no. 2, pp. 167-170, 1996/08/01/ 1996.

[149] E. Gheorghiu and K. Asami, "Monitoring cell cycle by impedance spectroscopy: experimental and theoretical aspects," *Bioelectrochemistry and Bioenergetics,* vol. 45, no. 2, pp. 139-143, 1998/05/01/ 1998.

[150] F. F. Becker, X.-B. Wang, Y. Huang, R. Pethig, J. Vykoukal, and P. R. C. Gascoyne, "The removal of human leukaemia cells from blood using interdigitated microelectrodes " *Journal of Physics D: Applied Physics* vol. 27, no. 12, pp. 2659-2662, 1994.

[151] V. Raicu, G. Raicu, and G. Turcu, "Dielectric properties of yeast cells as simulated by the two-shell model," *Biochimica et Biophysica Acta (BBA) - Bioenergetics,* vol. 1274, no. 3, pp. 143-148, 1996/06/13/ 1996.

[152] Y. Hayashi, L. Livshits, A. Caduff, and Y. Feldman, "Dielectric spectroscopy study of specific glucose influence on human erythrocyte membranes," *Journal of Physics D: Applied Physics,* vol. 36, no. 4, pp. 369-374, 2003/01/29 2003.

[153] M. Sancho, G. Martínez, and C. Martín, "Accurate dielectric modeling of shelled particles and cells," *Journal of Electrostatics,* vol. 57, no. 2, pp. 143-156, 2003.

[154] K. Asami, Y. Takahashi, and S. Takashima, "Dielectric properties of mouse lymphocytes and erythrocytes," *Biochim Biophys Acta,* doi: DOI: 10.1016/0167-4889(89)90183-3 vol. 1010, no. 1, pp. 49-55, Jan 17 1989.

[155] A. Irimajiri, T. Hanai, and A. Inouye, "A dielectric theory of "multi-stratified shell" model with its application to a lymphoma cell," *Journal of Theoretical Biology,* doi: DOI: 10.1016/0022-5193(79)90268-6 vol. 78, no. 2, pp. 251-269, 1979.

[156] R. D. Miller and T. B. Jones, "Electro-orientation of ellipsoidal erythrocytes. Theory and experiment," *Biophys J,* vol. 64, no. 5, pp. 1588-95, May 1993.

[157] R. Pethig and G. H. Markx, "Applications of dielectrophoresis in biotechnology," *Trends Biotechnol,* Review vol. 15, no. 10, pp. 426-32, Oct 1997.

[158] M. Castellarnau, A. Errachid, C. Madrid, A. Juarez, and J. Samitier, "Dielectrophoresis as a Tool to Characterize and Differentiate Isogenic Mutants of Escherichia coli," *Biophysical Journal,* vol. 91, pp. 3937-3945, 2006.

[159] J. C. Maxwell, *A tretise on electricity and magnetism* 3ed. Dover Publications, 1954.

[160] T. Sun and H. Morgan, "Single-cell microfluidic impedance cytometry: a review " *Microfluidics and Nanofluidics,* vol. 8, no. 4, pp. 423-443, 2010.

[161] N. Bhagwat *et al.*, "An integrated flow cytometry-based platform for isolation and molecular characterization of circulating tumor single cells and clusters," *Scientific Reports,* vol. 8, no. 1, p. 5035, 2018/03/22 2018.

[162] A. Furniturewalla, M. Chan, J. Sui, K. Ahuja, and M. Javanmard, "Fully integrated wearable impedance cytometry platform on flexible circuit board with online smartphone readout," *Microsystems & Nanoengineering,* vol. 4, no. 1, p. 20, 2018/07/30 2018.

[163] Y. Zhang *et al.*, "Crossing constriction channel-based microfluidic cytometry capable of electrically phenotyping large populations of single cells," *Analyst,* 10.1039/C8AN02100G vol. 144, no. 3, pp. 1008-1015, 2019.

[164] Y. Zhao *et al.*, "Development of microfluidic impedance cytometry enabling the quantification of specific membrane capacitance and cytoplasm conductivity from 100,000 single cells," *Biosensors and Bioelectronics,* vol. 111, pp. 138-143, 2018/07/15/ 2018.

[165] D. Holmes and H. Morgan, "Single cell impedance cytometry for identification and counting of CD4 T-cells in human blood using impedance labels," *Anal. Chem.,* vol. 82, no. 4, pp. 1455-61, Feb 15 2010.

[166] C. K. Fuller *et al.*, "Microfabricated multi-frequency particle impedance characterization systems.," in *Micro Total Analysis Systems*, 2000: Springer, Dordrecht.

[167] N. Haandbaek, S. C. Burgel, F. Heer, and A. Hierlemann, "Characterization of subcellular morphology of single yeast cells using high frequency microfluidic impedance cytometer," *Lab Chip,* vol. 14, no. 2, pp. 369-77, Jan 21 2014.

[168] M. A. Mansor, M. Takeuchi, M. Nakajima, Y. Hasegawa, and M. R. Ahmad, "Electrical Impedance Spectroscopy for Detection of Cells in Suspensions Using Microfluidic Device with Integrated Microneedles," *Applied Sciences,* vol. 7, no. 2, p. 170, 2017.

[169] F. G. and H. R., "Cell Electrorotation," in *Electrical Maniulation of Cells*, P. Lynch and M. R. Davey, Eds. U.S.: Springer, 1996.

[170] K. A. Michael, S. R. Hiibel, and E. J. Geiger, "Dependence of the dielectrophoretic upper crossover frequency on the lipid content of microalgal cells," *Algal Research,* vol. 6, pp. 17-21, 2014/10/01/ 2014.

[171] M. P. Hughes, H. Morgan, and F. J. Rixon, "Measuring the dielectric properties of herpes simplex virus type 1 virions with dielectrophoresis," *Biochim Biophys Acta,* vol. 1571, no. 1, pp. 1-8, May 10 2002.

[172] I. Ermolina, H. Morgan, N. G. Green, J. J. Milner, and Y. Feldman, "Dielectric spectroscopy of Tobacco Mosaic Virus," *Biochimica et Biophysica Acta (BBA) - General Subjects,* vol. 1622, no. 1, pp. 57-63, 2003/06/20/ 2003.

[173] P. Marszalek, J. J. Zielinsky, M. Fikus, and T. Y. Tsong, "Determination of electric parameters of cell membranes by a dielectrophoresis method," *Biophys J,* doi: 10.1016/S0006-3495(91)82312-8 vol. 59, no. 5, pp. 982-7, May 1991.

[174] F. H. Labeed, H. M. Coley, H. Thomas, and M. P. Hughes, "Assessment of Multidrug Resistance Reversal Using Dielectrophoresis and Flow Cytometry," *Biophysical Journal,* vol. 85, no. 3, pp. 2028-2034, 2003.

[175] A. E. Vasdekis, "Single microbe trap and release in sub-microfluidics," *RSC Advances,* 10.1039/C3RA40369F vol. 3, no. 18, pp. 6343-6346, 2013.

[176] M. Tanyeri, E. M. Johnson-Chavarria, and C. M. Schroeder, "Hydrodynamic trap for single particles and cells," (in eng), *Applied physics letters,* vol. 96, no. 22, pp. 224101-224101, 2010.

[177] M. Evander *et al.*, "Noninvasive Acoustic Cell Trapping in a Microfluidic Perfusion System for Online Bioassays," *Analytical Chemistry,* vol. 79, no. 7, pp. 2984-2991, 2007/04/01 2007.

[178] P. R. Start, S. D. Hudson, E. K. Hobbie, and K. B. Migler, "Breakup of carbon nanotube flocs in microfluidic traps," *Journal of Colloid and Interface Science,* vol. 297, no. 2, pp. 631-636, 2006/05/15/ 2006.

[179] M. A. Unger, H.-P. Chou, T. Thorsen, A. Scherer, and S. R. Quake, "Monolithic Microfabricated Valves and Pumps by Multilayer Soft Lithography," *Science,* vol. 288, no. 5463, pp. 113-116, 2000.

Chapter 3: Point-and-planar electrode microwell platform
(Adapted from published book chapter)

Applications of Electrokinetics and Dielectrophoresis on Designing Chip-Based Disease Diagnostic Platforms
Ezekiel O. Adekanmbi and Soumya K. Srivastava
Submitted: August 21st, 2018; Reviewed: November 21st, 2018; Published: May 17th, 2019
DOI: 10.5772/intechopen.82637

Chapter summary

In Chapter 2, the three commonly utilized methods used to characterize bioparticles were discussed with various electrode configurations. Some electrode fabrications required focused-ion beam (FIB) technology while others required the photolithography process. This electrode set up could be expensive and cumbersome to design and fabricate. Besides, they are generally metal-based electrode with electrode immobility that limits the real-time exploration of cell behavioral effects at various inter-electrode distance i.e. electrode spacing is fixed. Other characterization platforms, where a single measurement takes as long as 30 min, could lead to electrode degeneration after multiple runs [209] and the suspended bioparticle may lose viability before technical replicate experiments are completed. More so, if different device platforms are used for replicate experiments, the challenge of device variation could occur, and this may lead to error in measurements unless such variations are statistically verified to be inconsequential. Even though the variations can be discarded by proofs, using multiple devices with the current characterization methods could be expensive, since, most device fabricating vendors prefer high-volume production and often times, low-volume production can be astronomically expensive especially for low-resource laboratories.

In this chapter, the point and planar electrode microwell (PPM) is introduced as a device platform for bioparticle characterization that works on the principle of dielectrophoresis. The fabrication of PPM using silicone-based polymer and high-grade platinum electrode is discussed. The influence of inter-electrode spacing on dielectrophoretic force is explored numerically using a commercial software package COMSOL Multiphysics and verified experimentally for both eukaryotic and prokaryotic cells. This chapter ends with a mini introduction to chapter four, where the comparison between microwave and radio frequency plasma cleaners for irreversible hydrophilic sealing techniques for PPM is detailed.

3.1 Device architecture

Point-and-planar electrode microwell (PPM) is introduced, here, to overcome the challenges mentioned above. PPM consists of two platinum electrodes, variable-height perforated poly(dimethylsiloxane) (PDMS) sandwiched between two 1 mm thick borosilicate glass (Figure 3.1). The microwell in the PDMS is about 3 mm in diameter to enhance faster equilibration of the bioparticle

suspension. Microwell smaller than 3 mm diameter leads to enormous distractions due to diffusion and larger diameter causes electrode-tip to lift off leading to the electrode-pair being on different planes, thereby, impairing judgement regarding pDEP and nDEP cell response visualization using microscopy. The electrodes are in a fixed-variable mode i.e. the planar electrode is fixed but the point electrode can be varied with respect to its position in space. This variable inter-electrode distance allows for the exploration of the bioparticle response dependence i.e. nDEP and pDEP on the strength of the electric field at a fixed voltage. Too large interelectrode distance would prolong the bioparticle's residence time in the nDEP or pDEP domain as the frequency of the signal is varied. Since the integrity of the cells can be altered at longer residence time, the accuracy of such measurements might be affected. When the electrode spacing is too small, some bioparticles may be forced to experience pDEP too strongly and this may increase biofouling at the electrode thus leading to electrode degradation. Balancing this electrode spacing with the applied AC voltage can help prevent bioparticle lysis or electrolysis at the electrodes within the characterization PPM platform.

Another significant advantage of PPM is the cost involved in fabrication, since it is not expensive to fabricate due to the usage of flexible electrode design and polydimethylsiloxane (PDMS) polymer. Apart from the aforementioned advantages, PPM also has the flexibility of being constructed with variable height. This enhances optical clarity during experimentation with bioparticle of relative sizes. The response time to transition from nDEP to pDEP and vice versa is short (~2 min) and this confers another advantage to use PPM. To fabricate PPM, an elastomeric material (sylgard 184 silicon elastomer base) is mixed with its cross-linking agent and the mixture is degassed (using Dekker Vacuum pump in a converted desiccating chamber) to remove any air resulting in an optically clear slurry that is thermally cured at 70^{o}C for 90 min in a Blue-M oven. Cured elastomer is peeled, diced, and perforated prior to the onward cleaning, sealing, and final assembly of the characterization device platform. Figure 3.1 shows the steps required for making the microwell system.

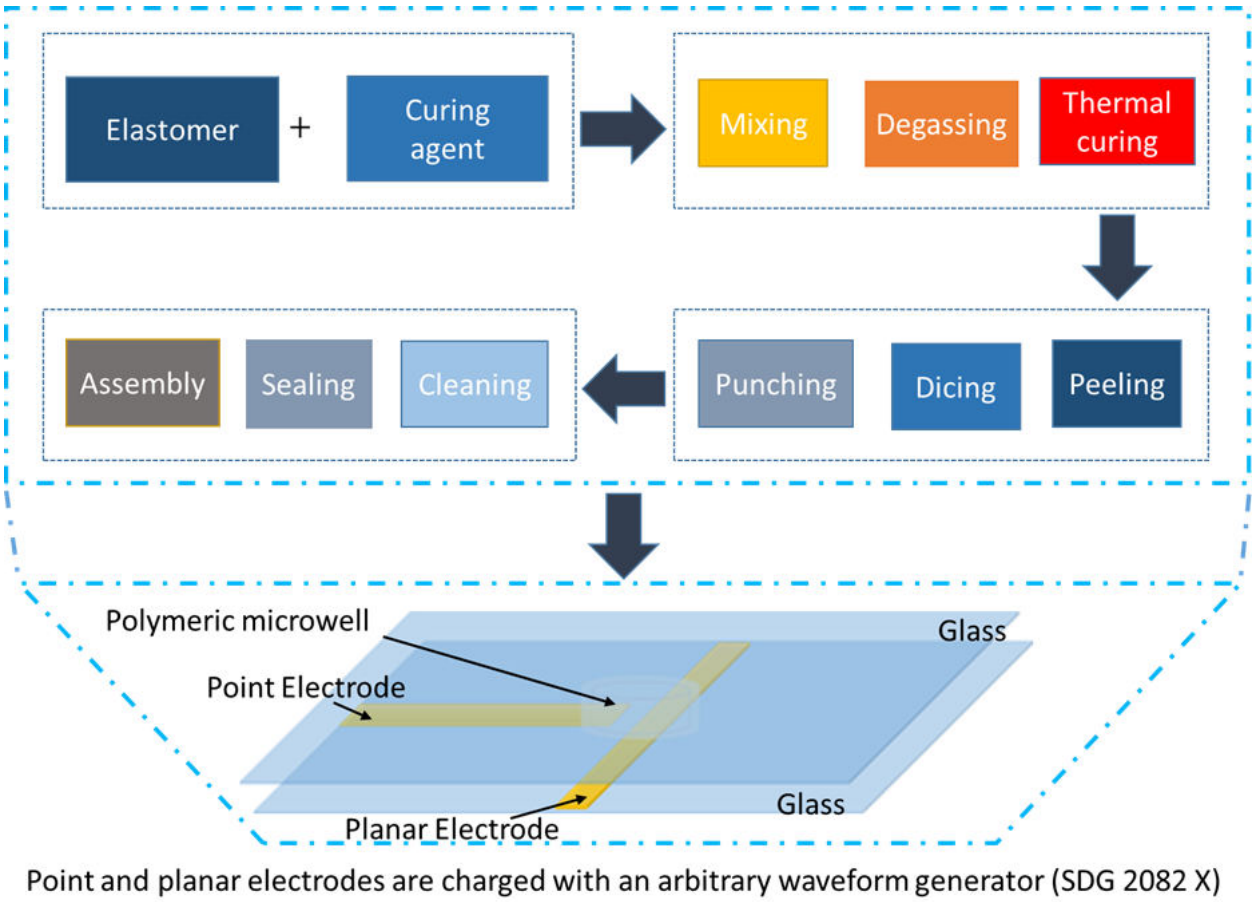

Figure 3. 1 *The construction of point and planar electrode microwell (PPM) platform. A choice elastomer as justified in section 3.2.1 was used to create the microwell while the microwave plasma generation system mentioned in section 3.2.3 was used for it sealing and rendering it hydrophilic.*

3.2 Device Operating Principle

The PPM device platform works on the principle of dielectrophoretic crossover frequency measurement [210-214]. The DEP force and the Clausius Mossotti factor given in chapter 2, eqns. 2.6 and 2.7, guides the operation of PPM. Whenever two equal but parallel plates with opposite signs (positive and negative) are separated by a predetermined distance, an electric field is produced between them. This electric field (direct current (DC) electric field in this case), represented in Figure 3.2, is uniform.

When a positive or negative net charge is introduced between these plates (Figure 3.2 B and C), the positively charged particle will move towards the negatively charged electrode (cathode) while the negatively charged particle will migrate to the positively charged electrode (anode) in a manner that is consistent with the basic principle of electrostatics. This sign-guided movement of charged particles in a uniformly distributed electric field is termed electrophoresis (EP). If, however, a neutral particle is placed between the electrodes (Figure 3.2 D), the principle of charging by induction takes place. From

physical science, neutral particles are known to contain equal number of protons and electrons. When a neutral

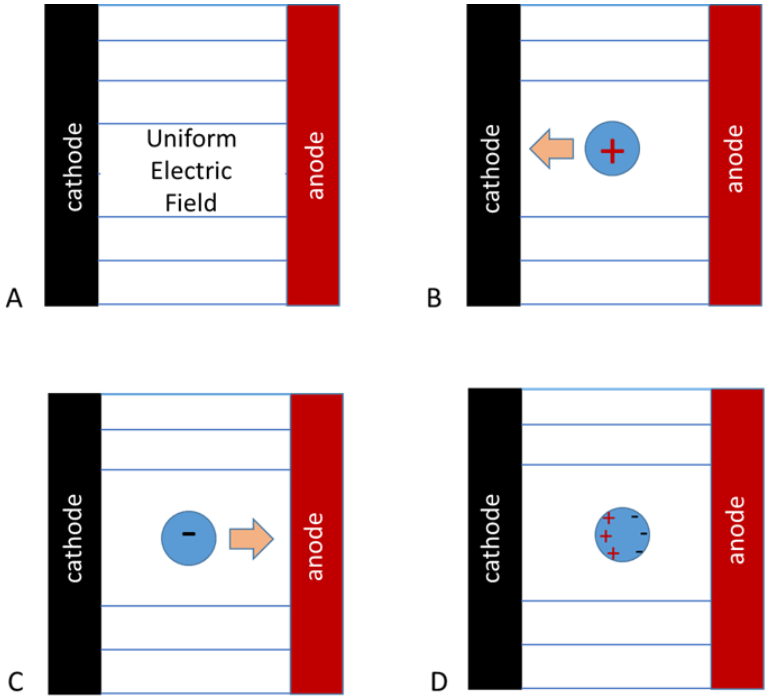

Figure 3. 2 *(A) Cartooned representation of uniform electric field between two parallel and equal-length electrode functionalized with DC signal. (B) positively charged particle is attracted by the cathode (C) negatively charged particle is attracted by the anode. (D) a neutral particle becomes charged by induction, hence, no net attraction to either poles.*

particle is placed in a uniform electric field, the side closer to the anode develops negative charges while the other side develops positive charges. The charges that are developed on either side of the particle aid in equal electrostatic interactions with the respective electrodes. This prevents any net movement of the particle.

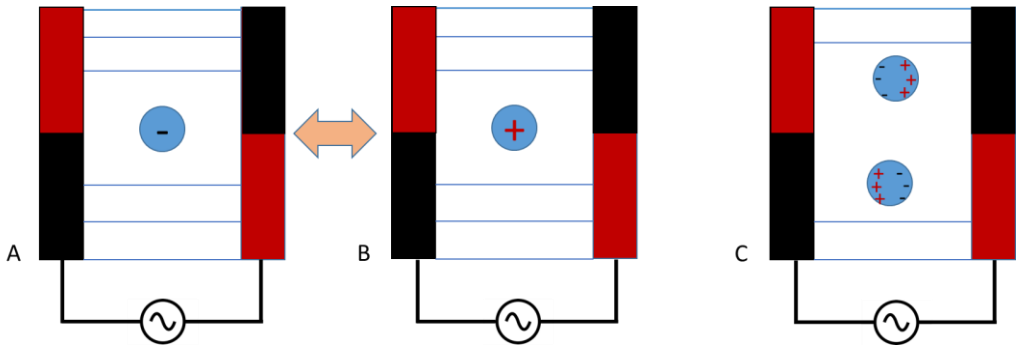

Figure 3. 3 *Charged particles (A) positive and (B) negative between two same-length electrodes connected to an AC source. (C) Neutral particle between two same-length electrodes connected to an AC source. (The red and black at each electrode indicates the sinusoidal signal switch from positive to negative)*

The no-net-movement of the particle stems from equal strength of the electric field everywhere between the two electrodes. This neutral particle, which is now said to have become polarized, forms a dipole within the uniform electric field. Depending on the nature of the particle, a torque may be generated (if the particle is elongated or have unequal polarizability) or not (if the particle is spherical or isotropic in its polarizability) even though there is no net translational movement [215].

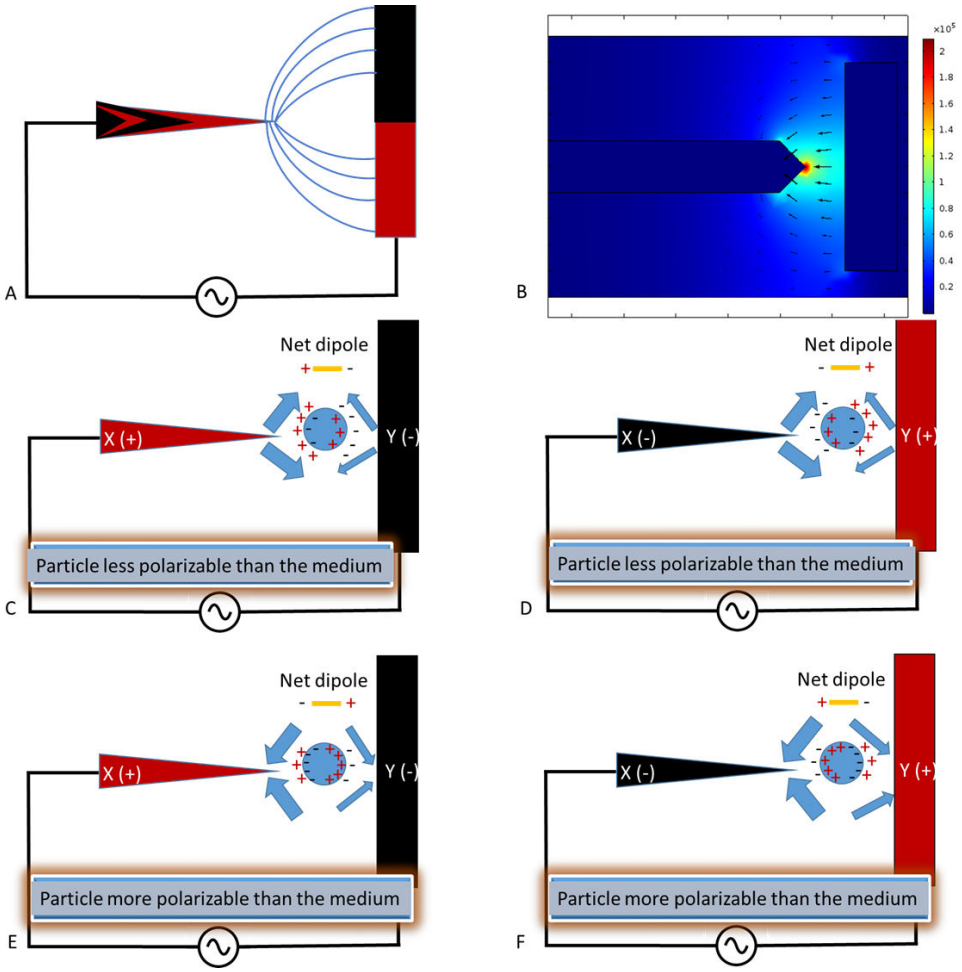

Figure 3. 4 *Non-uniform field effects on neutral but polarizable bioparticles. (A) non-uniform field lines representing the unequal field strength is numerically demonstrated in (B) where COMSOL simulation of PPM functionalized with 8 V_{pp},100 kHz AC signal was performed. (C) shows neutral particle experiencing negative dielectrophoretic (nDEP) force within the field. (D) When the charge on the electrode in (C) is switched, the same nDEP effect is observed. (E) Here the particle is more polarizable than the medium and positive dielectrophoresis (pDEP) is in effect. (F) Switching the polarity of the electrodes in (E) resulted in the same pDEP effect observed by the bioparticle. Hence, there is no dependency on electrode polarity, the response of cells will be the same. The bigger arrows point to the dominant dielectrophoretic force and the cells response.*

The phenomenon by which a neutral particle develops a dipole, i.e. polarization, has been discussed in Chapter 2, section 3.0. If the DC voltage source in Figure 3.2 is replaced with an alternating current (AC) source, then Figure 3.2 is no longer true, since, at any instance, the charges on the electrode keep alternating between negative and positive values. As a result, there is no net movement observed,

if the charged particles are placed between the electrode even though some pseudo-stationary vibrations / oscillations of the particles may be observed (Figure 3.3A and B). If the charged particle is replaced along a neutral particle as shown in Figure 3.3C, similar observation as with DC source is seen but with slight back-and-forth oscillation of the particle due to the charge switching by the electrodes.

With the point-and-planar electrode arrangement (Figure 3.4), the electric field is rendered non-uniform in agreement with the principle of dielectrophoresis (DEP). However, because the dielectrophoretic force relies not only on the properties of the bioparticles but also on the particle's suspending medium, Figure 3.4 will be explained in terms of both the particle and the suspending medium characteristics.

Assuming a neutral (polarizable) bioparticle is suspended in a very conductive medium, both the particle and the medium will be polarized under an external electric field effect. At any instant within the AC field between electrodes X and Y, the electrode polarity is such that X is positive, and Y is negative. So, the neutral particle suspended between electrodes X and Y will be polarized as shown in Figure 3.4C. Because the medium is highly conductive, many counter ions from the medium will build up at the interface between the particle and the medium resulting in a net dipole as shown in Figure 3.4C. In the non-uniform electric field set up between electrodes X and Y, the strength of the electric field is high at X than at Y (Figure 3.4B).

With the medium more polarizable than the particle, and the strength of the field higher at X, the negative-negative repulsive force at X is greater than the positive-positive repulsive force at Y, hence the particle is pushed away from X towards Y: negative dielectrophoresis (nDEP). If the electrode polarity is switched, the same nDEP effect on bioparticles will be observed (Figure 3.4D). When the reverse occurs such that the particle is more polarizable than the medium (Figure 3.4E), there is a switch in the net dipole orientation and the attractive force by the anode (X) on the dipole is more than that of the cathode. Hence, the dipole is pulled towards X: positive dielectrophoresis (pDEP). If at another instant the electrode polarity is switched such that the X is the cathode and Y is the anode (Figure 3.4F), the same pDEP effect will be observed since the orientation of the dipole is a function of the electrode polarity. At equal polarizability of the particle and the medium, there will be no net movement of the particle. In other words, the particle appears non-responsive to the external field effects as discussed in Chapter 2, termed as crossover frequency.

3.3 Device Fabrication

There are three factors to be considered while constructing a point-and-planar microwell system: materials, field gradient (a function of inter-electrode spacing), and assembly method. Here, each of these factors is discussed with emphasis on materials and field gradient. Chapter 4 is completely dedicated to device assembly with detailed surface effects analysis for bio-applications.

3.3.1 Choice of materials

In electrokinetics (a branch of physics that studies the motion of neutral or charged particles under the influence of electric currents), several materials can be used to house bioparticles for diverse analyses. Examples include glass [216, 217], ceramics [218-220], silicon [221, 222], polymer [223-225], composites [226, 227], hydrogel [228, 229], or paper [230, 231]. The choice of materials depends on the material properties and the purpose of the microdevice platform. However, polymer materials are more commonly used currently [223, 225]. The polymers used for microfluidic applications can be thermoplastic (polycarbonate [232], polyethylene glycol diacrylate (PEGDA) [233], poly-methyl methacrylate (PMMA) [234], fluorinated ethylene propylene (Teflon FEP) [235, 236], polyurethane (PU) [237], polystyrene [238]), elastomer poly(dimethylsiloxane) (PDMS) [239, 240], or thermoset polyester (TPE) [241, 242].

Here, PDMS elastomer is chosen because of its unique flow properties, non-toxic nature, high transparency, high deformability, high gas permeability, low auto-fluorescence, and low cost [243]. PDMS also has the advantage of being cured with moderate heat or at ambient condition without any need for ultraviolet or argon light source. This PDMS is complimented with borosilicate glass to enhance visibility under the microscope. To supply the electric field, platinum (Pt) electrodes are being utilized because of their high corrosion resistance, phase boundary impedance, and charge injection capacity [244].

3.2.2 Choice of inter-electrode spacing

The distance or spacing between the two Pt electrodes determines the magnitude of the electric field between them. The shape of the point electrode (Figure 3.4) also determines the spatial distribution of the electric field. It is important to note that if there is a change in shape and distance, then there is a shift in nDEP and pDEP residence times, thus shifting the crossover frequency. A substantial shift in crossover frequency occasioned by a shift in nDEP and pDEP domain will affect the estimated dielectric properties i.e. capacitance and conductance of the particle. Details of the effects of electrode geometry and interelectrode spacing on crossover frequency values has been given in Chapter 8, section 8.1.1. In this chapter, the effect of electrode spacing is numerically tested on the DEP factor (i.e. the magnitude of the dot product of the electric field, |E. E|) that will influence the dielectrophoretic force experienced by any polarizable particle suspended between the electrodes. This gradient of electric field, |E. E|, is originally embedded in the DEP equation. i.e. eqn. 2.6. Thus the equation representing the DEP force [245] modified from eqn. 2.6 can be written as;

$$\mathrm{F_{DEP}} = 4\pi r^3 \varepsilon_0 \varepsilon_m \mathrm{Re[CM]}(\mathrm{E}.\nabla)\mathrm{E} \qquad (3.1)$$

With vector transformation as given by Pethig, in reference to Hsu *et al.* [246] gives:

$$2(\mathrm{E}.\nabla)\mathrm{E} = \nabla(\mathrm{E}.\mathrm{E})\text{-}(\mathrm{E}.\nabla)\mathrm{E}\text{-}\mathrm{E}\times(\nabla\times\mathrm{E})\text{-}(\mathrm{E}\times(\nabla\times\mathrm{E}) = \nabla(\mathrm{E}.\mathrm{E}) \qquad (3.2)$$

leading to: $$F_{DEP} = 2\pi r^3 \varepsilon_0 \varepsilon_m \mathrm{Re}[CM] 2(E.\nabla)E \quad (3.3)$$

The DEP eqn. 3.3 is the same as given in eqn. 2.6. Hence, the knowledge of |E. E| gives an indication of the variation in the dielectrophoretic force within the microwell.

The numerical approach for this investigating the electrode spacing effect involves designing three different geometries for the point electrode while fixing the planar electrode (Figure 3.5). The electrodes were charged with 8 V_{pp} ($\pm$4V) to set up a distribution (gradient) of electric field while Laplace equation (($\nabla^2\varphi = 0$), in stationary mode, was solved via AC/DC module in COMSOL Multiphysics software. The Laplace equation was solved without any recourse to either Navier-Stokes (for the transport of momentum) or convection-diffusion equation (for the transport of mass) to track only the effects of the electric field. This decoupling of the forces saved both time and computational resources while still achieving the goal of the project. Details of the use of Laplace equation to explore the distribution of electric field effects have already been reported [247]. Different electrode shapes were used so that the region of high field strength can be spatially recognized to assist the pinning-down of both pDEP and nDEP regions during experiments. Being able to compute the spatial gradients of the electric field is very important not only for bioparticle characterization but also to enrich and sort bioparticles.

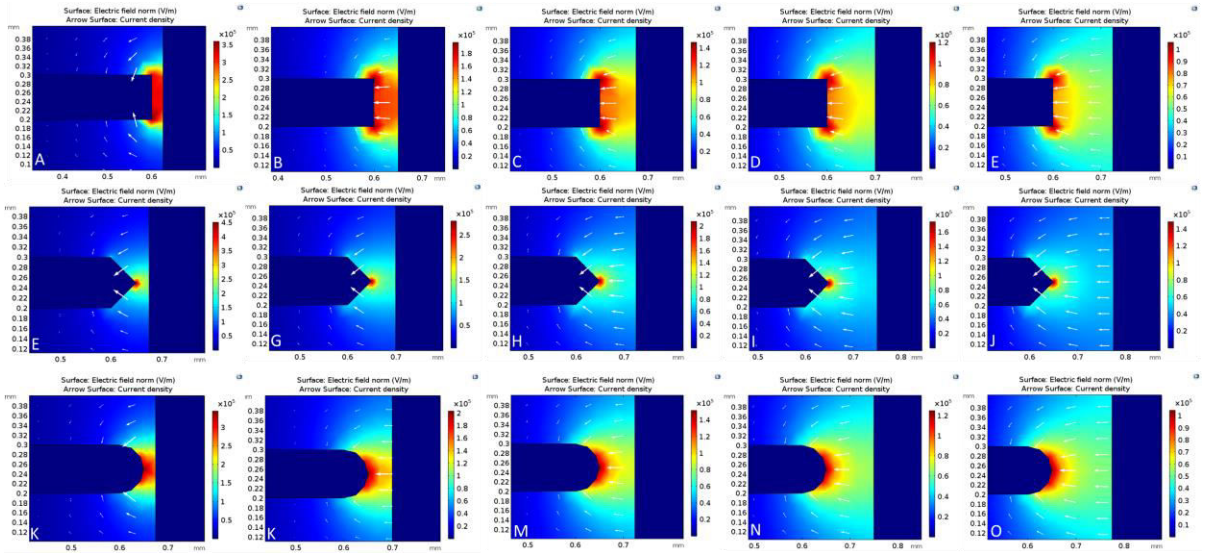

Figure 3. 5 *Effects of electrode shape and inter-electrode spacing on the electric field norm and current density. A-E (top row), F-J (middle row), and K-O (bottom row) consists of progressively varying inter-electrode distance i.e. 25 µm, 50 µm, 75 µm, 100 µm, and 125 µm for three different point-electrode shapes: rectangular (top row), triangular (middle row), and semi-circular (bottom row). Triangular-shaped design has the highest field strength while semicircular has the least.*

As shown in the COMSOL simulation (Figure 3.5), the distribution of the electric field is different for various electrode spacing and shapes of the point electrode. As the distance between the electrodes increases from 25 µm to 125 µm, the maximum electric field strength reduces across the

three designs. In the triangular design, for instance (Figure 3.5 F-J middle row), the maximum field strength at 25 µm and 125 µm are 4.5 X 10^5 V/m and ~1.5 X 10^5 V/m respectively. Also, maximum field strength at 25 µm are 3.6 X 10^5 V/m, 1.05 X10^5 V/m for the square and semicircular design respectively. At 125 µm, their respective field strengths are 3.4 X 10^5 V/m, 1.04 X 10^5 V/m. This shows that the maximum field strength among the designs at a fixed inter-electrode spacing is of the order: $-\nabla V_{triangle} > -\nabla V_{square} > -\nabla V_{semicircle}$. However, at a fixed inter-electrode distance of 125 µm, the maximum field strength of ~1.5 X 10^5 V/m was the highest observed for the triangle design but the field strength was uninfluenced by the square or semicircular shapes. Further, the effect of dielectrophoretic force on these electrode shapes and spacing is explored when a polarizable particle is suspended between the electrodes.

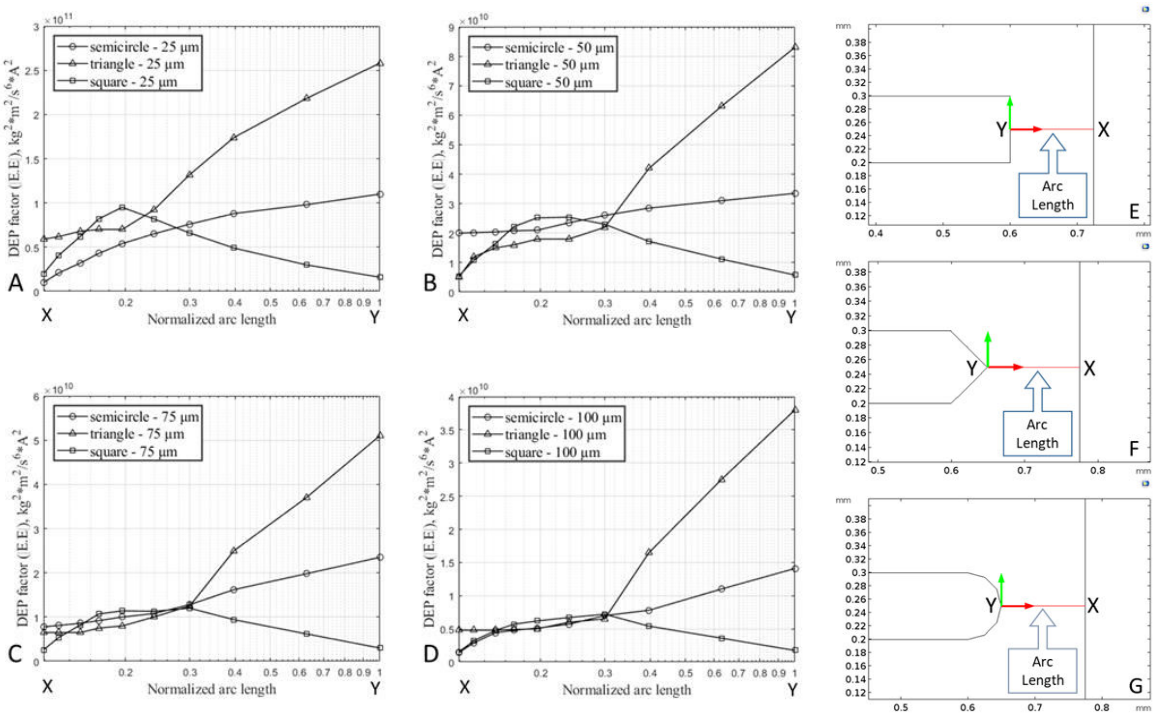

Figure 3. 6 *The plot of the variation of DEP factor along the arc length. A-D represent the variation in DEP factor for 25 µm -100 µm spacing (DEP factor for 125 µm spacing is in Figure 3.7). E-G are the arc lengths for square, triangular, and semicircular electrode shapes respectively with X being the low end and Y, the high end of the DEP factor.*

A cut plane tool was used to define a one-dimensional path along the horizontal axis such that the end of the point electrode is symmetrically connected to the planar electrode. This is commonly defined as the arc length (Figure 3.6 E-G). By numerically calculating the DEP factor as mentioned in eqn. 3.2, its absolute values were tracked along the defined arc length and plotted against the normalized values of the arc length. Figure 3.6 A-D show the variation of the DEP factor at each of the inter-electrode spacing for the three designs. At the lowest spacing (25 µm), triangular and semicircular design show progressive decrease in DEP factor from point Y to X unlike the square pattern that initially

shows a progressive increase up to 80% of the arc length before changing course toward the downward trend. When other spacings were analyzed, the square shaped electrode still displayed a similar trend while other shapes maintained their trend even though there was a progressive decrease in the DEP force experienced by the bioparticle from 50 µm -125 µm.

The physical significance of this result is that, experimentally, bioparticles are expected to cluster around the Y region during pDEP for semicircular and triangular electrodes. However, based on Figure 3.6, bioparticles will not cluster at Y when pDEP is experienced by them. Rather, they will only cluster close to Y depending on the inter-electrode distance. This observation was tested experimentally for both square (Figure 3.7A) and triangle-like (Figure 3.7C) shapes using prokaryotic and eukaryotic cells. The essence of using these two cell types is to show the versatility of the point-and-planar microwell device platform. Figure 3.7B shows bovine red blood cells (RBCs) experiencing pDEP and not attaching completely to the point electrode. This is because the highest DEP factor, according to Figure 3.6 is not at the point electrode (Y), but somewhere in between the two point and planar electrodes. Further experimental validation of the simulation was conducted using bacteria as shown in Figure 3.7D. Figure 3.6 shows that apart from the square shaped electrode, the other two shapes i.e. triangle and semicircular would have their highest DEP factor at Y. As seen in Figure 3.7D, the cells were perfectly attached at the surface of the point electrode during the pDEP regime. In Chapter 8, the details of the device validation are presented and further confirmation on the dependency of the electrode shape and spacing to the crossover frequency will also be discussed.

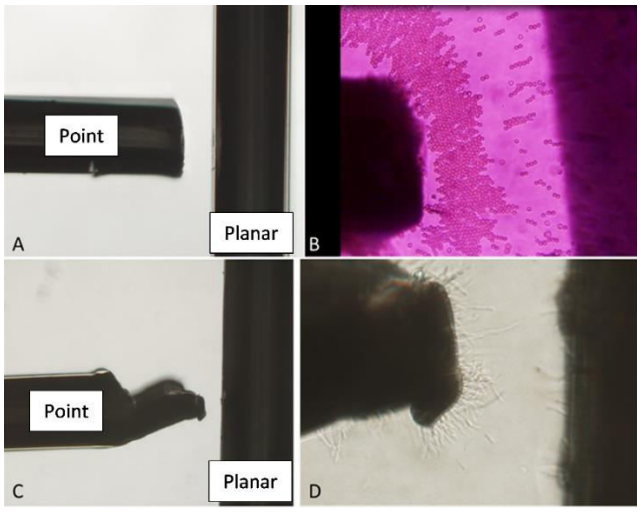

Figure 3. 7 *Positive dielectrophoresis regime in both eukaryotic and prokaryotic cells (A) and (C) are the pre-experimental microwell device platform set-up for square and pseudo-triangular shapes at 100 µm and 75 µm inter-electrode spacing respectively. (B) and (D) are bovine red blood cell and Cupriavidus necator bacteria experiencing pDEP as eukaryotes and prokaryotes respectively. Cells in (B) are farther apart from the point electrode compared to (D) that are present on the surface.*

When the DEP force factor was plotted for each shape as seen in Figure 3.8 (B-D), the dielectrophoretic trend for each of the shapes become more pronounced. The DEP factor for all the three shapes at 25 µm electrode spacing stands alone with very high DEP forces experienced by the bioparticles. The square shape is also consistent in trend but with a parabolic shaped trend. In Figure 3.8 D, the square shape maintained it hilly nature with a gradual shift in the peak value from left to right. Experimentally, for all electrode shapes at 25 µm spacing, utilizing bovine RBCs at 8 V_{pp} always resulted in electrolysis. However, the observed cell movement was too slow at 125 µm electrode spacing irrespective of the electrode shape. Hence, the PPM device platform through this dissertation was fixed to be operated between 50 -100 µm spacing.

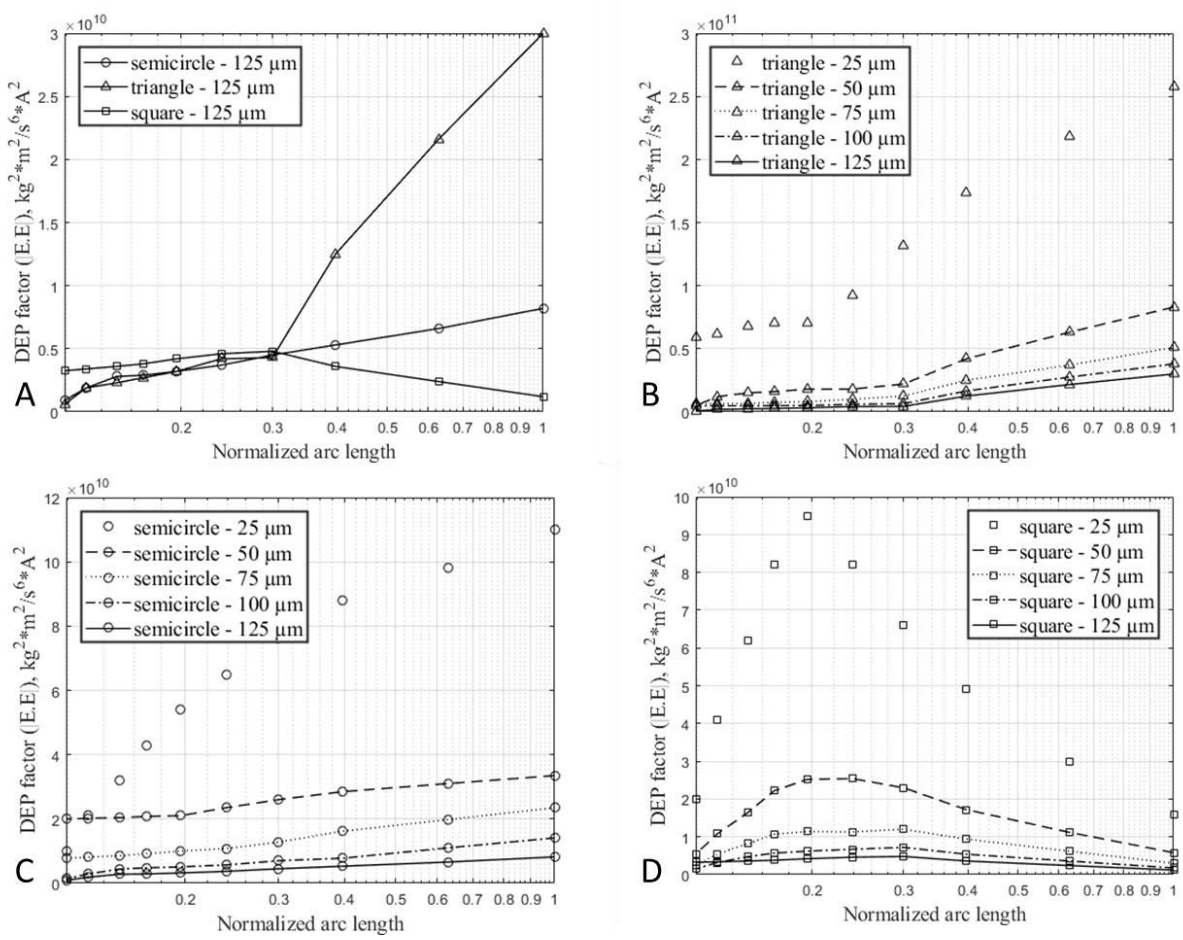

Figure 3. 8 *(A) The plot of the variation of DEP factor with arc length for 125 µm spacing. B-D are the plots combining the variation DEP factor for each shape. At 25 µm spacing the DEP factor is distinctly higher than all other spacing that were explored.*

3.4 Choice of sealing for rendering hydrophilicity

It is common to generate electroosmotic surface flow by sealing of microdevices using the plasma generated through a large span of radio frequency, RF (3 kHz-300 GHz) [248]; however, the generation of plasma in a narrow frequency range, 300 MHz - 300 GHz is possible, also known as

microwave frequency range. Prior to sealing, i.e. creating hydrophilic closed channels, the height of the PDMS channel / platform should be analyzed / predicted based on the size of the bioparticle of interest. The height is usually controlled by the volume of the silicone - curing agent mix as well as the characteristics of the curing mold. When the height is large, it creates more space between the illumination entrance and the objective lens of the microscope. This space, filled with air or water (medium) leads to increased diffraction and reduced clarity/sharpness of the image being viewed under the microscope; although, this space can contain higher volume of sample suspension preventing from drying up. The heat generated from the illumination lamp (argon or otherwise) could cause microliter volume of liquid to heat up and evaporate quickly, a Joule heating phenomenon. This evaporation would cause DEP force to be non-effective as their will be no net dipole within the electric field gradient. Therefore, balancing between the height and the diameter of the microwell is an important laboratory skill that is sharpened with practice.

For hydrophilic sealing, an in-house equipment (MESA-Mgen) generating microwave was constructed, analyzed, and validated against commercially available plasma cleaners i.e. Harrick plasma. The sealing not only ensured a leak-free interface between the polymer and the glass, it also cleansed the surface-off any contaminant. The plasma treatment ensured interaction of the alkyl group on the surface of the polymer to that of the glass and chemically changed them to hydroxyl (-OH) functional group. This in turn lead to hydrophilic nature of the microwell wall (i.e have lower surface energy and lower contact angle) thereby preventing any beading up/ formation of buffer-air convex interface (relative to the air) that adversely interferes with both the optics and spatial distribution of bioparticles. The operation of MESA-Mgen along with its comparison to the commercially available plasma cleaner is the focus of chapter 4.

3.5 Conclusion

The fabrication and numerical / experimental investigation of the point-and-planar microwell (PPM) platform for bioparticle characterization has been discussed in this chapter. The device is fabricated using an elastomeric material (PDMS) with embedded platinum electrodes in point-and-planar configuration sandwiched between borosilicate glass and PDMS. PDMS was chosen because of its excellent properties including non-toxicity, high transparency, high deformability, high gas permeability, low auto-fluorescence, low cost, and ease of curing. Platinum electrode have high corrosion resistance, acceptable phase boundary impedance, and charge injection capacity, making the best choice for electrodes. The two electrodes, planar that is fixed and point with different shapes: triangular, square and semicircular were investigated for high field strength and DEP force.

In terms of high field strength, simulation results showed $-\nabla V_{triangle} > -\nabla V_{square} > -\nabla V_{semicircle}$. The spacing between the planar and point electrode of 25 µm produced DEP factor ($|E.E|$) that was far

higher than the other interelectrode spacing (50-125 µm) for all electrode shapes. Also, the region of higher |E. E| was located at the point electrode for all the point electrode shapes exceptfor the square design where the highest DEP factor was located between the point and the planar electrode depending on the inter-electrode spacing. This observation was verified experimentally with square and pseudo-triangular electrode shapes. Due to the very high and very low DEP factor for 25 µm and 125 µm respectively (as observed from experiments) that created electrolysis and slow bioparticle movements respectively, it was concluded that the point-and-planar microwell device platform is operable between 50-100 µm inter-electrode spacing.

References

[1] M. A. Gencoglu A., "Chemical and morphological changes on platinum microelectrode surfaces in AC and DC fields with biological buffer solutions," *Lab Chip,* vol. 9, pp. 1866-73, 2009.

[2] N. A. K. Bashar Yafouz, Fatimah Ibrahim, "Dielectrophoretic manipulation and separation of microparticles using microarray Dot Electrodes," *Sensors (Basel),* vol. 14, pp. 6356-6369, 2014.

[3] E. A. Castellarnau M., Madrid C., Juares A., Samitier J., "Dielectrophoresis as a tool to characterize and differentiate isogeni mutants of Escherichia coli," *Biophysical Journal,* vol. 91, pp. 3937-3945, 2006.

[4] F. H, "Frequency-modulated wave dielectrophoresis of vesicles and cells: periodic u-turns at the crossover frequency," *Nanoscale Research Letter,* vol. 13, p. 169, 2018.

[5] K. K. Lewpiriyawong N, Yang C, Ivanov V., Stocker R., "Microfluidic characterization and continuous searation of cells and particles using conducting poly (dimethyl siloxane) electrode induced alternating current dielectrophoresis," *Analytical Chemistry,* vol. 83, pp. 9579-85, 2011.

[6] C. I. A. Weng P. Y., Yeh C. K., Chen P.Y., Juang J. Y, "Size-depedent dielectrophoretic crossover frequency of spherical particles," *Biomicrofluidics,* vol. 10, p. 011909, 2016.

[7] H. A. Pohl, *Dielectrophoresis: The behavior of neutral matter in nonuniform electric fields*. New York: Cambridge University Press, 1978.

[8] H. L.-y. Zhu Li, Zhang Wei-yi, "A new fabrication metho for glass microfluidic devices used in micro chemical system," *Sensors and Actuators B: Chemical,* vol. 148, pp. 135-146, 2010.

[9] G. L. Qiang Chen, Qing-Hui Jin, Jian-Long Zhao, Qiu-Shi Ren, Yuan-Sen Xu, "A rapid and low-cost procedure for fabrication of glass microfluidic devices," *Journal of microelectromechanical systems,* vol. 16, pp. 1193-1200, 2007.

[10] J. N. H. Govindarajan Natarajan, "3D cermaic microfluidic device manufacturing," *Journal of Physics: Conference Series,* vol. 34, pp. 533-539, 2006.

[11] B. B. Walter Smetana, Ibrahim Atassi, Philipp Kugler, Erwin Gaubitzer, Michael Edetsberger, Gottfried Kohler, "A ceramic microfluidic device for monitoring complex biochemical reactive systems," *Biomedical Engineering Systems and Technology. Communications in Computer and Information Science,* vol. 52, 2009.

[12] C. I. R. Pamela N. Nge, and Adam T. Woolley, "Advances in microfluidic materials, function, intergration and applications," *Chemical Reviews,* vol. 113, pp. 2550-2583, 2013.

[13] H. M. Harris N. R., Beeby S., Shen Y., White N. M., Hawkes, J. J., Coakley W. T., "A silicon microfluidic ultrasonic separator," *Sensors and Actuators B: Chemical,* vol. 95, pp. 425-434, 2003.

[14] L. X. ZhenBang Qi, Yi Xu, Junjie Zhong, Ali Abedini, Xiang Cheng, David Sinton, "Disposable silicon-glass microfluidic devices: oreicse, robust and cheap," *Lab chip,* pp. 3872-3880, 2018.

[15] L. E. L. Holger Becker, "Polymer microfluidic devices," *Talanta,* vol. 56, pp. 267-287, 2002.

[16] C.-W. Tsao, "Polymer Microfluidics: SImple, Low-cost Fabrication Process bridging academic lab research to commercialized production," *Micromachines (Basel),* vol. 7, p. 225, 2016.

[17] M. T. Arroyo, L. J. Fernández, M. Agirregabiria, N. Ibañez, J. Aurrekoetxea, and F. J. Blanco, "Novel all-polymer microfluidic devices monolithically integrated within metallic electrodes for SDS-CGE of proteins," *Journal of Micromechanics and Microengineering,* vol. 17, pp. 1289-1298, 2007/06/05 2007.

[18] Y. Gao, G. Stybayeva, and A. Revzin, "Fabrication of composite microfluidic devices for local control of oxygen tension in cell cultures," *Lab on a Chip,* vol. 19, pp. 306-315, 2019.

[19] C.-C. Huang, M.-D. Wu, D. Liang, J. Yu, P.-J. Shih, and W.-P. Shih, "Fabrication and Application of Iron(III)-Oxide Nanoparticle/Polydimethylsiloxane Composite Cone in Microfluidic Channels," *Journal of Nanomaterials,* vol. 2012, p. 10, 2012.

[20] S.-Y. Cheng, S. Heilman, M. Wasserman, S. Archer, M. L. Shuler, and M. Wu, "A hydrogel-based microfluidic device for the studies of directed cell migration," *Lab on a Chip,* vol. 7, pp. 763-769, 2007.

[21] H.-J. Koo and O. D. Velev, "Design and characterization of hydrogel-based microfluidic devices with biomimetic solute transport networks," *Biomicrofluidics,* vol. 11, p. 024104, 2017/03/01 2017.

[22] A.-l. Zhang and Y. Zha, "Fabrication of paper-based microfluidic device using printed circuit technology," *AIP Advances,* vol. 2, p. 022171, 2012/06/01 2012.

[23] A. K. Yetisen, M. S. Akram, and C. R. Lowe, "Paper-based microfluidic point-of-care diagnostic devices," *Lab on a Chip,* vol. 13, pp. 2210-2251, 2013.

[24] D. Ogończyk, J. Węgrzyn, P. Jankowski, B. Dąbrowski, and P. Garstecki, "Bonding of microfluidic devices fabricated in polycarbonate," *Lab on a Chip,* vol. 10, pp. 1324-1327, 2010.

[25] T. Yu, S. Yang, C. Fu, M. Liu, L. Hsu, and C. Liu, "Integration of organic opto-electrowetting and poly(ethylene) glycol diacrylate (PEGDA) microfluidics for droplet manipulation," in *2011 16th International Solid-State Sensors, Actuators and Microsystems Conference*, 2011, pp. 2307-2310.

[26] J. M. Li, C. Liu, X. D. Dai, H. H. Chen, Y. Liang, H. L. Sun, H. Tian, and X. P. Ding, "PMMA microfluidic devices with three-dimensional features for blood cell filtration," *Journal of Micromechanics and Microengineering,* vol. 18, p. 095021, 2008/08/13 2008.

[27] K. Ren, W. Dai, J. Zhou, J. Su, and H. Wu, "Whole-Teflon microfluidic chips," *Proceedings of the National Academy of Sciences of the United States of America,* vol. 108, pp. 8162-8166, 2011.

[28] W. H. Grover, M. G. von Muhlen, and S. R. Manalis, "Teflon films for chemically-inert microfluidic valves and pumps," *Lab on a chip,* vol. 8, pp. 913-918, 2008.

[29] I. Polenz, D. A. Weitz, and J.-C. Baret, "Polyurea Microcapsules in Microfluidics: Surfactant Control of Soft Membranes," *Langmuir,* vol. 31, pp. 1127-1134, 2015/01/27 2015.

[30] C. Y. Chan, V. N. Goral, M. E. DeRosa, T. J. Huang, and P. K. Yuen, "A polystyrene-based microfluidic device with three-dimensional interconnected microporous walls for perfusion cell culture," *Biomicrofluidics,* vol. 8, pp. 046505-046505, 2014.

[31] J. Friend and L. Yeo, "Fabrication of microfluidic devices using polydimethylsiloxane," *Biomicrofluidics,* vol. 4, p. 026502, 2010.

[32] E. Gencturk, S. Mutlu, and K. O. Ulgen, "Advances in microfluidic devices made from thermoplastics used in cell biology and analyses," *Biomicrofluidics,* vol. 11, pp. 051502-051502, 2017.

[33] G. S. Fiorini, G. D. M. Jeffries, D. S. W. Lim, C. L. Kuyper, and D. T. Chiu, "Fabrication of thermoset polyester microfluidic devices and embossing masters using rapid prototyped polydimethylsiloxane molds," *Lab on a Chip,* vol. 3, pp. 158-163, 2003.

[34] G. S. Fiorini and D. T. Chiu, "Disposable microfluidic devices: fabrication, function, and application," *BioTechniques,* vol. 38, pp. 429-446, 2005/03/01 2005.

[35] E. p. a. p. microfluidics. PDMS: A REVIEW [Online]. Available: https://www.elveflow.com/microfluidic-tutorials/microfluidic-reviews-and-tutorials/the-poly-di-methyl-siloxane-pdms-and-microfluidics/

[36] M. Schuettler, "Electrochemical porperties of paltinum electrodes in vitro: comparison of six different surface qualities," in *Annual International Conference of the IEEE Engineering in Medicine and Biology Society*, 2007, pp. 186-189.

[37] R. Pethig, *Dielectrophoresis : theory, methodology and biological applications*. Hoboken, NJ: John Wiley & Sons, Ltd, 2017.

[38] H. P. Hsu, *Applied vector analysis*, 1st ed. ed. San Diego: Harcourt Brace Jovanovich, 1984.

[39] E. B. Cummings and A. K. Singh, "Dielectrophoresis in Microchips Containing Arrays of Insulating Posts: Theoretical and Experimental Results," *Analytical Chemistry,* vol. 75, pp. 4724-4731, 2003/09/01 2003.

[40] D. A. K. JInwen Zhou, Amanda V. Ellis, Nicholas H. Voelcker, "Surface modification of PDMS-based microfluidic devices," *Microfluidics and Miniaturization,* vol. 33, pp. 89-104, 2011.

Chapter 4: Electro-osmotic surface effects generation in an electrokinetic-based transport device: a comparison of RF and MW plasma generating sources

(Published in Electrophoresis: February 14, 2019)

Ezekiel O. Adekanmbi[1], Jeremiah Dustin[2], Soumya K. Srivastava[1]*

[1] Department of Chemical and Materials Engineering, University of Idaho, Moscow, ID 83844-1021, United States

[2] Department of Nuclear Engineering, University of Idaho, Idaho Falls, ID 83402, United States

Abstract

It is a common practice in insulator-based dielectrophoretic separation to use and reuse PDMS-constructed microdevice for an extended period of time while performing biological and technical replicate experiments. This is usually done to rule out any effects of device variation on separation efficiency. Ensuring that all experimental conditions remain the same is critical to the conclusion that can be drawn from such repeated experiments. One important contributing factor to the flow of materials within the device is electro-osmotic velocity, which stems from the surface condition of the device construction materials. In this paper, we present an affordable microwave-based (MESA-Mgen) oxygen plasma cleaner developed for approximately less than $100 using readily obtainable parts from an average local hardware store with no specialized tools. This low-cost room-air microwave plasma generator was designed using a 400 W, 2450 MHz household microwave oven (Sharp®) for exploring the possibility of sealing polydimethylsiloxane (PDMS) devices onto glass with minimal budgetary commitment. Microfluidic channels generated using MESA-Mgen were evaluated for their electro-osmotic velocities while factors including contact angles, storage-solvent, half-way hydrophobicity period were also explored with MESA-Mgen, and the results were compared to those obtained from the commercially available plasma cleaner (COM-PC). These outcomes revealed that the microwave plasma generation system induced hydrophilicity and ensured leak-free sealing of PDMS substrates in a manner comparable with the commercially available method.

Abbreviations:

PDMS: Poly (dimethyl siloxane)

DMW: demineralized water

EWM: ethyl alcohol-water mixture

HHP: half-way hydrophobicity period

Keywords: Hydrophilic, microfluidics**,** Plasma Cleaner, PDMS microdevice, Sealing microdevice

4.1 Introduction

The flow of fluids in any microchannel can be driven through electrokinetics or mechanical means (micro pumps) [249]. In pump-driven flows, there exists a gradient in pressure distribution between the upstream and downstream flow regions [250]. Incorporating micro pumps into flow devices can increase their bulkiness and add to device microfabrication challenges [251]. It is more conventional to see micro pumps being used for fluid flow involving channels with embedded electrode [252]. However, embedded electrodes can cause fouling. An alternative to embedded electrode configuration is end-to-end electrode arrangement with spatial inter-electrode insulating hurdles [252]. With this arrangement, electric field generated by the electrodes can be used to drive the bulk of the fluid(s) flowing within the channel. This is referred to as electro-osmosis or electro-osmotic pumping [249].

The principle of electro-osmotic pumping takes it origin from the surface characteristics of the polymeric materials (PDMS, in this case), the glass coverslip used in forming the close-channel pathway through which these dielectric fluids flow, and the charge density associated with the flowing fluid [253-255]. Pure glass surface has hydrophilic SiOH groups [256, 257] which behaves like the Bronsted-Lowry acid releasing H+ ions when in contact with polar fluids [250]. However, PDMS polymeric material, which is usually the complementary channel wall surface has repeating units of -$OSi(CH3)_2$ terminals that render the surface hydrophobic. Forcing fluid to flow through hydrophobic fluid channel requires high field energy, which in turn could generate the undesirable phenomenon of electrolysis at the electrodes or Joule heating within the channel. Joule heating would increase the temperature within the device and this in turn will lead to increased dielectric loss.

Therefore, to make the PDMS surface hydrophilic like the glass surface, it must be treated [258, 259]. Numerous techniques have been used to treat PDMS devices some of which are incomplete curing, chemical sealing, surface coating, attachment of active groups, plasma oxidation, and thermal storage time [254, 257, 260]. Oxygen plasma treatment is one of the common surface treatment methods for insulator-based dielectrophoretic (iDEP) separation device. This treatment method is used to replace the $–Si(CH_3)_2$ terminal group with polar functional group -SiOH [261], which generates Si-O-Si bonds [259, 262] that aid the hydrophobic sealing of the treated PDMS on glass or other untreated (native) PDMS surface. One important observation during iDEP device making process is that numerical modeling of the separation device commonly utilizes electro-osmosis as the boundary condition for the fluid flow physics.

This electro-osmotic wall utilizes the electric field values obtained from the solution of the Laplace equation to impact velocity to the bulk fluid flowing within the channel. Both fluid flow and electric current modules, in numerical analysis, are usually solved as time-independent. However, in

experiments, this boundary condition may not be constant throughout the life span of the device owing to the tendency of the channel wall to gradually lose its hydrophobic surface after certain period of time. In this study, therefore, we built a relatively inexpensive device to accomplish plasma treatment and sealing of PDMS using a regular household microwave oven (MESA-Mgen) in a modified manner to McDonalds *et al.* [261] and Ginn *et al.* [263]. We use MESA-Mgen to treat PDMS and then investigate the electro-osmotic velocity parameters of the resulting fluidic channels and compared it with the commercially available cleaner (COM-PC).

Knowing how the electro-osmotic velocity vary within the microchannel could help propose a correlation factor that could account for some reproducibility challenges that are associated with insulator –based dielectrophoretic separation. Details of the fabrication, calibration and testing of MESA-Mgen and MESA-Mgen-treated polymeric materials are given in this present study. Also, the interrelation of the electric field with the treated polymeric materials at specified properties of the suspending medium, contact angle measurements and halfway hydrophobicity periods are explored. With research funding becoming more and more competitive, in-house development of certain research tools could help save cost. MESA-Mgen falls into this category of cost-saving effort toward achieving PDMS surface medication for use in insulator-based dielectrophoretic separation. It is also not uncommon to see researchers incorporating teaching and outreach into their research proposals owing to the need to carry the young generations along the STEM path. MESA-Mgen could also serve as a viable hands-on experience in surface modification arena.

4.2 Methods and Materials

We fabricated MESA-Mgen from a 400W Sharp-brand Household Microwave Oven. A 4” diameter acrylonitrile butadiene styrene (ABS) pipe cap was used as the plasma chamber while a 10.16 cm (4”) diameter sink gasket was adhered to the bottom of the pipe cap using a silicone sealant (3M). Two 1.27 cm (1/2”) diameter holes were drilled into the top of the cap to allow for an air inlet and suction line. High-density polyethylene (HDPE) tubing was used to connect a needle valve on the microwave exterior to form the air inlet. The other HDPE line was connected to a Winters PEM135 vacuum gauge in series with a TMS® single-stage rotary vane 3 CFM HVAC vacuum pump. MESA-Mgen was operated in a copy-exact form as COM-PC. This means that MESA-Mgen was operated in the same manner as recommended by the manufacturer of COM-PC so that both machines can be compared appropriately. Using the inginition pressure limits collated by Law et al, the chamber was pumped down to 0.27mbar. High-purity oxygen gas was introduced as the process gas to initiate the formation of various derivatives of the partially ionized oxygen gas: electrons, ions, neutral atoms/molecules, which have been well reported to be an organic component of plasma. To initiate and maintain the generated palsma, the pure oxygen gas was introduced controllably until the operating

pressure in the chamber was 20 mbar. After plasma exposure, it was necessary to verify the temperature of the exposed PDMS since the dielectric property of PDMS is a function of temperature at a specified frequency. This was done by microsealing low, mid- and somewhat high-melting solids in tiny capillary tubes and laying them on the surface of the PDMS during plasma treatment.

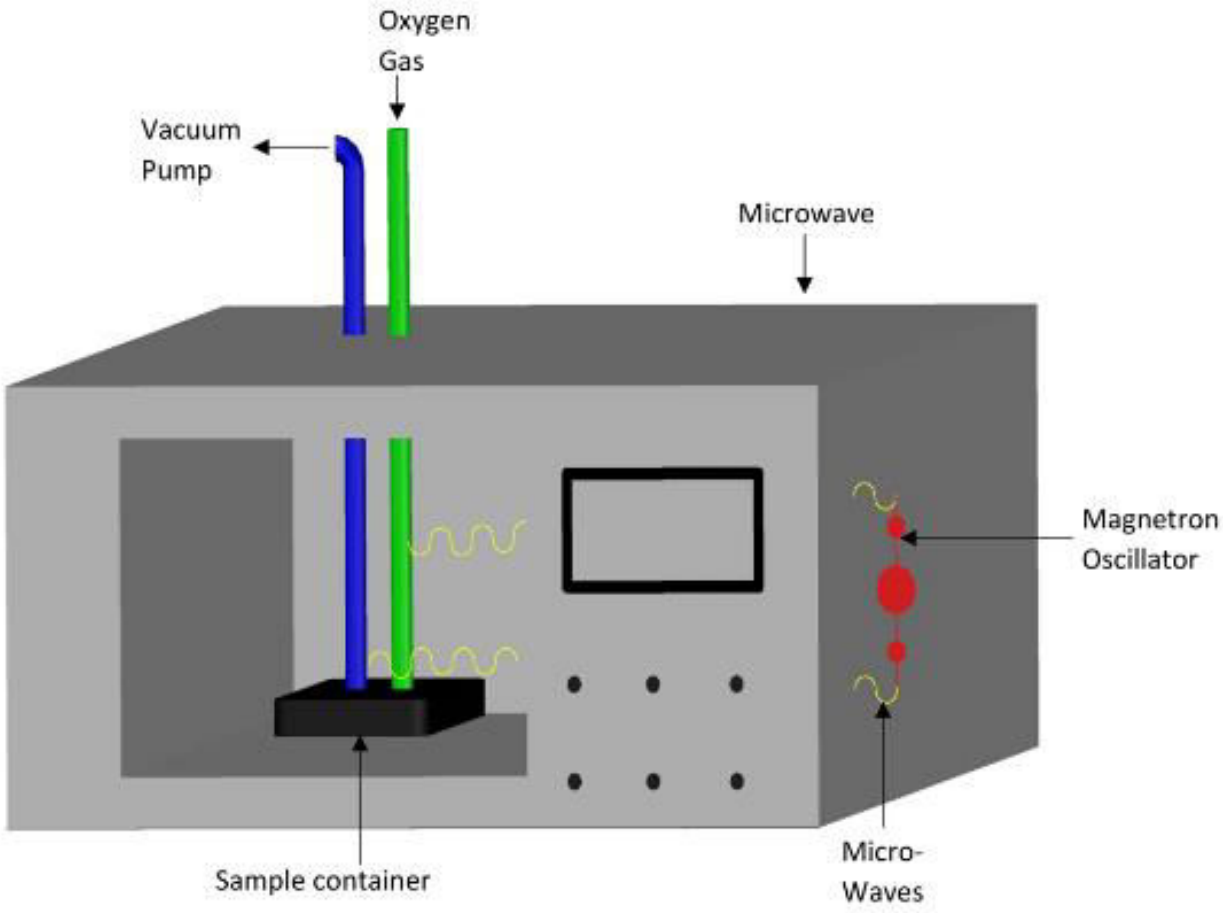

Figure 4. 1 Schematic diagram of the modified microwave oven

PDMS devices were fabricated by standard procedure [252, 264] and diced into 1" X 1" squares. 18 PDMS squares were randomly assigned as experimental units to two treatments (MESA-Mgen and COM-PC). It has been reported that plasma treated surface may lose its hydrophilicity within minutes [253, 262] owing to insufficient exposure period. Over exposed surface, on the other hand, can generate undesirable cracks on the PDMS surface [265]. Hence, each experimental unit was exposed to 1, 2, 4 and 5 min of plasma treatment separately. The water contact angle of untreated (native) PDMS was measured as 108^{o} using 2 µL droplet of isopure water and photographed with Imaging time Source DFK22AUC03 camera and IC Capture 2.2 software.

The first half of the 18 independent experimental units was treated with the 400 W MESA-Mgen with high-purity oxygen as the process gas. The initial static water contact angle of each of the 9 treated experimental units was measured. Treated units were stored under diverse environments to track their contact angles as a function of time. Usually, treated devices that are left in air seem to bounce back to their hydrophobic nature in a short time [263]. Treated PDMS returns to the path of hydrophobicity partly because of the reorientation of the -SiOH from the surface to the bulk part of the material [253], condensation of the hydroxyl group, and the storage conditions such as temperature, humidity and storage solvent [257].

There are certain characteristics that the storage solvent should possess. One such characteristic is that the storage solvent must be polar since PDMS swells in contact with nonpolar solvents [266]. PDMS-based electrokinetic devices are usually fabricated in line with the outcome of the numerical simulation and one of the factors that affect the specific operability of such devices is the channel dimension. Therefore, if PDMS-based electrokinetic devices are allowed to swell, the cross-sectional area of the channel will change [262]. This change in cross sectional area will inadvertently affect fluid flow profile which might cause device failure. Swollen PDMS during storage could also result in delamination of the PDMS if sealed onto glass [263].

As a result, demineralized water (DMW) was chosen as the first storage inorganic solvent owing to its polar nature and a very high cohesive energy density (~548 cal/cm^3): the energy associated with the intermolecular attractions within a unit volume of material [267]. The higher the cohesive energy density (a function of solubility parameter) of a solvent, the lesser the solvent's solubility capacity [262]. Devices stored in DMW were completely immersed in a DMW-filled petri dish and lowered into a vacuum chamber where air bubbles were removed, and the system temperature maintained constant at 68 ^oF. Owing to the comparable cohesive energy density of ethyl alcohol (12.7 cal/cm^3) in relation to its decreased swelling ability, the second solvent chosen was ethyl alcohol-water mixture (EWM) at an arbitrary 20:80 ratio respectively. The second set of sealed devices were stored in EMW under the same condition as pure DMW while the third set of sealed devices were left under room air as control.

Contact angles were independently measured for each of the treated units as a function of time with respect to their corresponding storage solvents. The relaxation time interval was 10 minutes ab initio until half-way hydrophobicity period (HHP), "the length of time required for the treated PDMS to return to half of its native contact angle (108^o) during relaxation", was reached. Thereafter, the time scale was changed to hourly interval, and then days. The whole process was repeated for another set of experimental units but with post-treatment storage in DMW and another set in EWM. It was necessary to obtained HHP because it gives an indication of the rate at which the electro-osmotic wall condition

would decay. More so, comparing the HHPs for the three storage conditions is necessary to explore the storage condition that would generate the highest HHP- a function of the length of time the device will still be useful under electro-osmotic condition. In these storage conditions, the PDMS static water contact angles were measured until HHP was reached or surpassed. The second half of the 18 independent experimental units were treated using COM-PC on high power setting (18 W) at the manufacturing operating condition of ≤ 0.27 mbar with high-purity oxygen as the process gas. Three (3) of these units were each stored in the three storage solvents and their contact angles were monitored with time like the MESA-MGen's. In each of the plasma generating machines, the number of replicates, 4, was calculated as given by Cochran and Cox with power: r = 0.9, and $\propto = 0.05$.

4.3 Results

Figure 4.2 shows the average post-treatment static water contact angles and how they vary with the oxidation time as well as the relaxation period. As seen for MESA-Mgen (Figure 4.2B), 1-minute plasma treatment resulted in the lowest oxidation effectiveness parameter (82^o). We define the oxidation effectiveness parameter as the difference between the native contact angle (108^o) of the PDMS and the post-treatment contact angle at t ≅ 0 s. The experimental unit (PDMS) plasma treated for 5 minutes gave the highest oxidation effectiveness parameter. This means that plasma treating the experimental units for 5 minutes generated more hydrophilicity ab initio. However, as time advanced, 1-minute plasma-treated units seemed more reluctant to return to hydrophobicity (Figure 4.2A and 4.2B). While 1-minute plasma treated units had an HHP of ~30 mins, the 2-, 4-, and 5-min plasma treated units had HHPs of 20, 15, and 12 mins respectively.

This means that in an electrokinetic-based microdevice, PDMS plasma treated for 1 min is expected to give lower electro-osmotic velocity decay rate when compared to the other units treated at the different oxidation times within the same relaxation period (the period within which the measurements were made after plasma treatment). Also, if any experiment were to be performed using the surface treated PDMS immediately, the different pathways of the curves in Figure 4.2A and 4.2B, which reveal the different contact angles relating to hydrophilicity generated at various oxidation (plasma treatment) times, suggest that the oxidation times are important. In an electrokinetic device, variable hydrophilicity may give some variation in the stern layer and cause a change in the Debye length provided the ionic strength of the passing fluid is fixed.

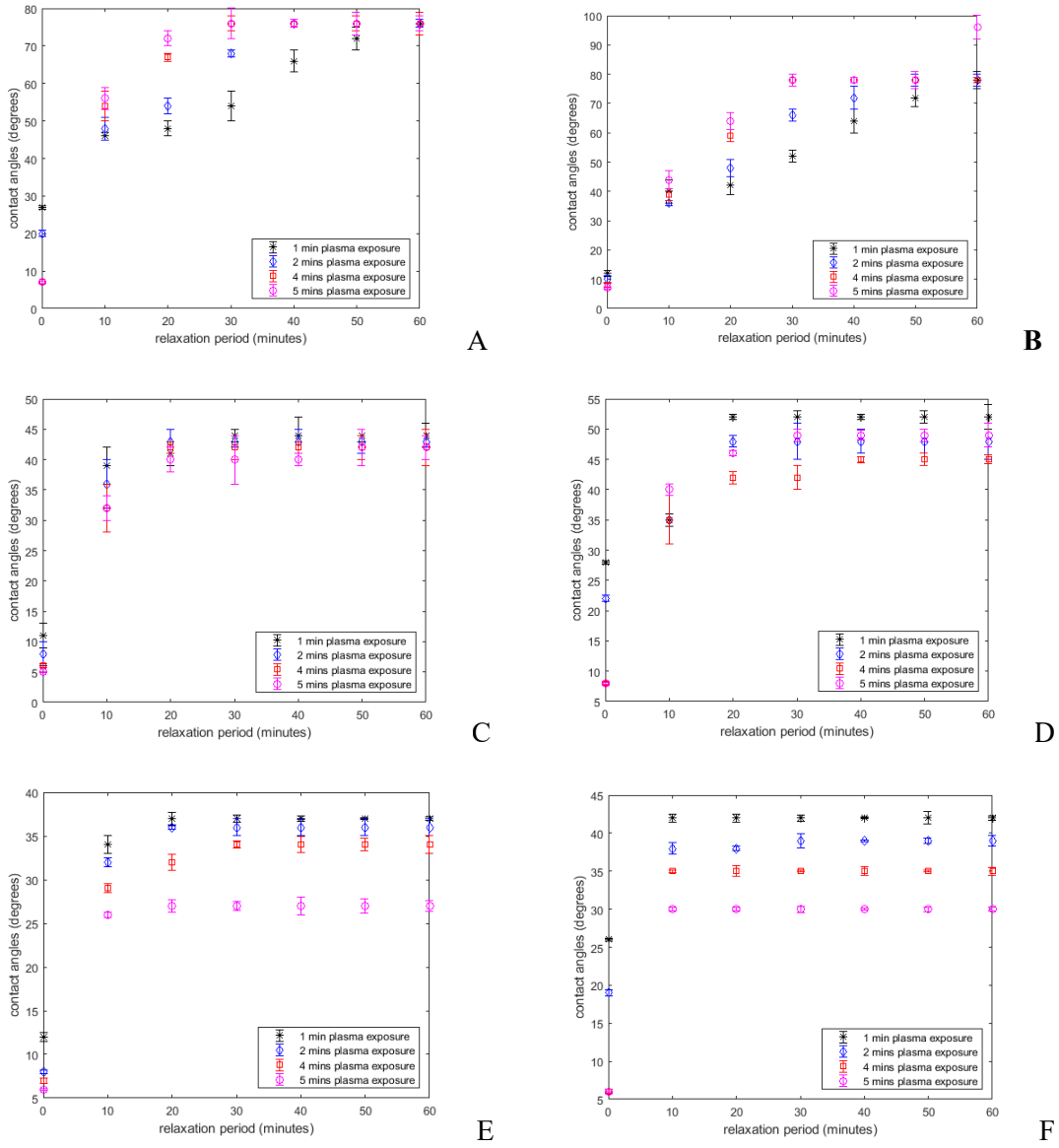

Figure 4. 2 *The plots of average post-treatment static contact angles for COM-PC (A, C, and E) and MESA-Mgen (B, D, and F)-treated PDMS as a function of relaxation period and oxidation time. Each data point is an average of 6 different measurements. A and B were stored in air, C and D in ethanol-water mixture (EWM) and E and F in demineralized water (DMW)*

At time 0 s, the contact angles of COM-PC-treated units (Figure 4.2A) were lower than those treated with MESA-Mgen (Figure 4.2B) irrespective of the oxidation periods. After 1 min oxidation, PDMS devices treated with COM-PC gave an average static contact angle of 12º while those treated with MESA-Mgen averaged 26º. Within 10 minutes, MESA-Mgen treated samples averaged a contact angle of 46 º while those treated with COM-PC were 39 º. This result suggests that the rate at which the generated -OH condenses after plasma treatment is higher in MESA-Mgen treated samples than in COM-PC treated samples. This disparity might have stemmed from the nature of chemical work done through the interaction of the plasma's reactive radical species with the PDMS surface. After this time

interval, the outcomes of both COM-PC and MESA-Mgen seems to follow similar trend until 1 hour. Samples treated with COM-PC were able to quickly exchange their -CH_3 for the -OH bond as compared to MESA-Mgen even though both of them utilized RF oscillating electric field generated through their respective magnetic inductions. The experimental units treated with COM-PC seems to have lower contact angle ab initio, however the contact angles jumped to almost the same value within 30 minutes. Since the utilization of PDMS is for certain t>0 period and that the statistical mixed model repeated measure analysis performed on both COM-PC and MESA-Mgen revealed a P>0.05 and Mauchly's test of P>0.05, we can accept the null hypothesis which states that the observed difference in the outcomes of these two treatment factors are not statistically significant and that the sphericity assumed during the mixed model analysis corroborates the contact-angle data representation.

When the devices treated with both COM-PC and MESA-Mgen were stored in DMW and EWM, they experienced substantial reluctance to return to hydrophobicity. Figure 4.2, C and D show the plots for devices that were stored in EWM after treatment. Both figures show static contact angle ramping within the first 20 minutes of storage in EWM and tend to plateau thereafter. The maximum constant value of the contact angle for COM-PC treated device (Figure 4.2C) was ~45º while that of MESA-Mgen was ~50 º. Again, statistical repeated measures based on the analysis of variance (ANOVA) revealed that the difference between the measurements was not significant. This is an indication that the storage medium was able to assist the retention of hydrophilicity in MESA-Mgen-treated devices in a manner like those treated with COM-PC. In Figure 4.2, E and F, the post-treatment data for devices stored in demineralized water (DMW) was presented. The curves flattened out at a maximum value of ~35º for COM-PC outcomes and ~43º for MESA-Mgen. Hydrophilicity is maintained at constant values for different oxidation times. Obviously, storing the devices in demineralized water after treatment lowers the contact angles considerable as compared to storing in EWM or air regardless of sources of plasma treatment time. The order of storage preference can be written as DMW>EWM>AIR.

Figure 4.3 compares the effects storage medium on the treated devices at a constant oxidation period of 1 min. When the devices were left in air, the HHP values for the outcomes of COM-PC and MESA-Mgen were 27 and 24 min respectively. When stored in EWM, MESA-Mgen-treated PDMS reached its HHP value in 30 min whereas COM-PC treated devices did not until 32 min. In DMW, both treatment factors resulted in devices with consistently lower static contact angles.

Long-time study of these storage solvent revealed a trend as shown in Figure 4.4. For devices left in air, both COM-PC and MESA-Mgen treatments gave comparable outcomes. However, when the devices were stored in EWM and DMW, COM-PC and MESA-Mgen treatments showed slight differed outcomes. But the difference, again, was not considered statistically significant because we failed to

reject the null hypothesis, which states that there is no significant difference between the two treatment outcomes.

After obtaining the HHPs, a new experimental unit was sealed onto plain uncoated glass slide. Prior to the surface treatment and subsequent sealing of the unit onto glass, 3 mm holes were punched with Miltex biopsy puncher to represent the inlet and the outlet channel reservoirs (see Figure 4.5). 50 g/ml dextrose buffer solution was prepared by dissolving 1.25 g of dextrose crystalline solids (weighed with 204 Mettler Electronic Weighing Balance) in 25 ml de-ionized water. The conductivity and pH of the medium (buffer) were measured to be 0.050 S/m and 6.98, respectively, using Accumet XL 200 Ph/mV/conductivity meter.

To verify that the sealing was leak-proof, each of the channel types was filled with 50 g/L dextrose

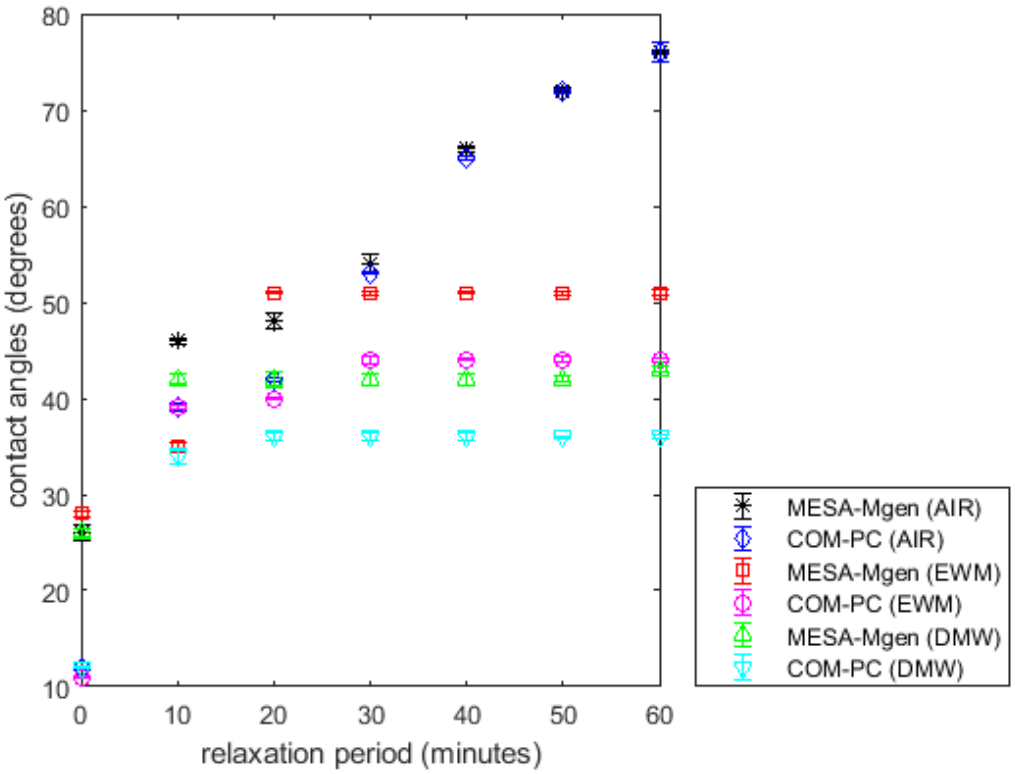

Figure 4. 3 *Effects of storage solvent at 1 min oxidation for PDC-32G and MESA-Mgen-treated samples (1-hr study)*

buffer using 5 µL mechanical pipette until a near static clear convex beads of buffer were seen as the meniscus of the buffer/air interface on both reservoirs. Thereafter, anhydrous $CuSO_4$ was poured around the sealed edges while the whole set-up was left for up to 30 minutes in a controlled environment. At the end of the 30-minute test period, it was found that the white color typified of CuSO4 did not change to blue indicating that the aqueous buffer solution did not have any contact with the test anhydrous

$CuSO_4$. The absence of leakage of fluid suggested that the sealing was substantially leak-proof when both MESA-Mgen and COM-PC were used. Having ensured that the sealing was leak-proof and that no hydrodynamic head was present, any effect of pressure gradients between the channel and the external environment was ruled out. The effects of gravity on the flow was also ruled out as being negligible since the channel depth was 10 µm. Owing to the goniometric observation that the retention of hydrophilicity was enhanced when the devices were stored in water, velocimetric analyses were carried out only on the sealed devices stored in DMW. We connected Labsmith HVS448 3000D High-Voltage Sequencer to the inlet and outlet reservoirs of a straight microchannel through platinum electrodes.

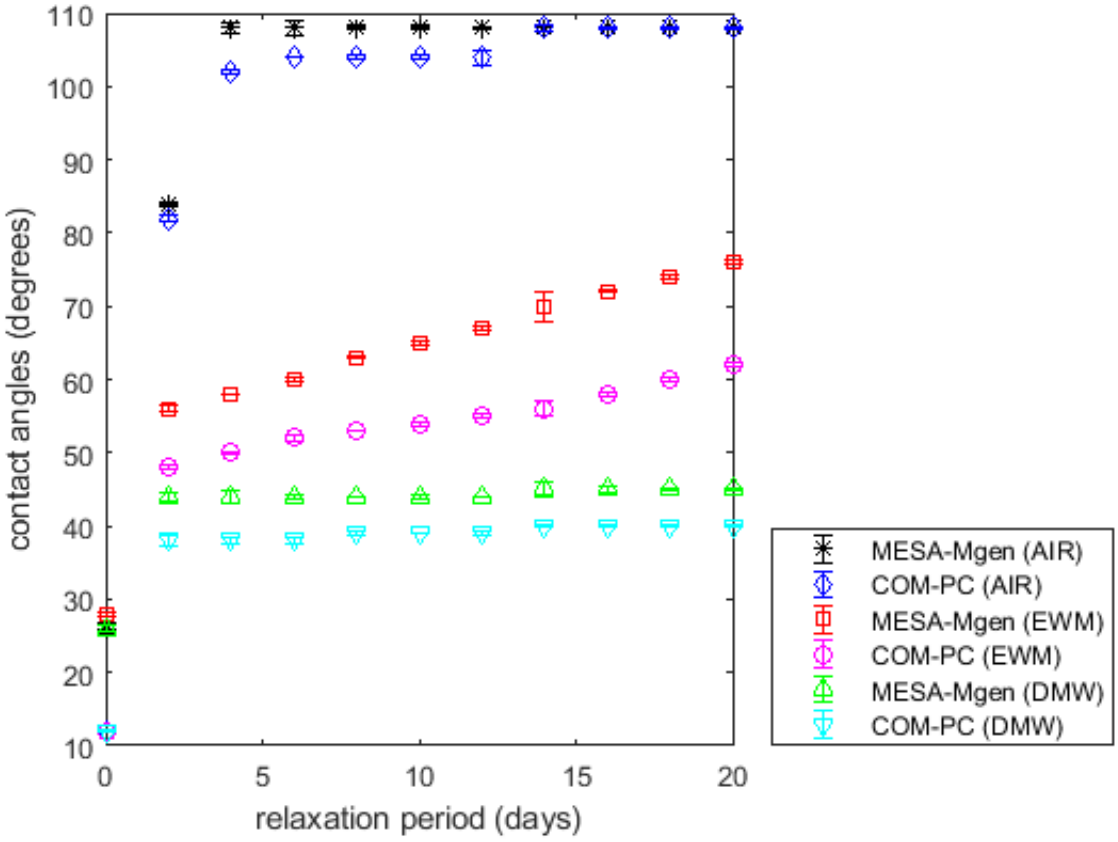

Figure 4. 4 *An extended study of the effects of storage medium at 1min plasma oxidation (3-week study)*

The whole channel was filled with 50 g/L dextrose buffer of pH 6.8 and conductivity 0.045 S/m. The buffer in the inlet reservoir was emptied and replaced with colloidal polystyrene particles (diameter 9 µm) whose particle-particle interactions have been substantially watered down through serial dilution (1:600 twice). By mounting the complete device set-up on Olympus IX71 inverted micoscope, the inter-reservoir distance was measured via computer connected to DP 70 camera.

Before the application of electric potential at the inlet and outlet reservoirs, the polystyrene particles were ensured to be almost static (only vibrating in their positional space). Inlet voltage was set to 2 V and the outlet set to ground. Particle movement was tracked and its total time along the microchannel length was recorded. The movement was purely due to electro-osmosis because the polystyrene particle, by convention, is a neutral particle even though it has slightly negative charge due to the surface charge arising from the fragment of the initiator used to start its polymerization reaction [268]. Tracking was initiated at a domain far away from the inlet reservoir (see Figure 4.5) to ensure fully developed flow and six different repeated measures were observed and recorded for 20 consecutive days to monitor the electro-osmotic velocity decay.

The average electro-osmotic velocity was determined as $\Delta L/\Delta t$. where ΔL is the distance between

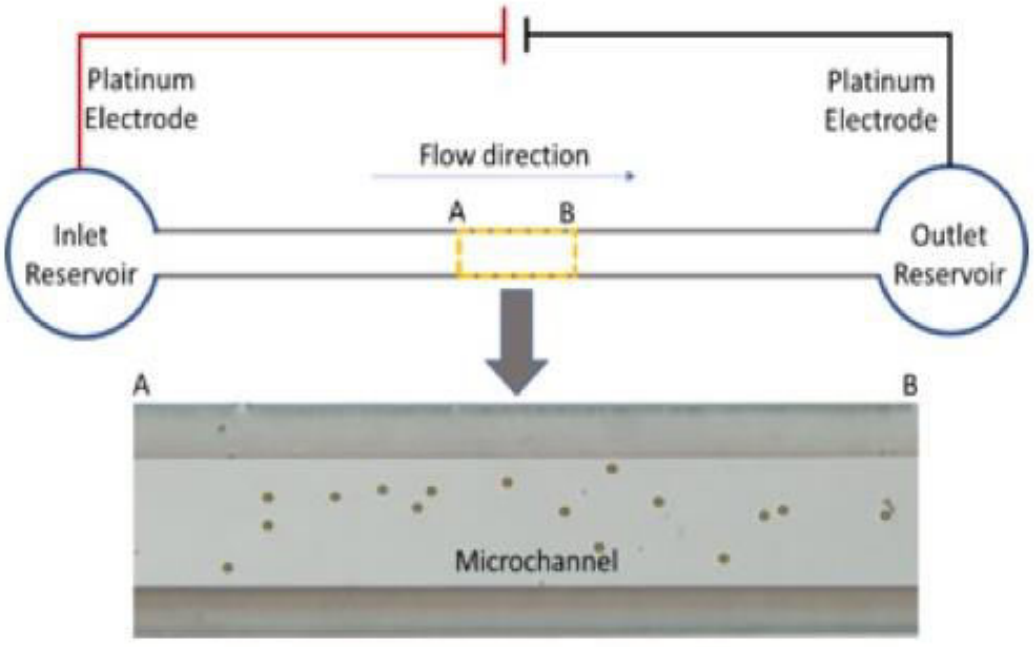

Figure 4. 5 *Migration of polystyrene particles in a uniform microchannel under the influence of electric field. The image shows a 2-D representation of the channel. Channel depth is 10 µm.*

points A and B and Δt is the resident time of a particle within the same AB interval. Particles were assumed to be moving at the same speed as the buffer. The electric field strength calculated from $E = \Delta V/\Delta l$ was expected to be uniform owing to the shape of the channel. For the curves in Figure 6, the potential difference used in calculating the field strength (E) within the 1.2 mm inter electrodes distance are 6V, 12V, 18V and 24V. This correspondingly generated E_1=5 kV/m, E_2=10 kV/m, E_3=15 kV/m and E_4=20 kV/m respectively.

4.4 Discussion and Conclusions

The mean electro-osmotic velocity (U_{EO}) as seen, for both COM-PC and MESA-Mgen outcomes are very similar. At lower field strength, the overlap between the two treatment factors was more pronounced. At 5 kV/m, there was a slight shift in values from day 1 to 4. Any other days afterwards had a decent overlap of values. Slight disparity in electro-osmotic velocity observed from day 3 to day 30 when the field strength was highest (20 kV/m). The main reason for plasma treatment in electrokinetic transport device is to generate electro-osmotic flow. As seen in Figure 6, there is no appreciable difference in U_{EO} values for COM-PC and MESA-Mgen. Therefore, MESA-Mgen works comparable with COM-PC. Also, U_{EO} tend to increase as the strength of the field increase. This corroborates the dependency of U_{EO} on field strength. First, PDMS has a lower zeta potential compared to glass and silicon materials. The zeta potential is the electrokinetic potential at the shear plane that separates the immobilized surface and mobilized fluid.

EOF velocity is proportional to the zeta potential for a paired liquid-solid interface. Therefore, higher

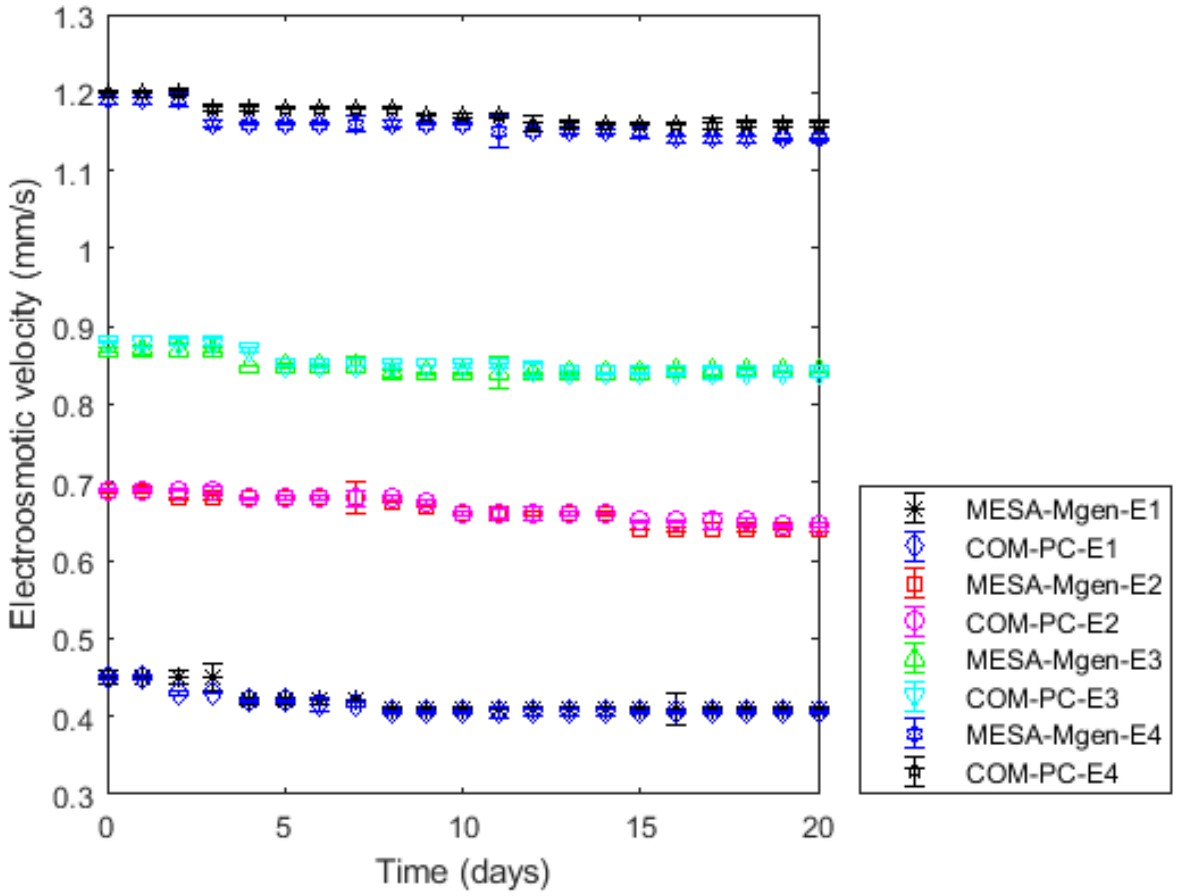

Figure 4. 6 *Mean electro-osmotic velocity of experimental units treated with PDC-32G and MESA-Mgen and stored in DMW as a function of time.*

applied electric fields are needed [9], [10], [11] for PDMS than for glass or silicon materials in order to achieve similar pumping flow rates. The use of higher applied electric fields results in problems like electrolysis at reservoirs and joule heating [10], [12], [13] which further lower down reliability of PDMS devices.

In terms of cost, COM-PC can start near $4,000. The total cost of MESA-Mgen, including vacuum pump, microwave, and fittings was less than $100. For research activities that are laden with finance, MESA-Mgen can be easily made in-house and used since it works comparatively like COM-PC. Even though the treated experimental units by MESA-Mgen reached HHP earlier that those treated using COM-PC, the time difference was not too significant, and the velocimetry showed that they are comparable. More so, when it becomes necessary to investigate some low-pressure discharges for non-routine applications like frictionless power absorption, it is easier to utilize MESA-Mgen since the construction is simple and the plastic head in the chamber can easily be replaced with the needed metallic wall.

Acknowledgements

Special thanks to Dr. Eric Aston for assistance with goniometry and Olympus inverted microscope, and Dr. David MacPherson for assistance with fabrication and testing.

The authors declare no conflict of interest

References

[1] S. Srivastava, A. Gencoglu, and A. Minerick, "DC insulator dielectrophoretic applications in microdevice technology: a review," *Anal. Bioanal. Chem.,* vol. 399, no. 1, pp. 301-321, 2011.

[2] E. Adekanmbi, "Application of Electrokinetics for disease diagnostics," MS, Chemical Engineering, Department of Chemical and Materials Engineering, University of Idaho, ProQuest, 2016.

[3] E. O. Adekanmbi and S. K. Srivastava, "Dielectrophoretic applications for disease diagnostics using lab-on-a-chip platforms," *Lab on a Chip,* 10.1039/C6LC00355A vol. 16, no. 12, pp. 2148-2167, 2016.

[4] S. K. Srivastava, A. Artemiou, and A. R. Minerick, "Direct current insulator-based dielectrophoretic characterization of erythrocytes: ABO-Rh human blood typing," *Electrophoresis,* vol. 32, pp. 2530-2540, 2011.

[5] D. Bodas and C. Khan-Malek, "Fabrication of long-term hydrophilic surfaces of poly(dimethyl siloxane) using 2-hydroxy ethyl methacrylate," *Sensors Actuators, B Chem* vol. 123, pp. 368-373, 2007.

[6] M. A. Eddings, M. A. Johnson, and B. K. Gale, "Determining the optimal PDMS–PDMS bonding technique for microfluidic devices," *J. Micromech. Microeng,* vol. 18, 2008.

[7] D. Bodas and C. Khan-Malek, "Formation of more stable hydrophilic surfaces of PDMS by plasma and chemical treatments," *Microelectron. Eng., ,* vol. 83, pp. 1277- 1279 2006.

[8] S. K. Sia and G. M. Whitesides, "Microfluidic devices fabricated in poly(dimethylsiloxane) for biological studies," *Electrophoresis,* Review vol. 24, pp. 3563-3576, 2003.

[9] S. R. Gaboury and M. W. Urban, "Microwave Plasma Reactions of Solid Monomers with Silicone Elastomer Surfaces," *Langmuir* vol. 9, pp. 3225-3233, 1993.

[10] P. Sajeesh and A. K. Sen, "Particle separation and sorting in microfluidic devices: a review," *Microfluidics and Nanofluidics,* vol. 17, no. 1, pp. 1-52, 2014.

[11] S. Tang and G. Whitesides, *Optofluidics Fundamentals* 2010, pp. 7-32

[12] A. Y. N. Hui, G. Wang, B. Lin, and W. T. Chan, "Interface of chip-based capillary electrophoresis-inductively coupled plasma-atomic emission spectrometry," *Lab Chip* vol. 5, pp. 1173-1177, 2005.

[13] J. C. McDonald and G. M. Whitesides, "Poly(dimethylsiloxane) as a material for fabricating microfluidic devices," *Account of Chemical Research* vol. 35, pp. 491-499, 2002.

[14] O. Bjorn, A. Wirsen, and A. C. Albertsson, "Oxygen microwave plasma treatmnet of silicone elastomer: kinetic behavior and surface composition," *J. Appl. Polym. Sci.,* vol. 91, pp. 4098-4104 2004.

[15] B. Ginn and O. Steinbock, "Polymer surface modification using microwave-oven-generated plasma," *Langmuir,* vol. 19, pp. 8117-8118, 2003.

[16] V. J. Law and D. P. Dowling, "Converting a Microwave Oven into a Plasma Reactor: A Review," *International Journal of Chemical Engineering,* vol. 2018, p. 12, 2018, Art. no. 2957194.

[17] S. K. Srivastava, J. L. Baylon-Cardiel, B. H. Lapizco-Encinas, and A. R. Minerick, "A continuous DC-insulator dielectrophoretic sorter of microparticles," *J. Chromatogr. A,* vol. 1218, no. 13, pp. 1780-1789, 2011.

[18] I.-J. Chen and E. Lindner, "The stability of radio-frequency plasma treated polydimethylsiloxane surface," *Langmuir,* vol. 23, no. 6, 2007.

[19] G. M. Whitesides. (2006, 27 July) The origins and the future of microfluidics. *Nature* [Insight Overview]. 368-373.

[20] S. K. Sia and G. M. Whitesides, "Microfluidic devices fabricated in Poly(dimethylsiloxane) for biological studies " *Eletrophoresis* vol. 24, no. 21, pp. 3562-3576, 2003.

[21] D. C. Duffy, J. C. McDonald, O. J. A. Schueller, and G. M. Whitesides, "Rapid Prototyping of Microfluidic Systems in Poly(dimethylsiloxane)," *Anal. Chem.,* Research vol. 70, pp. 4974-4984, 1998.

Chapter 5: Dielectric characterization and modeling of the separation of infiltrating ductal adenocarcinoma cells from peripheral blood via continuous insulator-dielectrophoresis

Ezekiel O. Adekanmbi[1], Soumya K. Srivastava[1*]
[1]Department of Chemical and Materials Engineering, University of Idaho, Moscow, ID, 83844-1021 USA

Abstract

The dielectrophoretic separation of infiltrating ductal adenocarcinoma cells (ADCs) from isolated peripheral blood mononuclear cells (PBMCs) in a ~1.4 mm long Y-shaped microfluidic channel with semi-circular insulating constrictions is numerically investigated. In this work, ADCs (breast cancer cells) and PBMCs' electrophysiological properties were iteratively extracted through the fitting of a single-shell model with the frequency-conductivity data obtained from AC microwell experiments. In the numerical computation, the gradient of the electric field required to generate the necessary dielectrophoretic force within the constriction zone was provided through the application of electric potential across the whole fluidic channel. By adjusting the difference in potentials between the global inlet and outlet of the fluidic device, the minimum (effective) potential difference with the optimum particle transmission probability for ADCs was found. The radius of the semi-circular constrictions at which the effective potential difference was swept to obtain the optimum constriction size was also found. Temperature variation in the device was negligible below the 50 V potential threshold and would neither affect the operability of the device nor alter the integrity of the cells. Independent particle discretization analysis was also made to underscore the accuracy of the numerical solution. The numerical results, which was obtained by the integration of fluid flow, electric current, and particle tracing module in COMSOL v5.3, reveals that PBMCs can be maximally separated from ADCs using a DC power source of 50 V. The article also discusses recirculation or wake formation behavior at high DC voltages (>100 V) even when sorting of cells are achieved. This result is the first step towards the production of a supplementary or confirmatory test device to clarify any medical hunt about breast cancer.

Keywords: Dielectrophoresis, electrophysiological properties, crossover frequency, wake or recirculation formation, dielectric spectra

Abbreviations:

DEP- Dielectrophoresis, PBMC- peripheral blood mononuclear cells, ADC- Adenocarcinoma cells, TP- Transmission probability

5.1 Introduction

Noncommunicable diseases (NCDs) kill more than 36 million people annually representing 63% of global deaths [269]. Breast cancer, a subset of NCDs, accounts for over 500,000 of these deaths [270] with an incidence of about 1.1 million new cases being reported per year [271]. In Unites states, as of March 2017, more than 3.1 million women with a history of breast cancer has been reported [272]. About 85% of these breast cancers occur in women who have no family history of breast cancer [272] and one in eight women develop breast cancer in her lifetime. As of now, the main cause of breast cancer cannot be pinned down exactly but scientists have hypothesized where breast cancer originates. Our bodies consist of many cells, which can be replaced as they age. Old cells tend to copy their DNA before splitting into new ones. However, the copying process could cause mutation which may result in cellular abnormalities called tumors. When tumor cells grow and invade neighboring tissues, they are termed cancerous [273, 274]. Breast cancer that starts in the cells of the glands are termed adenocarcinoma (ADCs), which can be invasive ductal (indicates that the cancer cells present in the milk ducts (Ductal Carcinoma in-situ) can begin to infiltrate and replace the normal surrounding tissues of the duct walls (accounts for 80% of breast cancer), also known as invasive lobular.

According to the National Cancer Institute, around 90% of breast cancers are adenocarcinomas. If untreated, breast cancers can grow bigger, taking over more surrounding breast tissue. When breast cancer cells break away from the original cancer, they can enter the blood or lymph vessels. Traveling through these vessels, cancer cells may settle in other areas of the breast or in the lymph nodes of the breast tissue, forming new tumors. This is called metastasis. These adenocarcinomas are the most difficult tumor to accurately identify the primary site [275]. Although features such as tubular myelin, intranuclear surface apoprotein tubular inclusions, Langerhans cells associated with neoplastic cells, cytoplasmic hyaline globules, glycogen, lipid droplets and cytoplasmic crystals have been used to diagnose adenocarcinoma, the procedure seems too elaborate, time consuming and costly since they are ultrastructural features that are needed to be observed through electron microscopes. The application of immunohistochemistry to diagnose these adenocarcinomas has also been explored using estrogen and progesterone receptor proteins, thyroid transcription factor-I and surfactant apoproteins [275]. However, specificity and sensitivity are the main issues associated with this method. While breast cancer cells that have spread beyond the ducts into other parts of the breast tissues or other organs through blood, the Peripheral Mononuclear Blood Cells (PBMCs) is usually chosen as the key source

agent for these cancerous cells since they are known to circulate in the peripheral blood of patients [276]. PBMCs are typically isolated from whole blood using density gradient centrifugation commonly in Ficoll-Pacque PLUS and the Histopaque 1077 media [277].

To discriminate and subsequently separate ADCs from PBMCs, increased interests have been rooted in exploring the utilization of cell physical properties in lieu of other methods including antibody-conjugation, which is time consuming and can impact ADCs' properties and viability [53]. Leveraging time physical characteristics in form of size-based filtration [278-280], density-gradient separation [281-283], and inertial-hydrodynamic discrimination [284-286] has worked well in the past until Shim *et al.* reported that size and density distributions of ADCs tend to overlap with those properties of PBMCs, leading to occasional inefficiency in the separation of ADCs based on size and density. Dielectrophoresis (DEP), which utilizes cell capacitance and conductance in a non-uniform electric gradient seems to be a novel alternative for isolating ADCs [249, 287-291]. DEP is a promising technique to manipulate cancer cells because it employs no moving parts, non-destructive for the bioparticles, and the use of low electric field on a micro-chip without the need of tagging makes it a portable system. Reduced response time and higher throughput and accuracy, with no requirement of labeling makes DEP a promising technique for cancer cell separations.

When a bioparticle is subjected to a non-uniform electric field, the dielectrophoretic forces and the dipole-dipole forces between the particles (dipole moments) are generated based on the differences between the electrical properties (capacitance and conductance) of cells and the surrounding fluid [290]. Traditionally, DEP based cancer cell separations employ metallic electrodes to capture or separate infected cells, by creating non-uniform electric fields using AC voltage [283, 292]. AC DEP device offers a major disadvantage in the form of decreased metal electrode functionality due to fouling when biological samples are manipulated [249, 293]. Also, these devices often have high cost associated with the fabrication containing metal parts [249, 294]. Insulator-based DEP (iDEP) is an alternative to electrode-based DEP. iDEP employs insulating objects created by microfabrication methods in channel to generate spatial non-uniformities in the field [295, 296]. iDEP is also referred to as electrodeless DEP, as electrodes are mounted far outside of the inlet and outlet and are immersed in electrolyte or buffer medium and are not in direct contact with cells. Another variation of iDEP is to employ low frequency AC along with DC to manipulate particles of interest (AC-iDEP). AC- iDEP systems offer an advantage over AC DEP, that they can be operated continuously unlike traditional electrode-based systems which are batch operated. With the electrodes placed away from inlet and outlets, here electroosmotic forces can be utilized for inducing flows, eliminating the need for the pumps for continuous operation [297].

Recently, contactless DEP has been explored by Davalos's group but only AC signals have been used to manipulate cancer cells [298]. This creates a gap in the exploration of cancer cell separation using DC signals. The aim of this work, therefore, was to determine experimentally if there are differences in the electrophysiological properties of normal peripheral mononuclear cells (PBMCs) and moderately differentiated infiltrating ductal adenocarcinoma cells (ADCs) and to use these differences, if they exist, to numerically attempt their separation (using DC signals) on a microchip - an important step towards the development of a supplementary diagnostic device for ADCs.

In this article, we develop a simulation-based COMSOL model for continuously separating breast cancer cells from peripheral blood mononuclear cells (PBMCs) in a microchannel with modified geometry by using an array of semi-circular insulating obstacles to create non-uniformity in electric field utilizing DC-iDEP. First, a PDMS-based microwell was constructed to house a horizontally arranged-100 µm-apart electrode (Fig. 5.1) to obtain the characteristic membrane properties of both ADCs and PBMCs. The properties, validated against the available data in the literature, are then utilized to in conjunction with Finite Element Method (FEM) to model and simulate the trajectory of both cells (ADCs and PBMCs) in a semicircular-insulator-based 2D microfluidic channel. While the characterization of the ADCs gives the innate electrical signatures that is characteristics of moderately differentiated infiltrating ductal adenocarcinoma, the utilization of FEM sets a workable model that could serve as a platform for fabricating a novel supplementary diagnostic device for ADCs.

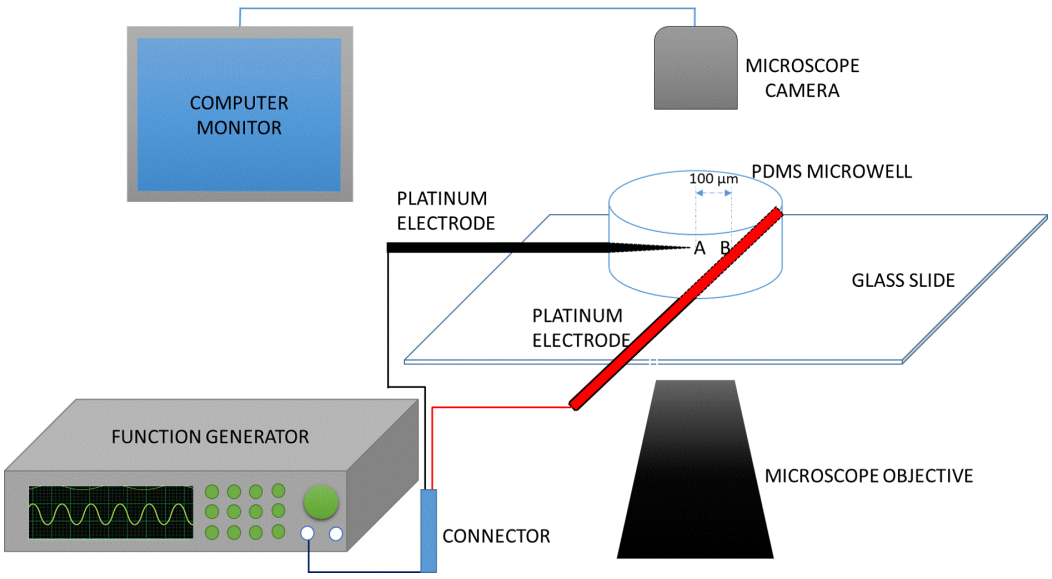

Figure 5. 1 *The experimental set-up for the measurement of DEP crossover frequency using a novel PDMS microwell platform to obtain electrophysiological properties i.e. conductivity and permittivity of PBMCs and ADCs that will aid in designing an early detection platform for breast cancer.*

5.2 Theory of dielectrophoresis

Crossover frequency measurement is a novel dielectrophoretic-based method of characterizing the dielectric properties of many biological particles. By crossover frequency, we mean the frequency at which cells suspended in a well characterized osmotic concentration medium, change their direction of motion towards or away from the high field region in an electric-field-gradient-based system. When a bioparticle (i.e. cell) is placed between two electrodes as shown in **Figure 5.1**, the cell can either move to A or B depending on its polarizability relative to the medium in which it is suspended. Cells move to A (pDEP) if they are more polarizable than the medium and to B (nDEP) if the reverse occurs. At varying conductivity of the suspending medium, various crossover frequency data (f_{xo}) can be generated. In this current work, these data are generated, plotted and fitted with a model (Eqn. 5.1) using least square regression and the confidence of the fit was found through the coefficient of regression analysis. According to Pethig [41], for a biological cell whose interfacial polarization between the plasma membrane and the cytoplasm results in a dispersion frequency far below 1 MHz for the cell effective dielectric permittivity and conductivity, the first crossover frequency, f_{xo1}, of the cell membrane is given by;

$$f_{xo1} = f_{xo1}(C_{mem}, G_{mem}, \sigma_m) \; \vdots \; f_{xo1} = \frac{1}{\sqrt{2}} \frac{\sigma_m}{\pi r C_{mem}} \sqrt{1 - \frac{RG_{mem}}{2\sigma_m} - 2\left(\frac{RG_{mem}}{2\sigma_m}\right)^2} \tag{5.1}$$

$$\forall \quad C_{mem} = \varepsilon_{mem}/d \tag{5.2}$$

$$G_{mem} = \sigma_{mem}/d \tag{5.3}$$

In terms of total particles and medium properties, f_{xo1} can also be represented as

$$f_{xo1} = \frac{1}{2\pi} \left\{ \frac{(o_m - o_p)(o_p + 2o_m)}{(\varepsilon_p - \varepsilon_m)(\varepsilon_p + \varepsilon_m)} \right\}^{1/2} \tag{5.4}$$

where C_{mem} is the specific membrane capacitance, G_{mem} the membrane conductance, σ_m the conductivity of the suspending medium, ε_{mem} the permittivity of the membrane, σ_{mem} the conductivity of the membrane, d is the characteristic dimension of the cell membrane and R, the radius of the particle

In an iDEP system, the DEP force, $\vec{F}_{DEP}$, acting on the particles due to the field gradient is a function of the particle and medium characteristics and is given as

$$\vec{F}_{DEP} = 2\pi\varepsilon_m r^3 \left(\frac{\sigma_p - \sigma_m}{\sigma_p + 2\sigma_m} \right) \nabla |\vec{E}_{DC}|^2 \tag{5.5}$$

Where the quantity $\left(\frac{\sigma_p - \sigma_m}{\sigma_p + 2\sigma_m} \right)$ is the Clausius-Mossotti factor (CM), which is the parameter that

DEP-viscous force balance for particle separation, electrokinetic forces (electroosmotic and electrophoretic forces) would have been utilized to pump the particles to the separation region through the electroosmotic channel wall condition and the electrostatic interaction of the electric field with the particles. Electroosmotic flow is generated due to action of electric field on charged interior surfaces having electrical double-layer (EDL). The nature and magnitude of the charge in EDL is characterized by the Zeta potential [299]. Electroosmotic mobility of fluid is a function of the Zeta potential of the microdevice i.e. microchannel construction material and is given by [300]:

where μ_{E0} is the electroosmotic mobility, ε_m is the permittivity of medium, ξ is the Zeta potential of the material and η is the viscosity of suspending medium (buffer). The electrophoretic mobility unlike the electroosmotic mobility that depends on the material, depends on the Zeta potential of the particle itself and is given by [301]:

$$\mu_{EO} = \frac{\xi_p \varepsilon_m}{\eta} \tag{5.7}$$

where ξ_p is the Zeta potential of the particle. At the separation region, the particle experiences a dielectrophoretic force that is impacted by the particle mobility. The DEP mobility is a function of CM factor and for a spherical particle it is expressed as [264]:

$$\mu_{DEP} = \frac{\pi d_p^2 \varepsilon_m}{12\eta} CM \tag{5.8}$$

where d_p is the particle diameter and η is the medium viscosity.

5.3 Materials and Methods

5.3.1 Microwell fabrication

Silicone elastomer mixed with its curing agent in 10:1 ratio (Sylgard 184, Dow Corning, USA) was placed in a desiccator chamber under 0.27-mTorr vacuum in order to remove the bubbles formed during the mixing process. After three successive degassing operations lasting for 15 min, at an interval of 5 min between each run, the clear PDMS was poured into a clean petri dish and cured in the oven at 70ºC for 1 h. This step was followed by dicing the PDMS into 1" X 1" squares. A 3-mm hole was punched into each of the diced PDMS to create a well onto which the cell suspension was pipetted. Scotch tape was used to remove any dirt/dust from the PDMS after which it is was irreversibly sealed to a borosilicate glass slide through plasma oxidation of 50 W RF power for 1 min. High purity platinum wire was connected to the microwell as shown in Figure 1. With the aid of an Olympus IX71 inverted microscope, the distance (100 μm) between the electrode tips was set. Loctite's self-mix epoxy was used to keep the electrode spacing intact. The epoxy also prevented any leakage of liquid when the

microwell was filled with cell suspension. This was evident when anhydrous copper sulfate was dispensed around the filled microwell, in a regulated environment, did not cause any change in color i.e. from its natural white to blue color.

5.3.2 Buffer and Cell preparation

The DEP buffer (dextrose solution) was prepared and characterized as described in our previous article [49]. The prepared 100 ml buffer was divided into five separate beakers. Into each beaker, except the first, calculated volume of phosphate buffer saline (PBS) was added to successively change the conductivity of the DEP buffer to obtain the following conductivities (in mS/m): 50, 60, 74, 88 and 97. Female normal peripheral mononuclear cells (PBMCs) and infiltrating ductal adenocarcinoma cells (ADCs) with no identifiable angiolymphatic invasion were obtained from Conversant Bio, Alabama, USA. Also, the cells obtained did not have any identifiable information about the patient itself except their gender and age (Institutional Review Board -IRB exempt). The cells were prepared for experiment according to the supplier's instructions. Thereafter, a known number of cells were transferred into each of the five DEP buffer solution where they were washed twice and diluted in 1:400 cell: buffer ratio before being pipetted into the DEP microwell for experiment.

5.3.3 Measurement of crossover frequency

After the assurance that the microwell was leakage-free, the platinum electrodes were connected to the two terminals of an 80 MHz Siglent SDG 2082X Arbitrary Waveform Generator, which supplied an 8V peak-to-peak sinusoidal AC signal of sweeping frequencies. 5 µL of the PBMCs suspension prepared as discussed in Sec 3.2 was transferred into the microwell and allowed to equilibrate. Then, about 4 µL was carefully siphoned from the well so that fewer cells (between 4-7 cells) were present in the field-of-view for the experiment. Having fewer cells does not only reduce the influence of particle-particle interaction, but also enhances clarity in visualizing cells for crossover frequency determination. The waveform generator was then switched on to generate electric field gradient around the electrodes. Movement of cells was monitored as a function of the changing field frequency until the crossover frequency was found. The experiment was repeated four times and the crossover frequency was found in each case. More experiments were run using the other modified medium at varying conductivities thus obtaining crossover frequency spectra. The PBMCs are majorly lymphocytes (>80%) ~10 µm in diameter while ADCs are ~20 µm in diameter. Measurement were made at room temperature conditions i.e. $\mathrm{T} = 24 \pm 1℃$.

5.3.4 Finite Element Modeling and Simulation

In this section, attention was given to the numerical modelling and simulation performed using the dielectric properties obtained from the crossover frequency measurements in section 3.3. COMSOL Multiphysics 5.3a was used to solve fluid flow, electrostatics, and particle tracing modules in an

integrated stationary and time-dependent fashion. The architecture of the separation device (Figure 5.2) was arrived at after a series of parameter modification that ensured a complete separation of ADCs from its mixture with PBMCs. The design was made in 2D because the width to depth ratio was more than 5:1.

Electric current node was used to solve, in steady states, the current conservation equation based on Ohms law and electric displacement relations using the electric potential as the dependent variable. This was solved in steady state because the charge relaxation time for the conducting media (water, in this case 3.6e-6 s) is less than the external time scale for device operation (10 s). Solving this Ohm's law with the charge conservation and electric displacement equations gives the electric field, E, which was used to compute the electroosmotic boundary condition used in the creeping flow analysis according to

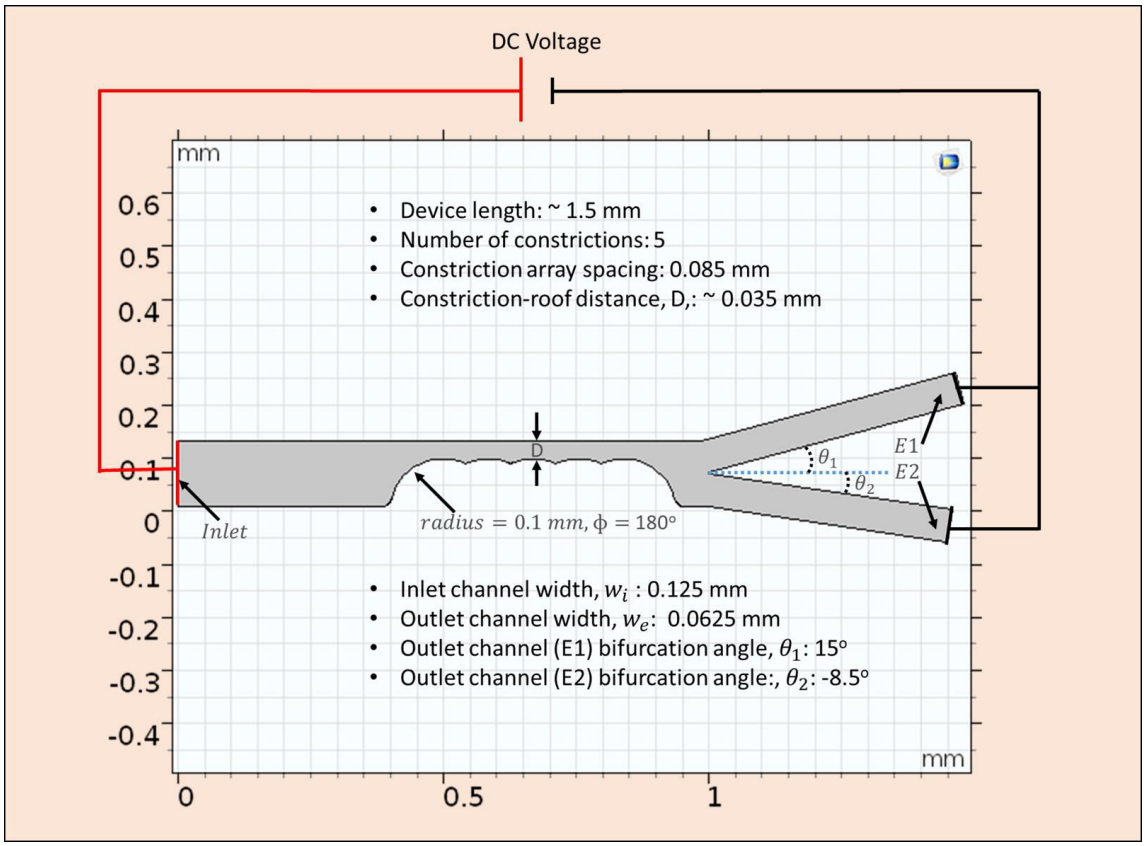

Figure 5. 2 *Optimal device design geometry obtained by COMSOL modeling and simulation utilizing the electrophysiological properties of PBMCs and ADCs from the PDMS microwell. Entire microfluidic platform is ~1.5 mm with semi-circular constrictions embedded in the channel. Inlet channel is 125 μm wide and the two outlet channel widths are ~62.5 μm. Pt electrodes in the inlet and outlet ports is connected to a DC power supply to further sort ADCs from healthy PBMCs.*

$u_{EO} = \mu_{EO}E$, where u_{EO} is the electro-osmotic velocity- the velocity of the bulk of the fluid flowing in the channel due to electric field effects. In the incompressible creeping flow analysis (as is the usual case in microfluidic channel where the Reynolds number is significantly less than unity and viscous

force is dominant), the steady state form Stoke equation together with the continuity equation was solved as the synergistic conservation of momentum and mass, which account for the velocity profile within the fluidic channel. The magnitude of this velocity as a function of the position within the channel was then used to solve the drag force (Table 5.1) acting on the particles flowing within the channel through numerical coupling. The drag force is then counterbalanced by the dielectrophoretic force, eqn. 5, at the region where the magnitude of electric field norm was modified as a result of the constrictions placed between the inlet and the outlet channels. Each particle moving through the microdevice was tracked using the particle tracing module solved in time-dependent mode. Tracking the particles enabled the statistics through which the device parameters (like voltage, device dimensions, etc.) that generated the desired separation of the particles were noted. Using a free triangular customized mesh, with different sizes, growth rate, and curvature factor for both constrictions and the remaining regions within the channel, the geometry was discretized and made ready for finite element analysis. Multifrontal massively parallel (MUMPS) solver, which performs Gaussian factorization, was used in the stationary mode to obtain the velocity profile and the electric field norms. MUMPS solved for the velocity profile and the electric field norms these values with a relative tolerance of 0.001 and without any recourse to lumping while computing the fluxes. GMRES, generalized minimal residual solver – a solver that approximates solutions by the vector in a Krylov subspace with minimal residual, was used in the transient domain to track the particles with respect to their position in space and velocity magnitude as a function of time. The final geometry of the device where complete separation occurs was 1.4 mm in length with 5 semi-circular constriction of radius 0.1 mm and inter-structural constriction spacing of 85 μm. The distance 'D' (Figure 5.2) between the constriction end and the upper channel wall was fixed to be 35 μm. This distance forbids two cancer cells to pass through the separation region at any given time. This design was made to prevent any form of shielding that may eventually result in incomplete separation. Table 5.1 provides a list of parameters, variables, type of study utilized in COMSOL, and equations associated with the modeling and simulation.

Table 5. 1 *List of parameters, variables, discretization, type of study utilized, and the equations associated that was incorporated into COMSOL package for optimizing the device geometry and sorting of ADCs from healthy PBMCs.*

Physics/ Parameters	**Tag**	**Dependent variable**	**Discretization**	**Study**	**Equation**
Electric current	ec	V	Lagrange Quadratic	Stationary	$\nabla.J = Q_{j.v}$ $J = \sigma E + J_e$ $E = -\nabla V$ Wall insulation $(n.J = 0)$
Fluid Flow	spf	u	P2+P1	Stationary	$\nabla.[-pI + \mu(\nabla u + (\nabla u)^T] + F = 0$ $\rho\nabla.(u) = 0$ Wall electro-osmosis $u = \mu_{eo}E_t$ $\forall \quad \mu_{eo} = \frac{\epsilon_r\epsilon_0}{\mu}\xi;\ E_t = E-(E.n)n$
Particle tracing	ptf	q, v	Formulation Newtonian Drag law Stokes	Transient	$\frac{d(m_p v)}{dt} = F_t$ $F_D = \frac{1}{\tau_p}m_p(u-v)$ $\tau_p = \frac{\rho_p d_p^2}{18\mu}$ $F_{DEP} = 2\pi r_p^3\epsilon_0 real(\epsilon_r^*)real(K)\nabla\lvert E\rvert^2$ $K = \frac{\epsilon_{r,p}^*-\epsilon_r^*}{\epsilon_{r,p}^*+2\epsilon_r^*}\forall\ \epsilon_r^* = \epsilon_r$ in stationary field
Meshing	**Calibration**		**Mesh Type**	**Max size**	**Boundary layer transition**
	Fluid dynamics		Free triangular	0.001 mm	Smooth transition to interior mesh
Stationary solver	MUMPS				
Transient Solver	GMRES				

5.4 Results and discussions

In this section, we finally discuss and present the important results to prove that breast cancer can be detected early enough using whole blood. This simulation study demonstrating sorting of ADCs from PBMCs will further be validated experimentally (beyond the scope of this article). Our results are categorized into sections demonstrating: 1) experimental evidence of electrophysiological characterization of both healthy PBMCs and breast cancer ADCs, 2) validation of our microwell technique by comparing with studies from literature and 3) modeling and simulation parameters like meshing, stationary analysis, transient analysis.

5.4.1 Electrophysiological characterization of PBMCs and ADCs experimentally

In estimating the properties of both PBMCs and ADCs movement of cells toward or away from high field region was tracked until the crossover frequencies were found in case at changing properties

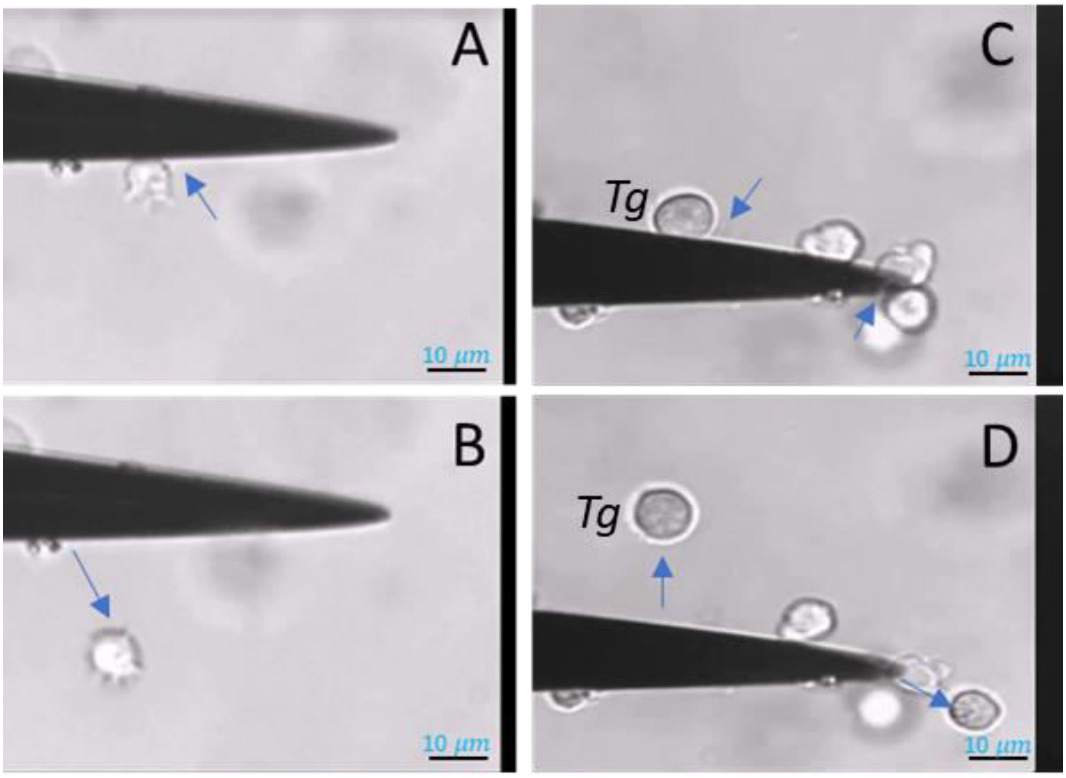

Figure 5. 3 *ADC cells experiencing DEP in the microwell at varying AC frequencies- (A) shows the ADC cells experiencing positive DEP (pDEP) wherein the cells move towards the high-field region or the triangular electrode in here and (B) shows the ADC cells experiencing nDEP behavior wherein the cells move away from the high field region. (C) and (D) are the images resulting from manual tracking of the target cell (labeled Tg) as demonstrated in ref. [302].*

of the suspending medium. Figures 3A and B shows an ADC cell experiencing positive and negative DEP force (pDEP and nDEP) respectively. In figs. 3C and D, we manually tracked the movement of the target cell as previously demonstrated for prostate cancer in Hele-Shaw flow cell by Huang et al [302]. The crossover frequency data for PBMCs and ADCs were fitted using eqn. 1. This equation is

an ideal model owing to the spherical nature of lymphocytes. Table 5.2 provides the dielectric properties obtained from our experiments and are compared to the other published literature values in case of PBMCs. However, the authors believe that this is the first time that ADCs were characterized using a novel electrokinetic technique to obtain their dielectric properties i.e., permittivity and conductivity as shown in Table 2.

Table 5. 2 *Dielectric properties i.e. conductivity and permittivity obtained from our novel electrokinetic technique based on cell response obtained at crossover frequency for ADCs and healthy PBMCs using an osmotic concentration suspending medium maintained at osmotic conductivity and permittivity. Literature reported values has been compared with our novel technique for PBMCs only as a measure of validation [38].*

Property	**ADCs (infiltrating ductal adenocarcinoma cells)**	**PBMCs (Lymphocytes)**		**Suspending medium**
	Crossover freq. technique	**Crossover freq. technique**	**Literature reported [38]**	
Conductivity (S/m)	1.3	0.67	0.66	0.055
Permittivity	69	62	59.62	80

5.4.2 Parameters affecting COMSOL modeling and simulation to obtain high sorting efficiencies

In this section, we discuss the factors that affect the optimization of the device geometry to achieve high sorting efficiencies that further influence early breast cancer detection obtained through sorting ADCs from healthy PBMCs.

5.4.2.1 Meshing of the device design in COMSOL

Meshing is one of the factors that strongly affect modelling requirements. Choosing the right mesh element types and sizes is highly pivotal to the accuracy of the simulation results in any finite element problem. Under-meshing can result in solutions that are far less than accurate while over meshing can result in large amount of computational time due to the mesh using too many unnecessary elements. To prevent under meshing, we used mesh elements greater than 40,000. Over meshing was, however, checked and prevented by using meshing sequence with local and global attributes. The local mesh density at the constrictions was sufficiently increased by reducing mesh size while the remaining part of the geometry (where dielectrophoretic force would not have significant effects) was meshed at increased mesh size.

This meshing sequence, which was based on Lagrange quadratic representation, reduced the total number of mesh element by 45.17 % and computation period by 51.06 %. Since the

dielectrophoretic force, which causes cells to separate based on their movement away or towards the high field region, acts significantly at the channel constriction zone, it was necessary to verify if the maximum element size (MES) at the constriction would affect the transmission probability of ADCs and to what extent would that effect be. As shown in Figure 4, the accuracy of the solution (which is a function of the transmission probability) depends on the choice of mesh size. The mesh characteristics that was found to be optimum at the applied effective potential difference is as given in Table 1.

Figure 5.4 demonstrates the gradation of the discretization regime of the constriction zone as the maximum element size (MES) is progressively reduced. At MES=0.05 mm the density of the triangular mesh is very low indicating that the inter-nodal distance within the discretized zone is large. This large distance depicts an inefficient solution capacity for the gradient of the electric field, which is evident in the low transmission probability (TP) for the ADCs (Figure 5.5). Transmission Probability, TP, is referred to as the ratio of the number of particles at a specified exit to the total number of the particles at the inlet .

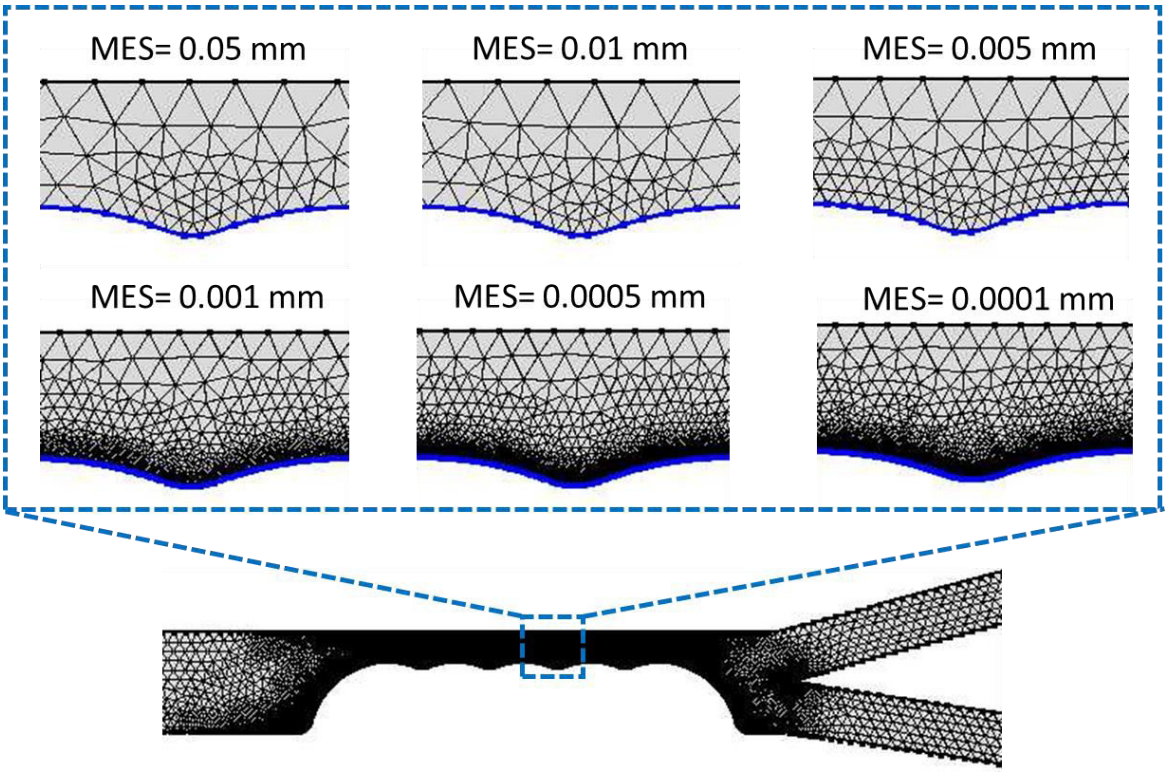

Figure 5. 4 *The discretization of the separation region i.e. along the semicircular constrictions where maximum DEP effect is observed that causes the cells to move into categorized streamlines by adopting variable mesh element size (MES).*

In other words, large mesh size at the constriction zone was not able to correctly solve for the electric field gradient which is necessary for dielectrophoretic influence on the particles. When the mesh size was progressively reduced, the number of elements increased correspondingly. This in turn increased the separation efficiency at the constriction zone, hence the dramatic ramping up of the

percentage of ADCs that were sorted from healthy PBMCs. It is important to note that the progressive reduction in MES increases the computation time i.e. with MES at 0.0005 mm and 0.0001 mm requiring 800% and 960% more time than at 0.001 mm. Since the TP value for MES=0.001 mm, 0.0005 mm and 0.0001 mm are comparatively similar and >97%, the computation was carried out at 0.001 mm with an error margin of ~ <0.00020%. At these values [0.001, 0.0005 and 0.0001 mm], it is safe to conclude that the stationary and transient solutions (within the margin of error) of the coupled physics do not vary with mesh condition as the TP values tend to be approximately constant. MES value beyond 0.0001 mm showed critical error warning sign in COMSOL and was computationally very expensive.

5.4.3 Stationary field analysis

The numerical computation comprises of two stationary fields: a) creeping (fluid) flow and b) electric

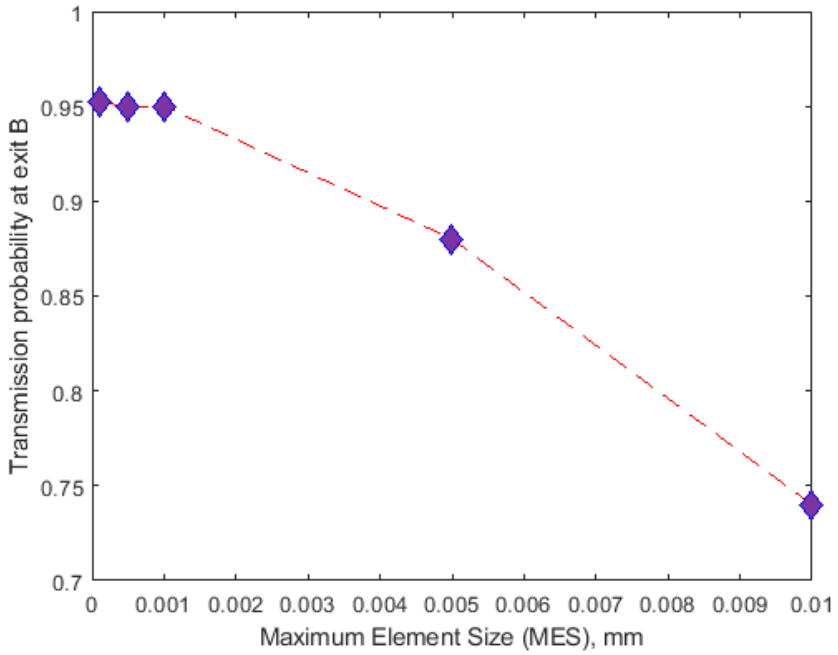

Figure 5. 5 *Transmission probability of ADCs as a function of the maximum element size at the separation zone i.e. around the semicircular constriction region. Since MES at 0.001 mm, 0.0005 mm, and 0.0001 mm are almost similar, the simulation was completed fixing MES at 0.001 mm.*

current (ec). The electric current was solved in the stationary mode to generate the electric field that not only generated the electro-osmotic effects at the channel wall but also provided the distribution of fieldstrength, E, whose gradient provided the necessary dielectrophoretic force at the constrictions.

As shown in Figure 5.6A, when DC potential difference was applied across the channel (from the inlet to outlet) and there was a distribution of the electric field as governed by the Laplace equation. The tips of the constrictions within the channel, generated the highest field strength region that was important for dielectrophoretic separation. In Figure 5.6, the effect of the field gradient is visually more pronounced when the flow field lines were plotted together with the electric field norm. Glaringly, the

gradient of the field which was utilized by the dielectrophoretic force acting at the constrictions interfere with the velocity field. The dielectrophoretic velocity introduced at the constrictions added to the already existing electrophoretic and electro-osmotic velocities apart from the increase in velocity that was introduced by the continuity equation owing to the reduction in flow area. Figure 5.6C shows the ripple effects generated from the surface of the constrictions outwards. The resultant effects of this streamline interference could be seen in Figure 5.6D, E, and F at varying DC voltage i.e. 10 V, 110 V, and 60 V respectively. The number of constrictions were fixed at 5 and diameter of the constriction was considered to be 100 μm.

5.4.3.1 Effects of applied potentials and constriction radius on transmission probability

It is important to verify the effects of the electric field strength at various applied potentials and constrictions on the separation efficiency of the microdevice platform. As a result, the radius of the constrictions was varied keeping the number (#) of constrictions fixed at 5 at a given time thus solving the Laplace equation each time using different applied potential without varying the mesh conditions (Figure 5.7). The number of constrictions was fixed as an optimization test constraint with respect to the length of the device as well as the exploration of the possibility of initiating cellular separation with minimal insulating constrictions as previously demonstrated by Adekanmbi et al [49].

Transmission probability of the total number of PBMCs (from inlet to outlet) as a function of the constriction gap i.e. *D* in Figure 5.2 and applied voltage using a fixed number of constriction entities i.e. 5 was calculated and plotted as shown in Figure 5.7. Transmission probability (TP) is congruent to normalizing the amount of PBMCs recovered by the initial amount of PBMCs in the inlet mixture. This means, a TP value of 1 represents 100% separation of the PBMCs from its mixture with ADCs. The essence of calculating the transmission probability was to verify the selectivity of the device and to track operating parameters that would be optimal for the operability of the device. Figure 5.7 demonstrates the effect of varying the constriction diameter and the applied voltage on the transmission probability of PBMCs

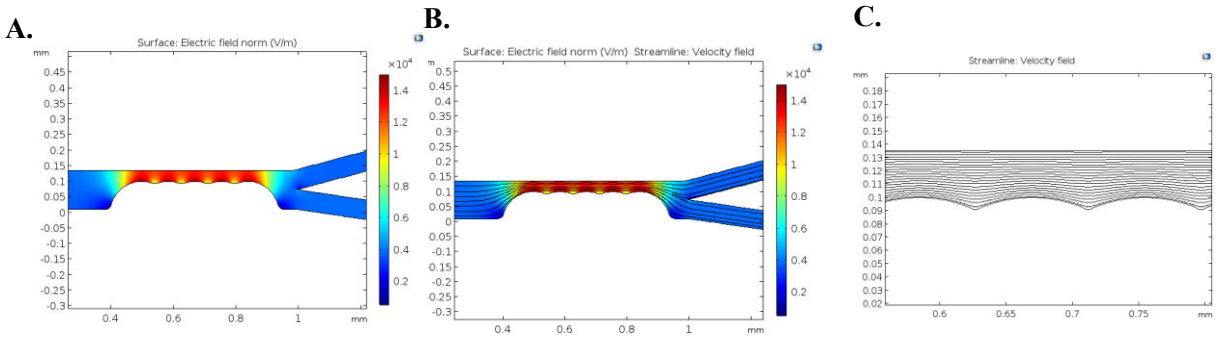

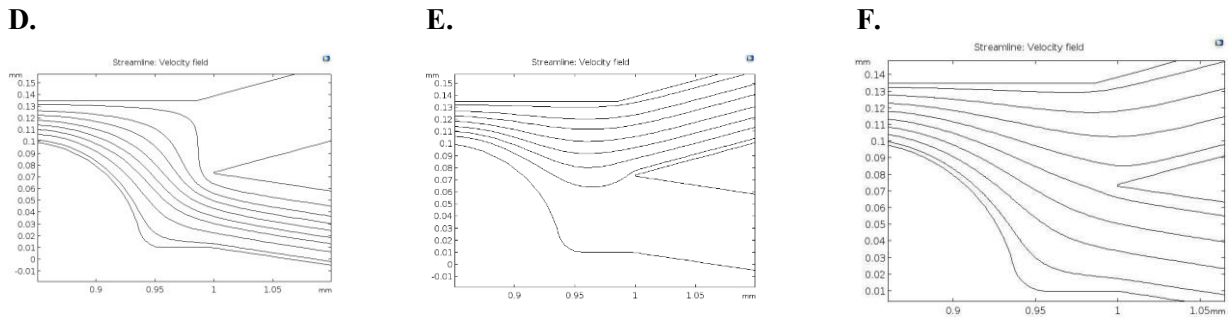

Figure 5. 6 *Field and velocity profiles obtained from solving the electrostatics and stokes equations in stationary mode. A is the electric field norm, B is the combination of the field norm with velocity streamlines, C is the zoomed image showing the effect of the constriction zone on velocity streamlines. D, E, and F show streamlines based on changing DC voltage at 10 V, 110 V and 60 V respectively. The constriction diameter and number were fixed to be 100 μm and 5 respectively.*

The TP value for each of the constriction diameter was progressively increased with the changing potential. At a given DC voltage, the recovery of PBMCs was highest when the constriction diameter was 100 μm. More so, from 50 V to 80 V, 100 μm constriction diameter gave a perfect separation of the PBMCs. None of the constriction diameters gave 100% separation except 110 μm at 80 V. These variations in transmission probability could be attributed to the changing electric field strengths as the applied voltage and constriction diameter change.

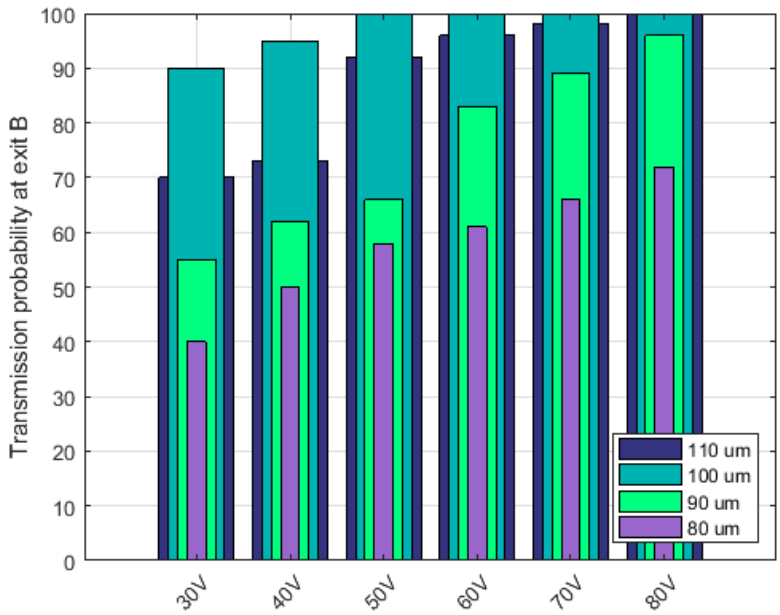

Figure 5. 7 *Effects of constriction clearance / size i.e. diameter and DC voltage on the transmission probability of ADCs. Diameter of the constrictions were varied- 80, 90, 100, and 110 μm keeping the number (#) of constrictions fixed i.e. 5 at a given time. Perfect sorting was observed for constriction diameter of 100 μm at voltages >50 V_{DC}.*

Changing the applied DC potential affected the electrokinetic and dielectrophoretic forces operating within the channel. Electrokinetic contributions within the channel affects the particle

velocity and hence the resident time within which the particles are expected to experience strongest DEP force at the constriction zone.

At <50 V, the electro-osmotic velocity of the bulk fluid medium was low enough to move the particles slowly to the constriction zone where there is ample residence time for the cells to experience sufficient induced dielectrophoretic force that would cause them to be separated adequately. However, since DEP force depends on square of the field gradient, the low DC potential (< 50 V) could not generate the required electric field gradient that is sufficient to induce strong negative dielectrophoretic force necessary for sorting the cells into their respective differential outlets.

Since increasing electric potential could result in increased Joule heating of the microdevice leading to unwholesome modification of the electrokinetic and dielectrophoretic effects, 100 µm constriction diameter was considered to be the ideal dimension for the separation device platform. Furthermore, operating at a lower voltage i.e. ~60 V_{DC} seems to reduce the risk of Joule heating within the insulator-based dielectrophoretic device.

5.4.4 Transient analysis

Particle tracking analysis was used to trace the movement of both ADCs and PBMCs along the whole microdevice platform. Particles were seen moving through the channel inlet until they were acted upon by the dielectrophoretic force at the constriction which tend to move the particles either towards or away from the constriction surface depending on the properties of the medium, ADCs, PBMCs, and the generated electric field gradient. From the equation of the dielectrophoretic force (eqn. 5.5), the force experienced by both PBMCs and ADCs at the constriction depends on the square of the electric field gradient as well as the radius of the particle to the third power. The membrane conductivity of both ADCs and PBMCs are both less than that of the medium. Therefore, it is expected that both of them would experience negative DEP.

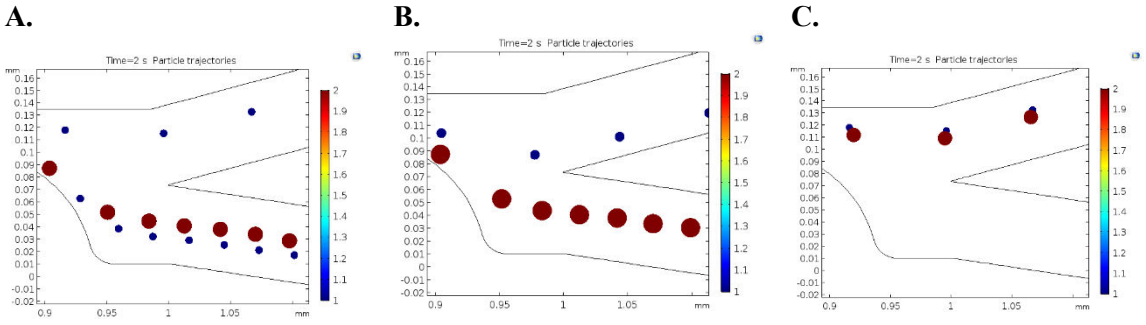

Figure 5. 8 *Particle trajectories showing partial (A and C) and complete separation (B) at various voltage conditions. The constriction diameter was fixed at 100 µm along with number of constrictions at 5. (A) shows incomplete separation at <50 V_{DC}, (B) complete separation at 50 V_{DC}, (C) no separation at >100 V_{DC}.*

Figure 5.8 demonstrates the scenario where ACDs and PBMCs were partially and completely separated while sweeping the applied voltage for a constriction number of 5 and diameter of 100 µm at

fixed medium properties. Figure 5.8A depicts incomplete separation at DC voltage below 50 V. At this applied voltage the strength of the applied electric field was not sufficient enough to push away the PBMCs. At 50 V, the generated field gradient had made the DEP force more negative such that the PBMCs were pushed away enough from the high field region to cause their separation from ADCs (Figure 5.8B). No separation was observed at higher DC voltages i.e. >100 V (Figure 5.8C). However, there was separation at ~100 V but with some interesting modification to the flow streamlines as shown in Figure 5.9.

In Figure 5.9A, the operating DC voltage is 60 V while Figure 5.9B is at 100 V. At 120 V (Figure 5.9C), some streamlines are being recirculated and this recirculation became more and more pronounced as the applied voltage increased to 200 V (Figure 5.9D, E and F). Figure 5.9D shows the close-up section of the bifurcation zone at 200 V, where in more recirculation of streamlines are being observed. Figure 5.9E is a close-up representation of the streamline recirculation showing some of the cells that were forced to move in a circular reverse direction to the DEP force. As shown in Figure 5.9F, some of the cells that were heading towards the exit ports are also forced to move towards the inlet i.e. recirculated back into the main channel.

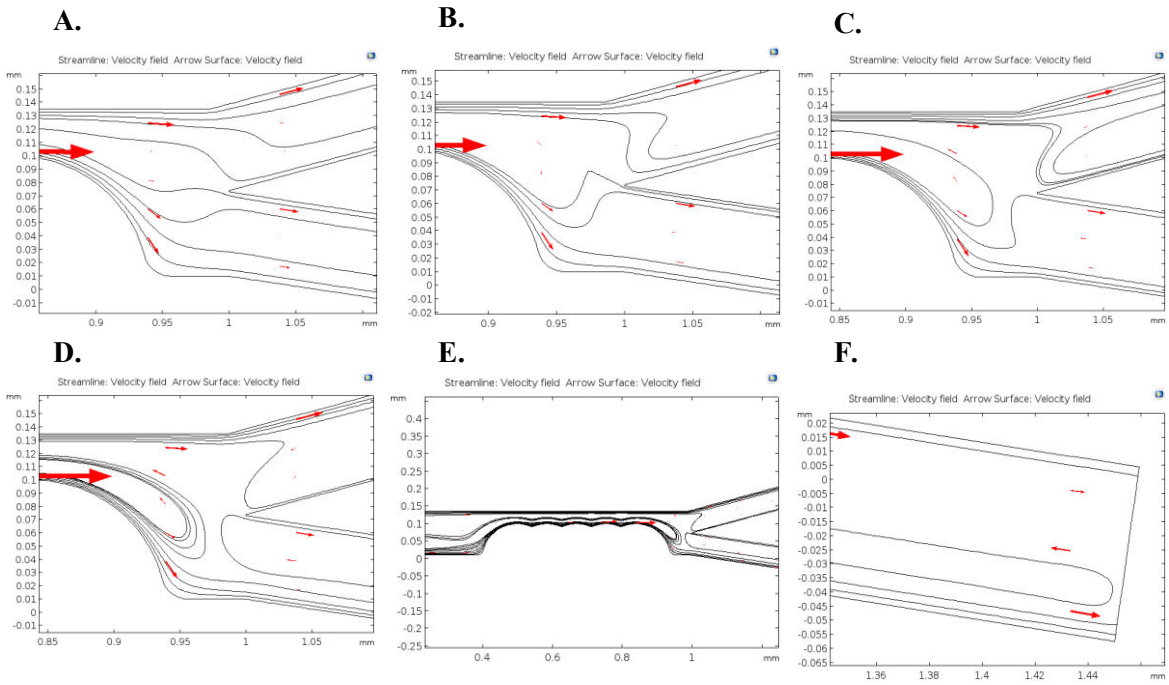

Figure 5. 9 *Velocity streamlines at various applied DC voltage conditions at fixed number of constrictions (5) and constriction size (100 µm); (A) and (B) shows streamlines at 60 V_{DC} and 100 V_{DC} respectively; (C) partial recirculation observed at 120 V_{DC}; (D) increasing recirculation at 200 V_{DC}; (E) shows the recirculation effects that caused non-compliant behavior of cells to the DEP force; and (F) close-up of some cells that tend to reach the exit showing recirculation as well.*

This interesting development may be associated with the inter-relation of the high potentials with the electric current within the channel, which, could generate a substantial amount of temperature

rise that interferes with the conductivity of the fluid-particle system. Since dielectrophoretic force is a function of conductivity of the fluid-particle system, DEP is hampered as Joule heating becomes more predominant due to the increased temperature. This simulation neglected particle-particle interaction on the basis of experiments since the cell suspension were to be diluted to an extent where in the cells will substantial be far apart that their interaction can be considered inconsequential.

5.4.5 Validation of the DEP microwell technique

The electrophysiological properties for PBMCs obtained data through our novel microwell platform via DEP cross-over frequency measurement were validated by comparing the reported data in literature obtained through DEP electro-rotation measurement as reported by Chan et al. [38]. The samples used in this research and the reported literature values were from non-pregnant young female (<50 Years of age) since pregnancy tends to substantially lower the specific membrane conductance of PBMCs [38]. The electrophysiological properties for PBMCs obtained from our experiments and the literature reported values were used to run the simulation independently under the same operating conditions.

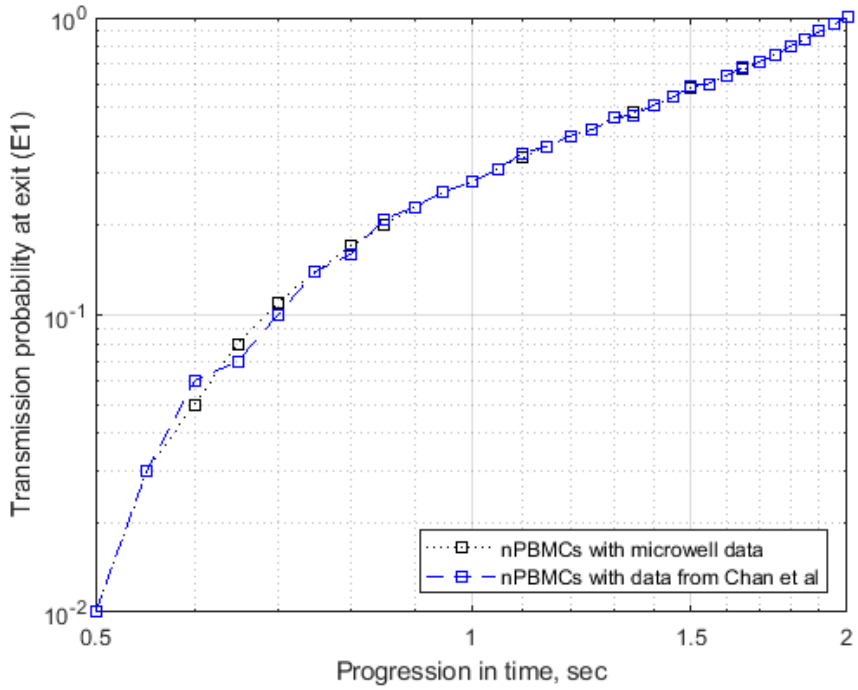

Figure 5. 10 *Validation of the electrophysiological properties of healthy PBMCs obtained from the DEP microwell platform using cross-over frequency measuement and the literature reported values based on electro-rotation excperiments [38]. Both the samples were derived from a non-pregnant young women (< 50 years of age).*

The results of the comparative simulation where a log-log plot of transmission probability (TP) and the progression time were plotted as shown in Figure 5.10.. Statistically, the P value obtained for

this comparison was 0.1 (at 0.01 significance level) implying that we do not have enough evidence to reject the null hypothesis of "no significant difference" between the two outcomes.

5.5 Conclusions

Continuous dielectrophoretic separation of infiltrating ductal adenocarcinoma cells (ADCs) from isolated peripheral blood mononuclear cells (PBMCs) using direct current in a semi-circular insulator-based microchannel has been numerically studied. The electrophysiological properties for PBMCs used in simulations were obtained in a novel DEP microwell platform that characterized the behavior of the cells under varying AC frequency by measuring the DEP crossover of the cells. The first and second crossover frequency obtained were curve-fitted using a single shell model to obtain the conductivity and permittivity of the PBMCs. PBMCs vary in size and the sample used in this experiment was majorly small size lymphocytes i.e. ~10 μm in diameter.

Dielectrophoretic force is a function of the gradient of the electric field-a factor that also depend on the applied voltage as well as the constriction radius. In order to induce sufficient field gradient for the dielectrophoretic separation of ADCs from PBMCs, the applied DC potential and the constriction diameter were dynamically varied until a regime of perfect simulation was obtained at constriction diameter of 100 μm and applied DC potential of ~50V. Number of constrictions in the channel also affects separation efficiency and 5 semi-circular constrictions lead to optimal sorting of ADCs from PBMCs. This insulator-DEP based method of separating infiltrating ductal adenocarcinoma cells (ADCs) from isolated peripheral blood mononuclear cells (PBMCs) using direct current provided a cheaper, less cumbersome, easier-to-use, and yet efficient approach when compare with previous methods that used deformability, magnetism, or dielectric affinity column. Discretization of domain (meshing) in numerical analysis is an important factor that affect the accuracy of the solution obtained from solving any associated physics within a microchannel. In this paper, effort was made to strike a balance between the computational requirements of the mesh size and the desired transmission probability. Mesh size (local and global) was carefully chosen such that the resultant solution of the simulation did not vary with meshing. To aid our understanding of the choice of applied potential and how it relates with the separation efficiency, we found out that increasing the voltage beyond 100 V_{DC} would lead to no separation i.e. both PBMCs and ADCs moved into one exit channel.

Another interesting phenomenon was observed at higher voltages (>100 V) along with separation was recirculation behavior of cells. Some of the cells that were moving towards the exit channels were forced to change their direction back to the inlet. Recirculation increased especially between the constriction region and the bifurcation into exit channels with increasing DC potential. This behavior or wake formation is due to increased Joule heating as the temperature rises in the

microfluidic platform with increasing DC potential since DEP is a function of the conductivity of the medium.

This DEP spectroscopy technique based on crossover measurement allows characterizing the intracellular differences and physical properties of cells, without any labeling, without affecting cell integrity and viability. Finally, this method confirms a high potential of emerging lab-on-chip (LOC) platforms in the early diagnosis and the treatment of breast cancer especially in young women where mammography is ineffective and/or painful.

Acknowledgements: We would also like to acknowledge the past undergraduate researchers Amanda Vu and Sheila Briggs for their help in DEP microwell experiments.

Funding: This research did not receive any specific grant from funding agencies in the public, commercial, or not-for-profit sectors. However, we would like to acknowledge the partial funding granted by IDeA Network of Biomedical Research Excellence (INBRE) via supporting summer INBRE undergraduate fellow.

References

[1] B. Cao, F. Bray, A. Ilbawi, and I. Soerjomataram, "Effect on longevity of one-third reduction in premature mortality from non-communicable diseases by 2030: a global analysis of the Sustainable Development Goal health target," *The Lancet Global Health,* vol. 6, pp. e1288-e1296, 2018.

[2] E. Obermayr, G. Bises, G. Pfeiler, M. Gneist, F. Wrba, M. de Santis, R. Zeillinger, M. Hudec, and C. Dittrich, "Detection of EpCAM positive and negative circulating tumor cells in metastatic breast cancer patients AU - Königsberg, Robert," *Acta Oncologica,* vol. 50, pp. 700-710, 2011/06/01 2011.

[3] E. Adekanmbi and S. Srivastava, "Dielectrophoretic applications for disease diagnostics using lab-on-a-chip platform," *Lab Chip,* p. 2148, 2016.

[4] *Breast cancer statistics*. Available: https://www.breastcancer.org/symptoms/understandbc/-statistics

[5] J. den Toonder, "Circulating tumor cells: the Grand Challenge," *Lab on a Chip,* vol. 11, pp. 375-377, 2011.

[6] N. M. Karabacak, P. S. Spuhler, F. Fachin, E. J. Lim, V. Pai, E. Ozkumur, J. M. Martel, N. Kojic, K. Smith, P.-i. Chen, J. Yang, H. Hwang, B. Morgan, J. Trautwein, T. A. Barber, S. L. Stott, S. Maheswaran, R. Kapur, D. A. Haber, and M. Toner, "Microfluidic, marker-free isolation of circulating tumor cells from blood samples," *Nature Protocols,* vol. 9, p. 694, 02/27/online 2014.

[7] S. P. Hammar, "Metastatic adenocarcinoma of unknown primary origin," *Human Pathology,* vol. 29, pp. 1393-1402, 1998/12/01/ 1998.

[8] M. Mego, "Emerging role of circulating tumor cells in cancer management," *Indian journal of medical and paediatric oncology : official journal of Indian Society of Medical & Paediatric Oncology,* vol. 35, pp. 237-238, Oct-Dec 2014.

[9] (Feb 5). *Whole Blood is the Best Biospecimen for Isolating Peripheral Blood Mononuclear Cells*. Available: https://www.dls.com/biopharma/blog/3-reasons-whole-blood-is-necessary-for-pbmc-isolation

[10] P. R. Gascoyne and S. Shim, "Isolation of circulating tumor cells by dielectrophoresis," *Cancers (Basel),* vol. 6, pp. 545-79, Mar 12 2014.

[11] S. Nagrath, L. V. Sequist, S. Maheswaran, D. W. Bell, D. Irimia, L. Ulkus, M. R. Smith, E. L. Kwak, S. Digumarthy, A. Muzikansky, P. Ryan, U. J. Balis, R. G. Tompkins, D. A. Haber, and M. Toner, "Isolation of rare circulating tumour cells in cancer patients by microchip technology," *Nature,* vol. 450, p. 1235, 12/20/online 2007.

[12] G. Deng, M. Herrler, D. Burgess, E. Manna, D. Krag, and J. F. Burke, "Enrichment with anti-cytokeratin alone or combined with anti-EpCAM antibodies significantly increases the sensitivity for circulating tumor cell detection in metastatic breast cancer patients," *Breast Cancer Research,* vol. 10, p. R69, August 07 2008.

[13] D. Wlodkowic and J. M. Cooper, "Tumors on chips: oncology meets microfluidics," *Current Opinion in Chemical Biology,* vol. 14, pp. 556-567, 2010/10/01/ 2010.

[14] B. D. Plouffe, L. H. Lewis, and S. K. Murthy, "Computational design optimization for microfluidic magnetophoresis," *Biomicrofluidics,* vol. 5, pp. 13413-13413, 2011.

[15] Y. Liu, D. Hartono, and K. M. Lim, "Cell separation and transportation between two miscible fluid streams using ultrasound," *Biomicrofluidics,* vol. 6, pp. 12802-1280214, Mar 2012.

[16] P. R. C. Gascoyne, X.-B. Wang, Y. Huang, and F. F. Becker, "Dielectrophoretic separation of cancer cells from blood," *IEEE Trans. Ind. Appl.,* vol. 33, pp. 670-678, 1997.

[17] F. F. Becker, X.-B. Wang, Y. Huang, R. Pethig, J. Vykoukal, and P. R. C. Gascoyne, "Separation of human breast cancer cells from blood by differential dielectric affinity," *Proc. Natl. Acad. Sci.,* vol. 92, pp. 860-864, 1995.

[18] H.-S. Moon, K. Kwon, S.-I. Kim, H. Han, J. Sohn, S. Lee, and H.-I. Jung, "Continuous separation of breast cancer cells from blood samples using multi-orifice flow fractionation (MOFF) and dielectrophoresis (DEP)," *Lab on a Chip,* vol. 11, pp. 1118-1125, 2011.

[19] X. Y. Fang Yang, Hong Jiang, William M. Butler, Guiren Wang, "Dielectrophoretic separation of prostate cancer cells," *Technology in Cancer Reserach and Treatment,* vol. 12, 2013.

[20] D. D. Zerbino, "[Biopsy: its history, current and future outlook]," *Likars'ka sprava,* pp. 1-9, 1994 Mar-Apr 1994.

[21] J. An, J. Lee, S. H. Lee, J. Park, and B. Kim, "Separation of malignant human breast cancer epithelial cells from healthy epithelial cells using an advanced dielectrophoresis-activated cell sorter (DACS)," *Anal Bioanal Chem,* vol. 394, pp. 801-9, Jun 2009.

[22] M. Alshareef, N. Metrakos, E. J. Perez, F. Azer, F. Yang, X. Yang, and G. Wang, "Separation of tumor cells with dielectrophoresis-based microfluidic chip," *Biomicrofluidics,* vol. 7, pp. 011803(1-12), 2013.

[23] S. K. Srivastava, P. R. Daggolu, S. Burgess, and A. R. Minerick, "Dielectrophoretic characterization of erythrocytes: Positive ABO blood types," *Electrophoresis,* vol. 29, pp. 5033-5046, 2008.

[24] S. Srivastava, A. Gencoglu, and A. Minerick, "DC insulator dielectrophoretic applications in microdevice technology: a review," *Anal. Bioanal. Chem.,* vol. 399, pp. 301-321, 2011.

[25] R. Pethig, "Dielectrophoresis: Status of the theory, technology, and applications," *Biomicrofluidics,* vol. 4, pp. 1-35, 2010.

[26] R. Pethig, "Review Article—Dielectrophoresis: Status of the theory, technology, and applications," *Biomicrofluidics,* vol. 4, p. 022811, 06/29 05/24/received06/01/accepted 2010.

[27] A. Gencoglu and A. Minerick, "Chemical and morphological changes on platinum microelectrode surfaces in AC and DC fields with biological buffer solutions," *Lab on a Chip,* vol. 9, pp. 1866-1873, 2009.

[28] S. Ozuna-Chacón, B. H. Lapizco-Encinas, M. Rito-Palomares, S. O. Martínez-Chapa, and C. Reyes-Betanzo, "Performance characterization of an insulator-based dielectrophoretic microdevice," *Electrophoresis,* vol. 29, pp. 3115-3122, 2008.

[29] C.-F. Chou, J. O. Tegenfeldt, O. Bakajin, S. S. Chan, E. C. Cox, N. Darnton, T. Duke, and R. H. Austin, "Electrodeless Dielectrophoresis of Single- and Double-Stranded DNA," *Biophys. J.,* vol. 83, pp. 2170-2179, 2002.

[30] E. B. Cummings and A. K. Singh, "Dielectrophoresis in Microchips Containing Arrays of Insulating Posts: Theoretical and Experimental Results," *Anal. Chem.,* vol. 75, pp. 4724-4731, 2003.

[31] H. Moncada-Hernández and B. H. Lapizco-Encinas, "Simultaneous concentration and separation of microorganisms: insulator-based dielectrophoretic approach," *Anal. Bioanal. Chem.,* vol. 396, pp. 1805-1816, 2010.

[32] H. Shafiee, J. L. Caldwell, M. B. Sano, and R. V. Davalos, "Contactless dielectrophoresis: a new technique for cell manipulation," *Biomed. Microdevices,* vol. 11, pp. 997-1006, 2009.

[33] R. R. Pethig, *Dielectrophoresis: Theory, Methodology and Biological Applications*: Wiley, 2017.

[34] S. Ghosal, "Fluid mechanics of electroosmotic flow and its effect on band broadening in capillary electrophoresis," *ELECTROPHORESIS,* vol. 25, pp. 214-228, 2004.

[35] V. Tandon, S. K. Bhagavatula, W. C. Nelson, and B. J. Kirby, "Zeta potential and electroosmotic mobility in microfluidic devices fabricated from hydrophobic polymers: 1. The origins of charge," *ELECTROPHORESIS,* vol. 29, pp. 1092-1101, 2008.

[36] R. W. O'Brien and L. R. White, "Electrophoretic mobility of a spherical colloidal particle," *Journal of the Chemical Society, Faraday Transactions 2: Molecular and Chemical Physics,* vol. 74, pp. 1607-1626, 1978.

[37] S. K. Srivastava, J. L. Baylon-Cardiel, B. H. Lapizco-Encinas, and A. R. Minerick, "A continuous DC-insulator dielectrophoretic sorter of microparticles," *J. Chromatogr. A,* vol. 1218, pp. 1780-1789, 2011.

[38] E. O. Adekanmbi, M. W. Ueti, B. Rinaldi, C. E. Suarez, and S. K. Srivastava, "Insulator-based dielectrophoretic diagnostic tool for babesiosis," *Biomicrofluidics,* vol. 10, p. 033108, 2016.

[39] C. Huang, H. Liu, N. Bander, and B. Kirby, "Enrichment of prostate cancer cells from blood cells with a hybrid dielectrophoresis and immunocapture microfluidic system," *Biomedical Microdevices,* vol. 15, pp. 941-948, 2013/12/01 2013.

[40] B. J. Kirby, *Micro- and Nanoscale Fluid Mechanics: Transport in Microfluidic Devices*. Cambridge: Cambridge University Press, 2010.

[41] G. Qiao, W. Duan, C. Chatwin, A. Sinclair, and W. Wang, "Electrical properties of breast cancer cells from impedance measurement of cell suspensions," in *International Conference on Electrical Bioimpedance*, 2010, p. 4.

[42] E. O. Adekanmbi and S. K. Srivastava, "Dielectrophoretic applications for disease diagnostics using lab-on-a-chip platforms," *Lab on a Chip,* vol. 16, pp. 2148-2167, 2016.

[43] K. L. Chan, H. Morgan, E. Morgan, I. T. Cameron, and M. R. Thomas, "Measurements of the dielectric properties of peripheral blood mononuclear cells and trophoblast cells using AC electrokinetic techniques," *Biochimica et Biophysica Acta (BBA) - Molecular Basis of Disease,* vol. 1500, pp. 313-322, 2000/03/17/ 2000.

Chapter 6: Application of crossover frequency measurements for the characterization of biosorption of rare-earth elements by *Cupriavidus necator*

Ezekiel O. Adekanmbi[1], Bennett A.C. Carv[1], Anthony T. Giduthuri[1], Jonathan Counts[1], James G. Moberly[1], Soumya K. Srivastava[1*]

[1]Department of Chemical & Materials Engineering, University of Idaho, Moscow, ID 83844

Abstract

This work presents the dielectric characterization of rare-earth elements biosorption by *Cupriavidus necator* using dielectrophoretic crossover frequency quantification. A 3 mm-diameter microwell was used to obtain the membrane dielectric properties of human erythrocytes (blood group O) as a baseline for validating our novel dielectrophoretic crossover frequency technique. Dielectric properties obtained from our crossover frequency technique were compared with those obtained from the modified electrorotation experiments using paired t-test. Student's t-test performed on the crossover measurements for each of the cases (at 7 degrees of freedom and α=0.05) gave a t-stat value of -1.482 which is less than the t-critical value of -2.385 for a one-tail test indicating agreeable similarity. Quantified dielectric properties of native *Cupriavidus necator* (REE^-) and those exposed to rare-earth elements (REE^+): Europium, Neodymium, and Samarium revealed a substantial change in the surface characteristics of the *Cupriavidus necator* after exposure to REE solution. The response of C-nec to changes in REE exposure is substantially different in Europium but similar between Neodymium and Samarium REEs. There was no significant change in the cytoplasmic properties of C-nec suggesting a dominant adsorption scenario.

Introduction

Rare earth elements (REEs) are essential for manufacturing modern electronics, certain medical diagnostic and imaging time equipment, and electric motors due to their unique magnetic, phosphorescent, and catalytic properties[2-6]. Their demand has increased over the years because of these properties. However, they are limited in supply owing to limited number of production sites globally. Besides, the environmental challenges associated with mining and separation of REEs are major issues and alternative methods for obtaining these elements are needed[7, 8]. Over the years several environmentally-friendly methods of recovering REEs, including biological methods, have been attempted[9]. Of these techniques, biosorption has gained attention[5, 10-12]. Biosorption is a method of using biological material e.g. bacteria, to bind and concentrate metals[13]. *Bacillus subtilis*[14-18], *Myxococcus xanthus*[19], *Escherichia coli*[16, 18, 20], *Pseudomonas fluorescens* [18, 21], *Arthobacter nicotianae*[22], and many other bacteria have been utilized as biosorbents for REEs[20, 23-25]. Removal of REE (and metals, in general) by bacteria stems from the interaction of

the bacteria with the rare earth elements[26]. This interaction can take four different forms: surface adsorption, adsorption on extracellular biopolymer, biologic absorption and adsorption on extracellular biominerals[27]. Most commonly, the interaction is through adsorption onto the cell membrane, uptake into the cytosol, or both [5, 28-31]. Adsorption affects the membrane characteristics (e.g., membrane dielectric, membrane net surface charge) of microorganism while uptake influences the cytoplasm (e.g., membrane potential, cytosolic dielectric). The traditional means of characterizing biomass for biosorption is limited and time consuming, hence we are presenting, for the first time, an electrokinetic method termed as dielectrophoresis for the characterization of biosorption (adsorption or uptake) of REEs by gram negative bacteria - *Cupriavidus necator*.

Dielectrophoresis (DEP) is a phenomenon that has been used to obtain the intrinsic electrophysiological identities of diverse biological materials [32-34]. DEP is the force induced on polarizable particles in non-uniform electric fields resulting in the translational motion of the particles according to their distinct dielectric identities and the interaction of the field-induced polarization with the applied field [35, 36]. The DEP force is dependent on many factors including characteristics of the external field, electrophysical nature of the polarizable particles and their suspending medium. While it is very common to use DEP for selective trapping, enrichment, and manipulation of biomolecules[37-39], it can also be used to obtain their intrinsic electric properties[40-43]. Various methods have been used to characterize dielectric properties of biological materials including electrorotation[44-46], DEP collection spectra[47], crossover frequency measurement[48], and capture voltage spectrum[49]. Until now, DEP has not been used to identify biomass which accumulates REEs. In this study, we present, for the first time, the dielectrophoretic evaluation of the behavior of *Cupriavidus necator* in its native (REE^-) and REE-binding (REE^+) states under non-uniform electric field using the method of crossover frequency measurement. This is the first step toward the design of DEP-based diagnostic platform technology to improve screening of biomass for sorption of REEs.

Materials and Methods

Microorganism medium and cultivation conditions:

Cupriavidus necator (ATCC # 17697) used for biosorption assays were grown on medium consisting of (per liter) 1.2 grams ammonium sulfate, 0.83 grams magnesium chloride hexahydrate, 0.097 grams calcium chloride dihydrate, 10 grams anhydrous citric acid, 1 gram yeast extract, and 11 grams 1,4-Piperazinediethanesulfonic acid (PIPES) buffer. One milliliter per liter of medium of a concentrated trace elements solution was added consisting of 68 mg zinc chloride, 67 mg cupric chloride dihydrate, 64 mg cobalt chloride, 75.8 mg manganese chloride, 11.7 mg sodium molybdate dihydrate, and 31 mg boric acid per liter. The pH of the medium was adjusted to 7.2 using sodium hydroxide and autoclaved in sealed serum bottles to sterilize prior to use. For all assays, *C. necator* was

grown in an orbital shaker at 135-rpm and 35°C. Parent solutions of *C. necator* were inoculated (2% v/v) into media from freezer stocks, grown to early stationary phase, inoculated into new media, and grown to early stationary phase (~12 hrs.) prior to use in biosorption assays. Stationary phase cells in non-growth media were used for biosorption assays to minimize potential differences between cells in different periods of growth that might impact metal uptake and apparent electrophysiological properties.

Chemical speciation predictions:

Chemical speciation of transition metals in aqueous solution, including rare earth elements, vary with pH. Visual MINTEQ ver. 3.1 was used to predict the speciation of europium, neodymium and samarium in the acetic acetate buffered saline (AABS). Prediction of precipitation was also monitored formation is expected to result in decrease biosorption performance. In addition, precipitates present may clog the microdevice, therefore should be minimized. Precipitates would also render the methods used to measure REEs invalid as REE precipitates may pellet with cells during centrifugation, showing increased "biosorption" when none is occurring. A prediction of the potential chemical species was performed with the Visual MINTEQ 3.1 software package [50] that is freely available. Thermodynamic sweeps were performed over temperatures from 15 degrees Celsius to 75 degrees Celsius with 10-degree increments at a constant pH of 5 were run and over pH values of 2 to 10 at 0.5 pH increments at constant temperature of 35 degrees Celsius. Results for these predictions were used for experimental design and result analysis.

Biosorption assay:

AABS was used during contact of REEs with *C. necator* biomass to minimize the potential for growth medium component complexation or precipitation and additional growth of *C. necator* cells. AABS consisted of 43.65 mg per liter of sodium chloride adjusted to a pH of 5 with 0.1 M sodium acetate buffer. Using sequential centrifugation (20,000 RCF for 15 minutes) and washing steps, *C. necator* cells were rinsed three times in AABS prior to use. After the final wash, the supernatant was decanted and the pellet was vortexed with 35 ml of ~500 μM single element REE in AABS and incubated at 35°C for one hour to allow biosorption of metals. Incubated cells were sequentially centrifuged and washed with AABS for 30 min at 30,000 RCF. Dilutions of the washed cell pellet were suitable for testing in the DEP microdevice.

REE concentration effect panel: An REE concentration panel was used to determine the average absorption capacity for each REE being investigated. Prior to each experiment, REE solutions were prepared for biosorption. The REE concentration panel consisted of approximately 8%, 12%, 16%, 20%, 40%, and 60% of stock solution concentrations. The REE solutions were made by adding a set volume in milliliters of REE stock solution to a 50 mL Falcon tube. The Falcon tube was then filled to

50mL with AABS solution of pH 5. Of the 50 mL of solution, 15 mL was saved for analysis while 35 mL was used to suspend bacteria pellet for biosorption to occur. All experiments were performed at 35ºC.

Temperature effect panel: These experiments were used to determine the effect on biosorption by temperature. REE solutions were made up the same way as for the concentration pellet with the concentration being held at 16% stock concentration. The biosorption process was performed at 15ºC, 35ºC, 55ºC, and 75ºC.

pH effect panel: These experiments were used to determine the effect on biosorption by pH. REE solutions were made up the same way as for the concentration pellet with the concentration being held at 16% stock concentration. The biosorption process was performed at pH 4.5, 5, 5.5, and 6. Temperature was held constant at 35ºC.

DEP Microorganism pretreatment:

Prior to dielectrophoretic experimentation, D-glucose (50 g/L) isotonic medium was divided into six sets. The conductivity of each set as modified with predetermined amount of potassium chloride (KCl) till values between 0.01-0.06 S/m were obtained. *C. necator* in its natural state (REE^-) and *C. necator* in its metal-bound states (REE^+) were centrifuged at ambient temperature at 10,000 rpm for 10 min to avoid cell damage due to centrifugal compaction. The resultant pellets were isolated and resuspended in ~ 600µL of each of the six isotonic medium prepared above. This was centrifuged again, and the isolated pellets were resuspended with a fresh solution A with a solution volume that resulted in the final cell density of 1.5 X 10^3 cells/ml with 12% margin of error. The cell number was estimated using Marienfeld's counting chamber. Two (2) µL of the final cell suspension was used for crossover frequency measurement.

Microwell fabrication and experimental set-up:

Sylgard 184 Silicone Elastomer (Dow Corning, Midland, MI, USA) were mixed with its accompanied curing agent and cured as described previously [51]. Cured poly (dimethyl siloxane) (PDMS) was cut into 50 X 50 mm^2 squares. Microwells of 3 mm diameter were created in the PDMS squares to house a pair of perpendicularly arranged high grade, 0.008" diameter, 99.95 % pure platinum wires that were exposed to plasma using an in-house microwave plasma cleaner [52] and then sealed onto a 0.5 mm thick borosilicate glass slide. High grade 0.008" diameter platinum wires were arranged as shown in Fig. 10A and the distance between them was set using an Olympus IX inverted microscope. One electrode served as a point electrode while the other electrode served as the planar electrode. Once electrodes were positioned using the microscope, Loctite® epoxy mixture was used to permanently adhere the electrodes into position so that the distance between each electrode was fixed.

Crossover measurement:

Two (2 µl) microliters of the cell suspension (conductivity 0.0.1 S/m) was pipetted into the microwell. After the microorganism had settled in the microwell, platinum electrodes were connected to function generator (Siglent SDG 2082X) and operated with a sinusoidal amplitude of 8 Vpp and frequency was changed manually from 0-800 KHz to observe nDEP, crossover, and pDEP. The experiment was repeated six (6) times using the same sample to obtain an average crossover of the technical replicates. Three biological replicates of the experiment were made with different samples. Both technical and biological replicates experiments were performed using each of the remaining five medium conductivity 0.02-0.06 S/m) to suspend the bacteria (REE^- and REE^+)

Microwell design validation:

Red blood cells (RBCs) were used as a biological material of known parameters to validate the microwell design. RBCs were obtained from a commercial source (Research Innovation Incorporated, VA, USA) and pretreated as reported by Gascoyne *et al.* [53]. RBC crossover frequencies were measured using the DEP method described above. The movement of RBCs in terms of nDEP and pDEP were noted alongside the static crossover point where the time-averaged DEP force on the RBCs were zero. The measurements were completed in approximately one minute. A hypothesis, that no significant difference occurred between modified electrorotation reported by Gascoyne and the point-planar crossover frequency measurement results (reported here) was evaluated using a paired t-test.

Dielectric property extraction:

The relationship between first crossover frequency and medium conductivity as given by Gascoyne et al.[54] is;

$$f_{co1} = \frac{1}{\sqrt{2}} \cdot \frac{\sigma_m}{\pi r C_{mem}} \sqrt{1 - \frac{rG_m}{2\sigma_m} - 2\left(\frac{rG_{mem}}{2\sigma_m}\right)^2} \tag{6.1}$$

The relationship between the second crossover frequency and medium conductivity is also given as

$$f_{co2}^2 = \frac{1}{4\pi^2} \frac{1}{\varepsilon_0^2} \frac{(\sigma_m - \sigma_{cyto})(\sigma_{cyto} + 2\sigma_m)}{(\varepsilon_{cyto} - \varepsilon_m)(\varepsilon_{cyto} + 2\varepsilon_m)} \tag{6.2}$$

where f_{co1} and f_{co2} are the first and second crossover frequencies respectively, σ_m – medium conductivity, ε_m – medium permittivity, G_{mem} – specific membrane conductance, C_{mem} – specific membrane capacitance, ε_{cyto} – cytoplasmic permittivity, σ_{cyto} – cytoplasmic conductivity, ε_o – permittivity of vacuum and *r* is the characteristic bioparticle size. Equation 6.1 is used to fit the crossover frequency *vs.* medium conductivity data to obtain C_{mem} and G_{mem} while Equation 6.2 is for fitting second crossover frequency data to obtain σ_{cyto} and ε_{cyto}.

Result and discussion

Chemical Speciation:

Aqueous chemical speciation predictions of Eu, Nd, and Sm in AABS are presented here. Within the pH and temperature spectrum studied, Eu occurs in four distinct species at measurable concentrations: Eu^{3+}, $EuCl^{2+}$, Eu-Acetate^{2+}, and $EuOH^{2+}$. As shown in **Figure 6.1,** with increasing pH, Eu^{3+} decreases as $EuOH^{2+}$ increases. Above pH 6.5, europium hydroxide precipitates are predicted to form (saturation indices approach or exceed 0). Precipitates are undesirable as they are less likely to be biosorbed by organism, may falsely increase perceived biosorption, and may clog the microdevice. From these results, it is inferred that Eu biosorption experiments should remain below pH 6. From **Supplemental Figure 1**, it is shown that Nd^{3+} decreases while $NdOH^{2+}$ increases with increasing pH above 7. No Nd-chloride species are predicted to form. Neodymium hydroxide hydrolysis products begins oversaturate above pH 7.5. From these results, it is inferred that Nd biosorption experiments should remain below pH 7. From **Supplemental Figure 2**, it is shown that Sm^{3+} decreases while $SmOH^{2+}$ increases with increasing pH. Sm hydroxide hydrolysis products begins oversaturate above pH 7. From these results, Sm biosorption experiments should be performed below pH 6.5. To avoid potential precipitate

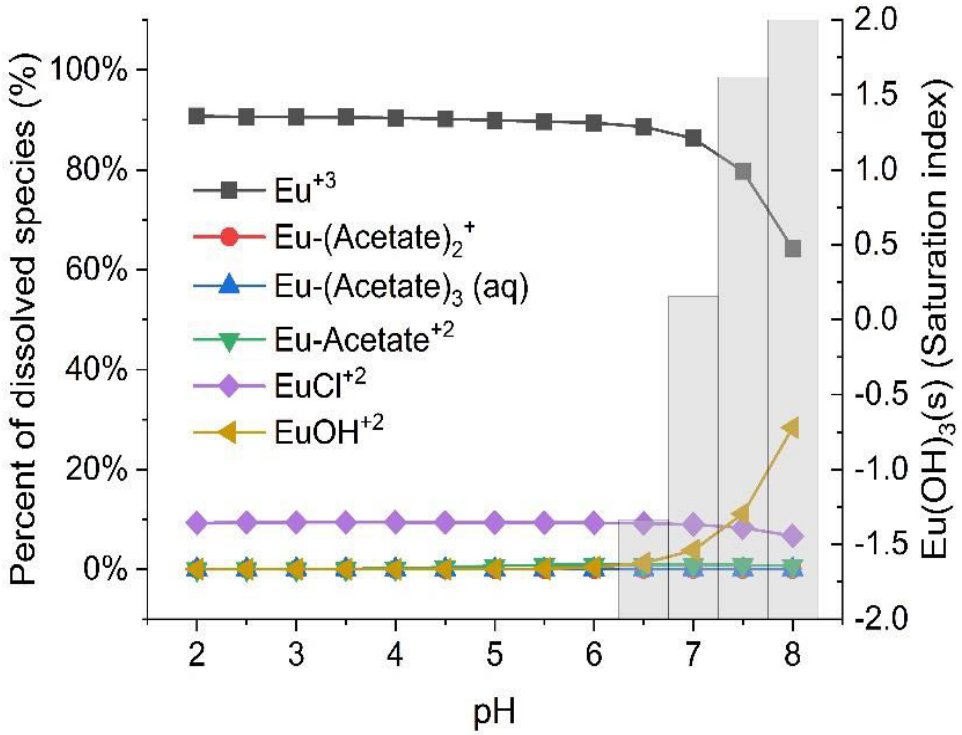

Figure 6.1: *Predicted chemical speciation of dissolved europium (60µM) in acetic acetate buffered saline at 25°C and saturation indices of $Eu(OH)_3$. Above pH 6.5 Eu-hydroxides are predicted to form.*

formation, biosorption experiments were carried out at pH 5 (unless otherwise stated).

Biosorption assay

REE concentration effect panel: Figure 6.2 presents the biosorption of different concentration of Eu onto approximately 0.07 grams (wet weight) of *C. necator* biomass in AABS at 35°C and pH 5. With increased Eu concentration, biomass saturates and more Eu is observed free in solution. Similar trends were observed for Sm and Nd (data not shown). This information provides a basis for biomass loading and REE dosing for further sorption evaluations.

Temperature effect panel: Because of the potential for increases in temperature within a microdevice operated for long periods, an evaluation of REE sorption to biomass under different temperatures was assessed. Amount of REE sorbed to biomass increased with increasing temperature (Figure 6.3). Since *C. necator*'s uptake is greater at higher temperatures, temperatures of up to 75°C may be acceptable for this bacterium to experience in microdevice without desorption occurring. However, cells expressed a different phenotype at 75°C compared to the lower temperatures studied. The 75°C exposure

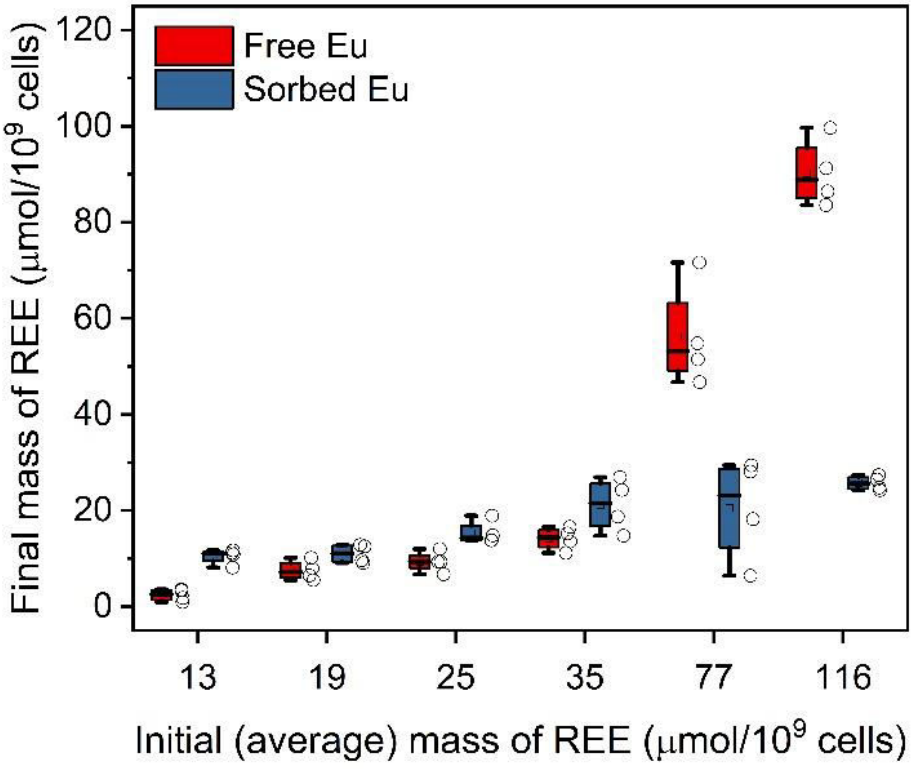

Figure 6.2: *Box and whisker plot of partitioning of Eu to C. necator biomass in AABS after 1-hr exposure at 35°C at pH 5. Boxes represent 25-75% of data while whiskers represent 1.5 times standard deviation. The mean of each dataset is represented by a line within the box and circles represent each measurement from quadruplicate samples. Initial biomass loading for each was approximately 0.07g wet weight.*

that were formed appeared to have a white coloration and where much weaker (more easily ruptured) than the pellets from the lower exposure temperatures. This increase in biosorption may be due to denaturing of proteins at higher temperatures that make the cell more permeable and expose more reactive sites for REE sorption. Since cells experienced a noticeable change in phenotype between the 55°C and 75°C, to ensure that the cells are have the same characteristics during separation in the DEP device, it may be advisable to ensure temperatures do not exceed 55°C within the device for *C. necator* cells

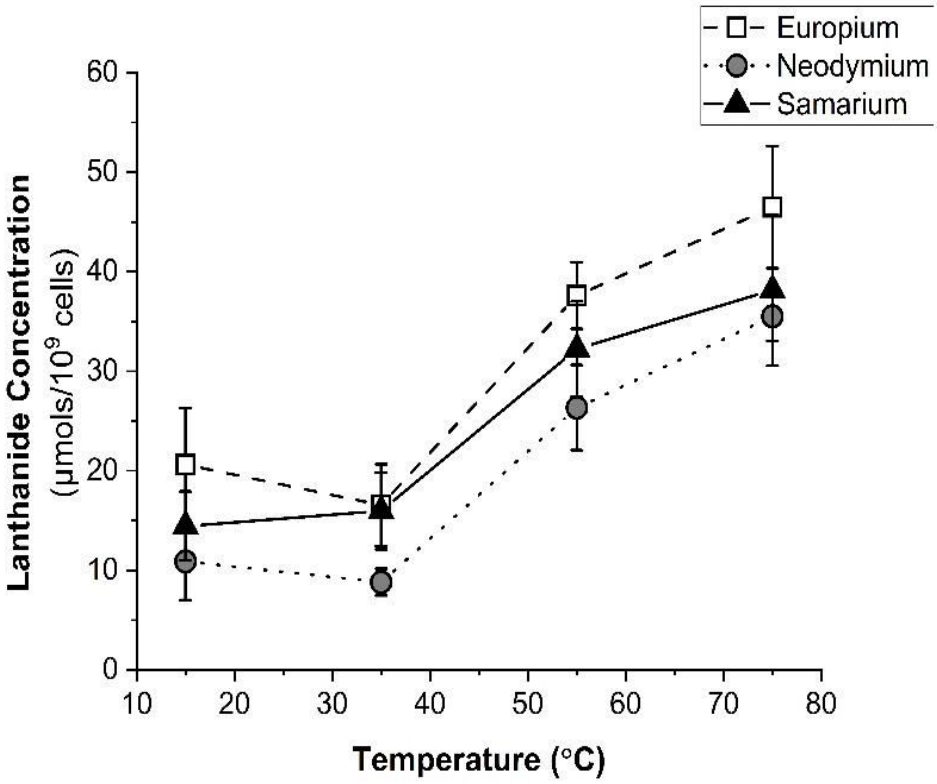

Figure 6.3: *Temperature profile for biosorption by C. necator of Eu, Nd, and Sm, at pH 5 and an average exposure concentration of 35 µmols per billion cells for Sm and Nd and 43 µmols per billion cells for Eu.*

pH Effect Panel: Since pH is known to have effects on both the speciation of REEs and functional groups that may be involved with binding with REEs during biosorption, pH variation studies were performed. Microdevices may experience pH differences when running for a long time, as well, exposing the cells to a gradient as it moves along the device. From Figure 6.4, as pH is increased, the biosorption capacity of Eu, Nd, and Sm decreases and then level out as preferred pH conditions for *C. necator* are approached. At

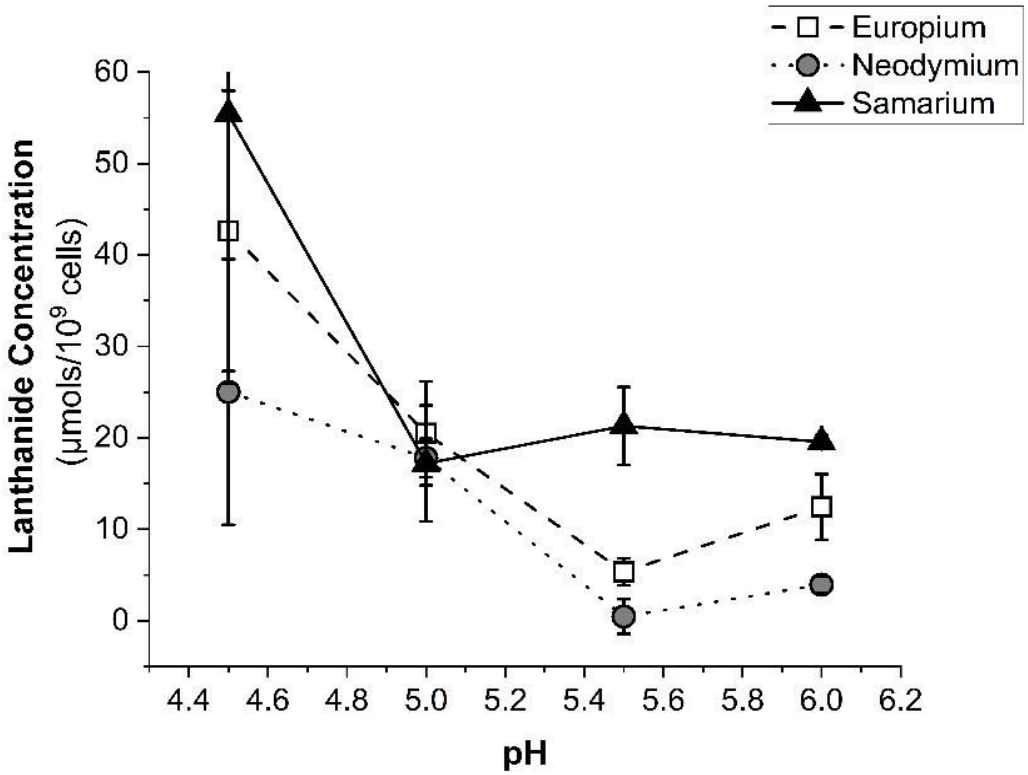

Figure 6.4: *Effect of pH on biosorption by C. necator of Eu, Nd and Sm at 35°C and exposure of approximately 30 µmols per billion cells for Eu and Nd and 40 µmols per billion cells for Sm.*

the pH around 5.5 and up, the rare earth elements start to approach the pH where hydrolysis reactions occur that may form precipitates. From these results, it appears that *C. necator* may be more effective at lower pH. Increases in sorption may be related to the speciation of the REEs in solution as the ionic form (REE^{3+}) dominates and these forms may be more readily adsorbed to the surface or transported into the *C. necator* cells then the complexes that are formed at the higher pH values. The pH adjustment may be attributed to the bacteria adjusting its environmental pH [55, 56]. This phenomenon has been observed in other bacteria to occur and is referred to as acid homeostasis [56]. A potentially counter intuitive path for increased uptake is that C. neactor biomass may uptake REEs to reduce internal increase in intracellular pH. For acidophilic microorganisms, an increased uptake of positively charged ions, like potassium, to increase the Donnan potential and decrease proton flux across the cell membrane [57]. Another complicating factor is the acetic acid used in the buffer, which becomes more neutrally charged at lower pH values (pKa of 4.75) and more easily transits the cell membrane. Once across the membrane and into a more neutral cytoplasm, acetic acid may dissociate, increasing the overall H^+ concentration in the cytoplasm and further triggering uptake responses [58].

Microwell measurement calibration:

Medium conductivity versus first crossover frequency of healthy human RBCs from the point-planar microwell design (this study) and electrorotation from Gascoyne *et al.* [53] is presented in Figure 6.5. The data obtained through the point-planar microwell, were fitted with eqn. (1) normalized with the average characteristic dimension of the cell.

It is evident from Fig. 5 that subjecting RBCs to the same pretreatment conditions [8.5% (w/v) sucrose and 0.3% (w/v) dextrose solution] should give comparable results whether we used electrorotation or point-and planar microwell platform provided that there is no change in the specific capacitance, specific conductance, and the dimensional ratio of the cells. In both cases (reported and experimental), the crossover frequency increases with the conductivity of the medium because the specific capacitance has to be kept constant. Student's t-test performed on the crossover measurements for each of the cases gave a t-stat value of -1.482 which is less than the t-critical value of -2.385 for a one-tail test. Hence, we fail to reject the null hypothesis since there is no significant difference between the modified electrorotation and the point-planar microwell crossover frequency measurement. These crossover frequency values are then used to estimate the dielectric properties of interest: membrane capacitance and membrane conductance. The parameter

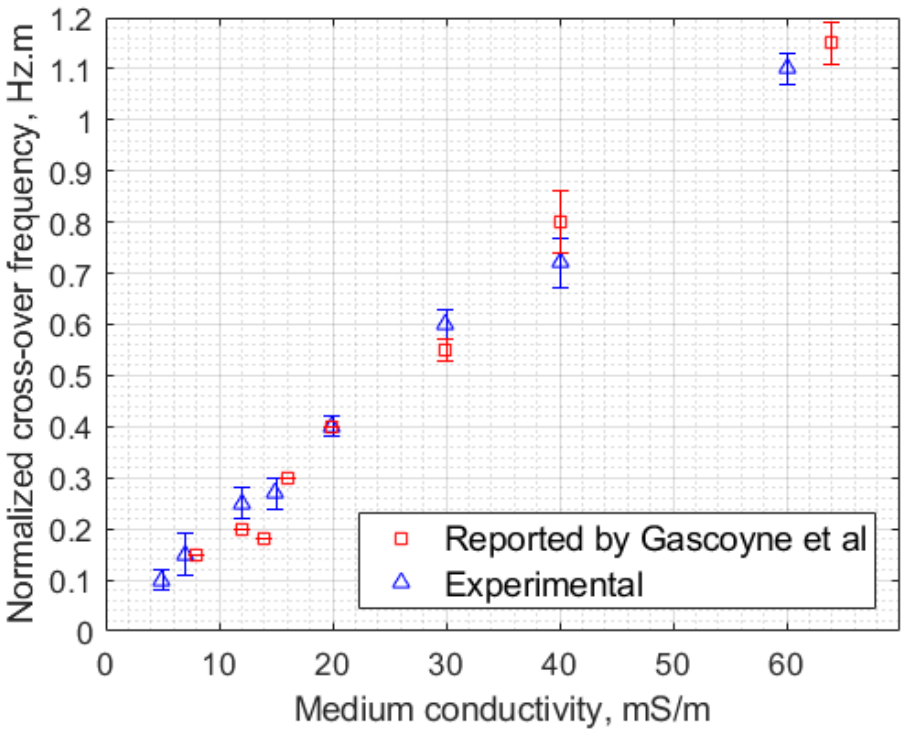

(A)

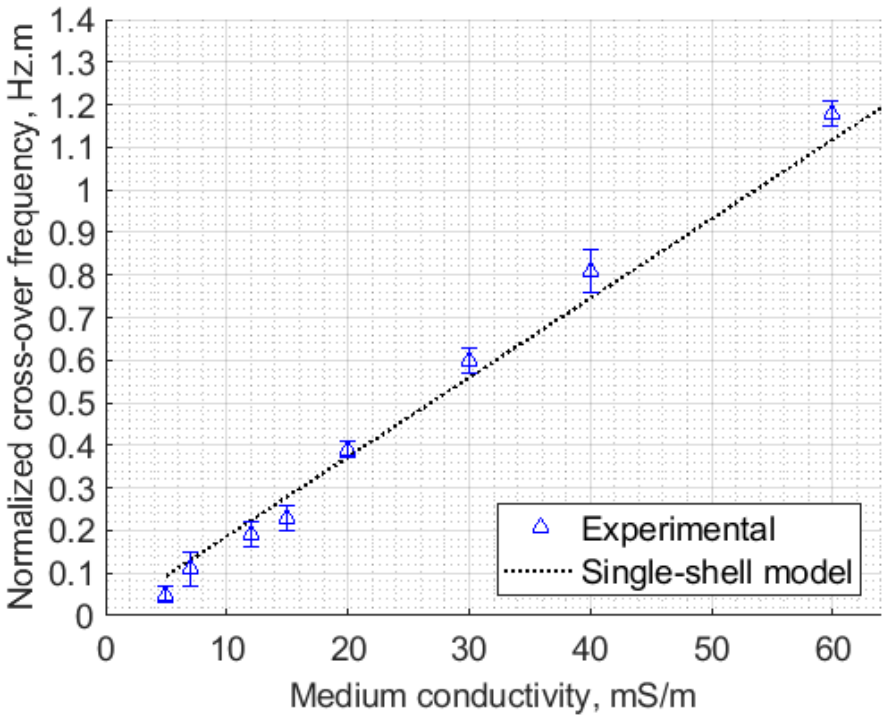

(B)

Figure 6. 5: *(A) Plots showing the crossover frequency vs medium conductivity data reported by Gascoyne et al.[1] and data obtained using the point-planar microwell experiment. Each of these data sets were obtained with 6 independent samples. (B) The experimental data were fitted with the oblate spheroid model given in equation 1*

estimates of membrane properties as obtained from the point-planar microwell experiments are compared with the reported data [53] and are given in Table 6.1.

The results in Figure 5 indicate that when the RBCs are suspended in the same medium and are subjected to nonuniform electric gradient via dielectrophoresis, their properties are the same (within the error of margin) as when they are measured via electrorotation. These results means that our point and planar microwell platform can now be dependably utilized to characterize REE^{+} and REE^{-}.

Table 6.1: *Estimate of membrane properties from point-planar microwell experiments in comparison to the reported values in literature [53]*

Specific Membrane properties	**Human Red Blood Cell (group O)**	
	Gascoyne et al (1997) [53]	**Microwell fit values**
Capacitance	11.8	10.5 ± 1.7
Conductance	271	266 ± 6.0

Analysis of C-nec and C-ree:

The same procedure for the calibration of RBCs from the previous section were used in obtaining the membrane properties of REE^{-} and REE^{+}. Figure 6.6A shows the typical arrangement of electrodes within the polymer-based microwell. The distance between the point and planar electrode

was fixed at ~75 µm as suggested by COMSOL® simulations to ensure that the field gradient is suffice for a relatively rapid response to the dielectrophoretic force. In Figure 6.6B, the microorganisms are seen aligning with the field lines. At this state, the Clausius-Mossotti factor depicts a higher polarizability of the suspending medium as compared to that of the C-nec themselves. All C-nec bacteria move away from the point electrode (high field region) showing nDEP behavior. Figure 6.6C shows the microorganisms experiencing major attraction towards the high-field region (pDEP). The C-nec are shown aligning between the planar and point electrode with significant interactions between them (showing chain formation of cells). The numerically-described distribution of electric field in a simple point-planar electrode arrangement is as shown in Figure 6.6D where the arrows show the spatial existence of particle within the field space.

With medium conductivities ranging between 5-60 mS/m, microorganism behavior was recorded based on the crossover frequencies. These crossover frequencies were averaged for fitting with single-shell model to reveal the dielectric constant (relative permittivity) as well as the conductivity of these bacteria (C-nec and C-ree). According to Equation 1, the relation between crossover frequency and medium conductivity has two unknowns: conductance and capacitance. These are related to relative permittivity and conductivity as described by Gascoyne et al [53]. These Estimation of these membrane properties are obtained through curve fitting.

Table 6.2: *Membrane properties calculated using MATLAB optimization algorithm from crossover frequency data obtained for C-nec and C-nec treated with three different REEs (C-ree)- Europium (C-Eu), Neodymium (C-Nd), and Samarium (C-Sm).*

Membrane Properties	**REE^-**	**REE^+ (Eu)**	**REE^+ (Nd)**	**REE^+ (Sm)**
Relative permittivity	12±0.010	15±0.040	14±0.010	14±0.009
Conductivity (S/m) *10^{-6}	0.05	0.03	0.02	0.02

The dielectric constant for C-nec was different from REE treated C-nec microorganisms (C-ree). With C-nec, the relative permittivity value of 12 underscores the idea that for a single-shell model, the cytoplasmic covering (membrane) behaves like a dielectric material which has the capacity to store charge when subjected to an external electric field. However, when C-nec was exposed to Europium (Eu) solution, the overall dielectric constant of its membrane increases to 15 (**Table 6.2**).This increase in permittivity suggests that there are changes associated with the outer surface of the bacteria and this may be due to the adsorption of Eu on the surface of the bacteria. Our hypothesis is that, because the outer surface of C-nec is negatively charged and europium (Eu) ions are positively charged, the electrostatic force of attraction may add neutral layers onto the surface of the C-nec that resulted in an

increased capacitance, thus increasing the dielectric constant. The trend seen in the conductivity of the membrane is not unexpected as conductivity and resistance are inversely related. However, the equality in the electrical properties for neodymium (Nd) and samarium (Sm) directs to the fact that it might be

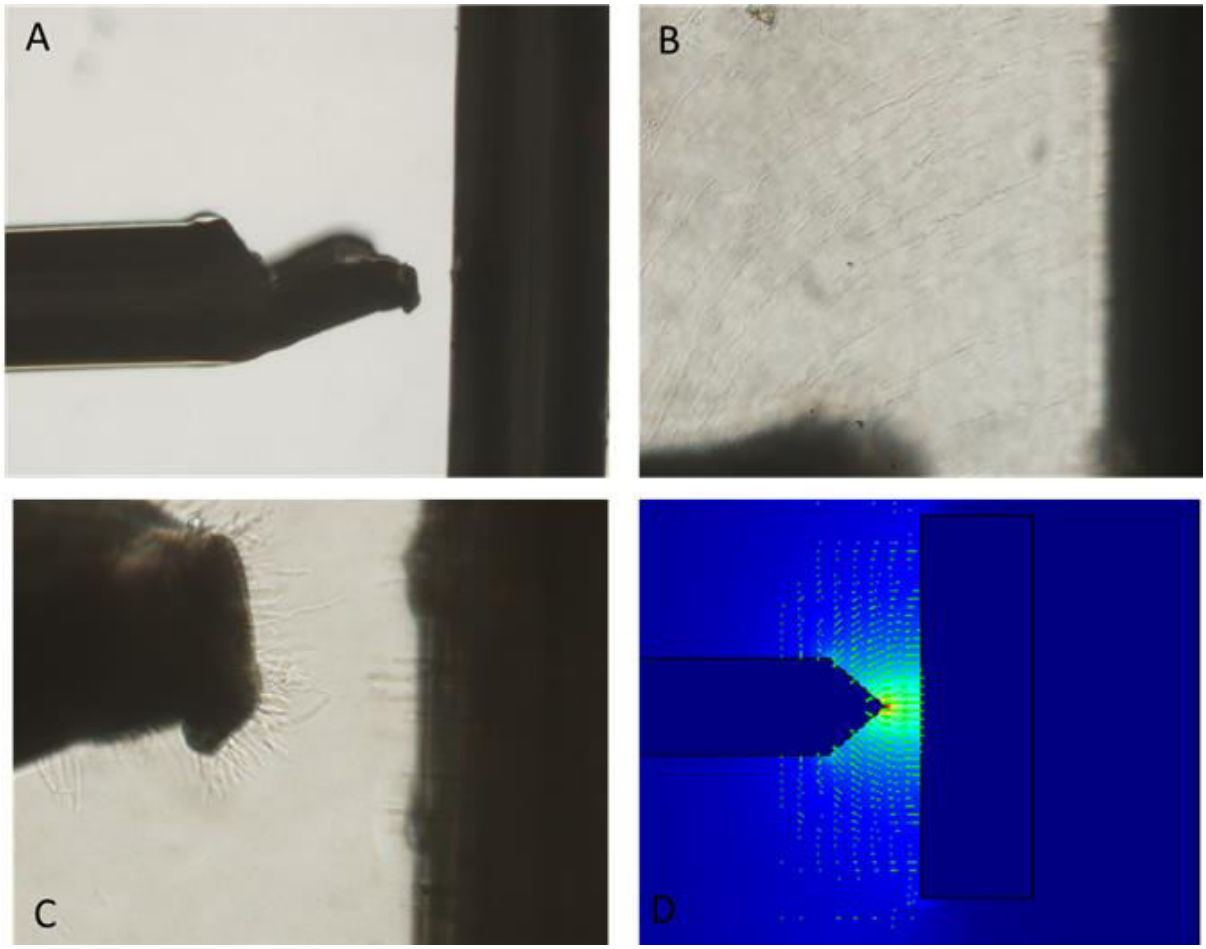

Figure 6.6: *(A) The electrode arrangement within the microwell at 10X magnification. The distance between the electrodes is 75 µm. Each of the electrodes is connected to the positive and negative ends of the function generator in an arbitrary manner since the charge source is alternating in nature. (B) Native C. necator cells undergoing nDEP as theoretically backed-up in chapter 3. (C) Native C necator cells experiencing pDEP by moving to the high-field region (point electrode). Magnification: 40X (D) Distribution of electric field in a point-planar electrode arrangement as solved in COMSOL Multiphysics (version 5.3a). The C necator cells in B and C were suspended in 50g/l dextrose medium of conductivity 56mS/m*

impossible to separate REE^{+} that have Nd from REE^{+} that has Sm using non-uniform electric field effects. This is because in an insulator-based dielectrophoretic separation device, cells are separated based on Clausius-Mossotti factor, which depends on their conductivities. Further frequency variation was employed to obtain the second crossover frequency that is related to the cytoplasmic properties of the bacteria as shown in Equation 2. However, after repeated experimentation, the second crossover frequency remain unchanging indicating that the cytoplasmic properties were not affected. Hence, the cytoplasmic dielectric properties were not quantified. The constant second cross over frequency is also

an indication that when the bacteria was exposed to REE for 1 h, the interaction between the bacteria and the metals is predominantly through adsorption.

Conclusions:

This present study has been able to establish that *Cupriavidus necator* can be used for the biosorption of the tested rare earth elements (Europium, Neodymium and Samarium). When the bacteria were exposed to solutions containing the rare earth elements, their average surface electrical characteristics, (permittivity and conductivity) as measured through the cross-over frequency method, changed but the second cross over frequency did not change. This suggests that the interaction between C. necator and the REEs when they were in contact for 1 hr was predominantly through adsorption. The difference in membrane permittivity of the REE^{+} is an indication that the capacity of C. necator to adsorb the tested REEs differs. Since the electrical properties of REE^{-} and REE^{+} differ, it indicates that through crossover frequency measurement, we can screen biosorbent with respect to their ability to adsorb REEs. Via this screening, we can obtain high-efficiency biomass for the recovery of REEs. Finally, a simple, easy-to-use and very cost-effective method of cell characterization using point-planar microwell set-up for crossover frequency measurement performed considerably like the more expensive electrorotation method tipping the former as an effective cell characterization technique.

Acknowledgment:

This work was supported by the National Science Foundation (NSF) through the CBET division # NSF-CBET # 1500815.

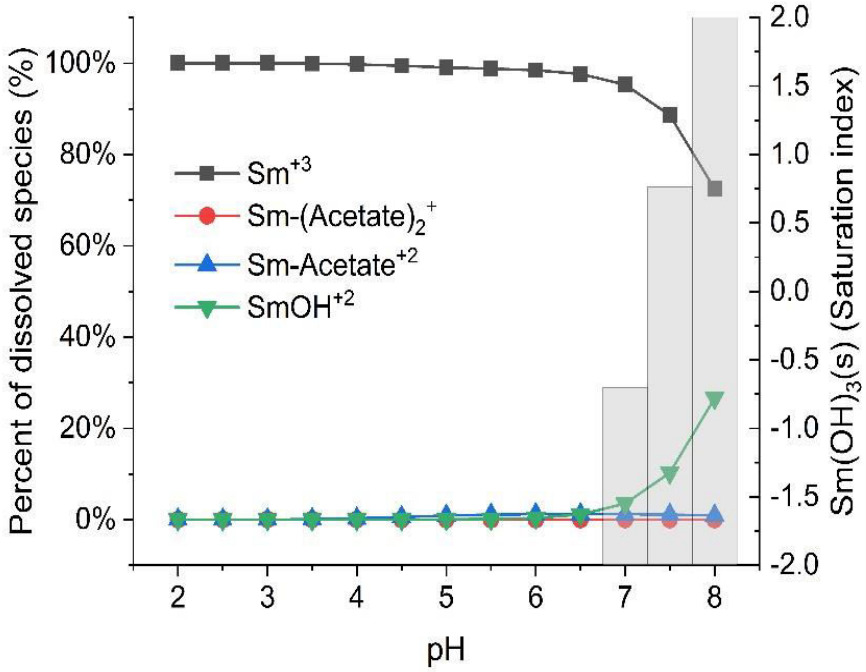

Supplemental Figure 2: *Predicted chemical speciation of dissolved samarium(60μM) in acetic acetate buffered saline at 25°C and saturation indices of $Sm(OH)_3$. Above pH 7 Sm-hydroxides are predicted to form.*

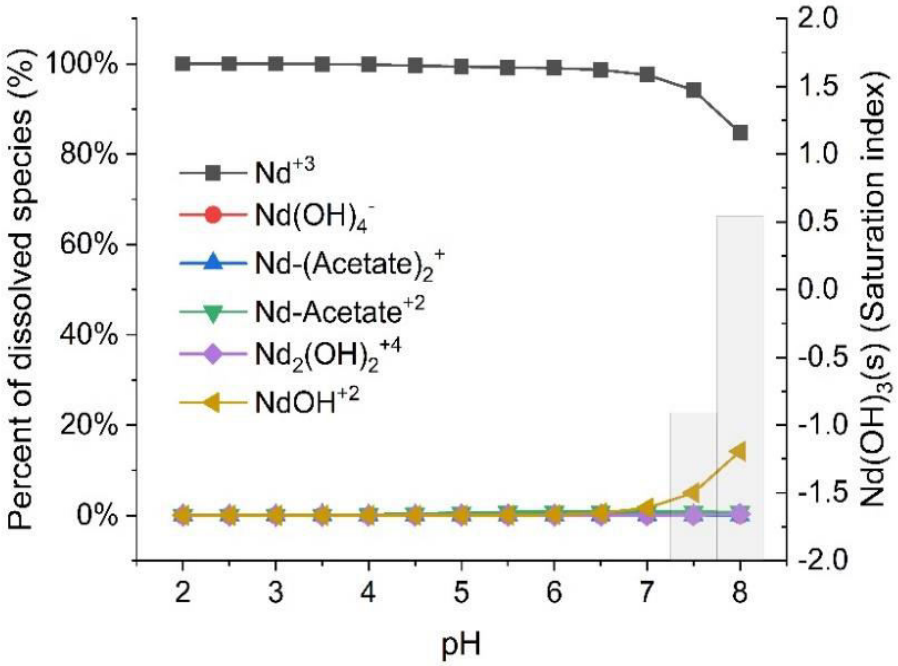

Supplemental Figure 1: *Predicted chemical speciation of dissolved neodymium (60μM) in acetic acetate buffered saline at 25°C and saturation indices of $Nd(OH)_3$. Above pH 7.5 Nd-hydroxides are predicted to form.*

References:

[1] R. P. Peter Gascoyne, Jutamaad Satayavivad, Frederick F. Becker, Mathuros Ruchirawat, "Dielctorphoretic detection of changes in erythrocyte membranes floowing malarial infection," *Biochimia et Biophysica Acta* vol. 1323, pp. 240-252, 1997.

[2] K. Hart, "Rare Earth metals and their roles in renewable energy- benefits and challenges," K. Hart, Ed., ed, 2018.

[3] B. Zawisza, K. Pytlakowska, B. Feist, M. Polowniak, A. Kita, and R. Sitko, "Determination of rare earth elements by spectroscopic techniques: a review," *Journal of Analytical Atomic Spectrometry,* 10.1039/C1JA10140D vol. 26, no. 12, pp. 2373-2390, 2011.

[4] A. Negrea *et al.*, "Rare Earth Elements Removal from Water Using Natural Polymers," *Scientific Reports,* vol. 8, no. 1, p. 316, 2018/01/10 2018.

[5] N. Das and D. Das, "Recovery of rare earth metals through biosorption: An overview," *Journal of Rare Earths,* vol. 31, no. 10, pp. 933-943, 2013/10/01/ 2013.

[6] B. Rohrig, "Smartphones: Smart Chemistry," ed, 2015.

[7] W. Leal Filho, "Chapter 17 - An Analysis of the Environmental Impacts of the Exploitation of Rare Earth Metals," in *Rare Earths Industry*, I. Borges De Lima and W. Leal Filho, Eds. Boston: Elsevier, 2016, pp. 269-277.

[8] A. El-Taher, F. Alshahri, and R. Elsaman, "Environmental impacts of heavy metals, rare earth elements and natural radionuclides in marine sediment from Ras Tanura, Saudi Arabia along the Arabian Gulf," *Applied Radiation and Isotopes,* vol. 132, pp. 95-104, 2018/02/01/ 2018.

[9] P. H. Brown, A. H. Rathjen, R. D. Graham, and D. E. Tribe, "Chapter 92 Rare earth elements in biological systems," in *Handbook on the Physics and Chemistry of Rare Earths*, vol. 13: Elsevier, 1990, pp. 423-452.

[10] A. A. Korenevsky, V. V. Sorokin, and G. I. Karavaiko, "Biosorption of rare earth elements," in *Process Metallurgy*, vol. 9, R. Amils and A. Ballester, Eds.: Elsevier, 1999, pp. 299-306.

[11] N. S. Gad, "Biosorption of rare earth elements using biomass of Sargassum on El-Atshan Trachytic sill, Central Eastern Desert, Egypt," *Egyptian Journal of Petroleum,* vol. 25, no. 4, pp. 445-451, 2016/12/01/ 2016.

[12] E. S. Kazak, E. G. Kalitina, N. A. Kharitonova, G. A. Chelnokov, E. V. Elovskii, and I. V. Bragin, "Biosorption of Rare-Earth Elements and Yttrium by Heterotrophic Bacteria in an Aqueous Environment," *Moscow University Geology Bulletin,* vol. 73, no. 3, pp. 287-294, 2018/05/01 2018.

[13] S. J. Kim, J. H. Chung, T. Y. Kim, and S. Y. Cho, "Biosorption of heavy metals and cyanide complexes on biomass," in *Studies in Surface Science and Catalysis*, vol. 159, H.-K. Rhee, I.-S. Nam, and J. M. Park, Eds.: Elsevier, 2006, pp. 141-144.

[14] T. Ozaki, J. Gillow, A. Francis, T. Kimura, T. Ohnuki, and Z. Yoshida, "Association of Eu(III) and Cm(III) with Bacillus subtilis and Halobacterium salinarum," *Journal of Nuclear Science and Technology,* vol. 39, no. sup3, pp. 950-953, 2002/11/01 2002.

[15] S. Markai, Y. Andrès, G. Montavon, and B. Grambow, "Study of the interaction between europium (III) and Bacillus subtilis: fixation sites, biosorption modeling and reversibility," *Journal of Colloid and Interface Science,* vol. 262, no. 2, pp. 351-361, 2003/06/15/ 2003.

[16] Y. Takahashi, X. Châtellier, K. H. Hattori, K. Kato, and D. Fortin, "Adsorption of rare earth elements onto bacterial cell walls and its implication for REE sorption onto natural microbial mats," *Chemical Geology,* vol. 219, no. 1, pp. 53-67, 2005/06/15/ 2005.

[17] G. Haferburg, D. Merten, G. Büchel, and E. Kothe, "Biosorption of metal and salt tolerant microbial isolates from a former uranium mining area. Their impact on changes in rare earth element patterns in acid mine drainage," *Journal of Basic Microbiology,* vol. 47, no. 6, pp. 474-484, 2007/12/01 2007.

[18] Y. Takahashi, T. Hirata, H. Shimizu, T. Ozaki, and D. Fortin, "A rare earth element signature of bacteria in natural waters?," *Chemical Geology,* vol. 244, no. 3, pp. 569-583, 2007/10/15/ 2007.

[19] M. L. Merroun, K. Ben Chekroun, J. M. Arias, and M. T. González-Muñoz, "Lanthanum fixation by Myxococcus xanthus: cellular location and extracellular polysaccharide observation," *Chemosphere,* vol. 52, no. 1, pp. 113-120, 2003/07/01/ 2003.

[20] K. Tanaka *et al.*, "A specific Ce oxidation process during sorption of rare earth elements on biogenic Mn oxide produced by Acremonium sp. strain KR21-2," *Geochimica et Cosmochimica Acta,* vol. 74, no. 19, pp. 5463-5477, 2010/10/01/ 2010.

[21] Y. Suzuki *et al.*, "Sorption of Eu (III) on Pseudomonas fluorescens in the Presence of Citric Acid," *Journal of Nuclear and Radiochemical Sciences,* vol. 6, no. 1, pp. 91-93, 2005.

[22] T. Tsuruta, "Selective accumulation of light or heavy rare earth elements using gram-positive bacteria," *Colloids and Surfaces B: Biointerfaces,* vol. 52, no. 2, pp. 117-122, 2006/10/01/ 2006.

[23] T. Ozaki, T. Kimura, T. Ohnuki, and A. J. Francisc, "Associations of Eu (III) with Gram-Negative Bacteria, Alcaligenes faecalis, Shewanella putrefaciens, and Paracoccus denitrificans," *Journal of Nuclear and Radiochemical Sciences,* vol. 6, no. 1, pp. 73-76, 2005.

[24] C. R. Anderson and K. Pedersen, "In situ growth of Gallionella biofilms and partitioning of lanthanides and actinides between biological material and ferric oxyhydroxides," *Geobiology,* vol. 1, no. 2, pp. 169-178, 2003/10/01 2003.

[25] B. T. Ngwenya *et al.*, "Macroscopic and spectroscopic analysis of lanthanide adsorption to bacterial cells," *Geochimica et Cosmochimica Acta,* vol. 73, no. 11, pp. 3134-3147, 2009/06/01/ 2009.

[26] Y. Andrès, A. C. Texier, and P. Le Cloirec, "Rare earth elements removal by microbial biosorption: A review," *Environmental Technology,* vol. 24, no. 11, pp. 1367-1375, 2003/11/01 2003.

[27] H. Moriwaki and H. Yamamoto, "Interactions of microorganisms with rare earth ions and their utilization for separation and environmental technology," *Applied Microbiology and Biotechnology,* vol. 97, no. 1, pp. 1-8, 2013/01/01 2013.

[28] I. Michalak, K. Chojnacka, and A. Witek-Krowiak, "State of the Art for the Biosorption Process-a Review," (in English), *Applied Biochemistry and Biotechnology,* Review vol. 170, no. 6, pp. 1389-1416, Jul 2013.

[29] M. Fomina and G. M. Gadd, "Biosorption: current perspectives on concept, definition and application," (in English), *Bioresource Technology,* Article vol. 160, pp. 3-14, May 2014.

[30] F. Veglio and F. Beolchini, "Removal of metals by biosorption: a review," *Hydrometallurgy,* vol. 44, no. 3, pp. 301-316, 3// 1997.

[31] N. Das, "Recovery of precious metals through biosorption — A review," *Hydrometallurgy,* vol. 103, no. 1–4, pp. 180-189, 6// 2010.

[32] H. A. Pohl, *Dielectrophoresis: The Behavior of Neutral Matter in Nonuniform Electric Fields.* . Cambridge: Cambridge University Press, 1978.

[33] T. Jubery, S. K. Srivastava, and P. Dutta, "Dielectrophoresis separation of bioparticles in microdevices: A review," *Electrophoresis,* vol. 35, no. 5, pp. 691-713, 2014.

[34] S. Srivastava, A. Gencoglu, and A. Minerick, "DC insulator dielectrophoretic applications in microdevice technology: a review," *Anal. Bioanal. Chem.,* vol. 399, no. 1, pp. 301-321, 2011.

[35] P. D. Soumya Srivastava, SC Burgess, AR Minerick, "Dielectrophoretic characterization of eryhtrocytes: Postive ABO blood types," *Electrophoresis,* vol. 29, no. 24, pp. 5033-5046, 2008.

[36] S. K. Srivastava, J. L. Baylon-Cardiel, B. H. Lapizco-Encinas, and A. R. Minerick, "A continuous DC-insulator dielectrophoretic sorter of microparticles," *J. Chromatogr. A,* vol. 1218, no. 13, pp. 1780-1789, 2011.

[37] R. S. Thomas, H. Morgan, and N. G. Green, "Negative DEP traps for single cell immobilisation," *Lab on a Chip,* 10.1039/B819267G vol. 9, no. 11, pp. 1534-1540, 2009.

[38] H. A. Pohl, *Dielectrophoresis: The behavior of neutral matter in nonuniform electric fields*. New York: Cambridge University Press, 1978.

[39] S. K. Srivastava, A. Gencoglu, and A. R. Minerick, "DC insulator dielectrophoretic applications in microdevice technology: a review," *Analytical and Bioanalytical Chemistry,* vol. 399, no. 1, pp. 301-321, 2011/01/01 2011.

[40] P. Gascoyne, R. Pethig, J. Satayavivad, F. F. Becker, and M. Ruchirawat, "Dielectrophoretic detection of changes in erythrocyte membranes following malarial infection," *Biochimica et Biophysica Acta (BBA) - Biomembranes,* vol. 1323, no. 2, pp. 240-252, 1997/01/31/ 1997.

[41] K. A. Michael, S. R. Hiibel, and E. J. Geiger, "Dependence of the dielectrophoretic upper crossover frequency on the lipid content of microalgal cells," *Algal Research,* vol. 6, pp. 17-21, 2014/10/01/ 2014.

[42] P. V. Jones, A. F. DeMichele, L. Kemp, and M. A. Hayes, "Differentiation of Escherichia coli serotypes using DC gradient insulator dielectrophoresis," (in eng), *Analytical and bioanalytical chemistry,* vol. 406, no. 1, pp. 183-192, 2014.

[43] P. R. C. Gascoyne, J. Noshari, F. F. Becker, and R. Pethig, "Use of dielectrophoretic collection spectra for characterizing differences between normal and cancerous cells," *IEEE Transactions on Industry Applications,* vol. 30, no. 4, pp. 829-834, 1994.

[44] L. Huang, P. Zhao, and W. Wang, "3D cell electrorotation and imaging time for measuring multiple cellular biophysical properties," *Lab on a Chip,* 10.1039/C8LC00407B vol. 18, no. 16, pp. 2359-2368, 2018.

[45] H. P. Schwan, "Dielectric spectroscopy and electro-rotation of biological cells," *Ferroelectrics,* vol. 86, no. 1, pp. 205-223, 1988/10/01 1988.

[46] K. L. Chan, P. R. Gascoyne, F. F. Becker, and R. Pethig, "Electrorotation of liposomes: verification of dielectric multi-shell model for cells," (in eng), *Biochimica et biophysica acta,* vol. 1349, no. 2, pp. 182-196, 1997.

[47] Z. Çağlayan, K. Sel, Y. D. Yalçin, S. Ö. Ş, and H. Külah, "Analysis of the dielectrophoretic (DEP) spectra of biological cells," in *2017 19th International Conference on Solid-State Sensors, Actuators and Microsystems (TRANSDUCERS)*, 2017, pp. 1644-1647.

[48] P.-Y. Weng, I. A. Chen, C.-K. Yeh, P.-Y. Chen, and J.-Y. Juang, "Size-dependent dielectrophoretic crossover frequency of spherical particles," (in eng), *Biomicrofluidics,* vol. 10, no. 1, pp. 011909-011909, 2016.

[49] L. Wu, L.-Y. Lanry Yung, and K.-M. Lim, "Dielectrophoretic capture voltage spectrum for measurement of dielectric properties and separation of cancer cells," (in eng), *Biomicrofluidics,* vol. 6, no. 1, pp. 14113-1411310, 2012.

[50] J. P. Gustafsson, "Visual MINTEQ ", 3.1 ed, 2013.

[51] E. O. Adekanmbi, M. W. Ueti, B. Rinaldi, C. E. Suarez, and S. K. Srivastava, "Insulator-based dielectrophoretic diagnostic tool for babesiosis," *Biomicrofluidics,* vol. 10, no. 3, p. 033108, 2016/05/01 2016.

[52] E. O. Adekanmbi, J. Dustin, and S. K. Srivastava, "Electro-osmotic surface effects generation in an electrokinetic-based transport device: A comparison of RF and MW plasma generating sources," *ELECTROPHORESIS,* vol. 0, no. 0.

[53] P. Gascoyne, R. Pethig, J. Satayavivad, F. F. Becker, and M. Ruchirawat, "Dielectrophoretic detection of changes in erythrocyte membranes following malarial infection " *Biochimica et Biophysica Acta (BBA) - Biomembranes,* vol. 1323, no. 2, pp. 240-252, 1997.

[54] D. M. Vykoukal, P. R. C. Gascoyne, and J. Vykoukal, "Dielectric characterization of complete mononuclear and polymorphonuclear blood cell subpopulations for label-free discrimination," *Integrative Biology,* vol. 1, pp. 477-484, 2009.

[55] B. Nagy, C. Mânzatu, A. Măicăneanu, C. Indolean, L. Barbu-Tudoran, and C. Majdik, "Linear and nonlinear regression analysis for heavy metals removal using Agaricus bisporus macrofungus," *Arabian Journal of Chemistry,* vol. 10, pp. S3569-S3579, 2017/05/01/ 2017.

[56] T. A. Krulwich, G. Sachs, and E. Padan, "Molecular aspects of bacterial pH sensing and homeostasis," *Nature reviews. Microbiology,* vol. 9, no. 5, pp. 330-343, 04/05 2011.

[57] C. Baker-Austin and M. Dopson, "Life in acid: pH homeostasis in acidophiles," *Trends in Microbiology,* vol. 15, no. 4, pp. 165-171, 4// 2007.

[58] P. Lund, A. Tramonti, and D. De Biase, "Coping with low pH: molecular strategies in neutralophilic bacteria," *FEMS Microbiology Reviews,* vol. 38, no. 6, pp. 1091-1125, 2014.

Chapter 7: Utilization of dielectrophoresis for the quantification of rare earth elements adsorbed on *Cupriavidus necator*

Ezekiel O. Adekanmbi[1], Anthony T. Giduthuri[1], Soumya K. Srivastava[1*]

Abstract

A new method of quantifying rare earth elements (REEs): light RREs (Neodymium - Nd (III), Samarium - Sm (III)) and heavy REE (Europium - Eu (III)) was investigated utilizing native *Cupriavidus necator* as biosorbent and dielectrophoresis (DEP) as the quantification technique. *C. necator* was characterized as a control (through the measurement of first and second crossover frequency) in a polymer (PDMS)-based point-and-planar microwell (PPM) platform at 8 Vpp (peak-to-peak voltage) AC signal and variable frequencies. Allied *C. necator* (*Cupriavidus necator* in its metal-bound state) was then characterized for each of the rare earth metals adsorbed. The first crossover frequency (f_{co1}) was correlated with the amount of metal adsorbed that was obtained through spectrophotometry. The influence of pH, bio-sorbent dosage, initial REE concentration, and metal incubation period was also investigated. The crossover vs. concentration curve is plotted and that serves as a calibration curve such that when the crossover frequency of a biosorbent with adsorbed metal solution is known, the quantity of metal adsorbed could be correlated using the calibration curve without any spectrophotometric analysis.

7.1 Introduction

Rare earth elements (REEs), comprising mainly the lanthanides, scandium and yttrium[1], are a set of elements that have entrenched their importance into the fabric of our modern world. Due to the filling of their *4f* orbitals, they show similar physical and chemical properties[2]. These physico-chemical properties include magnetic, catalytic, optoelectronic and metallurgical properties that have made them highly suitable for applications in diverse cutting-edge technologies [3]. REEs have been reported as useful elements in renewable energy[1, 3-5], smart phones[6], military defense systems[5], biomedical devices[7] and many other technological sectors[8-13]. REEs, even though abundant in nature, are described as rare because they are difficult to acquire in economically viable quantities at a single location. One of the challenges associated with the recovery of REE is the environmental pollution caused from heavy usage of chemicals[14]. In recent years, biosorption i.e. the use of microbial biomass, has been focused on as a cost-effective environmentally friendly biological alternative for the recovery of rare earths[4]. The biosorption process involves the exposure of microbes to the metal-rich solution e.g wastewater stream so that these metals ions are removed by the microbes while the unbound metal ions are left in the solution (supernatant). Diverse species of microbes, including fungi, algae, bacteria, and yeast, have been used sd biosorbents[15-20]. Efficient removal of metals by these microbes from their solution depends on the quantity of metals remaining in supernatant. This metal quantification of supernatants has been traditionally accomplished using absorption spectroscopy (ultraviolet–visible spectrophotometry (UV-

Vis)[21], emission spectroscopy (inductively coupled plasma mass spectrometry, (ICP-MS)[21-24], inductively coupled plasma - optical emission spectrometry, (ICP-OES)[25-26], X-ray fluorescence (XRF)[27], laser-induced breakdown spectroscopy (LIBS)[28-30] and electronic tongue system[31]. Amongst these methods, ICP-MS is the most commonly used technique for all type of metals especially if they are in water and sediments[2] due to various advantages which including favorable detection limits, high throughput, simultaneous measurement of more than one element[32]and its ability to provide elemental isotopic ratio information[33] as well as its large linear dynamic working range[33]. However, ICP-MS is very expensive requiring a skilled technician to operate and is often difficult to maintain[32]. Mass spectral interference by Argides, for example, makes it difficult for ICP-MS assays to be amenable to elements such as chromium, calcium and iron[32-33]. In addition to the shortcomings listed above, ICP-MS generally requires a clean room environment for maintaining ultra-low detection limits[33]. Apart from these, ICP-MS and other techniques mentioned above rely on the quantification of non-bound metal ions in the supernatant[34]. Here, a method that quantifies the amount of metal adsorbed by the biosorbent without requiring the usage of supernatant is proposed for the first time. This method involves the application of dielectrophoresis (DEP) to discriminate between native (unexposed biosorbent) and allied (biosorbent exposed to metal solution) biosorbents. DEP, which has been used to study many bioparticles[35-41], operates on the principle that a force can be exerted within a non-uniform electric field and can cause any polarizable bioparticle within the field to move[42-43]. However, at a certain AC frequency of the electric field, the bioparticle will cease to move despite the electric field effects; the frequency at this no-movement position is termed as the crossover frequency. Measurement of the crossover frequencies has been applied to characterize several bioparticles: eukaryotes, prokaryotes, archaea, virus, and polymer beads[43-48].

This research will be accomplished in tow steps: First gram-negative bacteria, *Cupriavidus necator* will be utilized to adsorb Europium (Eu^{3+}), Samarium (Sm^{3+}) and Neodymium (Nd^{3+}) ions from their solution and the supernatant will be quantified using UV-Vis spectrophotometer. Quantifying the elements in supernatant will allow us to obtain the amount of REE adsorbed by the bacteria. Second, the allied bacteria pellets extracted from the supernatant will be utilized to quantify the DEP crossover frequency that will be further correlated with the amount of metal adsorbed obtained through UV-Vis spectrophotometer in the first step. Thus, the amount of metal adsorbed can be obtained via the DEP crossover frequency of the bacteria. While this proposed method does not seek to replace spectroscopy completely, it has the potential to verify the efficiency of biosorption in an economical and faster way. This new method could also pave way towards identifying organisms that hyper-accumulate any metals in general and not limited to rare earths.

7.2 Materials and Methods

C. necator bacterial cells (biosorbent) were cultured according to procedure described in chapter 6 and the number of bacteria per ml of broth was determined. These cells were then washed, as previously described (*chapter 6: materials and methods section*), and incubated at 37ºC in a solution of Eu^{3+} (at *200, 400, 600, 800 and 1000 μM*) for 1 hr. Thereafter, the number of bacteria per ml of suspension was determined using a hemocytometer. Cell suspension was then centrifuged at 10,000 *rcf* (relative centrifugal force) for 15 mins. and the supernatant decanted. The remaining clustered cell mass was harvested and washed with 50 g/L of dextrose medium (with supernatant decanted) after which the first crossover frequency (f_{co1}) was quantified using our previously described point and planar microwell device platform (*Chapter 3*)[39]. The total supernatant was quantified for its metal content using UV-Vis spectrophotometer. Absorbance vs. concentration calibration curve for each of the metals was plotted using 10 - 50 μM metal solutions to ensure a linear non-dynamic absorbance span (Beer's law validity). Prior to obtaining DEP crossover response of *C. necator*, the number of *C. necator* per ml of dextrose medium suspension was recounted and adjusted in line with number of cells required for the dielectrophoretic experiment. The procedure was repeated three (3) times (technical replicate = 3) and the average f_{co1} was obtained. For each of the remaining REE solutions, Nd^{3+} and Sm^{3+}, the same procedure was repeated. The effects on different incubation periods [15 mins, 30 mins, 45 mins and 60 mins], REE solution pH [5.5, 6.0, 6.5, 7.0, and 7.5] and cell density (biosorbent dosage) $[0.5*10^9, 1*10^9, 1.5*10^9, 2*10^9 \frac{\text{cells}}{\text{ml of suspension}}]$ were investigated at a fixed REE solution concentration of 400 μM, thus quantifying the DEP crossover frequency responses.

When probing the biosorbent to investigate the DEP crossover dependencies on various factors like incubation periods, REE solution pH and cell density (biosorbent dosage), the amplitude of the function generator was varied between 6-8 Vpp with five (5) frequency variation per decade from 10kHz to 1MHz. The concentrations of the supernatants, obtained through the calibration curve for each of the REE solutions, were then related to the crossover frequency obtained to generate a standard frequency vs. concentration relation for allied *C. necator* cells. Simple linear regression was utilized to analyze the calibration data for both absorbance vs. concentration and crossover vs. concentration curves.

7.3 Results and Discussion

In this section, the results obtained from probing the biosorbent to investigate its adsorption efficiency and the corresponding crossover dependencies at various REE solution concentration, REE solution pH, biosorbent incubation period and biosorbent dosage are given.

7.3.1 Effects of initial concentration on crossover frequency

Once the spectrophotometric calibration curve was obtained using the supernatant after the biosorbents were extracted (supplementary figure 1), another set of experiments were implemented to characterize the extracted biosorbent (*C. necator*) pellets using the point and planar electrode microwell (PPM) device platform. The crossover frequency obtained from such experiments was related to the quantity of metal that the biosorbent had adsorbed as shown in Figure 7.1.

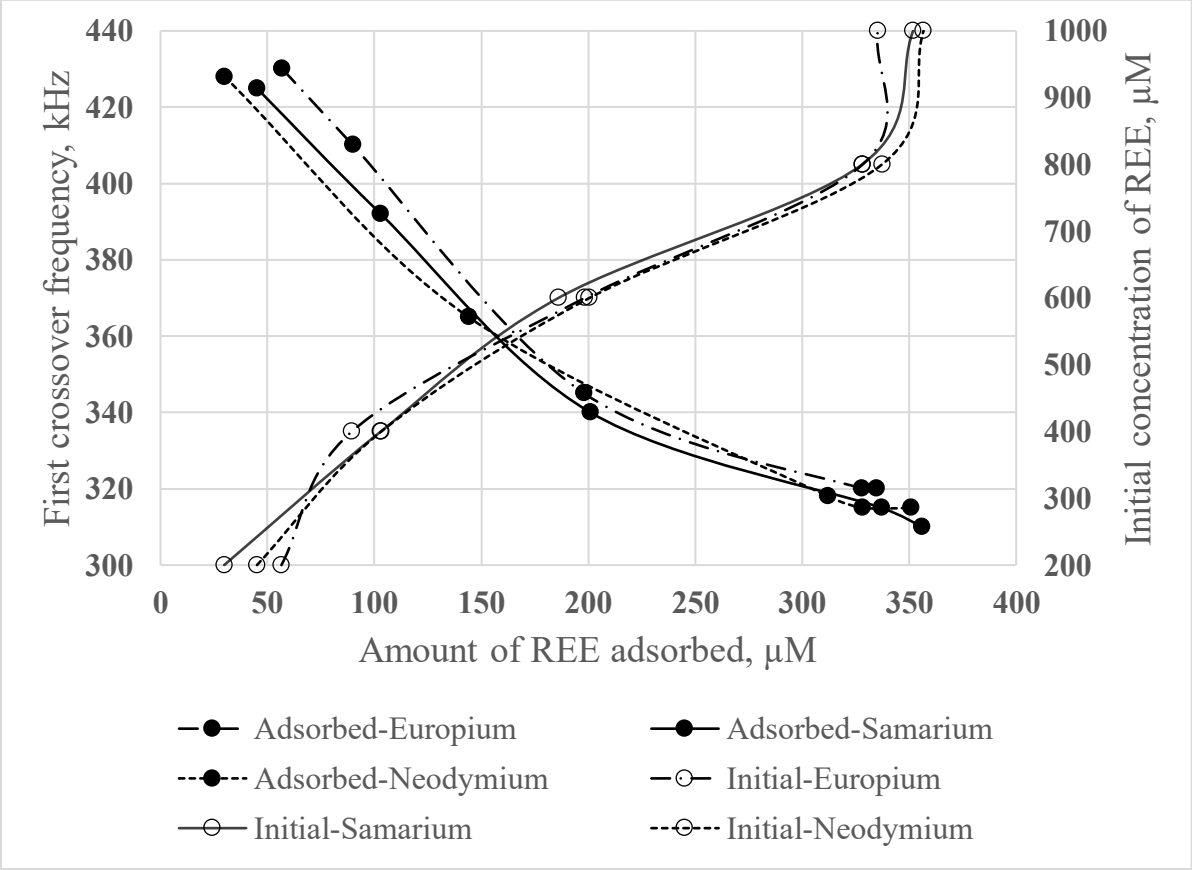

Figure 7. 1 *Dielectrophoresis calibration curves as a function of the concentration of Samarium, Europium and Neodymium. The curves were generated with one billion (1*10^9) C. necator cells incubated for one hour at 35^{o}C and pH 6. The values shown here are average values without any error bar to enhance clarity.*

It is shown that the crossover frequency of the allied biosorbent relates inversely to the quantity of REEs adsorbed. This observation can be explained from the surface characteristics of the bacteria. Bacteria as a living cell has an overall negative charge on their outer surface due to the presence of lipopolysaccharides. When they are suspended in the REE solutions, they adsorb REE ions to their surface through electrostatic attraction owing to the positive charges of the REE ions. This leads to the formation of Stern layer on the surface of the bacteria leading to cellular deactivation or even death. Since dead or inactivated cells have degraded external membrane[49] and thus adsorb metals better than the live cells[50] more REEs are adsorbed as the available initial concentration of the metal increase. Even

though dead cells usually have slightly lower permittivity than live cells, adsorption and potential degradation of the cell wall disrupts its osmotic balance thus increasing permittivity (and by extension, specific membrane capacitance). Since membrane capacitance is inversely proportional to the first crossover frequency[49], it is therefore expedient to observe the inverse relation between crossover frequency and REE concentration.

The effects of initial concentration on the cross over frequency of the each of the allied biosorbent was investigated using cell density of one billion ($1*10^9$) *C. necator* cells incubated in 200-1000 µM REE solutions at pH 6, 35°C for 1 hr (Figure 7.1). Adsorption of REEs by the biosorbent increased as the initial REE concentration in the solution increased. At 200 µM, more of Europium was adsorbed as compared to Neodymium and Samarium. However, at 1000 µM, lesser amount of Europium was adsorbed compared to the other two metals. This trend may be because of the unavailability of the active sites for adsorption i.e. the adsorption sites becoming saturated at higher concentration, since the initial high concentration (200 µM) of the REEs would have from the beginning provided strong driving force to combat any mass transport resistance within the system[51]. The crossover frequency measured at each of the different REE concentrations are observed on the second y-axis of the graph (Figure 7.1). In general, the first crossover frequency decreases as more REE ions are being adsorbed to due to the paucity of active sites caused by saturation. Another observation from Figure 7.1 is that the first crossover frequencies of *C. necator* when it adsorbs lesser REEs were more distinguishable among the three REEs than when more quantities were adsorbed. The relation of crossover with the amount of REE adsorbed is not completely linear. However, at the given conditions (in Figure 7.1), it can still be used as a correlation curve for each of the REEs such that when *C. necator* is exposed to any of the metal solutions, the concentration adsorbed can be found without the need of expensive ICP-MS technique.

7.3.2 Effects of pH on adsorbed metal

The effects of pH were explored from pH 5.5 to 7.5 on the adsorption capacity of *C. necator*. This specific range of pH values were chosen because of their appropriateness for dielectrophoretic crossover determination. DEP crossover frequency characterization is usually accomplished at neutral pH ranges between 6-7.5. One important observation during the biosorbent pellet extraction for the DEP crossover experiment was that at pH 5.5 and 6.0, the pellets were of the same volume as with other experiments. However, the pellets at pH 6.5 - 7.0 were observed to be large i.e. more in volume even though approximately same density of cell density was used at the outset of the experiment for all the pH ranges. This suggests that some form of complex salt formations may result at pH > 6 depending on the type of REE.

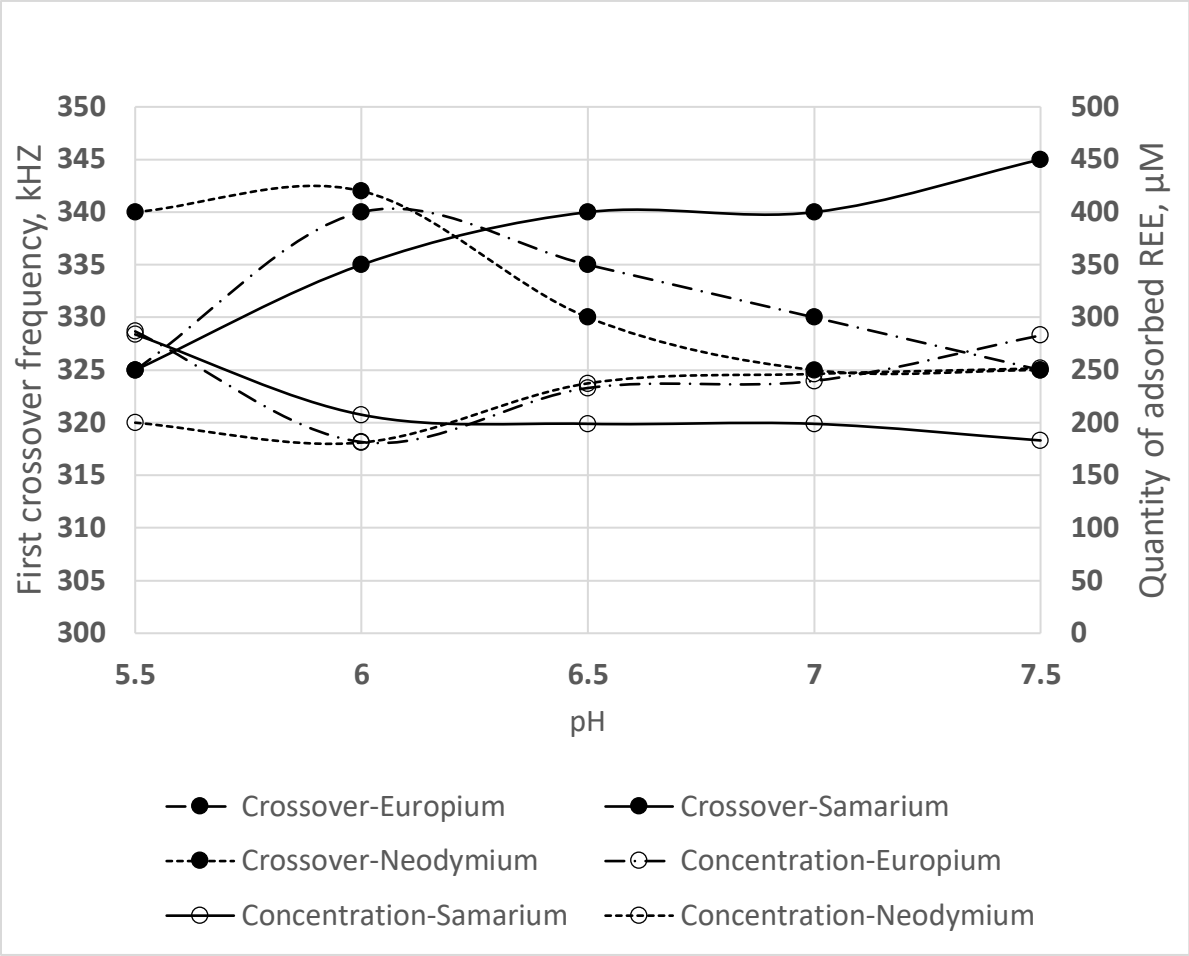

Figure 7. 2 *The variation of crossover frequency of allied C. necator as a function of pH of the REE metal solution. The C. necator bacterial cells were incubated for 1 hr at 37°C in a metal solution concentration 400µm. The dark broken lines represent the points where cell behavior changes curse.*

From Figure 7.2, the variation of crossover frequency with the concentration of adsorbed REEs are found to increase for all REEs between pH 5.5 and 6.0. After pH 6.0, the crossover frequency for Samarium increased but that of Europium and Neodymium decreased with increasing pH. The continued increase in crossover frequency of Samarium with pH also infers that lesser amounts of the REE are being adsorbed as the pH increases. This result is consistent with the published reports from other researchers[52]. At higher pH values, biosorption usually decreases since more hydroxyl (OH^-) ions are being introduced to mask the positive counter ions present in the solution, including the native elements themselves. Besides, higher pH could also mean increased repulsive forces due to the negatively charged cell surface, thus reducing biosorption and increasing complex salt formations. Bacteria possess negative charges on their surface that repel each other, a measure of their Zeta potential. When the biosorbents are suspended in a solution containing these REEs ions, the positive

ions are adsorbed onto their surface reducing the zeta potential (repulsive force) depending on the pH of the REE solution. Due to the negative charge on the cell surface, the Zeta potential is negative.

The higher the pH of the REE solution, the more negative the zeta potential of the bacteria. i.e. as the pH increases, the Zeta potential decreases leading to decreased electrostatic repulsion between cells thereby reducing the surface activity of the cell as observed in Figure 7.2 at pH 5.5 and 6. However, as mentioned in the previous chapter (results and discussion section), beyond pH 6.0, complexation of the bacteria with REE occurs resulting in surface chemistry changes leading to increased adsorption. Operating at too low pH could add more H+ ions to compete with the already present native element while reducing the zeta potential of the cell and enhancing coagulating. As stated earlier, the focus here is to utilize REE solutions at pH ranging between 5.5-7.5 because of the downstream utilization of point and planar microwell (PPM) device platform for biosorbent characterization to obtain electric properties. In the case of Samarium, the increased crossover frequency with increasing pH is comprehended as continued reduction in the amount of REE adsorbed. However, the increase in crossover for Europium and Neodymium was truncated at pH 6, afterwards, a downward trend was observed. The amount of adsorbed Europium soared, and Neodymium plateaued between pH 7 and 7.5, again attributing to the complex salt formation on the surface of biosorbent.

In chapter 6, Europium was predicted to display aberration at pH > 6 and neodymium at pH > 7. However, based on Figure 7.2, both Europium and Neodymium changed their direction at pH 6. Therefore, other dependencies were investigated by fixing the pH to be ~ 6. This was chosen due to the fact that 1) pH6 is the point of inflection between the usual and unusual behavior of biosorbent and 2) it is suitable for dielectric characterization experiments using PPM device platform. The focus of this work is to relate various adsorption factors to crossover frequency even though low adsorption at tis pH was observed. Also, the inconsistency in the relationship between the crossover frequency and the adsorbed REEs at pH > 6 poses a challenge in terms of quantifying the adsorbed metal merely from the first crossover frequency, thus forcing to maintain the pH between 5.5 and 6.0.

7.3.3 Effects of incubation period of biosorbent in REE solutions

The rate at which the metals were adsorbed onto the bacteria was monitored between 0-60mins at an interval of 15 mins. At the end of each interval, the crossover frequency of the resultant pellet was measured while the supernatant was quantified for the remaining unattached metal ions. When 1.0 dosage of biosorbent were incubated in 400 µM of REE solutions, it was observed that the highest adsorption was within the first 15 mins. The order of adsorption within this 15-min interval was Europium > Neodymium > Samarium representing an average of ~65 > ~60 > ~45 µM respectively. This order was maintained throughout the 60-min incubation period. There was also a progressive reduction in the rate of adsorption observed from the lower time intervals to the higher intervals i.e. 65

µM of europium was adsorbed with the first 15mins, between 15-30 mins 34 µM was adsorbed; 30-45 mins, and 45-60 mins, showed 31 µM and 15 µM of europium were adsorbed respectively. At each of these intervals, the crossover frequency progressively decreasing in agreement with the previous observations. This variation in the quantity of adsorbed metal ions as time progressed could be attributed to the number of adsorption site available for binding or the increased concentration gradient that existed between the biosorbents in solution.

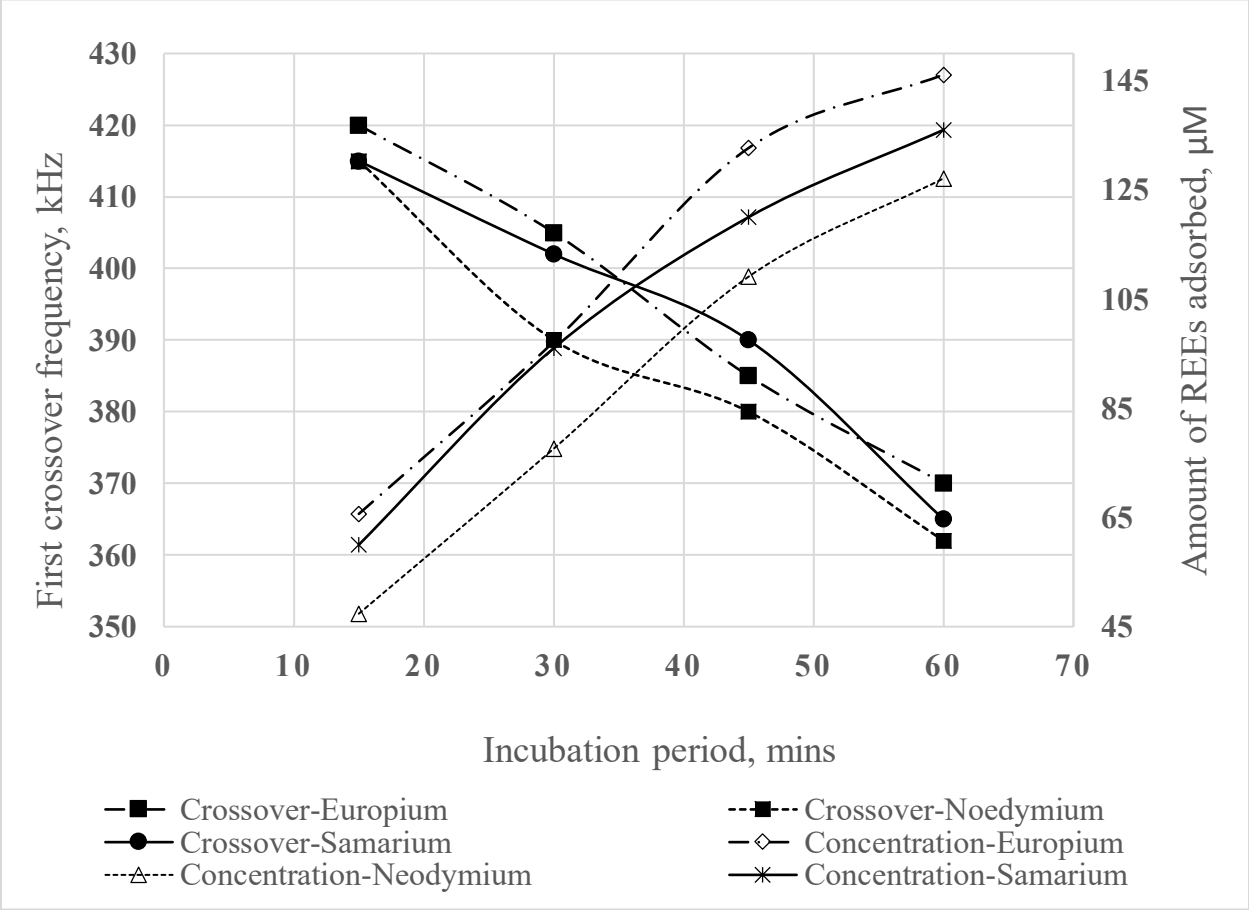

Figure 7. 3 *The variation of crossover frequency of allied C. necator as a function of incubation period. The solution pH was fixed at 6.0 and the incubation temperature, and metal-solution concentration were 37°C and 400µm respectively. The order of adsorption followed an exhibited trend: Europium > Neodymium > Samarium.*

7.3.4 Effects of cell density (biosorbent dosage)

The effect of biosorbent dosage on the crossover frequency of the allied *C. necator* is presented in Figure 7.4. A cell density of $0.5*10^9, 1*10^9, 1.5*10^9, 2*10^9 \frac{\text{cells}}{\text{ml of suspension}}$ represent 0.5,1.0,1.5 and 2.0 fractional biosorbent dosage per billion. When the dosage was 0.5, ~100 µM out of the 400 µM initial concentration of REEs were adsorbed within the 1hr of incubation, representing 25% efficiency. When the dosage was increased to 1.0, more REEs were adsorbed onto the bacteria with Europium >

Neodymium > Samarium. At biosorbent dosage between 1.5-2.0, there were no appreciable increase in the adsorbed REEs. This observation was related to the crossover frequency of the allied biosorbent at each biosorbent dosage explored here. As expected, the higher the adsorbed quantity of the REEs, the lower the DEP crossover frequency. This result again proves that when the crossover frequency of an allied biosorbent is known at certain experimental condition (Figure 7.4), the amount of metal adsorbed on its surface can be found. The overall increase in adsorption as the biosorbent dosage increases can be related to the increase in availability of negative charges (adsorption sites) brought about by the increases in number of cells. Like any other adsorption phenomena, when an adsorption sites had been occupied, there is a gradual reduction in the number of available sites for binding, hence, reduced quantity of the adsorbed REE.

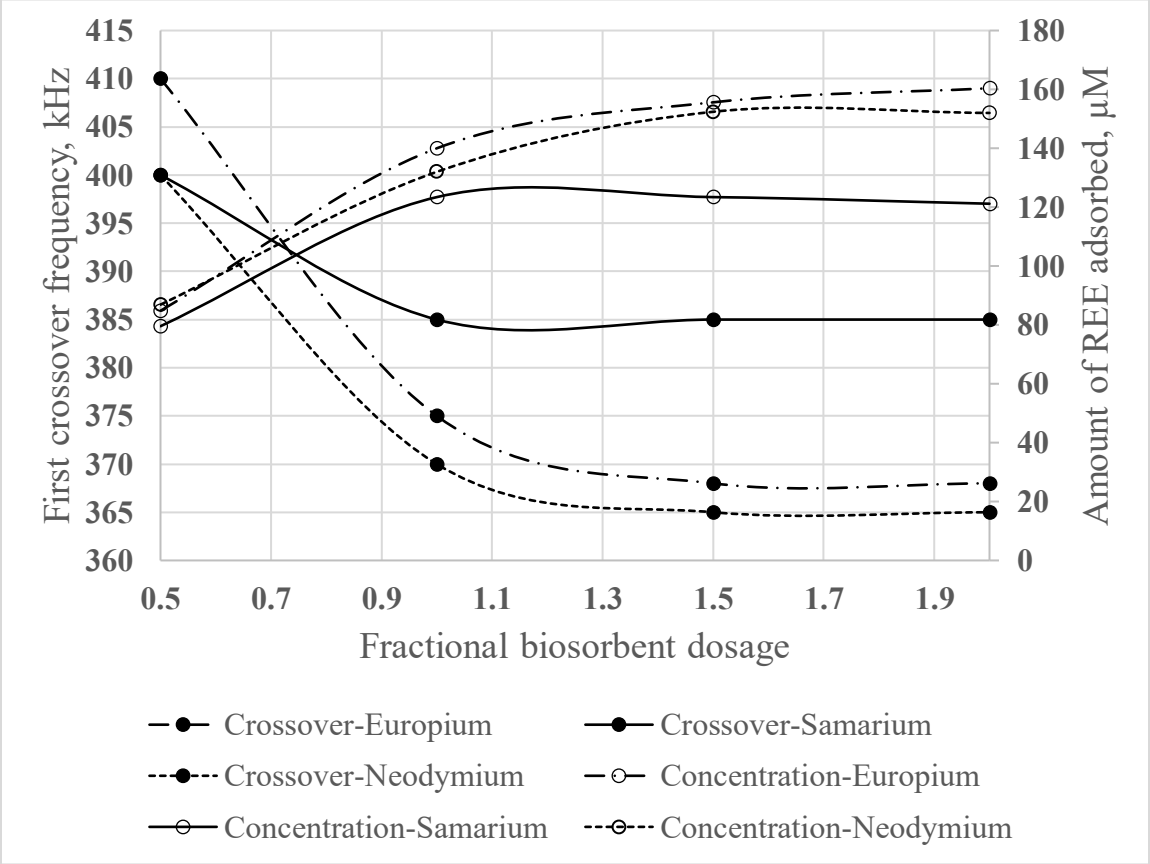

Figure 7. 4 *The variation of crossover frequency of allied C. necator as a function of biosorbent dosage. The pH was fixed at 6.0 and the incubation temperature, and metal-solution concentration were 37°C and 400 µm respectively.*

7.4 Conclusion

The research presented here is a proof of concept that the electrical property of *C. necator* can provide an indication of the amount of REE adsorbed by the biosorbent. By measuring the behavior of

allied *C. necator* i.e. REE-adsorbed bacteria under non-uniform electric field, the amount of metal adsorbed on the biosorbent surface can be quantified. The method described here is for pure REE solutions. Mixture of REEs as well as the addition of extraneous heavy REEs is the subject of our future research plan. To improve the capacity and efficiency of *C. necator* adsorption, it is recommended that specific REE-binding ligands be engineered on the biosorbent surface so that the bacteria can adsorb only specified REEs even when placed in a solution containing diverse metals. Thereafter, the Zeta potential of the biosorbent can be altered (through pH change) to release the corresponding adsorbed metals. If this quantification technique is to be incorporated as another method of quantifying adsorption of rare element onto a cell surface, the cell should be able to adsorb well at pH 6.

Supplementary figures

Calibration curves

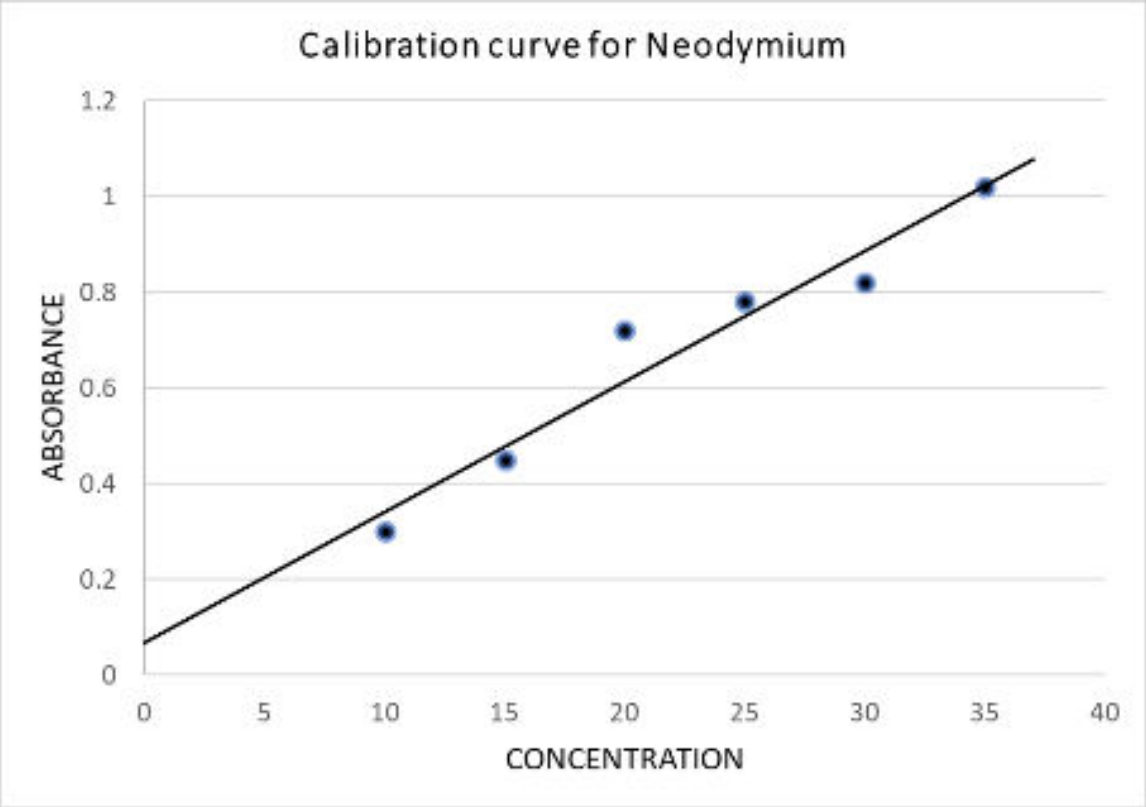

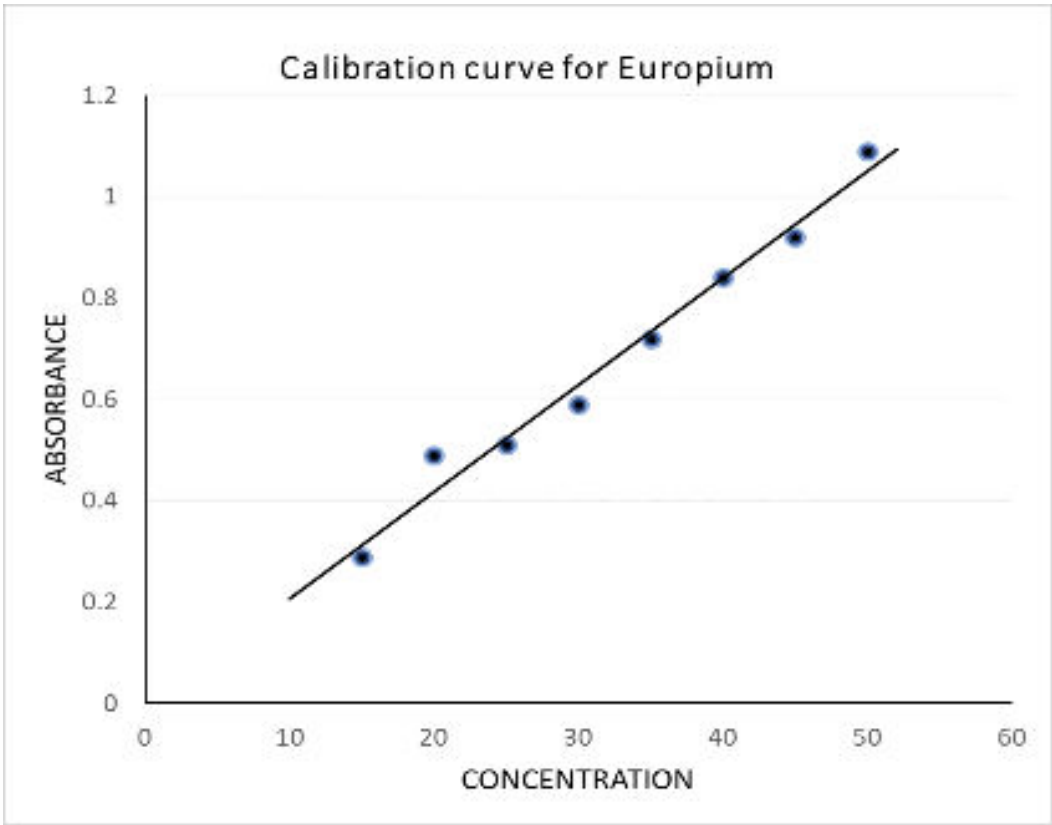
Calibration curve for Europium
ABSORBANCE
1.2
1
0.8
0.6
0.4
0.2
0
0
10
20
30
40
50
60
CONCENTRATION

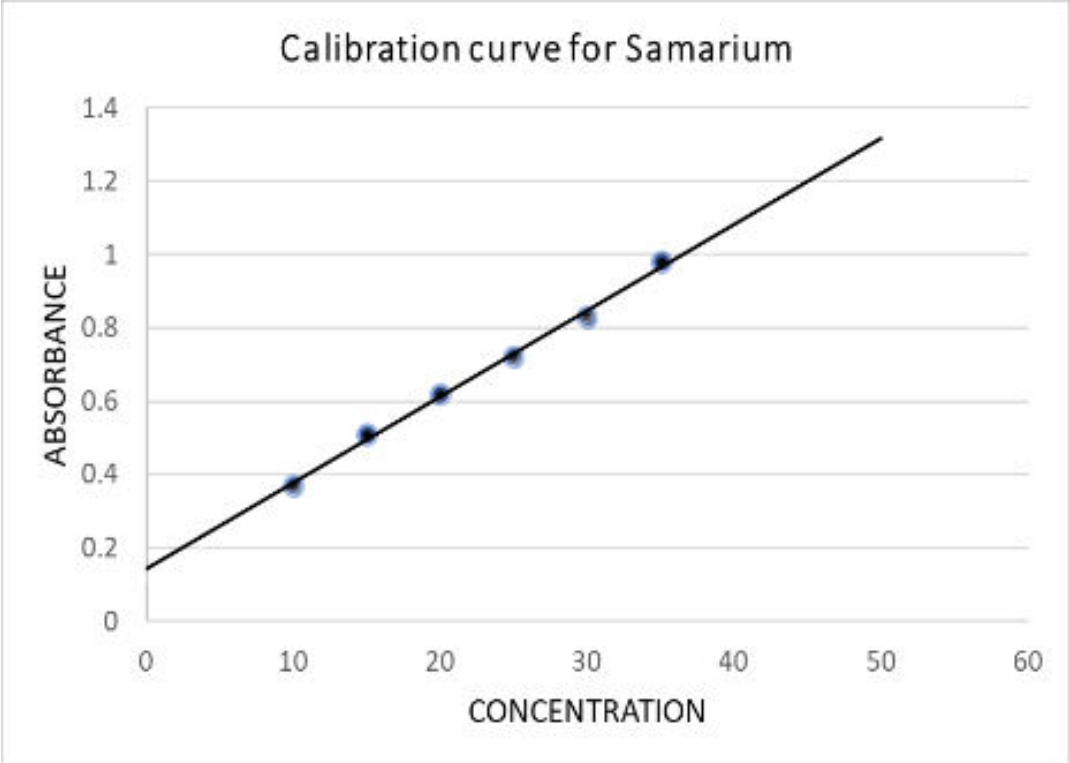
Calibration curve for Samarium
ABSORBANCE
1.4
1.2
1
0.8
0.6
0.4
0.2
0
0
10
20
30
40
50
60
CONCENTRATION

References

[1] Hart, K., Rare Earth metals and their roles in renewable energy- benefits and challenges. Hart, K., Ed. 2018.

[2] Zawisza, B.; Pytlakowska, K.; Feist, B.; Polowniak, M.; Kita, A.; Sitko, R., Determination of rare earth elements by spectroscopic techniques: a review. *Journal of Analytical Atomic Spectrometry* **2011,** *26* (12), 2373-2390.

[3] Negrea, A.; Gabor, A.; Davidescu, C. M.; Ciopec, M.; Negrea, P.; Duteanu, N.; Barbulescu, A., Rare Earth Elements Removal from Water Using Natural Polymers. *Scientific Reports* **2018,** *8* (1), 316.

[4] Das, N.; Das, D., Recovery of rare earth metals through biosorption: An overview. *Journal of Rare Earths* **2013,** *31* (10), 933-943.

[5] Chakhmouradian, A. R., Wall, F., Rare Earth Elements: minerals, mines, magnets, and more. 2012.

[6] Rohrig, B., Smartphones: Smart Chemistry. 2015.

[7] Willbold, E.; Gu, X.; Albert, D.; Kalla, K.; Bobe, K.; Brauneis, M.; Janning, C.; Nellesen, J.; Czayka, W.; Tillmann, W.; Zheng, Y.; Witte, F., Effect of the addition of low rare earth elements (lanthanum, neodymium, cerium) on the biodegradation and biocompatibility of magnesium. *Acta Biomaterialia* **2015,** *11*, 554-562.

[8] Charalampides, G.; Vatalis, K. I.; Apostoplos, B.; Ploutarch-Nikolas, B., Rare Earth Elements: Industrial Applications and Economic Dependency of Europe. *Procedia Economics and Finance* **2015,** *24*, 126-135.

[9] Greinacher, E., History of Rare Earth Applications, Rare Earth Market Today. In *Industrial Applications of Rare Earth Elements*, AMERICAN CHEMICAL SOCIETY: 1981; Vol. 164, pp 3-17.

[10] Lilia, C. C.; Ricardo, E. S., Applications of Europium Tetracycline Complex: A Review. *Current Pharmaceutical Analysis* **2008,** *4* (4), 238-248.

[11] Picot, A.; D'Aléo, A.; Baldeck, P. L.; Grichine, A.; Duperray, A.; Andraud, C.; Maury, O., Long-Lived Two-Photon Excited Luminescence of Water-Soluble Europium Complex: Applications in Biological Imaging time Using Two-Photon Scanning Microscopy. *Journal of the American Chemical Society* **2008,** *130* (5), 1532-1533.

[12] Enholm, E. J.; Trivellas, A., Samarium(II) iodide mediated transformation of carbohydrates to carbocycles. *Journal of the American Chemical Society* **1989,** *111* (16), 6463-6465.

[13] Sharma, P.; Singh, G.; Tomar, R., Synthesis and characterization of an analogue of heulandite: Sorption applications for thorium(IV), europium(III), samarium(II) and iron(III) recovery from aqueous waste. *Journal of Colloid and Interface Science* **2009,** *332* (2), 298-308.

[14] Rim, K.-T., Effects of rare earth elements on the environment and human health: A literature review. *Toxicology and Environmental Health Sciences* **2016,** *8* (3), 189-200.

[15] Diniz, V.; Volesky, B., Biosorption of La, Eu and Yb using Sargassum biomass. *Water Research* **2005,** *39* (1), 239-247.

[16] Palmieri, M. C.; Volesky, B.; Garcia, O., Biosorption of lanthanum using Sargassum fluitans in batch system. *Hydrometallurgy* **2002,** *67* (1), 31-36.

[17] Kazy, S. K.; Das, S. K.; Sar, P., Lanthanum biosorption by a Pseudomonas sp.: equilibrium studies and chemical characterization. *Journal of Industrial Microbiology and Biotechnology* **2006,** *33* (9), 773-783.

[18] Xu, S.; Zhang, S.; Chen, K.; Han, J.; Liu, H.; Wu, K., Biosorption of La3+and Ce3+ by Agrobacterium sp. HN1. *Journal of Rare Earths* **2011,** *29* (3), 265-270.

[19] Palmieri, M. C.; Garcia, O.; Melnikov, P., Neodymium biosorption from acidic solutions in batch system. *Process Biochemistry* **2000,** *36* (5), 441-444.

[20] Yao, T.; Wu, X.; Chen, X.; Xiao, Y.; Zhang, Y.; Zhao, Y.; Li, F., Biosorption of Eu(III) and U(VI) on Bacillus subtilis: Macroscopic and modeling investigation. *Journal of Molecular Liquids* **2016,** *219*, 32-38.

[21] Rabie, K. A., Sayed S.A., Lasheen T. A, Salama I.E., Europium seapration from a middle rare earths concentrate derived from Egyptian black sand monazite. *Hydrometallurgy* **2007,** *86*, 121-130.

[22] Li, Y.; Yu, H.; Zheng, S.; Miao, Y.; Yin, S.; Li, P.; Bian, Y., Direct Quantification of Rare Earth Elements Concentrations in Urine of Workers Manufacturing Cerium, Lanthanum Oxide Ultrafine and Nanoparticles by a Developed and Validated ICP-MS. *Int J Environ Res Public Health* **2016,** *13* (3), 350.

[23] Lawrence, M. G.; Greig, A.; Collerson, K. D.; Kamber, B. S., Direct quantification of rare earth element concentrations in natural waters by ICP-MS. *Applied Geochemistry* **2006,** *21* (5), 839-848.

[24] Clarice D.B., R. C. M., Juan A.V.A. Barros, Alex Virgilio, Daniela Schiavo, Ana Rita A. Nogueira, Joaquim A. Nobrega, Determination of rare earth elements in geological and agricaultural samples by ICP-OES. *Spectrocopy* **2017,** *32* (10), 32-36.

[25] Lichte, F. E.; Meier, A. L.; Crock, J. G., Determination of the rare-earth elements in geological materials by inductively coupled plasma mass spectrometry. *Analytical Chemistry* **1987,** *59* (8), 1150-1157.

[26] Taam, I.; Mantovano, J. L.; Gante, V.; Jesus, C. S. In *Quantitative analysis or rare earths by X-ray fluorescence spectrometry*, INAC 2013: International nuclear atlantic conference, Brazil, Brazil, 2013.

[27] Taam, I.; Mantovano, J. L.; Gante, V.; Jesus, C. S. In *Quantitative analysis of rare earths by X-ray fluorescence spectrometry*, INAC 2013: International nuclear atlantic conference, Brazil, Brazil, 2013.

[28] Martin, M.; Martin, R. C.; Allman, S.; Brice, D.; Wymore, A.; Andre, N., Quantification of rare earth elements using laser-induced breakdown spectroscopy. *Spectrochimica Acta Part B: Atomic Spectroscopy* **2015,** *114*, 65-73.

[29] Crock, J. G.; Lichte, F. E., Determination of rare earth elements in geological materials by inductively coupled argon plasma/atomic emission spectrometry. *Analytical Chemistry* **1982,** *54* (8), 1329-1332.

[30] Bhatt, C. R.; Jain, J. C.; Goueguel, C. L.; McIntyre, D. L.; Singh, J. P., Determination of Rare Earth Elements in Geological Samples Using Laser-Induced Breakdown Spectroscopy (LIBS). *Applied Spectroscopy* **2017,** *72* (1), 114-121.

[31] Kirsanov, D.; Legin, A.; Tkachenko, M.; Surzhina, I.; Khaidukova, M.; Babain, V., Development Of Electronic Tongue System For Quantification Of Rare Earth Metals In Spent Nuclear Fuel Reprocessing. *AIP Conference Proceedings* **2011,** *1362* (1), 104-106.

[32] Dziewatkoski, M., Inductively Coupled Plasma Mass Spectrometry Edited by Akbar Montaser (George Washington University). Wiley-VCH: New York. 1998. 964 pages. $125.00. ISBN 0-471-18620-1. *Journal of the American Chemical Society* **1999,** *121* (17), 4310-4310.

[33] Montaser, A.; Montaser, A., *Inductively coupled plasma mass spectrometry*. New York : J. Wiley: New York, 1998.

[34] Gerbino, E.; Mobili, P.; Tymczyszyn, E. E.; Frausto-Reyes, C.; Araujo-Andrade, C.; Gómez-Zavaglia, A., Use of Raman spectroscopy and chemometrics for the quantification of metal ions attached to Lactobacillus kefir. *Journal of Applied Microbiology* **2012,** *112* (2), 363-371.

[35] Gascoyne, P.; Satayavivad, J.; Ruchirawat, M., Microfluidic approaches to malaria detection. *Acta Trop* **2004,** *89* (3), 357-369.

[36] Srivastava, S. K.; Gencoglu, A.; Minerick, A. R., DC insulator dielectrophoretic applications in microdevice technology: a review. *Analytical and Bioanalytical Chemistry* **2011,** *399* (1), 301-321.

[37] Adekanmbi, E. O.; Ueti, M. W.; Rinaldi, B.; Suarez, C. E.; Srivastava, S. K., Insulator-based dielectrophoretic diagnostic tool for babesiosis. *Biomicrofluidics* **2016,** *10* (3), 033108.

[38] Cho, Y.-K.; Kim, S.; Lee, K.; Park, C.; Lee, J.-G.; Ko, C., Bacteria concentration using a membrane type insulator-based dielectrophoresis in a plastic chip. *ELECTROPHORESIS* **2009,** *30* (18), 3153-3159.

[39] Chiok, K. L.; Paul, N. C.; Adekanmbi, E. O.; Srivastava, S. K.; Shah, D. H., Dimethyl adenosine transferase (KsgA) contributes to cell-envelope fitness in Salmonella Enteritidis. *Microbiological Research* **2018,** *216*, 108-119.

[40] Adekanmbi, E. O.; Srivastava, S. K., Dielectrophoretic applications for disease diagnostics using lab-on-a-chip platforms. *Lab on a Chip* **2016,** *16* (12), 2148-2167.

[41] Hawkins, B. G.; Kirby, B. J., Electrothermal flow effects in insulating (electrodeless) dielectrophoresis systems. *ELECTROPHORESIS* **2010,** *31* (22), 3622-3633.

[42] Gascoyne, P. R. C.; Shim, S., Isolation of circulating tumor cells by dielectrophoresis. *Cancers (Basel)* **2014,** *6* (1), 545-579.

[43] Salmanzadeh, A.; Romero, L.; Shafiee, H.; Gallo-Villanueva, R. C.; Stremler, M. A.; Cramer, S. D.; Davalos, R. V., Isolation of prostate tumor initiating cells (TICs) through their dielectrophoretic signature. *Lab on a Chip* **2012,** *12* (1), 182-189.

[44] Bakewell, D. J.; Morgan, H., Quantifying dielectrophoretic collections of sub-micron particles on microelectrodes. *Measurement Science and Technology* **2003,** *15* (1), 254-266.

[45] Sanchis, A.; Brown, A. P.; Sancho, M.; Martínez, G.; Sebastián, J. L.; Muñoz, S.; Miranda, J. M., Dielectric characterization of bacterial cells using dielectrophoresis. *Bioelectromagnetics* **2007,** *28* (5), 393-401.

[46] Hölzel, R., Single particle characterization and manipulation by opposite field dielectrophoresis. *Journal of Electrostatics* **2002,** *56* (4), 435-447.

[47] Bunthawin, S.; Wanichapichart, P.; Tuantranont, A.; Coster, H. G. L., Dielectrophoretic spectra of translational velocity and critical frequency for a spheroid in traveling electric field. *Biomicrofluidics* **2010,** *4* (1), 14102-14102.

[48] Wu, L.; Lanry Yung, L.-Y.; Lim, K.-M., Dielectrophoretic capture voltage spectrum for measurement of dielectric properties and separation of cancer cells. *Biomicrofluidics* **2012,** *6* (1), 14113-1411310.

[49] Pethig, R. R., *Dielectrophoresis : Theory, Methodology and Biological Applications*. New York: John Wiley & Sons, Incorporated: New York, 2017.

[50] Li, X.; Li, D.; Yan, Z.; Ao, Y., Adsorption of cadmium by live and dead biomass of plant growth-promoting rhizobacteria. *RSC Advances* **2018,** *8* (58), 33523-33533.

[51] Gao, Y.; Zhang, S.; Zhao, K.; Wang, Z.; Xu, S.; Liang, Z.; Wu, K., Adsorption of La3+ and Ce3+ by poly-γ-glutamic acid crosslinked with polyvinyl alcohol. *Journal of Rare Earths* **2015,** *33* (8), 884-891.

[52] Ramstedt, M.; Leone, L.; Persson, P.; Shchukarev, A., Cell wall composition of Bacillus subtilis changes as a function of pH and Zn^{2+} exposure: insights from cryo-XPS measurements. *Langmuir : the ACS journal of surfaces and colloids* **2014,** *30* (15), 4367-4374.

Chapter 8: Validation and conclusions

Chapter summary

Dielectrophoresis (DEP) has been used extensively in this dissertation to explore various bioparticles in their native or allied states. This DEP technology utilized the crossover measurement technique through the fabrication and investigation of the point-and-planar microwell (PPM) device platform. While exploring the effects of the inter-electrode spacing in the PPM device platform on DEP factor in chapter 3, a pertinent question was raised: would the variation of inter-electrode spacing affect the crossover frequency response of the bioparticles? From numerical simulations via COMSOL, it was investigated that the DEP factor distribution is affected based on the electrode spacing and the type of the bioparticle probed. In this chapter, electrode spacing dependency on the crossover response of bioparticles will be sought experimentally. Additionally, it is important to validate that if the results from the PPM device actually represent the dielectric characteristics of the explored bioparticles. As a result, the validation of the PPM characterization device is detailed in this chapter. Other significant factors that could affect the validation of the PPM device platform are the cell age and osmolarity of the cells when suspended in a medium. These factor are explored in this chapter. Thereafter, the summary of each of the chapters are sequentially stated. The chapter ends with the future direction regarding the utilization of PPM device platform and general bioparticle characterization using dielectrophoresis.

8.1 Validation of the point-and-planar microwell device platform [recap]

Validation is the comparison between a known result from a different well-established technique or instrument and the results generated using a newly developed novel technique or an instrument to verify sensitivity and specificity. Hence it is important to inspect if the PPM device platform designed and fabricated here as an alternative to the well know electrorotation platform used for dielectric characterization of cells would yield comparable dielectric properties. A bioparticle that has been well characterized by other techniques like electrorotation is the group ‘O’ human red blood cells [1] (RBC). O type RBCs are used to validate the dielectric properties obtained from the point-and-planar microwell device platform designed in this research. Human red blood cells were obtained, prepared, and used as reported by Gascoyne *et al.* [1]. Briefly, packed erythrocyte fraction from group ‘O’ blood sample (Research Innovation Incorporated, VA, USA) was washed twice in phosphate buffer saline (pH 7.2) and were suspended in medium containing 8.5% (w/v) sucrose and 0.3%(w/v) dextrose of conductivity 56 mS/m. Gascoyne *et al.[1]* obtained the properties of the RBCs using the modified electrorotation method [1]. Here, same O type RBCs will be fed into the PPM device platform for obtaining the DEP crossover frequency response.

Prepared RBCs were fed into the PPM device and the DEP crossover frequency experiments were performed on them. The movement of the RBCs in terms of nDEP and pDEP were recorded alongside the no-movement crossover point where the time-averaged DEP force on the RBCs were zero. The frequency of the AC signal when the cells did not respond to the AC electric field effect, termed crossover frequency, was recorded at a particular medium conductivity. The conductivity of the medium was modified with potassium chloride salt (KCl) and the experiment was repeated to obtain a new DEP crossover frequency point. This process was repeated for a total of seven (7) medium conductivity values i.e. 0-60 mS/m. Each experimental run at a particular medium conductivity was completed in about a minute (~1 min) since the proclivity for net ion outflux from the cytoplasm to the suspending medium is enhanced with prolonged measurement period, thus leading to significant errors in crossover frequency measurements [1]. A hypothesis, that no significant difference in dielectric properties occurs between the modified electrorotation and the point-and-planar microwell platform in the DEP crossover frequency response results, was then set up. The hypothesis used the statistical student's paired t-test for analysis.

A plot of medium conductivity *vs.* first crossover frequency (f_{CO1}) of healthy human red blood cell was obtained as described by Gascoyne *et al.* [1], as shown in Figure 8.1. These data, obtained through the point-and-planar microwell device, were fitted using an optimization algorithm on eqn. 8.1 and normalized with the average characteristic dimension of the RBC.

$$\mathrm{r.f_{co1}} = \frac{\mathrm{A_{0p}}}{2\pi \mathrm{b C_{spmem}}}\left\{\left(\sigma_{\mathrm{m}} - \frac{\mathrm{br}}{\mathrm{A_{0p}}}\mathrm{G_{spmem}}\right) \mathrm{X} \left[\left(\frac{1-\mathrm{A_{0p}}}{\mathrm{A_{0p}}}\right)\sigma_{\mathrm{m}} + \frac{\mathrm{br}}{\mathrm{A_{0p}}}\mathrm{G_{spmem}}\right]\right\}^{\frac{1}{2}} \qquad (8.1)$$

It is evident from Figure 8.1 that subjecting RBCs to the same preparatory conditions as outlined in the electrorotation article by Gascoyne *et al.*: (8.5% (w/v) sucrose plus 0.3% (w/v) dextrose solution), provided comparable results irrespective of the method of analysis utilized i.e., the specific capacitance, specific conductance, and the dimensional ratio of the RBCs remained consistent.

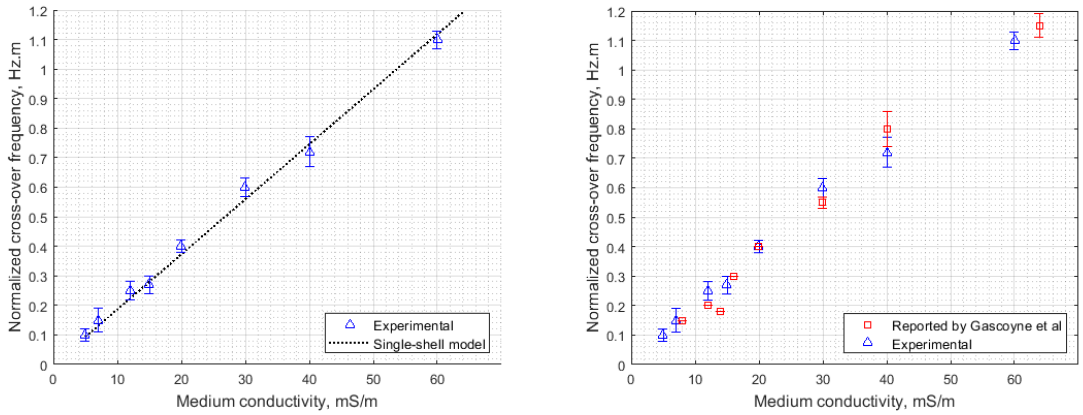

Figure 8. 1 *(A) Plots showing the crossover frequency vs. medium conductivity for the data reported by Gascoyne et al. [1] and the data obtained through the point-and-planar microwell device. Each of these data sets were obtained with 6 independent samples at varying medium conductivity. (B) The experimental data were fitted with the oblate ellipsoidal model given in eqn. 8.1. The error bars represent the measure of variation among the 6 independent technical replicates.*

In both cases (reported and experimental), the crossover frequencies increase along with the increase in medium conductivity because the specific capacitance is kept constant. More so, the intercepts on the y-axis are both positive. This observation indicates that the dielectric properties of the RBCs as well as the cell's dimension are both consistent, hence the non-linearity in dimension or intrinsic electrophysiological properties that introduces complexity into the analysis has been ruled out [2]. Student's t-test performed on the crossover measurements for each of the cases (at 7 degrees of freedom and α=0.05) gave a t-stat value of -1.482 which is less than the t-critical value of -2.385 for a one-tail test. Hence, we fail to reject the null hypothesis that there is no significant difference between the modified electrorotation and the point-and-planar microwell device crossover frequency measurement. The obtained crossover frequency response values are then used to estimate the dielectric properties of interest. The dielectric parameters of the membrane properties obtained from the PPM device platform are compared with the reported data using electrorotation [1] and is given in the table 8.1 below:

Table 8. 1 *Calculated membrane properties from the PPM device as compared to the reported values from electrorotation [1]*

Specific Membrane Properties (mF/m^2)	***Human Red Blood Cell (group O)***	
	Gascoyne et al[1]	***Microwell fit values***
Capacitance	11.8	10.5±1.7
Conductance	*271*	266±6.0

8.1.1 Effects of electrode shape and spacing on the first crossover frequency

As discovered in chapter 3 based on simulations, different electrode shapes and spacing resulted in changing DEP factor. Since DEP factor influences the dielectrophoretic force (Eqns. 3.1 and 3.2), both nDEP and pDEP responses of the RBCs will be affected. This may lead to a change in crossover frequency that is investigated here. This investigation essentially rules out any cell response variability issues that may arise when different shaped point electrodes are utilized in the PPM device platform. To verify these effects, human red blood cells obtained from Innovative Research Inc. were suspended in 50g/L dextrose solution. The spacing between the point and planar electrodes were adjusted through the point electrode only. Once the appropriate spacing has been established i.e. 25, 50, 75 and 100 μm, it was kept constant by using an epoxy sealant. The experiment was a 3 x 4 factorial design with two factors (electrode shape and electrode spacing) at 3 and 4 levels respectively. Statistical factorial analysis was performed using SAS software to verify the main effects of each of the factors as well as their interactions.

Table 8. 2 *The average crossover frequencies (in kHz) of human red blood cells using each of the spacing-shape designs at a fixed medium conductivity of 0.052 S/m. The precision of the triangle data is better than the other two designs. However, there are no statistically significant interactions observed between the spacing and the electrode shape when the crossover frequency data was analyzed using a two-factor experimental design.*

Design	**Spacing**			
	25 µm	**50 µm**	**100 µm**	**125 µm**
Square	265±4.82	269±0.13	268±2.06	266±3.90
Triangle	270±0.02	269±0.40	269±0.72	269±0.72
Semicircle	269±1.30	268±2.60	266±4.30	269±0.00

Results from Table 8.2 shows that operating the device at inter-electrode distance of 25-100 µm would neither change the crossover frequency nor the cell membrane properties. This observation is consistent with the literature [3, 4]. Therefore, operating at electrode spacing distances (25-100 µm) does not have any effect on the crossover frequency determination since this is the point where $F_{DEP} = 0$. This implies that the gradient of the electric field is inconsequential at the crossover frequency point.

8.1.2 Effects of cell storage time on membrane capacitance

In direct current (frequency-independent) dielectrophoresis (DC DEP), separating cells into individual components relies heavily on the membrane capacitance, thus influencing membrane conductance. If the dielectric characterization result is erroneous then the design and testing of the separation device will be flawed since the obtained dielectric parameters are utilized in modeling and

simulating the sorting device. One of the factors that can affect this dielectric property characterization is the age of the cell i.e. how fresh the sample is. This also means the length of the time the bioparticles (e.g., RBCs) are stored at 2-8 ºC before utilizing for experimental runs. Many molecular and clinical reports have provided extremely convincing evidence towards concluding that the long-time storage of erythrocytes are likely to decrease its quality [5-10]. Jeon *et al.* studied the change in properties observed when RBCs are stored for 40 days using optical tweezers [11]. A dramatic change in the DEP response of the cells were observed as the cells aged. Here, the PPM platform will be used to investigate the effect of cell storage time on membrane capacitance using 2-8 ºC storage conditions for four (4) days.

Freshly collected bovine erythrocytes (C-95053, WSU, USA) was washed twice in phosphate buffered saline (PBS) (pH 7.2) and were suspended in isotonic dextrose medium of conductivity 0.056 S/m. The experimental procedure was as given in section 8.1 and was repeated at various medium conductivities adjusted by using KCl. When the crossover frequency data were analyzed and plotted using the theoretical single shell model, there was a substantial shift in the properties correlating to the cell DEP response from day 1 to day 4. This shift can be related to the changes in the cell membrane as the cell ages. As days go by, the ability of the cell membrane to resist electric field (permittivity) weakens due to the degradation of the membrane. Since permittivity is directly proportional to membrane capacitance, which in turn is inversely proportional to the crossover frequency, it is expected that the crossover frequency will increase. This decrease in permittivity (associated with the increase in crossover frequency) is consistent with reported variation in DEP force with frequency using the optical tweezer technique [11].

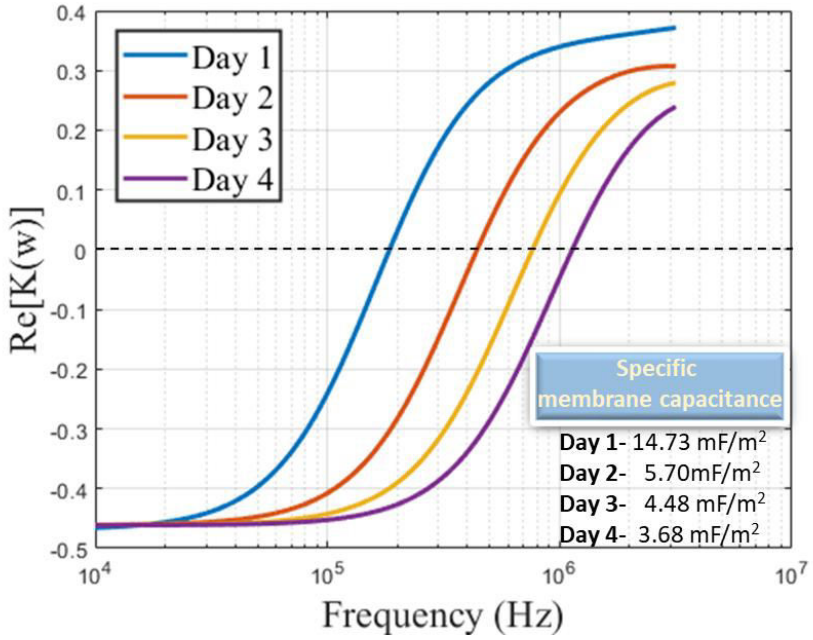

Figure 8. 2 *The variation of plot of the real part of the Clausius-Mossotti factor as a function of frequency. The horizontal broken line represent the plane where Re[K(w)] is zero. The points at which the sigmoidal curve intersects this line is the cross over frequency of the cells.*

8.1.3 Effects of osmotic stress on membrane capacitance

Another factor, as mentioned earlier, that could affect the characterization outcomes of any biological cell is the osmolality of the suspending medium. Osmolality of a medium is the concentration of such medium measured as the total number of solute particles per kilogram solvent. As mentioned in chapter 2, section 5.1, this factor can render a solution to be hypotonic, isotonic or hypertonic. Here, three sets of medium were prepared using different concentration of sodium chloride (NaCl): 0.45% NaCl solution (hypotonic), 0.9% NaCl solution (isotonic) and 2% NaCl solution (hypertonic). Freshly collected bovine erythrocytes (C-95053, WSU, USA) were prepared as stated in section 8.1.2 but suspended in each of the three NaCl solutions. The crossover frequency of each set of samples was found and used to calculate the membrane capacitance as shown figure 8.3.

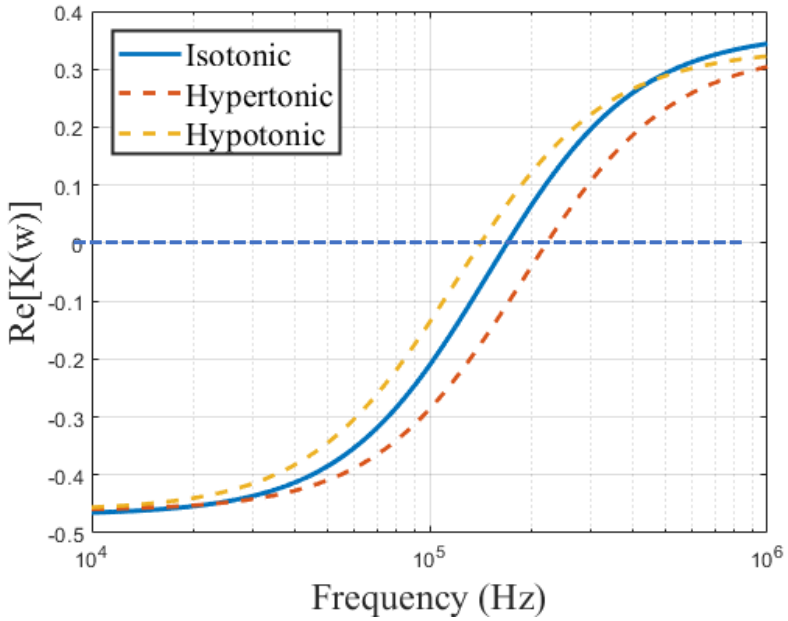

Figure 8. 3 *The variation of plot of the real part of the Clausius-Mossotti factor as a function of frequency. The points at which the sigmoidal curve intersects the horizontal line is the cross over frequency of the cells. Hypertonic solution resulted in cells having higher crossover frequency because the cell shrinks and smaller particles always have larger crossover frequencies.*

From Figure 8.3, it is evident that the crossover frequency of the bovine RBCs was effected when they were suspended in each of the test solutions. In the hypotonic solution, the size of the RBCs was slightly increased due to turgidity. This increase in size is reflected in Figure 8.3 as lower crossover frequency. An isotonic solution is seen as the preferred solution and thus gives the actual estimate of the cell membrane capacitance because the membrane is not compromised through water loss or gain. When the hypertonic solution was used, the crossover frequency increased due to the reduction in cell size. These results corroborate the essence of maintaining specific osmolality when characterizing biological cells.

8.2 Key Conclusions

Electrical characterization of bioparticles provides an opportunity to predict their behavior when placed in a nonuniform electric field. This characterization could reveal the permittivity and conductivity (and by extension, specific capacitance and specific conductance) of their membranes and cytoplasm (cell interior). Information about bioparticle's permittivity and conductivity can further yield results leading to healthy, infection, or death. This information can also provide the directional orientation of the cell in a microfluidic sorting or enriching platform in the midst of other cells either homogeneous or heterogeneous. The chapters in this dissertation have been organized with a view to providing an easy-

to-follow progression of cellular characterization from diagnostics to environmental applications. The overview of key conclusions from each chapter is presented below:

Chapter 2 detailed the three methods of electrical characterization of bioparticles: impedance cytometry, electrorotation, and dielectrophoresis. Dielectrophoretic characterization was further explored in terms of collection spectra, capture-voltage spectra, and crossover frequency measurement. Furthermore, chapter 2 details the structure of the three forms of life: prokaryotes, eukaryotes, and archaea, and including the membrane structure that serves as an insulating layer that rendered them to resist electric field at low frequencies of externally applied AC signals. The working principle of each of the three characterization techniques was also provided in chapter 2, in addition to the procedure commonly followed to obtain electrical properties of biological cells. The chapter concluded by reporting different bioparticle characterization studies achieved by other researchers using one of the three methods mentioned above.

The focus in this dissertation is on dielectrophoresis as a characterization method, a gap was identified in terms of developing a cost-effective platform. This led to the introduction of the point-and-planar microwell (PPM) device platform in chapter 3. This novel characterization microwell has the advantage of adjustable inter-electrode spacing that allows for real-time exploration of cell behavior at diverse spatial locations within the PPM device. The microwell also benefits from faster cellular response to electric field effect, thus, reducing the residence time for dielectric property quantification. This PPM device also has the advantage of preserving the integrity of the bioparticle. The rationale behind the choice of material for the fabrication of the microwell platform was also detailed. The device which works on the principle of DEP crossover frequency was numerically and experimentally investigated to determine the effect of electrode shape and inter-electrode spacing on DEP factor (|E. E|), a variable that determines the dielectrophoretic force a bioparticle. This resulted in narrowing down the inter-electrode spacing to between 50 – 100 μm. Validation of this PPM device was performed using human RBCs (erythrocytes group O) in comparison with results from electrorotation. This was reported in Chapter 8.

When the point-and-planar microwell was fabricated, there was a need to assemble it through irreversible hydrophilic sealing. This is commonly achieved through any commercially available radio-frequency (RF) plasma cleaning technology. However, in chapter 4, an in-house plasma cleaning machine that uses microwave (MW) frequency was constructed, characterized, and compared with the RF type to reduce the costs associated with commercial cleaners. Its performance was juxtaposed with RF's in terms of contact angle, storage solvent, half-way to hydrophobicity, and electroosmotic surface

effects of the elastomeric material treated with both machines. The outcomes revealed that RF and MW plasma generation work comparably similar.

After the complete assembly of the point-and-planar device as seen in chapter 4, this PPM device was used in chapter 5 to characterize infiltrating ductal adenocarcinoma cells (ADCs) and peripheral blood mononuclear cells (PBMCs). ADC, a type of breast cancer, is one of the non-communicable disease that kill more than 36 million people annually representing 63% of global deaths. The point-and-planar microwell provided the crossover frequency response of ADCs that were used to obtain conductivity and permittivity of the cells. This electrical information was used to numerically detect the cause of the age-long challenge of cellular recirculation or flow restriction in microdevice. This flow instability was observed experimentally, and researchers had failed to detect numerically. By obtaining the optimal experimental conditions numerically, will aid in a better realistic point-of-care device platform to detect many diseases.

In Chapter 6, attention was shifted from the application of point-and-planar microwell for disease characterization to the exploration of the changes that occur in the electrophysiological property of *Cupriavidus necator* in its native and allied states. Recovery of rare earth elements (REEs) from any waste-water streams through bacteria (biosorption) is a potent technique that have been used for ages. In this chapter, the behavior of the bacteria with and without any exposure to the REEs were tracked. Results showed that the second crossover frequency (f_{CO2}) of the bacteria in both native and allied states did not change indicating that the inner membrane of the gram negative bacteria was not substantially affected. This also proves that the uptake of REEs in solution by the bacteria was only a surface-related phenomenon i.e. adsorption. The first crossover frequency (f_{CO1}), however, were different implying that the point-and-planar microwell device was able to show that the membrane of the bacteria had been tampered substantially by REEs as a result of the exposure to the metal solutions.

The unique and novel results from chapter 6 led to further exploration of the utilization of the no-change-in-second-crossover advantage to REE quantification without any recourse to spectroscopy. In chapter 7, the bacteria were investigated for dependencies on pH, biosorbent density i.e. *C. necator*, exposure time to the REE solutions, and solute concentration i.e. REEs. The efficiency of the bacteria as a biosorbent at these conditions were measured through the quantification of supernatants by ultraviolet-visible (UV-Vis) spectrophotometer and correlated with the crossover frequency measurement. This crossover-concentration curve now serves as the calibration curve for the bacteria biosorption efficiency in lieu of spectrophotometry.

Each of the chapters (2-8) have their unique contributions to the current body of knowledge and those contributions are relayed below:

Chapter 2: This collated diverse useful work in cellular characterization provided detailed information about the procedure involved. Researchers now have a one-stop shop for easy access to various information regarding the electrical characterization of living cells. This review also revealed a gap regarding the challenges of cellular characterization, which this dissertation outrightly explored and addressed.

Chapter 3: This chapter contributed to the current body of knowledge by introducing a point-and-planar device platform that has the capacity to vary interelectrode distance for real-time measurement of bioparticle properties. This device helped to explain the different pDEP regions observed for various electrode shapes. Through this, researchers can now predict the pDEP zones prior to running real-time experiments that aids to DEP collection-spectra technique for dielectric characterization.

Chapter 4: Microwave plasma cleaner was designed in this chapter for the assembly of the point-and-planar microwell platform. This plasma cleaner was unique as it explored the possibility of saving cost of the device assembly in microfluidic area. Researchers can find this cost-saving device useful in exploring electroosmotic effects within their microchannels. This is a huge advantage to researchers especially in this era of dwindling research funds.

Chapter 5: Most published research in dielectrophoretic cancer diagnostics search for circulating tumor cells (CTCs) in the blood. These CTCs are an indication of late stage cancer. In this chapter, stage 0 (early stage) breast cancer was characterized and numerically explored for possible separation from healthy peripheral blood mononuclear cells. Two key contributions that fills the gap in dielectrophoretic arena from this chapter are (a) it is now possible to characterize stage 0 breast cancer, (b) The age-long problem of flow instability in microfluidics can now be solved through process modification as addressed in the chapter.

Chapters 6 and 7: These chapters detail the application of point-and-planar microwell device for environmental biotechnology applications. The very important contribution of these chapter is that researchers can now use the electrical properties of biosorbents to obtain the amount of metals they can adsorb on their surface without using any expensive spectrophotometric technique. This novel finding is the first to be reported and has the potential to attract attention amongst the experts in dielectrophoresis.

Chapter 8: This chapter finally validates the PPM platform to provide research confidence about its usage. This chapter also revealed an important variation in red blood cell properties due to their age and osmotic stress i.e. isotonicity and osmolarity has to be maintained. This is a very important

contribution to the DEP world as researcher can now use the knowledge gained in this research to develop a correlation factor for their cells (depending on their age) during characterization.

References

[1] P. Gascoyne, R. Pethig, J. Satayavivad, F. F. Becker, and M. Ruchirawat, "Dielectrophoretic detection of changes in erythrocyte membranes following malarial infection," *Biochimica et Biophysica Acta (BBA) - Biomembranes,* vol. 1323, pp. 240-252, 1997/01/31/ 1997.

[2] R. R. Pethig, *Dielectrophoresis : Theory, Methodology and Biological Applications*. New York: New York: John Wiley & Sons, Incorporated, 2017.

[3] P. Marszalek, J. J. Zielinsky, M. Fikus, and T. Y. Tsong, "Determination of electric parameters of cell membranes by a dielectrophoresis method," *Biophysical Journal,* vol. 59, pp. 982-987, 1991/05/01/ 1991.

[4] P.-Y. Weng, I. A. Chen, C.-K. Yeh, P.-Y. Chen, and J.-Y. Juang, "Size-dependent dielectrophoretic crossover frequency of spherical particles," *Biomicrofluidics,* vol. 10, pp. 011909-011909, 2016.

[5] G. J. C. G. M. Bosman, J. M. Werre, F. L. A. Willekens, and V. M. J. Novotný, "Erythrocyte ageing in vivo and in vitro: structural aspects and implications for transfusion," *Transfusion Medicine,* vol. 18, pp. 335-347, 2008/12/01 2008.

[6] E. Bennett-Guerrero, T. H. Veldman, A. Doctor, M. J. Telen, T. L. Ortel, T. S. Reid, M. A. Mulherin, H. Zhu, R. D. Buck, R. M. Califf, and T. J. McMahon, "Evolution of adverse changes in stored RBCs," *Proceedings of the National Academy of Sciences of the United States of America,* vol. 104, pp. 17063-17068, 2007.

[7] P. E. Marik and W. J. Sibbald, "Effect of Stored-Blood Transfusion on Oxygen Delivery in Patients With Sepsis," *JAMA,* vol. 269, pp. 3024-3029, 1993.

[8] F. R. Purdy, M. G. Tweeddale, and P. M. Merrick, "Association of mortality with age of blood transfused in septic ICU patients," *Canadian Journal of Anaesthesia,* vol. 44, pp. 1256-1261, 1997/12/01 1997.

[9] R. W. Taylor, J. O'Brien, S. J. Trottier, L. Manganaro, M. Cytron, M. F. Lesko, K. Arnzen, C. Cappadoro, M. Fu, M. S. Plisco, F. G. Sadaka, and C. Veremakis, "Red blood cell transfusions and nosocomial infections in critically ill patients*," *Critical Care Medicine,* vol. 34, pp. 2302-2308, 2006.

[10] C. J. Fernandes, Jr., N. Akamine, F. V. De Marco, J. A. De Souza, S. Lagudis, and E. Knobel, "Red blood cell transfusion does not increase oxygen consumption in critically ill septic patients," *Critical care (London, England),* vol. 5, pp. 362-367, 2001.

[11] H.-J. Jeon, H. Lee, D. S. Yoon, and B.-M. Kim, "Dielectrophoretic force measurement of red blood cells exposed to oxidative osmotic stress using optical tweezers and a microfluidic chip," *Biomedical Engineering Letters,* vol. 7, pp. 317-323, 2017/11/01 2017.